TECHNISCHE UNIVERSITÄT MÜNCHEN

Fakultät für Chemie

Structure and Function of the Invariant Light Chain

JASMIN RENATE KÖNIG

Vollständiger Abdruck der von der Fakultät für Chemie der Technischen Universität München zur Erlangung einer

Doktorin der Naturwissenschaften (Dr. rer. nat.)

genehmigten Dissertation.

Vorsitz: Prof. Dr. Bernd Reif

Prüfer*innen der Dissertation:

1. Prof. Dr. Johannes Buchner
2. Prof. Dr. Matthias Feige

Die Dissertation wurde am 19.05.2022 bei der Technischen Universität München eingereicht und durch die Fakultät für Chemie der Technischen Universität München am 18.08.2022 angenommen.

Gewidmet meiner Oma, Helga

ABSTRACT

The mammalian immune system is a complex defense apparatus against foreign pathogens and numerous other infectious agents, like viruses and cancer cells, to protect an organism from diseases. It conists of an innate immune response, which confers unspecific protection to a broad group of stimuli, and an adaptive (or acquired) immune response that is specific to each stimulus and has a memory function. Adaptive immunity can produce both, a T-cell mediated cellular response and a B-cell mediated humoral reaction. Antibodies are the protagonists of the humoral immune response. The production of functionally and structurally intact antibodies is a key process depending on a finely tuned B-cell development, which comprises various stages and checkpoints to control the quality of antibodies, especially of the heavy chain (HC).

The surrogate/invariant light chain (SLC) monitors the quality of the the immunoglobulin (Ig) HC as part of the pre-B-cell receptor (pre-BCR), which constitutes an important control checkpoint in early B-cell development. Unlike a conventional light chain (LC) harboring covalently linked variable (V_L) and constant domains (C_L), the SLC consists of two non-covalently associated, analogous proteins: VPREB and IGLL (λ5). Both proteins contain unfolded unique regions (UR) at their N- and C-terminal ends, respectively. Upon association of VPREB and λ5, the typical Ig fold in VPREB is completed by incorporation of the missing β-strand from the N-terminal part of λ5. The elucidation of the underlying molecular mechanisms of SLC and pre-BCR assembly is still at an early stage. Moreover, the SLC function regarding its structure-function relationship is largely unknown. However, this knowledge is of high importance since an improper B-cell development and a malfunctioning pre-BCR, attributed to a (partly) missing SLC, can lead to an incomplete immune response. This doctoral thesis is a first approach to dissect the association mechanisms of both, the SLC and the pre-BCR, with a focus on the special structural SLC features.

An efficient method for recombinant production of tag-less SLC wildtype (WT) proteins, variants and complexes was established. Characterization revealed VPREB to be unfolded in absence of λ5, while λ5 can attain its native conformation, both regardless of their URs. VPREB was shown to be homodimeric and λ5 to be a monomer. The VPREB dimer interface was identified to be located at the VPREB-V_H interface with some parts of the VPREB-λ5 interface, which can be attributed to decreased conformational dynamics. Furthermore, the dimer species of VPREB is shifted towards a monomer-dimer equilibrium with the added β-strand. The URs decrease the thermal stabilities in λ5 alone and in the SLC complex. For interaction of VPREB and λ5, it was shown previously that the additional β-strand of λ5 is indispensable. This thesis proved that it also is sufficient to induce folding of VPREB. The λ5 core region induces folding in the C_H1 domain as it was previously shown for C_L. However, also VPREB interacts via its IgV-like domain with C_H1 without inducing a folding reaction in any of the two proteins.

Unfolded VPREB alone has the highest affinity for the variable HC domain (V_H) compared to λ5 and the SLC complex. V_H and VPREB form a heterodimer exposing the interaction site for λ5 in VPREB as revealed by increased conformational dynamics. Also, in λ5, the additional β-strand, which is the main interaction site for VPREB, gets exposed upon V_H interaction. In both SLC proteins, the URs were shown to be crucial parts for V_H interaction. However, folding of VPREB is not induced upon interaction with V_H.

Taken together, a model of SLC and pre-BCR assembly was elaborated that supports a concerted binding of VPREB and ʎ5 to the HC, in which VPREB seems to bind first in its unfolded state to both, the V_H and C_H1 domain. After this first proof-reading step is approved by VPREB, ʎ5 interacts via its β-strand with VPREB while simultaneously inducing its folding. Consequently, the ʎ5-UR binds to V_H and the λ5 core region to C_H1 to induce the folding of this domain. One of the most important findings in this thesis is the surprisingly high antigen affinity of the Fab-SLC complex, which seems to be predominantly confered by the λ5-UR providing an excellent starting point for further research.

ZUSAMMENFASSUNG

Das Immunsystem von Säugetieren ist ein komplexer Abwehrapparat gegen fremde Krankheitserreger und zahlreiche andere Infektionserreger wie Viren und Krebszellen, der den Organismus vor Krankheiten schützt. Es besteht aus einer angeborenen Immunreaktion, die einen unspezifischen Schutz gegen eine breite Gruppe von Reizen bietet, und einer adaptiven (oder erworbenen) Immunreaktion, die für jeden Reiz spezifisch ist und eine Gedächtnisfunktion hat. Die adaptive Immunität kann sowohl eine durch T-Zellen vermittelte zelluläre Reaktion als auch eine durch B-Zellen vermittelte humorale Reaktion hervorrufen. Antikörper sind die Protagonisten der humoralen Immunantwort. Die Produktion von funktionell und strukturell intakten Antikörpern ist ein Schlüsselprozess, der von einer fein abgestimmten B-Zell-Entwicklung abhängt, die verschiedene Phasen und Kontrollpunkte umfasst, um die Qualität der Antikörper, insbesondere der schweren Kette, zu kontrollieren.

Die SLC überwacht die Qualität der schweren Kette des Immunglobulins als Teil des Prä-B-Zell-Rezeptors, der einen wichtigen Kontrollpunkt in der frühen B-Zell-Entwicklung darstellt. Im Gegensatz zu einer herkömmlichen leichten Kette mit kovalent verbundenen variablen und konstanten Domänen besteht die SLC aus zwei nicht kovalent verbundenen, analogen Proteinen: VPREB und IGLL (λ5). Beide Proteine enthalten an ihren N- bzw. C-terminalen Enden ungefaltete einzigartige Regionen. Bei der Assoziation von VPREB und λ5 wird die typische Ig-Faltung in VPREB durch den Einbau des fehlenden β-Strangs aus dem N-terminalen Teil von λ5 vervollständigt. Die Aufklärung der zugrundeliegenden molekularen Mechanismen der SLC- und Prä-BCR-Assemblierung befindet sich noch in einem frühen Stadium. Darüber hinaus ist die Funktion der SLC im Hinblick auf ihre Struktur-Funktions-Beziehung weitgehend unbekannt. Dieses Wissen ist jedoch von großer Bedeutung, da eine fehlerhafte B-Zell-Entwicklung und ein schlecht funktionierender prä-BCR, der auf eine (teilweise) fehlende SLC zurückzuführen ist, zu verschiedenen Krankheiten, zu einer unvolständigen Immunantwort führen kann. Diese Doktorarbeit ist ein erster Ansatz, die Assoziationsmechanismen von SLC und prä-BCR zu entschlüsseln, wobei der Schwerpunkt auf den speziellen strukturellen Merkmalen der SLC liegt. Es wurde eine effiziente Methode zur rekombinanten Produktion von SLC-Wildtyp-Proteinen, Varianten und Komplexen ohne Tag etabliert. Die Charakterisierung ergab, dass VPREB in Abwesenheit von λ5 entfaltet vorliegt, während λ5 seine native Konformation annehmen kann, und zwar unabhängig von ihren URs. VPREB erwies sich als Homodimer und λ5 als Monomer. Die VPREB-Dimer-Grenzfläche wurde an der VPREB-V_H-Grenzfläche mit einigen Teilen der VPREB-λ5-Grenzfläche lokalisiert, was auf eine verringerte konformationelle Dynamik zurückgeführt werden kann. Darüber hinaus wird die Dimer-Spezies von VPREB durch den hinzugefügten β-Strang in Richtung eines Monomer-Dimer-Gleichgewichts verschoben. Die URs verringern die thermischen Stabilitäten von λ5 allein und im SLC-Komplex. Für die Interaktion

von VPREB und λ5 wurde bereits gezeigt, dass der zusätzliche β-Strang von λ5 unverzichtbar ist. In dieser Arbeit wurde nachgewiesen, dass er auch ausreicht, um die Faltung von VPREB zu induzieren. Die λ5-Kernregion induziert die Faltung in der C_H1-Domäne, wie es zuvor für C_L gezeigt wurde. Allerdings interagiert auch VPREB über seine IgV-ähnliche Domäne mit C_H1, ohne dass eine Faltungsreaktion in einem der beiden Proteine induziert wird.

Ungefaltetes VPREB allein hat die höchste Affinität für die V_H-Domäne im Vergleich zu λ5 und dem SLC-Komplex. V_H und VPREB bilden ein Heterodimer, das die Interaktionsstelle für λ5 in VPREB freilegt, wie eine erhöhte konformationelle Dynamik zeigt. Außerdem wird in λ5 der zusätzliche β-Strang, der die Hauptinteraktionsstelle für VPREB darstellt, bei der Interaktion mit V_H freigelegt. Bei beiden SLC-Proteinen wurde gezeigt, dass die URs für die V_H-Interaktion entscheidend sind. Die Faltung von VPREB wird jedoch durch die Interaktion mit V_H nicht induziert.

Insgesamt wurde ein Modell der SLC- und Prä-BCR-Assemblierung erarbeitet, das eine konzertierte Bindung von VPREB und ʎ5 an die HC-Domäne unterstützt, wobei VPREB zunächst in seinem ungefalteten Zustand sowohl an die V_H- als auch an die C_H1-Domäne zu binden scheint. Nachdem dieser erste Korrekturleseschritt von VPREB genehmigt wurde, interagiert ʎ5 über seinen β-Strang mit VPREB und induziert gleichzeitig dessen Faltung. Im Folgenden bindet die ʎ5-UR an V_H und die Kernregion an C_H1, um die Faltung dieser Domäne zu induzieren. Eine der wichtigsten Erkenntnisse dieser Arbeit ist die überraschend hohe Antigen-Affinität des Fab-SLC-Komplexes, die anscheinend hauptsächlich durch die λ5-UR vermittelt wird und einen hervorragenden Ausgangspunkt für weitere Forschungen darstellt.

TABLE OF CONTENTS

1. INTRODUCTION

1.1 Protein Folding

1.1.1 The Principles of Protein Folding

Proteins are the “molecular machines” of the cells and consist of amino acid residues that are connected by peptide bonds. These essential macromolecules fulfill several functions, e. g. transport of molecules, catalyzing enzymatic reactions and deoxyribonucleic acid (DNA) replication. Beyond, proteins are important in cell signaling, immune responses, cell adhesion, the cell cycle and much more. Despite their numerous functions, proteins are only encoded by 20 different proteinogenic amino acids. According to the central dogma of molecular biology, which was first stated by Francis Crick in 1958, genes are transcribed into messenger ribonucleic acids (mRNAs) that are subsequently translated into the primary structure of proteins by ribosomes, a process also referred to as the protein biosynthesis (Zamecnik, 1962; Khorana, 1968; Crick, 1970; Barger, 2016). During ribosomal biosynthesis, the nascent linear polypeptide chain can already adopt its three-dimensional conformation (Anfinsen, 1973; Zhang and Zoya, 2011). Protein folding is essential because the function of proteins is directly related to their three-dimensional structure (Orengo et al., 1999). The native conformation and the pathway to attain this state is encoded in the amino acid sequence, also referred to as the Anfinsen´s dogma (Anfinsen, 1973), although nearly identical amino acid sequences do not always fold into similar structures (Alexander et al., 2007).

The first step in the protein folding process is the formation of the secondary structure. The secondary structure is defined as the local three-dimensional structure, such as alpha helices and β-strands, which are stabilized by intramolecular hydrogen bonds (Pauling and Corey, 1951a; 1951b; 1951c; 1951d; 1951e; Pauling et al., 1951). The Ramachandran Plot has been used to analyze crystal structures of proteins. The two dihedral/torsion angles φ (Phi) and ψ (Psi) represent the rotation angles of the polypeptide backbone around N-Cα and Cα-C, respectively. The plot reflects the possible or allowed and disfavored φ- and ψ-angles according to their steric degree of freedom (Ramachandran et al., 1963). The secondary structure elements arrange into their global three-dimensional shape to attain the protein´s tertiary structure (Richardson, 1981). The main driving force of protein folding are the hydrophobic interactions of non-polar amino acid side chains causing the hydrophobic portions to be buried in folded proteins. This is complemented by polar interactions between polar residues and water molecules causing the hydrophilic moieties to be exposed to the hydrophilic aqueous environment (Pace et al., 2011). These interactions are predominantly conferred by van der Waals interactions. Beyond, folding is also dictated by other non-covalent interactions like hydrogen bonds and salt bridges (Dill, 1990; Dobson, 2003). The formation of covalent bonds between two cysteine residues to form

disulfide bridges supports the formation of the tertiary structure (Anfinsen and Haber, 1961). Protein folding from an unfolded state to a folded state is a first-order reaction because the reaction rate is only dependent on the protein concentration (Jackson, 1997; Plaxco et al., 1998; Plaxco et al., 2000). Non-covalent interactions between several folded polypeptide subunits, i. e. protein molecules, results in the quaternary structure, which is defined as a multi-subunit protein complex (Kim and Baldwin, 1982; Hurtley and Helenius, 1989).

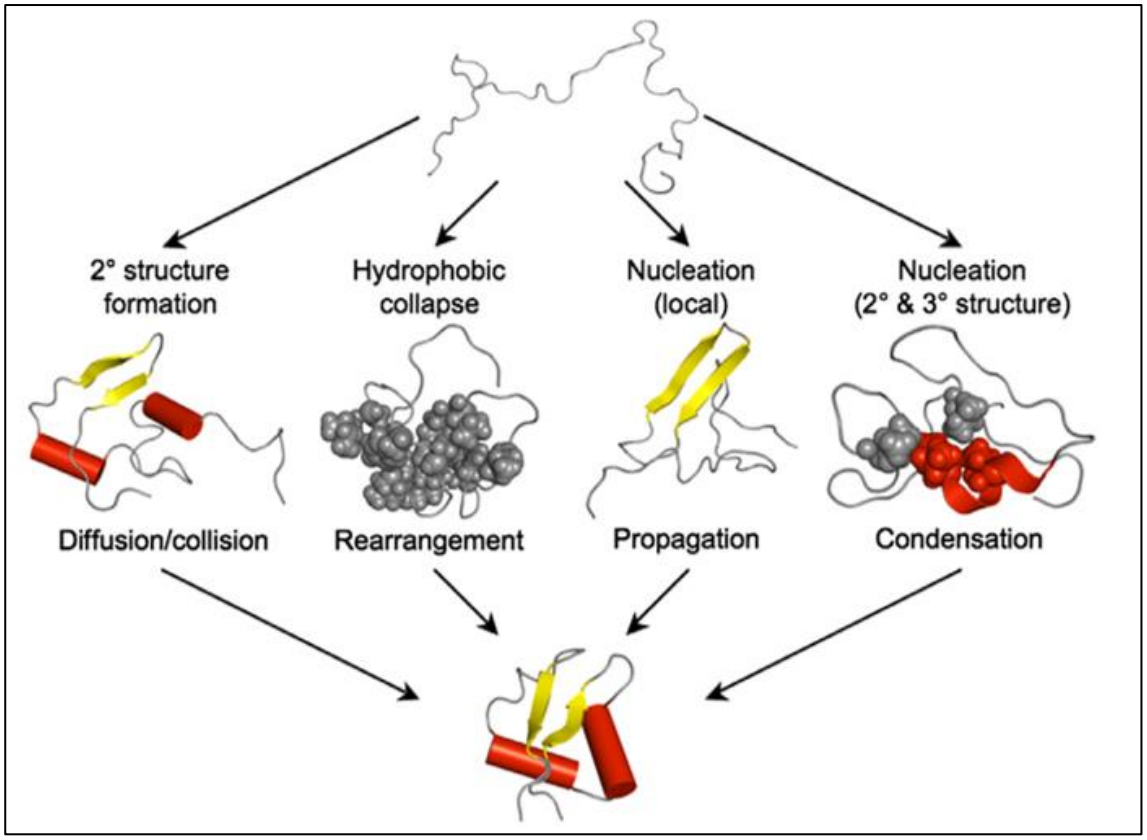

Figure 1: Folding Models for Protein Structure Prediction.
The framework/diffusion-collision model (left) divides the protein into microdomains, which are local elements that form the secondary structure first, which then collide and diffuse together to form the tertiary structure. The hydrophobic collapse model (middle left) describes a protein to bury its hydrophobic side chains in the inside and to carry its hydrophilic residues surface-exposed after collapsing. The nucleation propagation model (middle right) states that local interactions form a small nucleus consisting of secondary structure from which the propagation for the rest of the structure formation takes place. The nucleation condensation model (right) describes the parallel formation of secondary and tertiary structure. Figure and legend were taken from Nickson and Clarke, 2010, the legend was modified (Nickson and Clarke, 2010).

There are several folding models that can be used to predict a protein´s structure (Figure 1). One model already mentioned above is the so-called hydrophobic collapse model. Polar residues that interact with the aqueous surrounding place thermodynamic pressure to force the protein into its native conformation with a hydrophobic core (Dolgikh et al., 1981; Hart and Istrail, 1996; Pace et al., 2011). The second model is the diffusion-collision model, also called the framework model. In this model, the protein is divided into several parts, i. e. microdomains. Each of the microdomains is considered short enough to be scanned for all conformational alternatives

rapidly. This implies the secondary structure elements to be dynamic, diffuse together and collide in order to unite into a structural entity (Karplus and Weaver, 1976; 1994). The third model is the nucleation propagation model which states that local interactions form a small nucleus consisting of secondary structure from which the propagation for the rest of the protein takes place (Wetlaufer, 1973; Feige et al., 2008). The fourth model is the nucleation-condensation theory, which describes the parallel formation of secondary and tertiary structure (Fersht, 1995; Itzhaki et al., 1995; Fersht, 1998).

The hydrophobic core of the proteins has little surface exposure, which reduces the restriction of the translational movement of water molecules, i. e. water crowding, in the system. The hydrophobic effect upon protein folding leads to an increase of the water entropy and therefore to an energetically favoured state (Tanford, 1978; Privalov and Makhatadze, 1993; Pace et al., 1996; Kinoshita, 2009). Subsequently, folding guides the protein to adopt the most thermodynamic stable conformation, called the native state (Makhatadze and Privalov, 1993). In 1968, Cyrus Levinthal stated the Levinthal paradoxon, which implied that a very large number of degrees of freedom exist in an unfolded protein with 3^{300} possible conformations for a protein with 100 residues. If a protein would attain its structure by sequential sampling of all possible conformations, it would take a tremendous amount of time. Therefore, Levinthal concluded that, based upon the observation that proteins fold much faster, sequential sampling does not occur but instead proteins must fold through intermediate states (Levinthal, 1968; Anfinsen, 1972). This is achieved by adopting an energetically favoured state, the native state (Dill and Chan, 1997). The energy landscape is displayed as the folding funnel in Figure 2, which gives an overview of how enthalpy and entropy drive protein folding (Jahn and Radford, 2005). The y-axis depicts the increasing energy, which is referred to as the Gibbs free energy (Equation 1). The surface of the funnel shows the highest energy states with completely unfolded proteins. The more the energy is decreased the more the proteins get folded. The larger ΔG is between the folded and the denatured state of proteins, the more stable is the native conformation of the protein. The difference in G in [J] is determined by a high difference in enthalpy (H in [J]) and entropy (S in [J/K]) (Gibbs, 1873). As mentioned above, the entropy is influenced by hydrophobic interactions. Moreover, the enthalpy depends on solvation of the protein, represented by polar interactions, upon protein folding (Liu and Chan, 2005).

$$\Delta G = \Delta H - T \times \Delta S$$

Equation 1: Gibbs Free Energy (Gibbs, 1873).
G: Gibbs free energy [J]; H: Enthalpy [J]; T: Temperature [K]; S: Entropy [J/K]

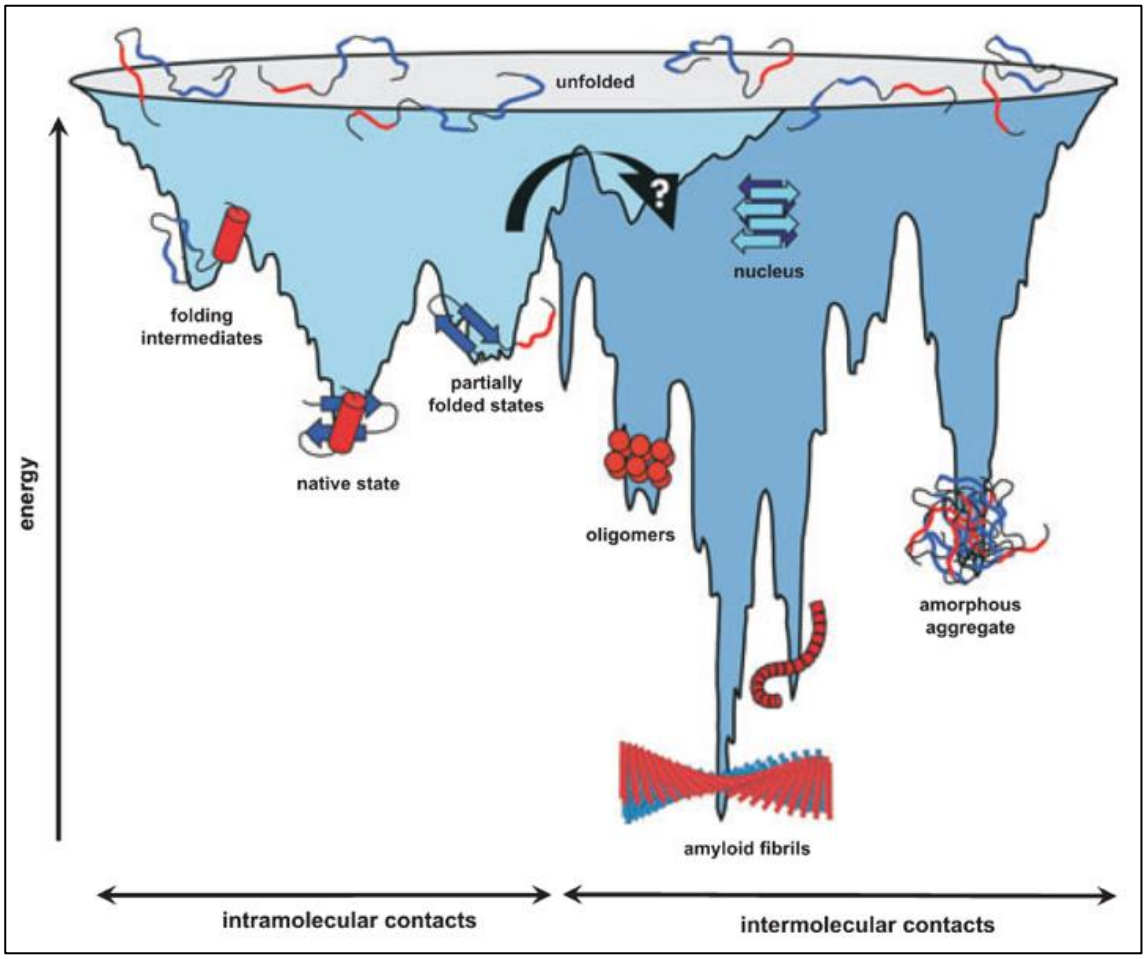

Figure 2: Schematic Overview of the Energy Landscape for Protein Folding and Aggregation.
The energy landscape shows the "funneling" events to the native state or amorphous aggregates. The y-axis displays the increase in energy and the increase in hydration (not displayed). To reach the native state from folding intermediates or partially folded states is achieved through intramolecular interactions, whereas oligomers, amorphous aggregates and amyloid fibrils result from intermolecular interactions. Figure and legend were taken from Jahn and Radford, 2005, the legend was modified (Jahn and Radford, 2005).

From folding intermediates and partially folded states, the native conformation with minimal Gibb´s free energy (Dobson, 2003) is achieved through intramolecular interactions. Oligomers, amorphous aggregates and amyloid fibrils require intermolecular interactions (Neira and Fersht, 1999; Bartlett and Radford, 2009). Aggregates can be formed from intermediates during *de novo* folding because of their exposure of hydrophobic surfaces (Clark, 2004). This is normally prevented by quality control and folding mechanisms in a cell, e. g. molecular chaperones (Seckler and Jaenicke, 1992; Walter and Buchner, 2002; Hartl and Hayer-Hartl, 2009). Aggregated proteins can be toxic and play a huge role in several diseases, e. g. Parkinson´s or Alzheimer´s disease where one hallmark is the accumulation of amyloid fibrils formed by misfolded proteins (Selkoe, 2003).

1.1.2 Molecular Chaperones in the Cell

The Anfinsen cage model states an important incision in protein folding and goes back to Christian B. Anfinsen who showed that proteins refold spontaneously without a source of energy (Anfinsen, 1973). The cage refers to protein folding machines, which encapsulate a new native protein. For some proteins folding was no longer considered as a spontaneous energy-independent process. In a process that involves transient interaction with chaperonin ATPases, the efficiency of correct folding was increased within a highly crowded intracellular environment. This suggests that proteins fold inside cells in the same way as they do in so-called macromolecular Anfinsen cages in pure dilute solution, which prevent and reverse unproductive interactions (Ellis, 1996). The two chaperonins GroEL (Hsp60) and GroES (Hsp10) provide a cage that protects the proteins from aggregation and aids them to fold more rapidly (Lorimer, 1994; Hartl et al., 2011; Horwich and Fenton, 2019). About 10-15% of all newly synthesized proteins interact with GroEL under non-stress conditions (Ewalt et al., 1997).

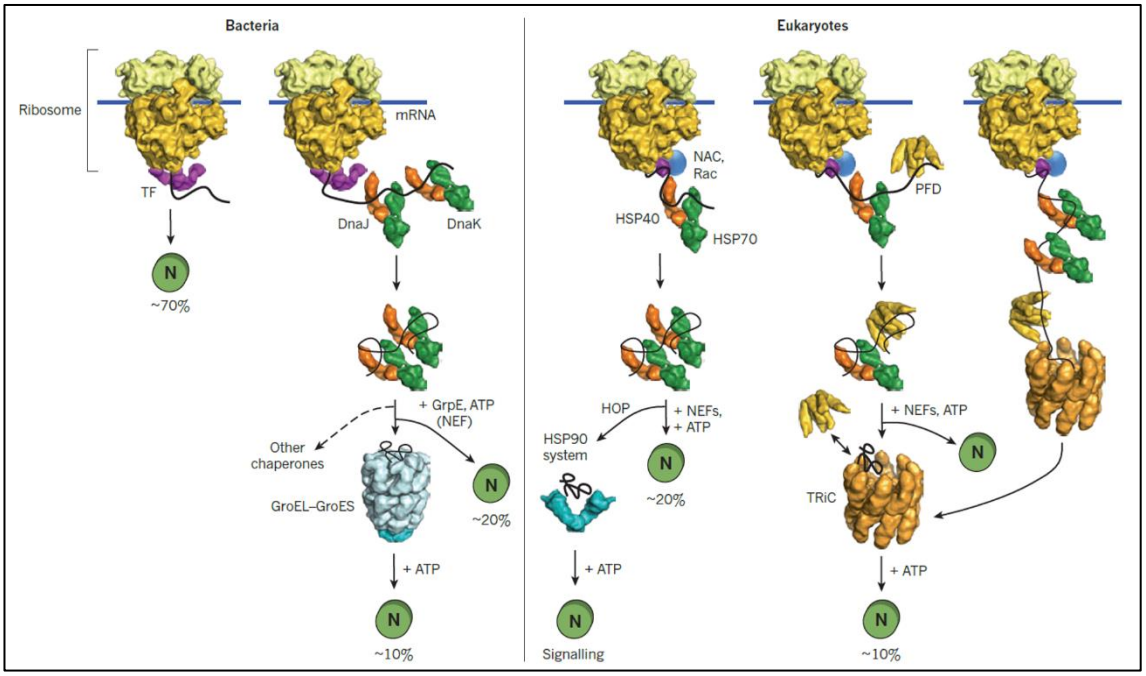

Figure 3: The Chaperone Network in the Cytosol.
Bacteria (left) and eukaryotes (right) contain chaperones that stabilize nascent polypeptide chains on ribosomes and initiate folding. The number of substrates is indicated as a percentage of the total proteome. Chaperones that bind in close proximity to the ribosomal exit site comprise e. g. the trigger factor (TF) in bacteria and HSP70 complexes (ribosome-associated complex (Rac) in *Saccharomyces cerevisiae*, MPP11 and HSP70L1 in mammalian cells) and nascent-chain-associated complex (NAC) in eukaryotes. These chaperones bind to hydrophobic segments. Non-ribosome-bound members of the HSP70 family (DnaK in bacteria and HSC70 in eukaryotes) function as second tier chaperones for longer nascent chains, mediating co- or post-translational folding. They distribute proteins to downstream chaperones, such as chaperonins (GroEL in bacteria and TRiC in eukaryotes) and HSP90. HOP promotes the transfer from HSC70 to HSP90. Dashed arrow means that the pathway is not fully understood. N, native protein; GrpE, protein GrpE; mRNA, messenger RNA; PFD, prefoldin. Figure and legend were taken from Hartl et al., 2011, the legend was modified (Hartl et al., 2011).

GroEL and GroES form part of a set of auxiliary proteins that cells have developed to ensure the proper folding process of proteins (Hartl et al., 2011; Horwich and Fenton, 2019). This is necessary because of the highly viscous and crowded environment in a cell with protein concentrations between 300 to 400 g L^{-1} in the cytosol (Zimmermann and Trach, 1991) and 100 – 400 g L^{-1} in the ER lumen (Stevens and Argon 1999). Many of these auxiliary proteins were discovered in the context of the heat shock response and therefore they are called heat shock proteins (Hsp) (Lindquist and Craig, 1988). This highly conserved protein machinery consisting of Hsps is referred to as the molecular chaperone network (Ellis and van der Vies, 1991; Georgopoulos and Welch, 1993). Besides chaperones and their cofactors, protein folding depends also on several other factors like the solvent, salt concentration, pH, and temperature (Ellis, 1987; Horwich and Fenton, 2019).

Different classes of molecular chaperones cooperate in evolutionary conserved folding pathways in the cytosol (Kim et al., 2013). Some of the classes are depicted in Figure 3. The members of these classes were initially named according to their molecular weight: Hsp40, Hsp60, Hsp70, Hsp90, Hsp100, and the small Hsps (sHps) (Kim et al., 2013). Most of these molecular chaperones are consitutively expressed and upregulated upon different stressors such as temperature, ethanol, oxidizing agents, and accumulation of unfolded proteins (Richter et al., 2010). They tend to bind to hydrophobic regions that are surface-exposed in unfolded or partially folded polypeptides during early folding stages or upon protein misfolding (Walter and Buchner, 2002; Araki and Nagata, 2011). The chaperone function as foldases is accompanied by ATP hydrolysis, except for sHsps that form large oligomeric structures binding to substrates and preventing them from aggregation. Only their release and refolding requires ATP-dependent chaperones (Haslbeck et al., 2005). Generally, chaperone function is a complex cellular interplay including many other factors like co-chaperones or nucleotide exchange factors (NEFs) (Young et al., 2004).

1.1.3 Quality Control in the ER

Quality control of proteins is used by cells of all kingdoms to maintain proteome integrity and protein homeostasis (Gottesman et al., 1997; Wickner et al., 1999; Yerbury et al., 2005). Generally, proteins are transported co-translationally into the ER where they fold and assemble (van Anken and Braakman, 2005; Zimmermann et al., 2011). Therefore, the ER is the entry point of proteins into the secretory pathway and provides a unique environment for protein folding with folding helpers like the before-mentioned chaperones (Wickner et al., 1999; Ma and Hendershot, 2004; Wiseman et al., 2022), that reside there in high concentrations (Stevens and Argon 1999). Downstream organelles usually do not support further protein folding. Therefore, a strict ER quality control (ERQC) system is essential (Ellgaard and Helenius, 2003). The ER possesses

numerous molecular chaperones and folding factors, e. g. the HC binding protein BiP, calnexin/calreticulin and their co-chaperones, and oxidoreductases (Braakman and Hebert, 2013). In addition to hydrophobic regions as mentioned in the previous chapter (section 1.1.3), chaperones also bing to free thiol groups of cysteines (Araki and Nagata, 2011).

Proteins, which are natively folded and assembled, leave the ER via vesicular transport to the Golgi complex (depicted in Figure 4), whereas partially folded and incompletely assembled proteins are retained in the ER. These proteins are then either subjected to further folding cycles or retro-translocated into the cytosol and degraded by the proteasome after ubiquitination in a process called ER-associated degradation (ERAD) (McCracken and Brodsky, 1996; Tsai et al., 2002) or targeted to lysosomal degradation (Yerbury et al., 2005).

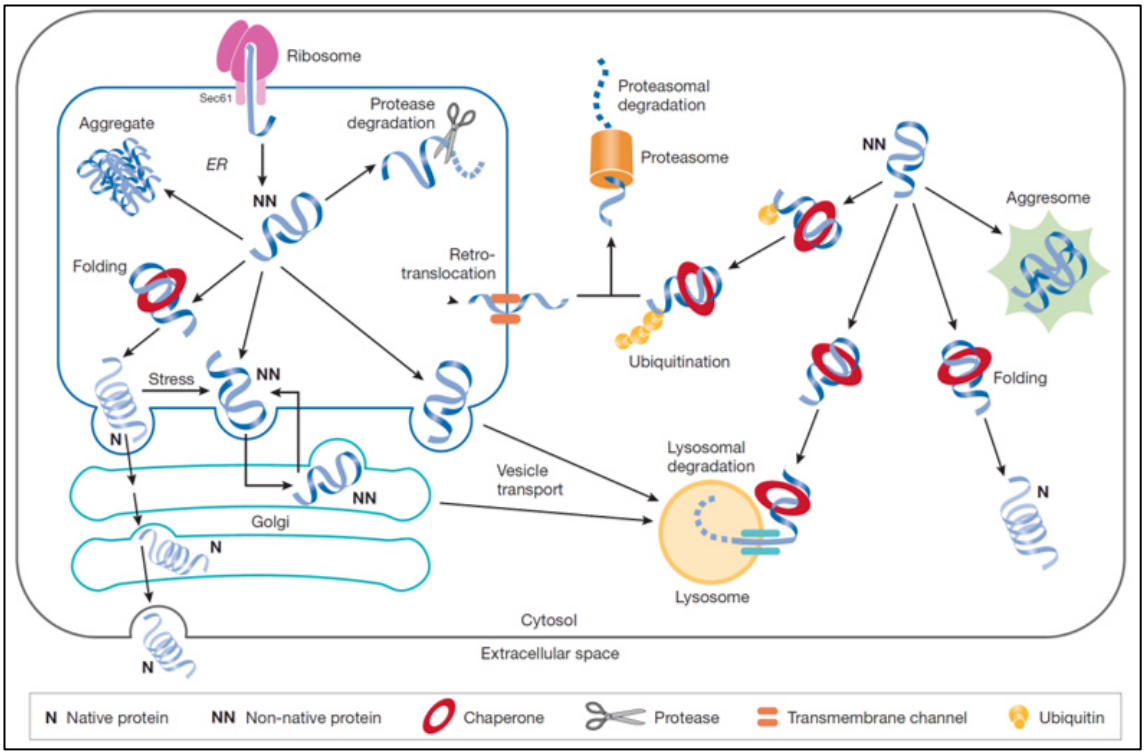

Figure 4: The Main Intracellular Controls of Protein Folding.
Non-native proteins are either recognized by chaperones and targeted for refolding or for proteolytic degradation by the proteasome or lysosome in the cytosol. Newly synthesized proteins or other non-native proteins are folded by chaperones in the ER. Cycling from ER to Golgi may occur at this stage. A protein is secreted from a cell in its native conformation. Proteins with non-native conformations cannot be proteolytically degraded within the ER. They are retro-translocated to the cytosol and degraded by the proteasome or transported to the lysosome. Aggregated non-native protein can also accumulate as insoluble deposits inside the ER or in the cytosol as an aggresome. Figure and legend were taken from Yerbury et al., 2005, the legend was modified (Yerbury et al., 2005).

Cells have evolved the unfolded protein response (UPR), which is a conserved mechanism to cope with increases in the ER unfolded secretory protein burden (Cox and Walter, 1996; van Anken and Braakman, 2005; Kannan et al., 2016; Hetz and Papa, 2018). The UPR induces an ER-to-nucleus signal transduction by activating different pathways. In consequence, further protein

synthesis is prevented while folding and degradation capacities of the ER and the degradion of misfolded proteins are simultaneously ameliorated. Three different transmembrane proteins are involved to transmit the UPR, as depicted in Figure 5 (Hetz, 2012): Inositol-requiring enzyme 1α (IRE1α), protein kinase RNA-like endoplasmic reticulum (ER) kinase (PERK), and activating transcription factor 6 (ATF6). The chaperone BiP keeps all three stress sensors in an inactive complex until the accumulation of un- and misfolded proteins in the ER leads to the dissociation of BiP and subsequent UPR activation (Bertolotti et al., 2000; Walter and Ron, 2011; Kopp et al., 2019).

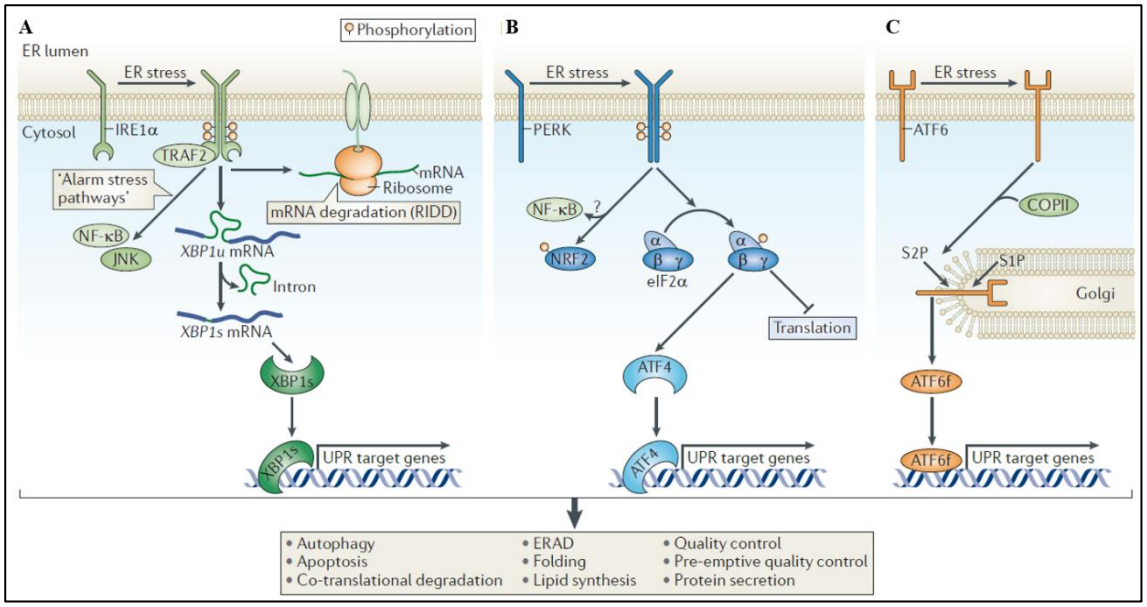

Figure 5: The Unfolded Protein Response (UPR).
The UPR stress sensors, inositol-requiring protein 1α (IRE1α), protein kinase RNA-like endoplasmic reticulum (ER) kinase (PERK) and activating transcription factor 6 (ATF6) transduce information about the folding status in the ER to the cytosol and nucleus to restore protein-folding capacity. **A** IRE1α dimerizes, which is followed by autotransphosphorylation. This triggers its RNase activity, which splices the mRNA of X box-binding protein 1 (XBP1u) to produce an active transcription factor (XBP1s). XBP1s controls the transcription of genes encoding proteins involved in protein folding, ER-associated degradation (ERAD), protein quality control and phospholipid synthesis. IRE1α also degrades certain mRNAs through IRE1-dependent decay (RIDD) and induces „alarm stress pathways" like JNK and NF-κB. **B** PERK gets dimerized upon ER stress which induces its autophosphorylation. This drives phosphorylation of eIF2α, which then induces *ATF4* mRNA translation, a transcription factor that controls the transcitpion of genes involved in autophagy, apoptosis, amino acid metabolism and antioxidant responses. **C** ATF6 is localized in the ER in unstressed cells and transported to the Golgi complex upon ER stress through interaction with the coat protein II (COPII) complex. There it is processed by site 1 protease (S1P) and S2P to release its cytosolic fragment ATF6f. ATF6f upregulates genes that encode ERAD components and XBP1. Figure and legend were taken from Hetz, 2012, the legend was modified (Hetz, 2012).

After the dissociation of BiP, IRE1α dimerizes and is activated upon auto-transphosphorylation of its cytosolic domain. IRE1α splices *XBP1* mRNA in the cytosol, which allows its translation. This produces an active transcription factor that upregulates genes involved in protein folding, ER-associated degradation (ERAD), protein quality control and phospholipid synthesis (Cox et al., 1993; Shamu and Walter, 1996; Walter and Ron, 2011). BiP dissociation also induces

homodimerization and autophosphorylation of PERK. PERK phosphorylates eIF2α, which leads to a global translation arrest and reduction of protein load in the ER (Liu and Kaufman, 2003; Kouroku et al., 2007). ATF6 is transported to the Golgi upon UPR activation, where it is activated by proteolytic cleavage. Active ATF6 upregulates genes that encode ERAD components and XBP1 (Shoulders et al., 2013; Wang et al., 2014).

1.1.4 Immunoglobulin Folding, Assembly and Structure

Immunoglobulins, also referred to as antibodies, were first reported in 1890 by Behring and Kitasato as an agent in the serum capable of neutralizing the diphtheria toxin (Behring and Kitasato, 1890). Antibodies belong to a superfamily with many functionally diverse proteins that share the immunoglobulin fold as a common structural feature (Williams and Barclay, 1988). In higher vertebrates, five different classes of immunoglobulins exist: IgA, IgD, IgE, IgG, and IgM with the last letter denoting the class of HC they contain (α, δ, ε, γ, and μ). The HCs can only combine with two different subtypes of LCs (λ and κ).

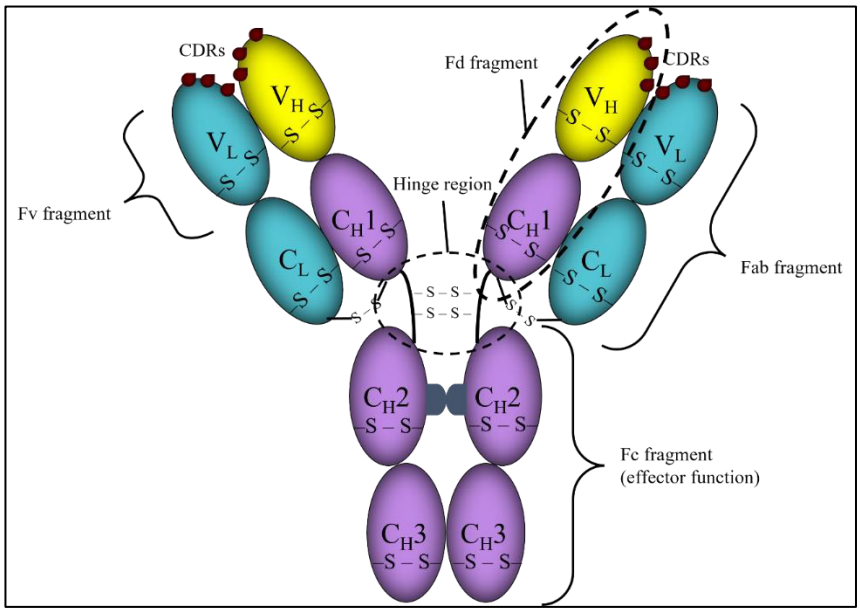

Figure 6: Schematic Overview of an IgG1 Antibody Molecule.
LCs are depicted in cyan, HCs in violet (constant domains) and yellow (variable domain). Sugar moieties are represented in grey semi-circles and S-S indicates a disulfide bridge. The black circles represent the three complementarity determining regions (CDRs) in the variable domains of the HCs and LCs, respectively.

While IgM antibodies are produced as the first immune response after antigen contact, monomeric IgG is the predominant isotype with the longest serum half-life. IgG1 is a Y-shaped heterotetrameric glycoprotein complex composed of two identical HCs and LCs, respectively (Figure 6). The LCs consist of a V_L and a C_L domain, while the HCs contain one V_H domain and three C_H domains, C_H 1-3. The complex has several disulfide bridges: two in the so-called hinge

region between the heavy-chains, one between the C-terminal cysteines in C_L and C_H1 each and an intramolecular disulfide bridge in every domain (Baumal et al., 1971).

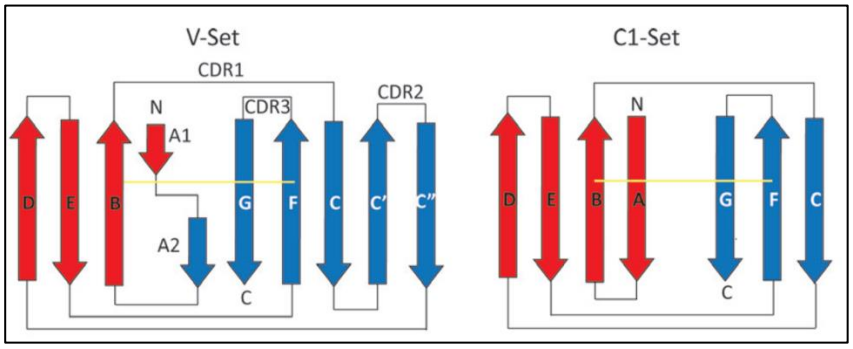

Figure 7: Two-dimensional Topology Diagrams of Ig Constant and Variable Domains (Bodelón et al., 2012).
Topology diagrams of variable (V set) and constant (C1-set) domains. Front and back sheets are shown in red and blue, respectively. The disulfide bond between the B and F strand is indicated as a yellow line. The CDRs are also depicted. Figure and legend were taken from Bodelón et al., 2012, the legend was modified (Bodelón et al., 2012).

Fully assembled antibodies can be divided into three parts: The crystallizable fragment (Fc) composed of C_H2 and C_H3 homodimers and two Fab fragments consisting each of a LC and the Fd fragment. The Fd fragment denotes the V_H and C_H1 domain (Huber et al., 1976). Antigen binding is conferred by the N-terminal variable domain of each chain, together representing the Fv part of the antibody. Each variable domain possesses three complementarity-determining regions (CDRs) which provide the amino acids that specifically interact with the antigen (Wu and Kabat, 1970; Kabat et al., 1977). Antibody diversity, specificity and variability is achieved by recombination of variable (V), diversity (D) and joining (J) gene segments, called VDJ gene rearrangement (Hozumi and Tonegawa, 1976; Maki et al., 1980; Tonegawa, 1983).
Differences in the folding of the highly similar structure of antibody domains could only be revealed by studying the individual domains. This was pioneered by Goto and co-workers by focusing on denaturing and refolding LCs (Goto et al., 1979). Further initial studies were on the C_L domain (Goto and Hamaguchi, 1982) and the C_H3 domain (Isenman et al., 1979), which revealed their autonomous folding and the importance of the rate-determining peptidyl-prolyl isomerization reaction that can be catalyzed and accelerated by peptidyl-prolyl *cis/trans* isomerases (PPIases) (Lang et al., 1987; Lilie et al., 1993). While the C_L domain is folding on its own (Feige et al., 2008), C_H1 is intrinsically disordered and can only fold upon binding to its native partner, the C_L domain (Feige et al., 2009). Antibodies fold and assemble in the ER lumen where HCs are retained until they are assembled with the LCs (Mains and Sibley, 1983). The topology of the antibody domain structure is highly conserved (Figure 7). Both, constant and variable domains, are composed of a β-barrel structure. The variable domains contain nine β-

strands (A, B, C, C´, C´´, D, E, F, G) and the constant domains seven (A, B, C, D, E, F, G). Intramolecular disulfide bridges are formed between the strands B and F (Bork et al., 1994).

BiP, as already mentioned above, is an Hsp70 family member present in the ER of eukaryotes (Haas and Wabl, 1983). It is retained in the ER, together with its associated proteins, by virtue of its C-terminal KDEL tetrapeptide (Munro and Pelham, 1987). Since the ER is, besides the intermembrane space of mitochondria (Sideris and Tokatlidis, 2010), one compartment in the cell with a more oxidative environment due to its redox system consisting of the small peptides GSH (reduced glutathione) and GSSG (oxidized glutathione), it is the location for oxidative folding (Montero et al., 2013). This system allows the formation of intra- and intermolecular disulfide bridges. The internal disulfide bond is a conserved feature of the immunoglobulin fold in antibodies and therefore important for the correct overall folding of antibodies (Feige et al., 2007).

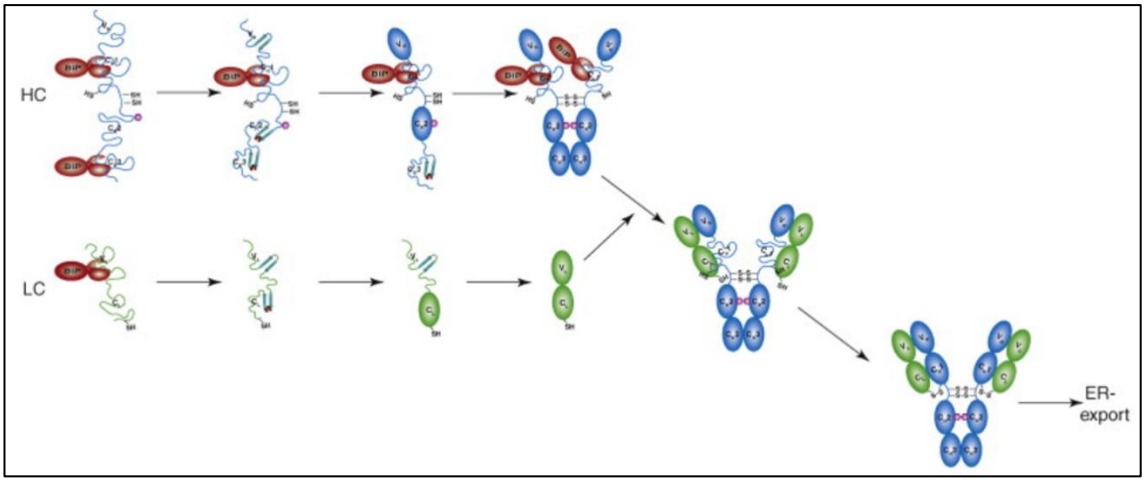

Figure 8: Overview of BiP-Assisted IgG Folding and Assembly in the ER.
Folding and formation of disulfide bridges and glycosylation of the HC and the LC begins co-translationally in the ER. BiP is a molecular chaperone that interacts with most of the domains transiently before folding is complete. All constant domains, except C_H1 and most variable domains, fold autonomously. C_H3 induces HC dimerization. C_H1 remains unfolded, reduced, and stably bound to BiP until the LC displces BiP and induces its folding. After this step, disulfide bridges between the LC and the HC are formed and IgG molecules are ready for secretion. Figure and legend were taken from Feige et al., 2010, the legend was modified (Feige et al., 2010a).

BiP associates with the unfolded C_H1 domain in the absence of LC synthesis and is therefore responsible for HC retention in the ER (Figure 8) (Hendershot et al., 1987a; Hendershot et al., 1987b). Folded LCs displace BiP from its binding to the unfolded C_H1 domain, thus facilitating folding of the C_H1 domain, which is a critical early step in the antibody quality control mechanism in the ER (Feige et al., 2009). The assembled IgG molecule is released from the ER and secreted (Feige and Buchner, 2014). Besides the LC, also the BiP co-chaperone ERdj3 plays an important role in antibody folding in mammalian cells because it modulates the BiP chaperone cycle at several steps (Shen and Hendershot, 2005; Marcinowski et al., 2011). Bap (BiP-associated protein) in mammals (Sil1 in yeast) is a nucleotide-exchange factor of BiP. It affects the

conformation of both BiP domains, including the lid subdomain for substrate binding. The largely unstructured N-terminal domain of Bap promotes substrate release from BiP (Rosam et al., 2018). Moreover, glycosylation of proteins take place in the ER, e. g. glycosylation of asparagine residues of the sequence N-X-T/S (X not being a proline), which increases the stability and allows interaction and assembly of proteins via their covalently attached sugar moieties (Helenius and Aebi, 2004). Glycosylation is an important step for many biological antibody functions (Arnold et al., 2007; Dalziel et al., 2014). In the case of antibodies, glycosylation at the constant domain controls antibody activity by altering their affinity for Fc receptors (Jennewein and Alter, 2017).

1.2 The Mammalian Immune System

1.2.1 Adaptive and Innate Immunity

The mammalian immune system is a defense apparatus against pathogens consisting of the innate and adaptive immunity. The ability of the immune system to fight infectious diseases is the result of the successful interaction of cells and proteins of the immune system. The evolutionary ancient and universal form of host defense is the innate immune system, which consists of a limited number of germline-encoded receptors. Immediate, non-speficic responses to foreign but not host structures are characteristic for innate immunity as well as non-lasting immunity (Alberts et al., 2002). Inflammatory responses are triggered by macrophages, polymorphonuclear leukocytes and mast cells through their innate immune receptors. These include pattern recognition receptors (PRRs) and their principal functions are opsonization, activation of complement and coagulation cascades, phagocytosis, activation of pro-inflammatory signaling pathways, and induction of apoptosis. Toll-like receptors (TLRs) and nucleotide-binding oligomerization domain (NOD)-like receptors are PRRs that recognize pathogen-associated molecular patterns (PAMPs) (Janeway, 1989; Medzhitov and Janeway, 1997; Janeway and Medzitov, 2002; Gregersen and Behrens, 2006).

The parts and functions of the innate immune system and their interplay with the adaptive immune system are illustrated in Figure 9. The innate immune system is supplemented by the adaptive immune system that is characteristic for its great variability and rearrangement of receptor gene segments. It specifically recognizes foreign antigens and has memory function (Janeway and Medzitov, 2002). It mediates reactivity with specific antigens via T-cell receptors (TCRs) on the cell surface of T-cells, referred to as the cellular immune response, and immunoglobulin receptors on the cell surface of B-cells (BCRs), also called the humoral immune response (Gregersen and Behrens, 2006). T-cells, also referred to as T lymphocytes, are a type of leukocytes, which are white blood cells. They are part of the cell-mediated immunity. After originating in the bone marrow, T-cells mature from thymocytes in the thymus. There, they multiply, acquire antigen receptors, and differentiate into helper, regulatory (suppressor), effector, cytotoxic and memory

T-cells. Afterwards, they are sent to peripheral tissues or circulate in the blood or lymphatic system (Alberts et al., 2002). Helper-T-cells (T_H cells), also known as $CD4^+$ cells, become activated when they are presented with peptide antigens by major histocompatibility complex (MHC) class II molecules, which are expressed on the surface of antigen-presenting cells (APCs) (Gutcher and Becher, 2007). T_H cells secrete chemical messengers called cytokines, when they are stimulated by the appropriate antigen, which initiates the differentiation of B-cells into plasma cells, known as antibody-producing cells. Regulatory T-cells control immune reactions. Cytotoxic (killer) T-cells (T_C), also known as $CD8^+$ T-cells, recognize their target by binding to antigens associated with MHC class I molecules, which are present on the surface of all nucleated cells. They are activated by various cytokines, bind to, and kill infected and cancer cells. Memory T-cells are long-lived and can quickly expand to large numbers of effector T-cells (Alberts et al., 2002).

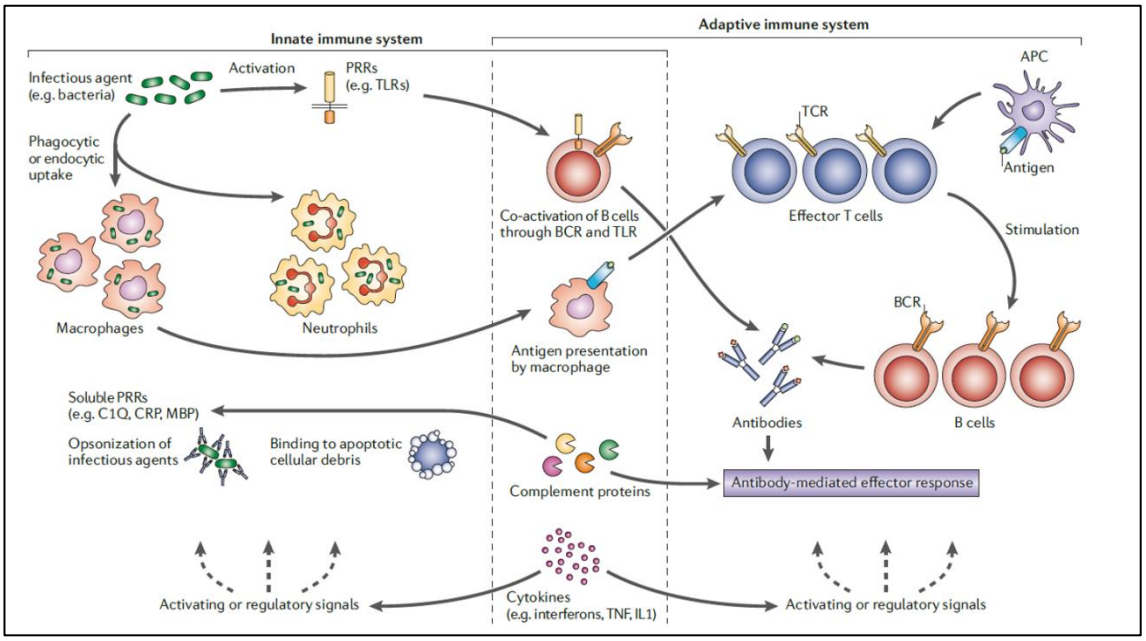

Figure 9: The Innate and Adaptive Immune System and their Overlap.
Innate immune mechanisms are characteristic for their immediate, non-specific responses to foreign infectious agents. These responses include phagocytosis and endocytosis. Some of these mechanisms are dependent on pattern-recognition receptors (PRRs), such as Toll-like receptors (TLRs) and NOD-like receptors, which recognize pathogen-associated molecular patterns (PAMPs) on a variety of microorganisms. Moreover, a variety of soluble PRRs, e. g. complement proteins, play a role in innate immunity by opsonizing microorganisms and binding to apoptotic cellular debris in a non-specific manner. Adaptive immune mechanisms include receptors, the T-cell receptors (TCRs) and immunoglobulin receptors on B-cells (BCRs) that are selected for reactivity with specific antigens. This requires the expansion and differentiation of the specific responder cells to establish a memory for the specific antigen response. The connection between innate and adaptive immunity is demonstrated e. g. in phagocytosed and endocytosed antigens by macrophages that are presented to T-cells, generating a highly specific T-cell response. Figure and legend were taken from Gregersen and Behrens, 2006, the legend was modified (Gregersen and Behrens, 2006).

B-cells or B lymphocytes confer humoral immunity by secreting antibodies (Murphy, 2012). B-cells mature in the bone marrow (Cooper, 2015) and bind a specific antigen through their BCRs,

against which it will initiate an antibody response (Murphy, 2012). There are three different pathways that B-cells can be activated by: T-cell dependent activation (Murphy, 2012), T-cell-independent activation (Murphy, 2012), and memory B-cell activation (McHeyzer-Williams et al., 2011). In T-cell-dependent activation, as the name indicates, B-cells are activated by antigens with the help of T-cells, whereas in T-cell-independent activation, B-cells are activated without the help of T-cells (Murphy, 2012). Activation of memory B-cells begins with the detection and binding of their target antigen (McHeyzer-Williams et al., 2011).

1.2.2 B-Cell Development

B-cell development is a hallmark event in the immune system to produce the antibody secreting B-cells. The absence of B-cells results in various diseases, e. g. agammaglobulinemia, in which the body is not able to execute an immune reaction against pathogens and patients often manifest upper or lower airway infection (Tsukada et al., 2012).

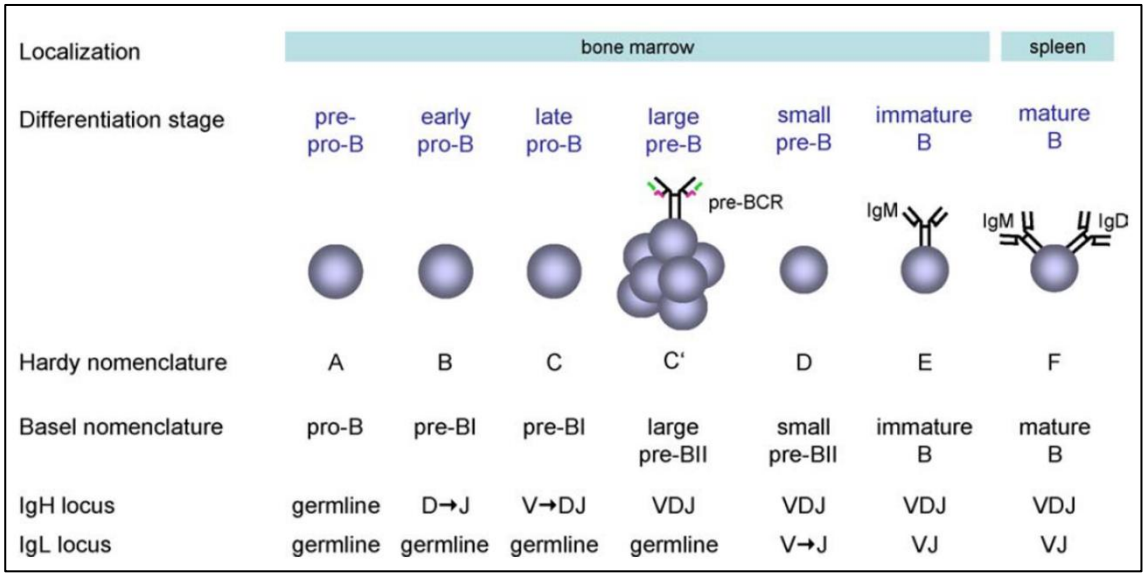

Figure 10: Schematic Illustration of B-Cell Development.
The respective stages are characterized by the rearrangement status at the IgH and IgL loci. The SLC components λ5 and VPREB are expressed until the large pre-B-cell stage. SLC expression stops at the small preB II cell stage and therefore pre-BCR cell surface expression stops. Then, LCs assemble with HCs and small pre-B-cells develop into IgM-positive immature B-cells. After selection against self-reactive BCR, immature B-cells leave the bone marrow and migrate to peripheral lymphatic organs while differentiating into mature and antigen-dependent responsive B-cells (surface IgM and IgG). Figure and legend were taken from Vettermann et al., 2006, the legend was modified (Vettermann et al., 2006).

B-cells are generated from pluripotent hematopoietic stem cells in the liver during mid-to-late fetal development and in bone marrow after birth (Hardy and Hayakawa, 2001). The bone marrow contains B lineage cells at all stages of development, from earliest progenitors to mature B-cells (Hardy and Hayakawa, 2001). B-cells at different stages are characterized by different cell surface phenotypes, i. e. different markers are expressed on their surface (Park and Osmond, 1987; Hardy

et al., 1991; Ehlich et al., 1993), and the stepwise recombination of the immunoglobulin gene loci (Yancopoulos and Alt, 1986; Rolink and Melchers, 1991).

During B-cell development, several checkpoints guarantee the development of competent B-cells. Before they become mature B-cells, several cell stages must be passed from progenitor (pro-) B-cells via precursor (pre-) B-cells, to immature and mature B-cells as illustrated in Figure 10. Recombination of the immunoglobulin gene loci is referred to as VDJ recombination of various gene segments encoding HCs and LCs and allelic exclusion (Tonegawa, 1983; Hesse et al., 1989; Melchers et al., 2000).

The earlierst B-cell progenitors, the pre-pro-B-cells, are phenotypically defined by expressing B220, CD43, IL-7R and c-kit and at this cell stage neither the IgH nor the IgL locus undergoes gene rearrangement (Allman et al., 1999; Ogawa et al., 2000). The pre-BCR components, λ5 and VPREB, are also expressed in the pre-pro-B-cell stage (Vettermann et al., 2006). In IL-7 rich niches of bone marrow, pre-pro-B-cells committed to B-cell lineage develop through differentiation into pro-B-cells (Hardy et al., 1991; Meffre et al., 1996; Schlissel, 2003; Tokoyoda et al., 2004). In the early pro-B-cell stage, Ig-gene rearrangement is started to rearrange their D_H and J_H gene elements in the IgH loci in the early phase and in late phase, V and DJ rearrangement takes place (Alt et al., 1981; Coffman and Weissman, 1983; Reth et al., 1985; Rolink and Melchers, 1991; Igarashi et al., 2002). This recombination process is mediated by semi-random induction of double-stranded DNA breaks by recombinase activating gene (Rag)-1 and Rag-2 proteins at recombination signal sequences followed by non-homologous end joining (NHEJ) (Schatz et al., 1989; Oettinger et al., 1990; Lieber et al., 2003).

Transition from late pro-B to large pre-B-cells is known to be the pre-BCR checkpoint (Burrows et al., 2002). At this point, no LC is expressed (Burrows et al., 1979). The transient surface expression of the pre-BCR is dependent on the successful pairing of HC with the SLC components, λ5 and VPREB (Karasuyama et al., 1990; Tsubata and Reth, 1990; Ye et al., 1996; Melchers, 2005). Large pre-B-cells undergo a limited clonal expansion phase of four to six cell divisions, which results in the selective expansion of HC-expressing pre-B-cells (Decker et al., 1991). After polyclonal expansion, late (small) pre-B-cells lose c-kit expression and are therefore not expandable any longer (Rolink et al., 1994; Ten Boekel et al., 1997). They migrate away from proliferation-inducing IL-7-rich niches of bone marrow and exit the cell cycle (Tokoyoda et al., 2004). At this stage, the IgL locus is rearranged by V_L to J_L recombination (Schlissel and Morrow, 1994). Afterwards, they develop into surface-IgM positive immature B-cells, if they produce a LC capable of pairing with the HC (Reth et al., 1985; Reth et al., 1987; Ehlich et al., 1993). Immature B-cells express also BCRs with the affinity for auto-antigens and subsequently become negatively selected and die in the bone marrow (Pelanda et al., 1997; Avalos et al., 2014). Cells that survive this negative selection leave the bone marrow via the blood stream to the spleen where they become mature B-cells (Cooper, 2015).

1.2.3 The Pre-B-Cell Receptor

The association of Igμ, which is produced after a successful recombination of the IgH gene, with the germline-encoded SLC to form the pre-B-cell receptor on the cell surface of pre-B-cells represents an essential checkpoint during B-cell development (Nishimoto et al., 1991; Karasuyama et al., 1996).

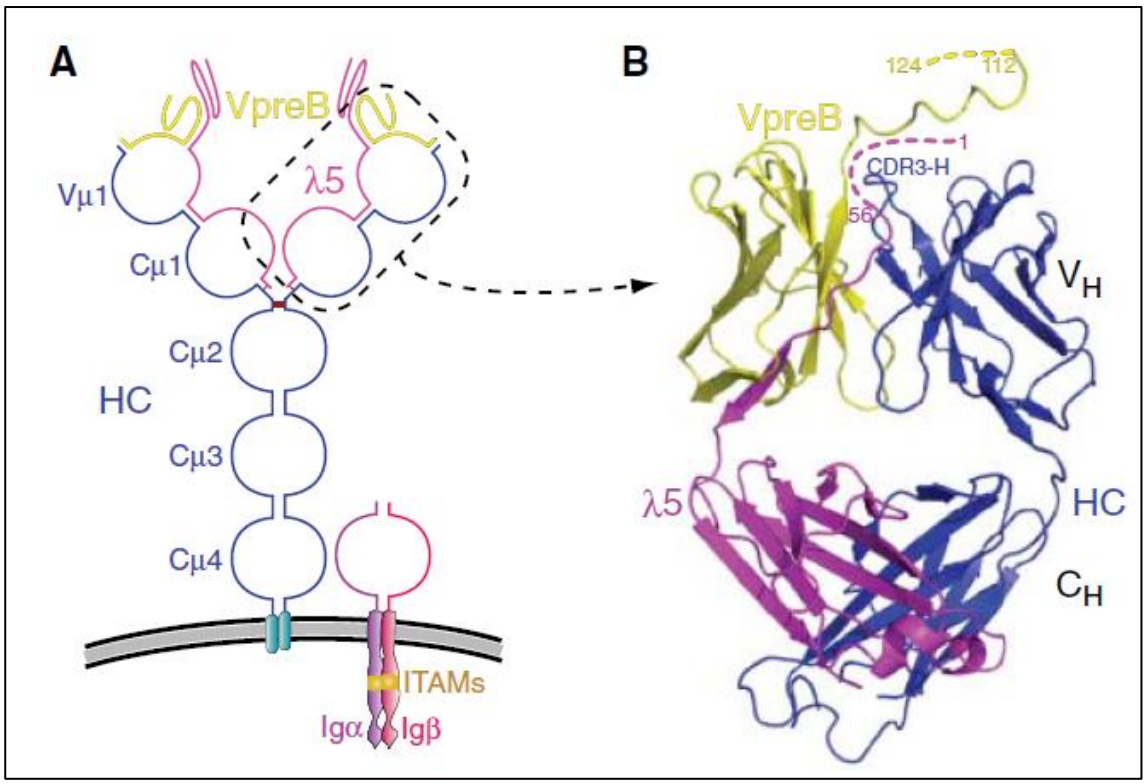

Figure 11: Structure of the Pre-BCR.
A Schematic representation of the pre-BCR complex with the Fab-like arm (dashed box) that was crystallized. **B** Protein structure of Fab fragment of the pre-BCR. VPREB is coloured in yellow, λ5 in violet and the Fd fragment consisting of V_H and C_H1 in blue. Missing parts in the URs of VPREB and λ5 are indicated as dashed lines. Figure and legend were taken from Bankovich et al., 2007, the legend was modified (Bankovich et al., 2007).

Similar in structure to the BCR, the pre-BCR consists of two Igμ chains and two SLCs that are associated with the signalling subunit Igα and Igβ (Figure 11) (Kerr et al., 1989; Karasuyama et al., 1990; Tsubata and Reth, 1990; Schiff et al., 1991). VPREB and λ5 can associate without the presence of the μHC (Misener et al., 1990). The Fab complex containing the Fd fragment and the SLC could be crystallized in 2007 (Bankovich et al., 2007). In contrast to a conventional LC, the SLC is a heterodimer composed of two germline-encoded invariant proteins, VPREB and λ5. Structural details about the SLC are given in section 1.3.2.

Pre-B-cell expression on the cell surface induces a signaling cascade that leads first to an increased pre-B-cell proliferation (Misener et al., 1991; Brouns et al., 1993). This should aid in the expansion of cells harboring a successfully recombined IgH gene (Jumaa et al., 2005).

Furthermore, pre-BCR signalling activates IgL gene rearrangement and is therefore indispensable for the continuation of B-cell differentiation (Reth et al., 1987). This is accompanied by a downregulation of the expression of the Rag1-Rag2 recombination machinery, which in turn causes the inhibition of further gene rearrangements and the ensurement of the expression of only one Igμ (Grawunder et al., 1995). At the same time, pre-BCR expression was found to upregulate Rag1-Rag2 expression and to promote the accessibility of the IgL gene for recombination (Meixlsperger et al., 2007). Crosslinking of the pre-BCR complex on the surface of pre-B-cells activates gene rearrangement of the IgL locus. VPREB and λ5 are necessary for spontaneous crosslinking (Tsubata et al., 1992).

The signaling caused by the engagement of pre-BCR and BCR likely induces the same transduction pathways (Guo et al., 2000). The first step after pre-BCR or BCR activation is the phosphorylation of tyrosine residues in immunoreceptor tyrosine-based activation motifs (ITAMs) in the cytoplasmic tails of Igα and Igβ by the spleen tyrosine kinase (SYK) (Sanchez et al., 1993; Flaswinkel and Reth, 1994) (Figure 12). Subsequently, SYK binds to phosphorylated ITAMs, which leads to an autophosphorylation of SYK as well as a phosphorylation by other SRC kinases like Lyn (Kurosaki et al., 1995; Rowley et al., 1995; Fütterer et al., 1998). Constitutively active SYK induces the phosphorylation of CD19 and/or the adaptor protein B-cell PI3K adaptor (BCAP/PIK3AP1) resulting in the recruitment and activation of PI3K (Aiba et al., 2008). This leads to a downstream phosphorylation cascade (Kanie et al., 2004), which ultimately results in phosphorylated protein kinase B (PKB/AKT) and 3-phosphoinositide-dependent protein kinase 1 (PDK1) (Vanhaesebroeck and Alessi, 2000; Manning and Cantley, 2007). SYK phosphorylates SLP65 (Wienands et al., 1998; Zhang et al., 1998). Active SLP65 downregulates λ5 expression, SLC production and activates Igκ gene recombination (Parker et al., 2005; Thompson et al., 2007).

Active PKB phosphorylates FOXO proteins. This leads to the inhibition of their transcriptional activity by promoting their export from the nucleus to the cytoplasm, where they are degraded (Coffer and Burgering, 2004). This scenario promotes proliferation and inhibits differentiation because of Rag2 degradation (Herzog et al., 2009). SLP65 is interfering with this by probably inhibiting PI3K and/or PKB (Okkenhaug and Vanhaesebroeck, 2003). This would not cause phosphorylation of FOXO and therefore no degradation. Instead, the FOXO protein promotes IgL gene recombination by RAG2 stabilization (Herzog et al., 2009).

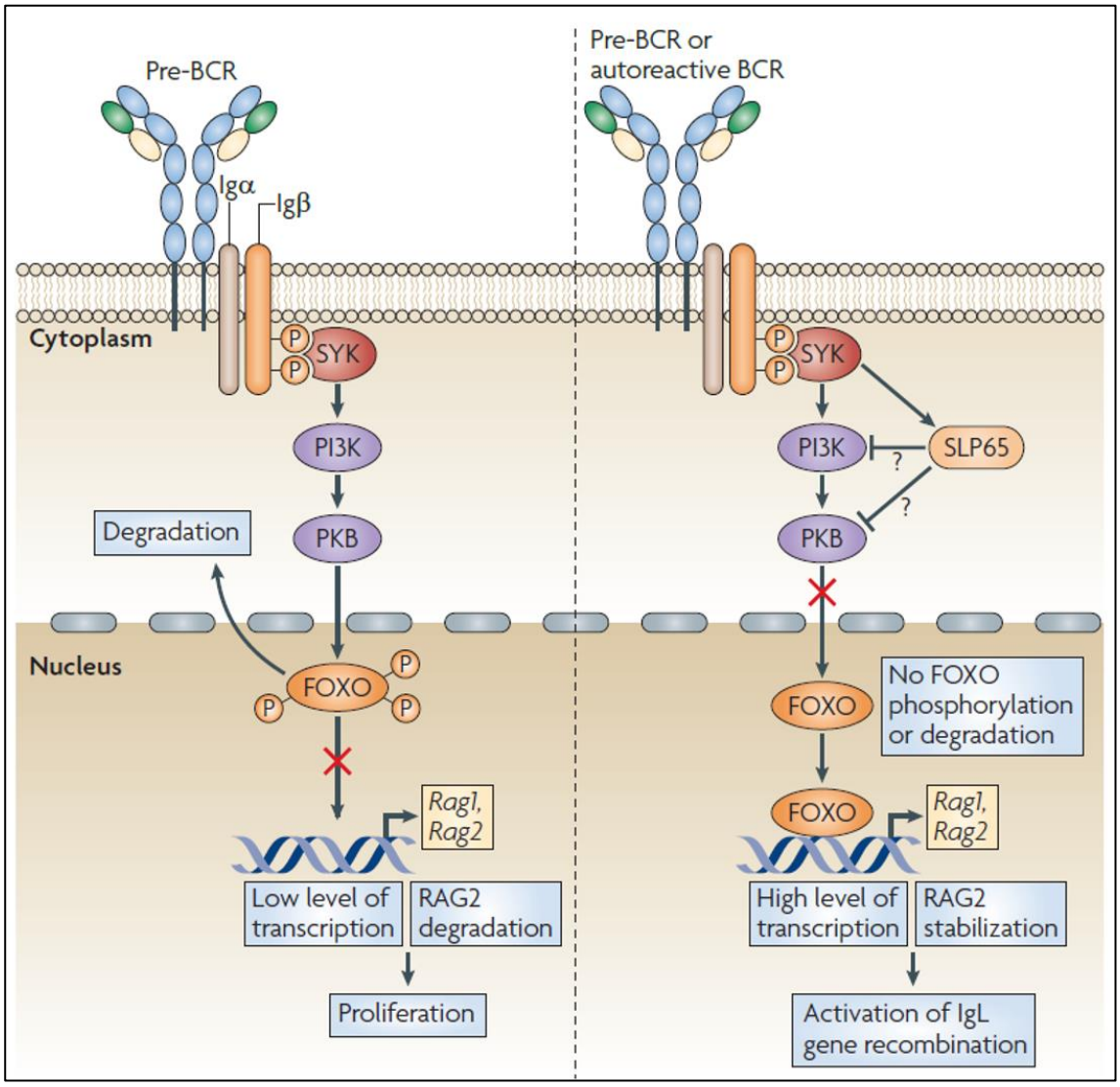

Figure 12: Overview of Pre-BCR Signaling and its Influence on Cell Cycle Progression.
Pre-BCR engagement leads to phosphorylation of Igβ by Syk. This in turn causes the autophosphorylation of Syk, which leads to a downstream activation of PI3K and PKB. During proliferation of the pre-B-cell, FOXO is phosphorylated by PKB, transported from the nucleus to the cytoplasm leading to its degradation. RAG2 is degraded and transcription is halted. Alternatively, Syk can activate SLP65 by phosphorylation, which then blocks either PI3K or PKB. This prevents FOXO from phosphorylation and degradation, RAG2 is stabilized, and a high level of transcription is maintained. This results in an activation of IgL gene recombination. Figure and legend were taken from Herzog et al., 2009, the legend was modified (Herzog et al., 2009).

1.3 The Surrogate Light Chain

1.3.1 The SLC Genes in Mice and Humans

The murine *λ5* gene is located on chromosome 16 (Sakaguchi et al., 1986; Kudo et al., 1987a) and is composed of three exons (Kudo et al., 1987b). Exon II and III as well as the intron in between show sequence homology to JλL and CλL exons, whereas homology to the *λL* chain genes is lost (Kudo et al., 1987b). The murine *λ5* gene does not undergo recombination (Sakaguchi and Melchers, 1986) and the translation product of the allelic variant of the *λ5* gene contains a

signal peptide of approximately 30 amino acids at its N-terminus (Jongstra et al., 1988). Different to humans, who have one *VPREB* gene, mice have three genes: *Vpreb1* and *Vpreb2*, that show homology to IgV gene segments (Kudo and Melchers, 1987) and *Vpreb3*, which shows 37% amino acid sequence homology to *Vpreb1* and resides on chromosome 10 (Shirasawa et al., 1993; Ohnishi and Takemori, 1994; Hagiwara, 1996). *Vpreb1* in mice is located 4.6 kb upstream of the *λ5* gene (Kudo and Melchers, 1987) and *Vpreb2* 1 Mb downstream of it in the opposite transcriptional orientation (Dul et al., 1996). The sequence homology between *Vpreb1* and *Vpreb2* is 97 % (Kudo and Melchers, 1987), within the coding regions there is even 99 % homology (Dul et al., 1996). The *Vpreb1* and *2* genes are transcribed, but *Vpreb2* at lower levels compared to *Vpreb1* (Dul et al., 1996). Murine *λ5* as well as the *Vpreb* genes have not been mapped relative to the λ LC locus (Kudo and Melchers, 1987) (Figure 13). Both, VPREB1 and 2 can assemble with λ5 and the μHC to form pre-B-cell receptor complexes in mice (Dul et al., 1996).

The immunoglobulin λ-like (*IGLL*) gene cluster in humans is located on chromosome 22 and the gene product of *VPREB1* is mapped within the Vλ gene complex (*IGL-V*), proximal to the Cλ LC genes (*IGL-C*) (Figure 13) (Goyns et al., 1984; Sakaguchi and Melchers, 1986; Bauer et al., 1988a; Mattei et al., 1991; Frippiat et al., 1995). The *IGLL* gene cluster consists of 3 genes: *14.1*, *16.1* and *Fλ1/16.2* (Chang et al., 1986; Schiff et al., 1989; Schiff et al., 1990), in which *14.1* is the only functional member that contains three exons (Bossy et al., 1991). *16.1* and *16.2* have over 95 % homology to *14.1* in exons II and III but lack exon I and associated regulatory elements (Schiff et al., 1989; Bossy et al., 1991). The *IGLL* genes are also referred to as *IGLL1* (*14.1*), *IGLL2* (*16.2*) and *IGLL3* (*16.1*), reflecting their position on chromosome 22 (Bauer Jr et al., 1993). *16.1* is located 1.5 Mb distal to *14.1* and *16.2*. *14.1* is proximal to *16.2* by about 30 kb (Bauer Jr et al., 1993). *14.1* lies about 690 kb distal to the 3´ *IGL-C7* gene in the *IGL* gene locus (Bauer Jr et al., 1993). In humans, the pre-B-cell specific genes of *VPREB* and *IGLL* do not belong to the same transcriptional unit, which is unlike compared to those in mice (Mattei et al., 1991). Murine *λ5* and human *14.1* are organized similarly with their sequences containing three exons: Exon I, II and III in mice contain 65, 38 and 106 codons compared to humans who have 69, 38 and 106 codons, respectively (Schiff et al., 1990). The immunoglobulin λ (*IGL*) locus and the *IGLL* cluster, expressed in B and pre-B-cells, respectively, are closely related members of a gene family (Bossy et al., 1991; Bauer Jr et al., 1993). The two clusters have diverged after duplication of a common ancestor, from which each cluster has independently but similarly evolved by successive duplications of the Jλ-Cλ or exon2-exon3 units (Bossy et al., 1991). Unlike other immunoglobulin genes, the genes of the *IGLL* cluster and the *VPREB* gene do not undergo rearrangement prior to expression (Bauer et al., 1988b; Hollis et al., 1989).

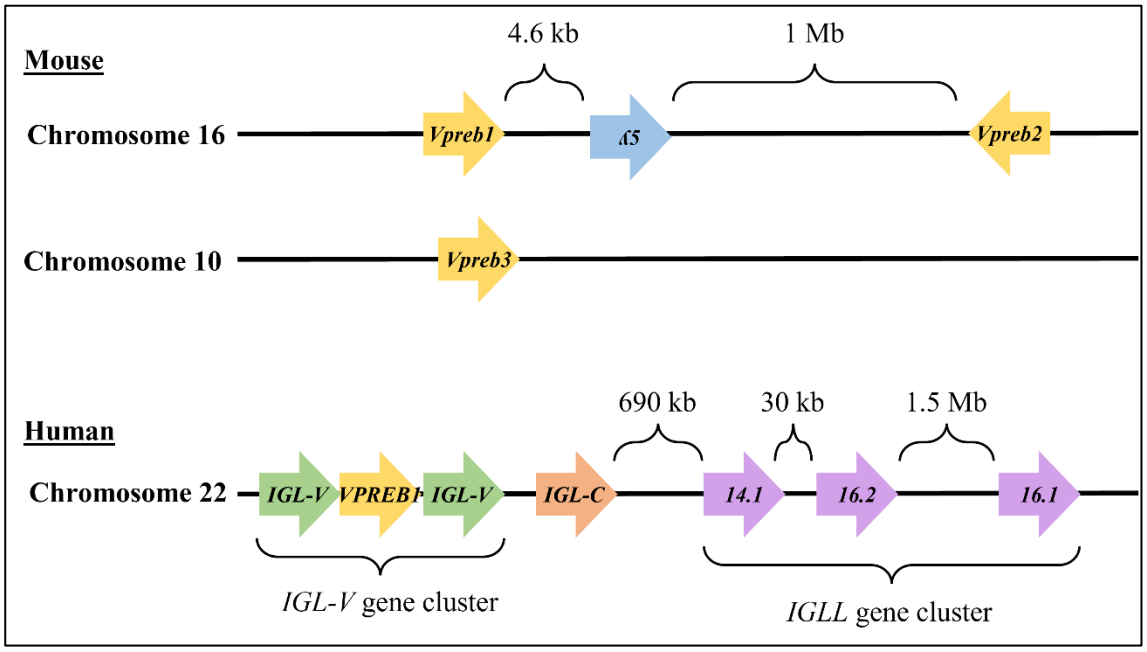

Figure 13: Chromosomal Organization of *VPREB* and *IGLL* Genes in Mice and Humans.
The murine *Vpreb* and *λ5* genes are depicted with their chromosomal location and orientation at the top and the human *VPREB* and *IGLL* genes at the bottom.

The *λ5* gene encodes a protein of 209 amino acids in mice (Kudo et al., 1987b). In humans the λ-like genes *14.1/16.1* encode a protein of 214 amino acids and an unprocessed molecular weight, i. e. containing the signal sequence, of 22944 Dalton. The C-terminus of this predicted protein is highly homologous to immunoglobulin λ light-chain joining and constant regions, whereas the N-terminal region does not share any homology with variable regions. It is called omega LC (Hollis et al., 1989). *Vpreb* codes for a protein of 142 amino acids including a 19 amino acid long signal peptide in mice. The 26 amino acids at its C-terminal end show as well no homology to any known nucleotide sequences (Kudo and Melchers, 1987).

1.3.2 Structure of the SLC

The SLC is composed of non-covalently linked λ5 and VPREB in mice, humans, rabbits and cows and in complex with the HC, λ5 is linked by a disulfide bridge via its C-terminal cysteine with C_H1 (Pillai and Baltimore, 1987; Karasuyama et al., 1990; Tsubata and Reth, 1990; Schiff et al., 1991; Bossy et al., 1993; Guelpa-Fonlupt et al., 1994; Jasper et al., 2003; Ekman et al., 2009). VPREB has the typical Ig fold already shown in Section 1.2.3 and Figure 11. Yet, it only contains eight of nine β-strands found in a conventional V_L (a, b, c, c´, c´´, d, e, f). It lacks the J region sequence that forms the ninth and final β-strand of a variable domain as shown in the top of Figure 15 (Melchers et al., 1993; Guelpa-Fonlupt et al., 1994; Melchers, 1999; Lanig et al., 2004; Melchers, 2005). λ5 is equivalent to a constant domain of a LC and possesses all seven β-strands and the eighth β-strand in addition which is essential for non-covalent interaction with VPREB (Guelpa-Fonlupt et al., 1994; Melchers, 1999; Minegishi et al., 1999; Lanig et al., 2004). The

additional strand of ʎ5 (g) is inserted between a and f, where normally the ninth β-strand is located in a V_L domain (Figure 14) (Lanig et al., 2004). When the additional β-strand of ʎ5 was added to recombinant VPREB, it allowed the production of a protein that resembles the native conformation of a V_L domain (Morstadt et al., 2008).

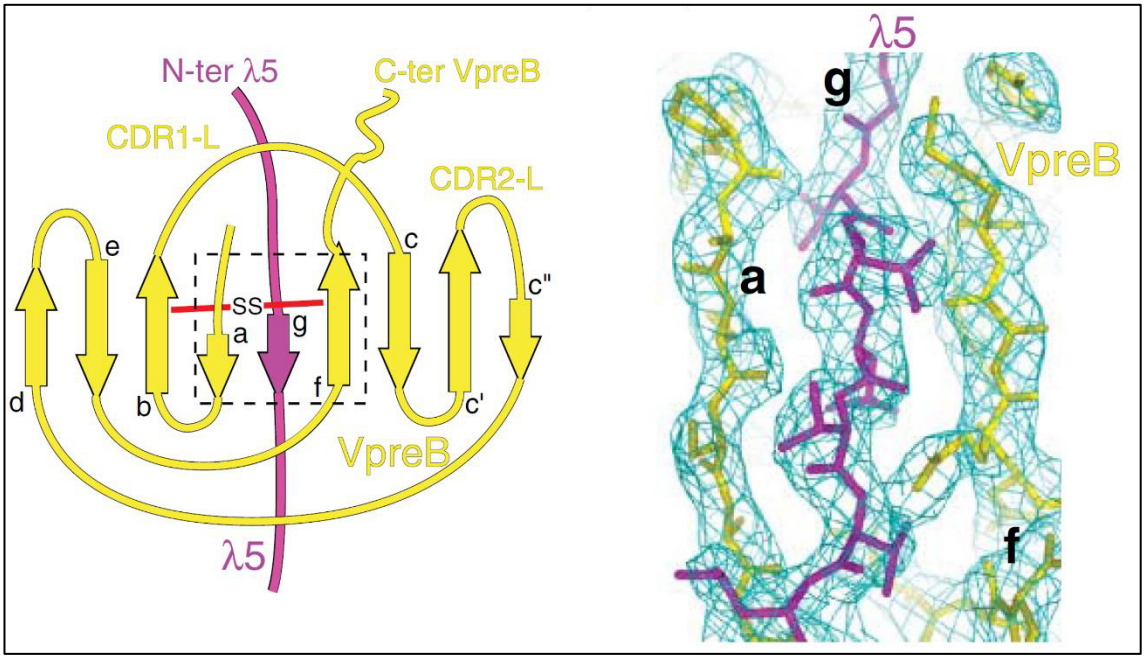

Figure 14: Topology of VPREB (yellow) with the UR of λ5 (violet).
VPREB contains eight out of nine β-strands of a conventional V_L domain (a, b, c, c´, c´´, d, e f). The internal disulfide bridge is formed between the b- and f-strand. The additional strand of ʎ5 (g) is inserted between a and f, where normally the ninth β-strand is in a V_L domain (left). The right shows electron density map of the a and f strand of VPREB and the g strand of ʎ5. Figure and legend were taken from Bankovich et al., 2007, the legend was modified (Bankovich et al., 2007).

Both SLC proteins are equipped with unfolded URs that have no sequence homology to any known protein. VPREB has a 24 amino acid long unique tail at its C-terminal end with nine negatively charged glutamates and four positively charged residues, one lysine and three histidines, resulting in a negatively charged UR. ʎ5 has a 50 amino acid long N-terminal UR with eight arginines, one lysine and one histidine. These ten positively charged residues provide for the overall positive charge of the UR (Guelpa-Fonlupt et al., 1994; Bradl et al., 2003). The opposite charged URs do not contribute to SLC assembly (Minegishi et al., 1999). The URs in both proteins protrude from VPREB and are located where normally the third CDR in a V_L domain is located as shown at the bottom of Figure 15 (Lanig et al., 2004).

Furthermore, the interaction of SLC and HC showed a decrease of roughly 30 % of interface contacts, like van der Waals interactions and hydrogen bonds, compared to LC and HC. However, it buries more surface area than the V_H/V_L interface which is due to a loss in framework interactions but a gain in interactions between URs and V_H, especially with CDR-H3 (Bankovich et al., 2007).

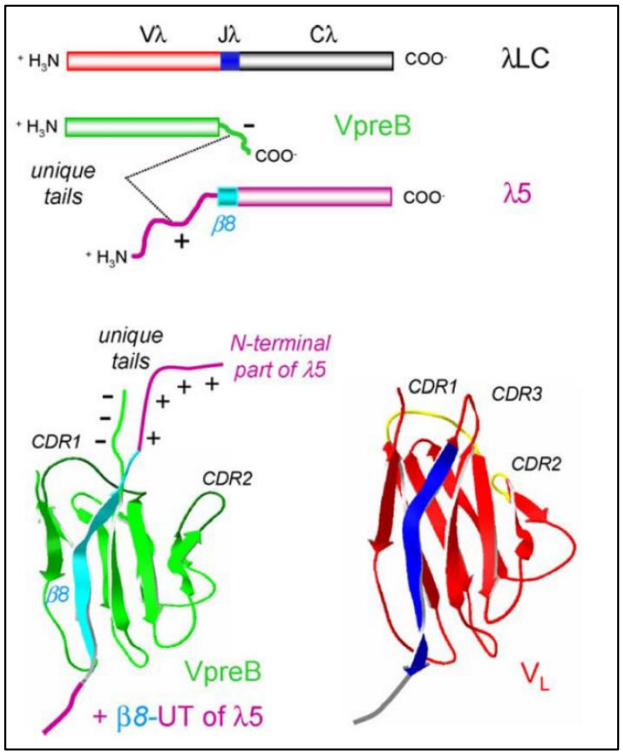

Figure 15: Schematic Alignment of SLC and LC and Modelling of VPREB.
The top shows the schematic alignment of VPREB and λ5 with the λLC. The bottom shows the model of the VPREB structure compared with a conventional V_L domain. Figure and legend were taken from Herzog et al., 2009, the legend was modified (Vettermann et al., 2006).

1.3.3 Function of the SLC

Although the knowledge about the SLC is still at an early stage, several functions were able to be dissected. The SLC, especially the ʎ5-UR and the eight arginines in it are implicated in pre-BCR clustering and pre-BCR mediated signal transduction (Ohnishi and Melchers, 2003; Guloglu et al., 2005). In humans, the absence of a functioning pre-BCR caused by the lack of λ5 expression, results in a blocked B-cell development (Minegishi et al., 1998). Furthermore, the ʎ5-UR was shown to limit the number of pre-BCR molecules on the cell surface (Minegishi et al., 1999; Fang et al., 2001; Ohnishi and Melchers, 2003). The λ5-UR is also a pre-BCR-specific autoreactive signaling motif that increases the size of the primary antibody repertoire by selective expansion of pre-B-cells with functional μHC (Vettermann et al., 2008). The URs of VPREB and λ5 play opposite roles in pre-BCR presentation on the surface. Deletion of the UR of λ5 ended in an increased surface deposition, while the deletion of the VPREB-UR yielded a decreased surface exposure (Knoll et al., 2012). The λ5-UR crosslinks the pre-BCRs for downregulation and stimulation, whereas the VPREB probes the fitness of the V_H domains and its UR fixes the pre-BCR on the surface (Knoll et al., 2012). In a study, λ5 alone was unable to bind properly to 19 tested μ chains in *Drosophila melanogaster* Schneider cells, while VPREB alone formed complexes with 5 of the μ chains (Seidl et al., 2001). This implies a possible role of the VPREB-HC complex in allelic exclusion of the HC locusing during B-cell development.

Only low levels of the pre-BCR are expressed on the surface of freshly isolated pre-B-cells (Cherayil and Pillai, 1991; Winkler et al., 1995; Wang et al., 2002; Su et al., 2003). More than 95 % of the assembled pre-BCR is retained in the ER (Brouns et al., 1996; Fang et al., 2001). The limited amount of pre-BCR on the cell surface is important to prevent the deletion of distinct pre-BCR idiotypes by overstimulation of antigen- or self-mediated pre-BCR signaling pathways (Nishimoto et al., 1991). This is in line with the finding that super cross-linking of pre-BCRs on the surface of pre-B-cells induces apoptosis (Kato et al., 2000).

The targeted inactivation of the *λ5* gene in mice resulted in an increase of the pro-B-cell compartment. The B-cell differentiation was not completely blocked but only impaired, while allelically excluded B-cells accumulated in peripheral lymphoid tissues with up to 50 % of wildtype levels (Kitamura et al., 1992; Rolink et al., 1993; Löffert et al., 1996; Ten Boekel et al., 1998; Rolink et al., 2000). In double (*Vpreb1* and *Vpreb2*)- and triple (*λ5, Vpreb1 and Vpreb2*)-deficient mice, the allelic exclusion remained intact, pre-B-cells passed the pre-BCR checkpoint but without proper expansion. IgL rearrangements took place but with a delayed appearance of peripheral B-cells (Mundt et al., 2001; Shimizu et al., 2002). In *SLC*-deficient mice, also pre-B-cell proliferation is impaired (Rolink et al., 1993; Grawunder et al., 1995). This impairment was also shown in *λ5*-deficient pre-B-cells (Rolink et al., 2000). Mice lacking the *Vpreb1* gene have a lower number of cells producing a functional pre-BCR, but the cells reaching the pre-BCR stage perform a normal function in terms of proliferation and differentiation indicating that Vpreb2 supports B-cell debelopment (Martensson et al., 1999). Mice with two *Vpreb1* alleles show an indistinguishable B-cell development from that of normal mice, whereas mice with two *Vpreb2* alleles have a 1.6-fold increased number of preBI cells and the number of preBII cells is decreased by 35 %. Mice with only one *Vpreb2* allele show a block in B-cell development (Mundt et al., 2006). Neither of the SLC proteins in mice, λ5, Vpreb1 or Vpreb2, nor the LC is required for μHC cell surface expression and signaling in mutant mice lacking any of these proteins (Galler et al., 2004). Vpreb was found to be normally expressed in B lineage cells of *λ5*-deficient mice, but unable for deposition on cell surface (Stephan et al., 2001). The SLC associates intracellularly with BiP among several other proteins in pro-B-cells before undergoing rapid degradation (Lassoued et al., 1996). Moreover, impaired pre-BCR formation or function has an influence on bone homeostasis independent of the presence of mature B-cells implicating a role in regulation of adult bone mass (Khass et al., 2019).

1.3.4 SLC Ligands

The SLC is implicated in the interaction with proteins other than the HCs. The two SLC proteins, λ5 and VPREB, are non-covalently associated with a 130 kDa N-linked glycoprotein with a 100 kDa protein core on pro-B and pre-BI cells (Cooper et al., 1986; Karasuyama et al., 1993; Shinjo et al., 1994; Winkler et al., 1995; Ohnishi et al., 2000). The glycoprotein was identified as a

cadherin type 1 membrane protein, called BILL-cadherin/cadherin 17 (*CDH17*), with seven extracellular cadherin domains, one being a pseudodomain without the catenin-binding site in its rather short cytoplasmic part comprising only about 25 amino acids (Kreft et al., 1997; Ohnishi et al., 2000; Wendeler et al., 2004). BILL-cadherin is a membrane-associated protein and together with an unknown protein with a molecular weight of 105 kDa and the SLC, it induces intracellular calcium flux and mediates calcium-dependent homotypic adhesion of cells without the catenin-binding site (Lemmers et al., 1999; Ohnishi et al., 2000). This might imply that the SLC together with BILL-cadherin functions as a pro-B-cell receptor before the association with the μHC to form a pre-B-cell receptor (Karasuyama et al., 1993; Winkler et al., 1995; Ohnishi et al., 2000). The signaling of the so-called pro-B-cell receptor is postulated to increase apoptotic sensitivity (Ohnishi et al., 2000). BILL-cadherin participates in the development of B lymphocytes at least at two stages, first at the transition from pro-B/pre-BI to pre-BII cells possibly in association with the SLC in the bone marrow and later at the point of development, accumulation and reactiveness of immature B-cells in the spleen (Ohnishi et al., 2005).

The pre-B-cell receptor interacts via its SLC with Galectin-1 (GAL1) in humans, an 135 kDa S-type lectin (Bradl and Jäck, 2001; Gauthier et al., 2002), which is secreted by stromal cells in the bone marrow (Chiariotti et al., 1999). It is involved in synapse formation between pre-B and stromal cells (Gauthier et al., 2002). Early B-cells move from the IL-7$^+$ to GAL1$^+$ supportive bone marrow niches during their development (Mourcin et al., 2011). GAL1 has a single carbohydrate recognition domain (CRD) with a short N-terminal sequence and occurs naturally as a non-covalently associated dimer (Bourne et al., 1994). It belongs to the family of galectins, a family of multivalent lectins that organize cell surface lattices (Brewer et al., 2002).

The interaction between the SLC and GAL1 is a direct sugar-independent protein-protein interaction with a K_D of 0.5 μM (Gauthier et al., 2002). The N-terminal UR of λ5 is the major binding element, whereas VPREB is not involved in the GAL1 interaction at all (Gauthier et al., 2002). The fixation of GAL1 by the SLC on pre-B-cells leads to the formation of a complex lattice consisting of the pre-B-cell receptor, GAL1, glycosylated counter receptors (Gauthier et al., 2002) as well as their stromal cell ligands ADAM15/fibronectin (Figure 16) (Rossi et al., 2006). The glycosylated counter receptors comprise the integrins $\alpha_4\beta_1$ (VLA-4) on pre-B-cells, $\alpha_5\beta_1$ (VLA-5) on stromal and pre-B-cells and $\alpha_4\beta_7$ on pre-B-cells in their active conformation (Rossi et al., 2006). The lattice is polarized at the contact zone between pre-B and stromal cells, which results in pre-B-cell receptor triggering (Gauthier et al., 2002). Furthermore, Erasmus et al. could show that GAL1 binding to the pre-BCR results in the formation of large, highly immobile pre-BCR aggregates (Erasmus et al., 2016). This aggregation was partially relieved by the addition of lactose to prevent the crosslinking of GAL1-pre-BCR complexes to other glycosylated membrane components (Erasmus et al., 2016).

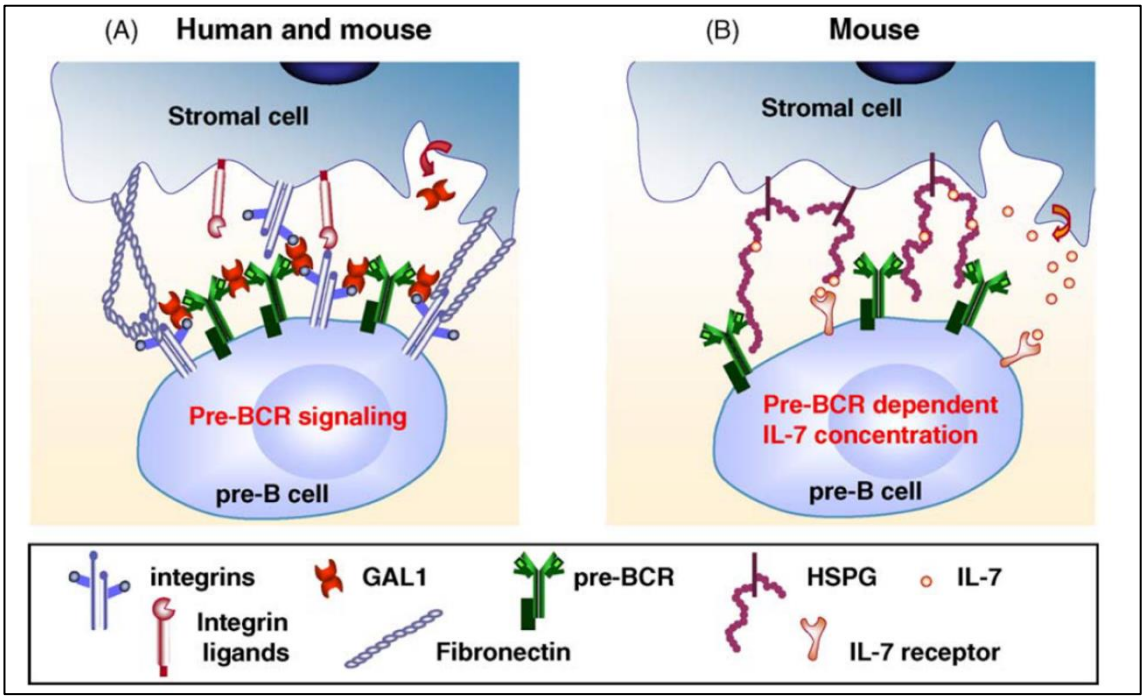

Figure 16: Schematic Overview of the Cell Synapse Between Pre-B and Stromal Cells in Humans and Mice (A) and in Mice Only (B).
A Galectine-1 (GAL1) is secreted by stromal cells and captured by λ5 of the pre-BCR and to GAL1 counter-receptors (integrins and fibronectin, in humans) that are interacting with their ligands on stromal cells and by the pre-BCR. The active integrin relocalization in the presence of GAL1 drives the pre-BCR into the cell synapse, consisting of pre-B and stromal cells and pre-BCR clustering. This leads to the initiation of pre-BCR signaling. **B** Heparan sulfate proteoglycan (HSPG) and heparan sulfate (HS) bind to λ5 of the pre-BCR and to IL-7 in mice. HS is involved in the recruitment of pre-BCR positive cells into specialized bone marrow niches. Figure and legend were taken from Espeli et al., 2006, the legend was modified (Espeli et al., 2006).

The UR of λ5 adopts a stable helical conformation in its center (Ser28-Arg37) that docks onto the hydrophobic surface of GAL1 adjacent to its carbohydrate binding site, whereas the rest of this domain is unfolded (Elantak et al., 2012). Crucial for this interaction and for the clustering of the pre-B-cell receptor are the hydrophobic and electrostatic interactions from the amino acids 22-45 in the UR of λ5 (Elantak et al., 2012). The aromatic ring of the tryptophane at position 30 is surrounded by a triad of hydrophobic side chains from GAL1, among which the aromatic ring of phenylalanine at position 30 directly faces the ring of the tryptophane at position 30 in the λ5 UR 22-45 (Elantak et al., 2012). The hydrophobic interactions are essential for relocalization of the pre-B-cell receptor at the cell synapse of pre-B and stromal cells (Elantak et al., 2012). The interaction of GAL1 and the pre-B-cell receptor induces local conformational changes in the GAL1 carbohydrate-binding site generating a reduction in the affinity of GAL1 and glycans (Bonzi et al., 2015).

In mice, the pre-B-cell receptor interacts with stroma cell-associated heparan sulfate (HS) via the UR of λ5, while the λ5 core region and VPREB are dispensable for this interaction (Bradl et al., 2003). This interaction can be blocked with the HS derivative, heparin (Bradl et al., 2003). Heparin induces internalization of a pre-B-cell receptor but not of a conventional B-cell receptor

on B lymphoid cell lines (Chen et al., 1991). Moreover, heparin blocks stroma cell-dependent maturation of B- and T-cell precursors in an *in vitro* culture system (Borghesi et al., 1999). GAL1-deficient mice show an impaired B-cell development at the pre-BII-cell stage due to inefficient pre-BII/stromal cell interactions (Espeli et al., 2009). In mouse bone marrow pre-BII cells, ligand-induced pre-B-cell receptor activation depends on the interaction of the pre-B-cell receptor, GAL1 and integrins leading to the clustering of the pre-B-cell receptor at the pre-BII/stromal cell synapse (Espeli et al., 2009).

1.3.5 Interaction of the V_H domain and the SLC

In early studies, it could be shown that the same V_H domain, only with differences in their CDR3 sequences, failed to pair with ʎ5 and LCs (Keyna et al., 1995; Kline et al., 1998). Later, it was shown that the structural requirements for a functional HC are the CDR length and the amino acid composition in the V_H domain. A nine amino acid long CDR3 (49 %) with a histidine at position one (73 %) were found to be favorable (Martin et al., 2003; Kawano et al., 2005). Another study showed that most remaining B-cells have a V_H CDR3 of 10 aa length with a glycine in the fourth position (Ye et al., 1996; Wang et al., 2001). Furthermore, many V_H domains found only in pro B-cells (roughly 50 %) are not able to pair with the SLC, which further supports the thesis that SLC acts as a proof-reader of the HC (Ten Boekel et al., 1997). The pre-BCR assesses the quality of µHCs and drives preferential expansion and differentiation of cells with higher quality of µHC (Kawano et al., 2006).

VPREB exists as a homodimer with a K_D of 0.5 µM as measured by SPR (Hirabayashi et al., 1995). It binds human as well as mouse V_H domains and a human V_L domain with a similar affinity at about 1 µM (Hirabayashi et al., 1995). VpreB can bind to human Fab fragments at sites different from the V_H-V_L interface (Hirabayashi et al., 1995). However, Gauthier et al. determined a K_D of 25 nM for VPREB and V_H (Gauthier et al., 1999).

The UR and the Ig-like domain of λ5 are both necessary to probe the H chain structure (Smith and Roman, 2010). The core domain of λ5 interacts with C_H1, which causes the release of the HC from its interaction with BiP. The URs of λ5 and VPREB bind to V_H to ensure a quality control of the HC and it was shown that two Fab-like fragments did not interact with each other (Gauthier et al., 1999) indicating that a ligand is required for pre-BCR clustering. A conserved N-linked glycosylation site at position 46 (N46) is necessary in V_H for pre-BCR function. Binding of SLC to the sugar linked to N46 in V_H mediates autonomous crosslinking and receptor formation (Übelhart et al., 2010). In conclusion, the plethora of HCs with different sequences, especially in their CDRs, makes it difficult to identify the selection mechanism by which the SLC chooses the HC.

1.4 Research Aims and Methodological Approach

Previous work on the SLC has mainly focused on *in vivo* experiments that investigated the consequences of SLC gene inactivation on B lineage cells in living animals or in cell culture. Beyond, the crystal structure of the Fab fragment containing the SLC instead of the LC was solved (Bankovich et al., 2007) and some studies were conducted regarding the interaction of the SLC with the V_H domain (Hirabayashi et al., 1995; Gauthier et al., 1999). The Fab-SLC complex has the same architecture as a conventional Fab-LC complex consisting of an Fd fragment and a LC. The SLC however shows remarkable difference as described in more detail in the introduction. Therefore, it is interesting to assess the SLC structure to gain more information about their molecular differences. How they behave alone and as a heterodimer remains elusive.

The mechanism of pre-BCR assembly, the role of the unusual structural features of the SLC and their specific functions as well as their impact on antigen or ligand interaction are still poorly understood. Therefore, the aim of this doctoral thesis is to dissect the SLC function *in vitro* with recombinantly produced proteins with a focus on the structure-function relationship of the SLC. This should help to outline a mechanism for pre-BCR assembly, expression, and secretion. This study is the continuation of the doctoral thesis of Natalia Sarmiento (Sarmiento Alam, 2015), who made first attempts to purify the SLC and structurally characterize it. However, her proteins contained tags, were not pure and not oxidized properly. Also, her interaction studies of the V_H domains with the SLC by SPR analysis and the ELISA assays for antigen interaction were only initial results that needed to be repeated and optimized for reproducibility and consistency.

Therefore, it was the goal of this thesis to establish a robust expression and purification system for the SLC proteins, ʎ5 and VPREB, and their variants, the SLC complex and the Fab complex, harboring the SLC instead of the LC bound to the Fd fragment. The aim is to achieve high expression levels, high yields, and a high purity of stable and correctly oxidized proteins. To realize these aims, recombinant protein expression will be carried out *in vitro* in *E. coli* cells. A standard protocol for purification and refolding of the recombinant proteins will be obtained.

The most outstanding features in both SLC proteins are their URs. Thus, mutants lacking the URs are created. Furthermore, the additional β-strand of ʎ5 was found to be essential in interaction with VPREB (Minegishi et al., 1999). Therefore, β-strand swapping mutants are generated, in which the β-strand was deleted in ʎ5 and added to VPREB. Additionally, three tryptophanes in the UR of ʎ5 and one tryptophane in the UR of VPREB are mutated to alanines to get an insight into their functions. All nine negatively charged glutamates in the UR of VPREB are mutated to

glutamines to confer a neutral charge and investigate the implications. An overview of all used SLC variants is given in Section 2.2.

Building up on the above-mentioned establishment of a robust expression and purification system, this thesis has several research goals with the focus on dissection of the unique structural features of VPREB and λ5:

1) Influence on Secondary, Tertiary, and Quaternary Structure and Stability
2) Influence on Conformational Stability
3) Influence on Complex Formation of VPREB and λ5
4) Influence on Complex Formation of C_H1 and SLC
5) Influence on Complex Formation of V_H and SLC
6) Influence on Antigen Interaction

For this purpose, far-ultraviolet (UV) circular dichroism (CD) and near-UV CD spectroscopy serves to analyze the secondary and tertiary structure, respectively. The quaternary structure is assessed by analytical ultracentrifugation (AUC) and glutaraldehyde crosslinking. Temperature-induced unfolding transitions followed by far-UV CD spectroscopy are used to obtain the melting temperatures (T_m). Changes in conformational dynamics is measured by hydrogen deuterium exchange coupled to mass spectrometry (HDX-MS). Complex formation between VPREB and λ5 variants, C_H1 and SLC variants and V_H and SLC variants is analyzed by folding kinetics followed by far-UV CD spectroscopy and binding affinities are measured by surface plasmon resonance (SPR) as well as isothermal-titration calorimetry (ITC). Furthermore, nuclear magnetic resonance spectrometry (NMR) is used to analyze the interaction of VPREB and λ5. Antigen interaction is analyzed by enzyme-linked immunosorbent assays (ELISA).

Taken together, these experiments are expected to lead to a better understanding of SLC and pre-BCR assembly as well as antigen interaction of the pre-BCR and the role of the URs in these processes.

2. RESULTS

2.1 Sequence Analysis and Structure Prediction of the Human SLC

Little is known about the structure of the single SLC proteins as well as the SLC heterodimer without the HC. Therefore, structural predictions were made, using AlphaFold (Jumper et al., 2021; Varadi et al., 2022), Phyre2 (Kelley et al., 2015), SWISS-MODEL (Guex et al., 2009; Bienert et al., 2016; Bertoni et al., 2017), Psipred (Jones, 1999; McGuffin et al., 2000) and IUPred (Mészáros et al., 2018; Erdos and Dosztányi, 2020).

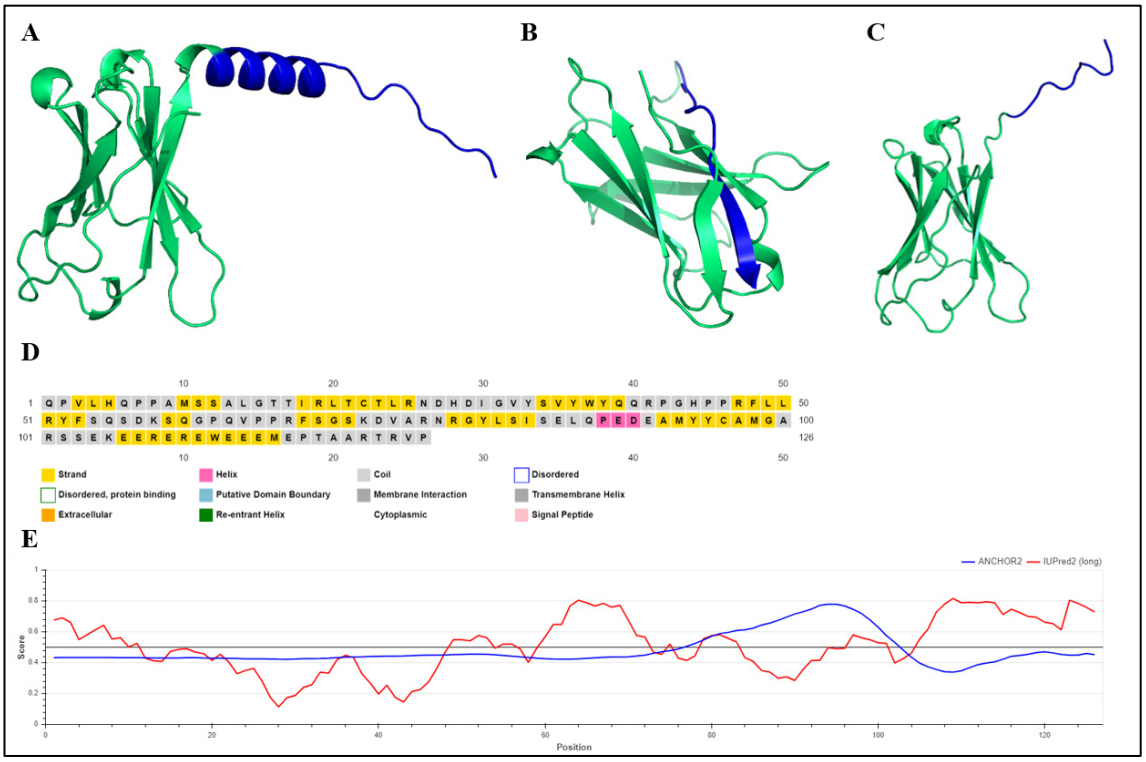

Figure 17: Secondary Structure Prediction for VPREB Using Structure Prediction Tools.
The 3D structures are depicted in A-C by using AlphaFold (**A**) (Jumper et al., 2021; Varadi et al., 2022), Phyre2 (**B**) (Kelley et al., 2015) and SWISS-MODEL (**C**) (Guex et al., 2009; Bienert et al., 2016; Bertoni et al., 2017; Waterhouse et al., 2018; Studer et al., 2020). Secondary structure was predicted using Psipred (**D**) (Jones, 1999; McGuffin et al., 2000). For prediction of unfolded regions, IUPred was used (**E**) (Mészáros et al., 2018; Erdos and Dosztányi, 2020).

The structural prediction of VPREB by AlphaFold (Figure 17A) showed it to be consisting of mainly β-strands and some parts of the UR (in blue) to be helical and random coil. Phyre2 even shows the UR to be part of the folded core consisting of mainly β-strands (Figure 17B). These two predictions are somewhat surprising because the UR of VPREB is expected to be completely unfolded and protruding (Bankovich et al., 2007). SWISS-MODEL fits the expectations since it predicts VPREB to consist of a core that contains mainly β-strands and an unfolded protruding UR (Figure 17C). Psipred predicts VPREB to consist of mainly β-strands in its core region and, surprisingly, also in its UR (Figure 17D). IUPred predicts the VPREB-UR (102-126), as expected,

as disordered and the core region to be mainly folded except a segment in the middle part (65-85), which show a high disorder tendency (Figure 17E). The ANCHOR2 graph predicts the disordered binding region roughly between 85 and 100, which comprise indeed part of the interaction sites with λ5 and V_H.

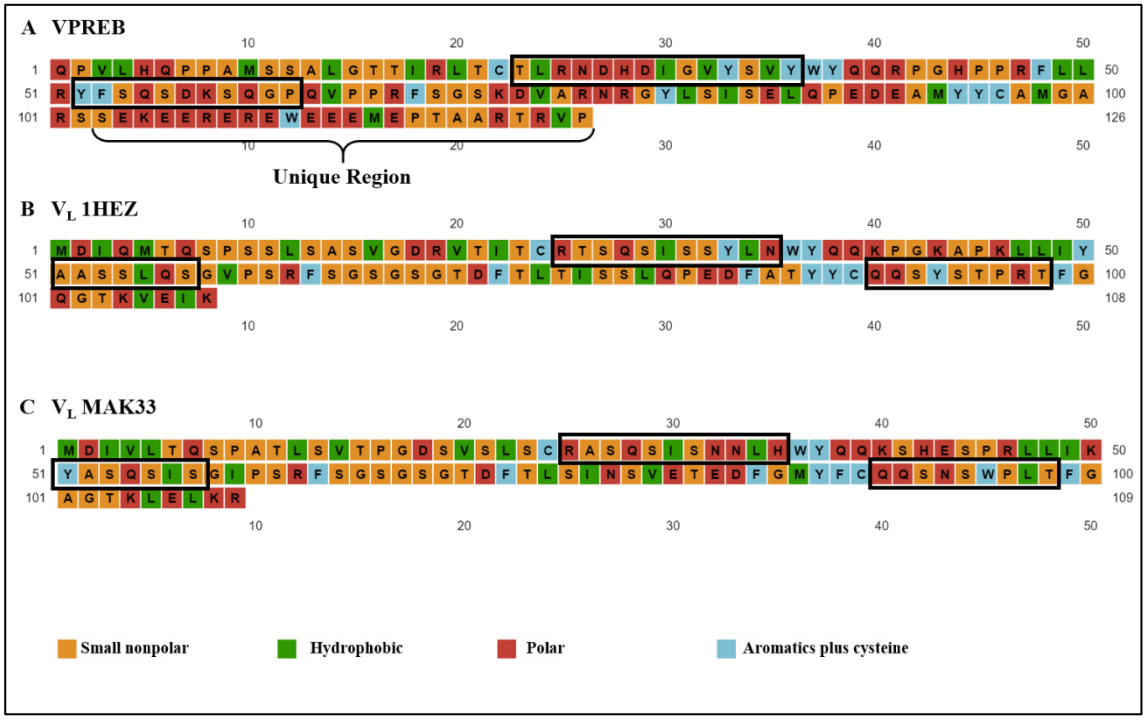

Figure 18: Amino Acid Types in VPREB (A) Compared to Human V_L 1HEZ (B) and Murine V_L MAK33 (C).
The amino acid types were predicted by Psipred (Jones, 1999; McGuffin et al., 2000). Small nonpolar amino acids are coloured in orange, hydrophobic amino acids in green, polar amino acids in red, aromatic amino acids and cysteines in blue. The CDRs are marked as black boxes and the UR in VPREB with a brace.

Psipred served as a web-tool to not only predict the secondary structure of a protein, but also gives an overview of polar, non-polar, hydrophobic as well as aromatic residues. This was used to compare VPREB with two V_L domains, murine MAK33 and human 1HEZ. As shown in Figure 18, VPREB has only two out of the three CDRs in a conventional V_L domain. The number of small non-polar amino acids is roughly the same in all three proteins. There are 45 small nonpolar amino acids in VPREB, 50 in V_L 1HEZ, and 46 in V_L MAK33. Also, the number of hydrophobic residues is not strikingly different between the three proteins. There are 21 hydrophobic amino acids in VPREB, 19 in V_L 1HEZ, and 22 in V_L MAK33. However, there is a major difference in the number of polar as well as positively and negatively charged amino acids between VPREB, V_L 1HEZ and V_L MAK33. VPREB possesses 46 polar amino acids of which 17 are positively charged and 19 are negatively charged, whereas V_L 1HEZ only has 26 polar amino acids with only 9 positively and 6 negatively charged amino acids and V_L MAK33 has 29 polar amino acids with 10 being positively and 8 being negatively charged. Remarkably, 9 out of the 17 negatively

charged amino acids and 5 out of the 19 positively charged amino acids are in the UR. This is a significant difference, which may contribute to VPREB dimerisation by electrostatic interactions (discussed in more detail in section 3.1). The number of aromatic residues is roughly the same between the three proteins with VPREB having 12, V_L 1HEZ also 12 and V_L MAK33 having 10. Furthermore, while VPREB has 10 proline residues, of which 2 are located in the UR, V_L 1HEZ only contains 5 proline residues and V_L MAK33 only has 4. This is an obvious difference between the three proteins. All three proteins contain two cysteines that form the typical intramolecular Ig disulfide bridge. Altogether, VPREB contains 18 amino acids more than V_L 1HEZ and 17 more than V_L MAK33, although it is missing a β-strand. However, this extension in length is due to the additional 25 amino acid long UR in VPREB.

The CDRs of VPREB were analyzed by abYsis (Swindells et al., 2017) and compared to the CDR pattern of V_L MAK33 and V_L 1HEZ (Figure 19). First, it should be noted that VPREB only has two CDRs, CDR1 and CDR2, compared to V_L 1HEZ and V_L MAK33 that have three CDRs, typical for V_L domains. The relative position of CDR1 and CDR2 is roughly the same as for the V_L domains. Notably, the length of the CDRs varies. While CDR1 for the V_L domains comprises 11 amino acids, the CDR1 for VPREB consists of 14 amino acids. Furthermore, CDR2 has 7 amino acids in the V_L domains and 11 amino acids in VPREB. The third CDR in VPREB is missing. Also remarkable is the unusual frequency of the amino acids in the CDRs of VPREB compared to the V_L domains, which means that rather atypical amino acids are used in certain positions. Figure 19D shows the CDR prediction of the VPREB ΔU + β mutant. Unlike VPREB, it contains a third CDR by adding the β-strand from λ5, which resulted in the generation of a third CDR, where normally the UR is located. However, compared to the V_Ls´ CDR3 domains, it is back-shifted but has an equal length of 9 amino acids. Moreover, VPREB ΔU + β exceeds the length of the murine and human V_L domains by 8 amino acids, which is due to the longer CDR1 and CDR2 regions in VPREB.

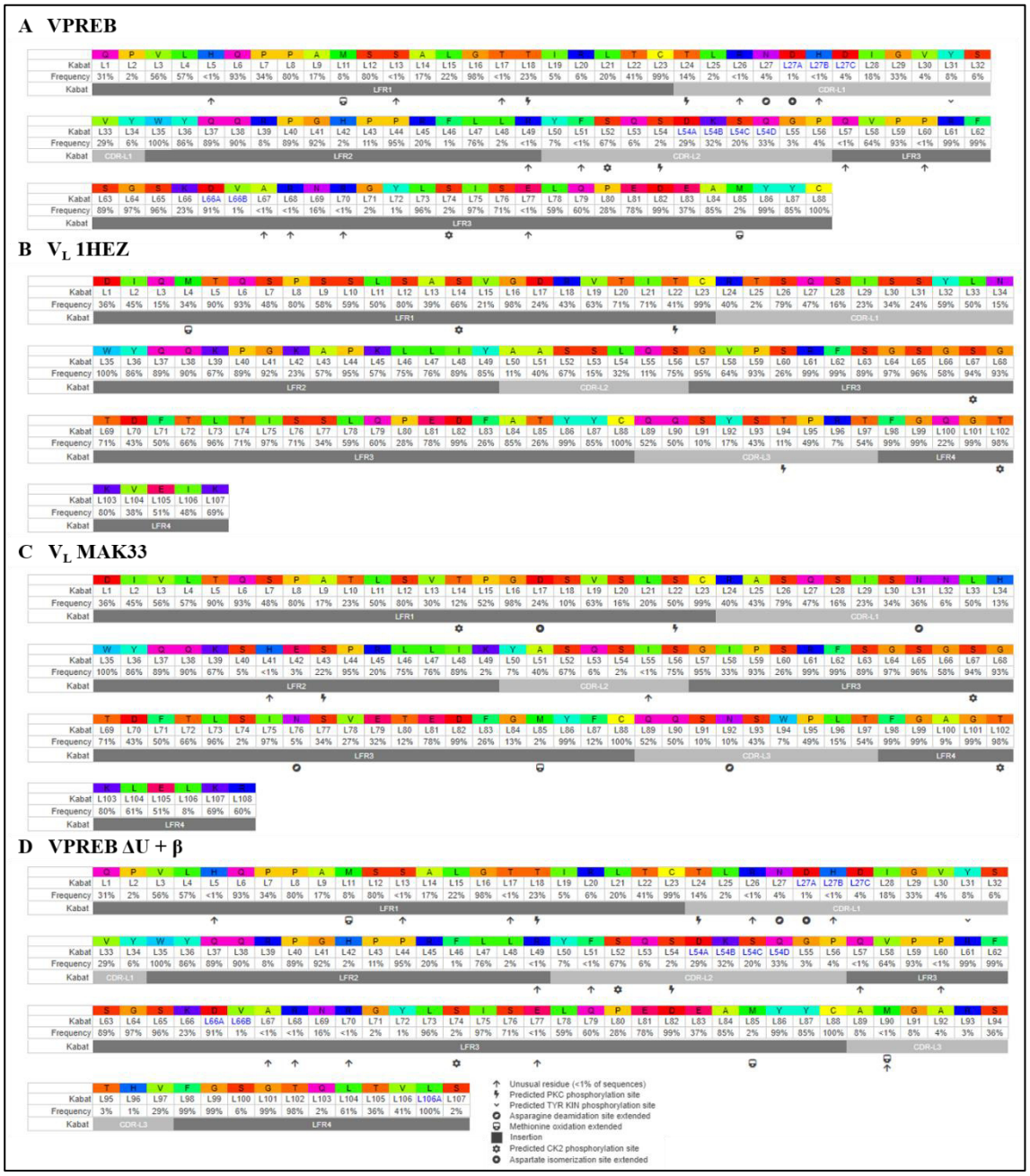

Figure 19: Prediction of CDRs in VPREB (A), V_L 1HEZ (B), V_L MAK33 (C) and VPREB ΔU + β (D) by abYsis (Swindells et al., 2017).

The structural predictions of ʎ5 (Figure 20) showed it to be a folded protein consisting of mainly β-strands with the N-terminal region to be unfolded. In AlphaFold (Figure 20A), the additional β-strand in red is part of the β-strand core of the protein, instead of protruding, while the UR is fully unfolded and protruding. Phyre2 (Figure 20B) shows a similar prediction to that of AlphaFold. The β-strand core is the same. Except, the additional β-strand is protruding in both predictions and unfolded. The UR was not predicted. SWISS-MODEL (Figure 20C) show the core to consist of β-strands as the typical Ig fold, the β-strand to be unfolded and protruding, with the end and a part of the UR to form two β-strands. Large parts of the UR are also not predicted. Contrary to the expectations, Psipred shows β-strand predictions towards the end of the unfolded

UR, whereas the rest of the UR is predicted to have a random coil structure as expected (Figure 20D). The core region is predicted to form β-strands as well as two helices. IUPred shows areas with their tendency to be unfolded. For the first part of the UR (1-20), it predicts a high tendency of disorder, whereas for the second part (20-50) it shows a high tendency to be folded (Figure 20E). This is expected because an α-helix was measured in this segment by NMR (Elantak et al., 2012). Also, at around amino acid position 118, the protein shows a very low propensity to be folded, which is rather surprising since the core region folds mainly in β-strands. ANCHOR2 predicted at amino acids 20-35 a disordered binding region with a low score, which is the region binding to GAL1 (Elantak et al., 2012).

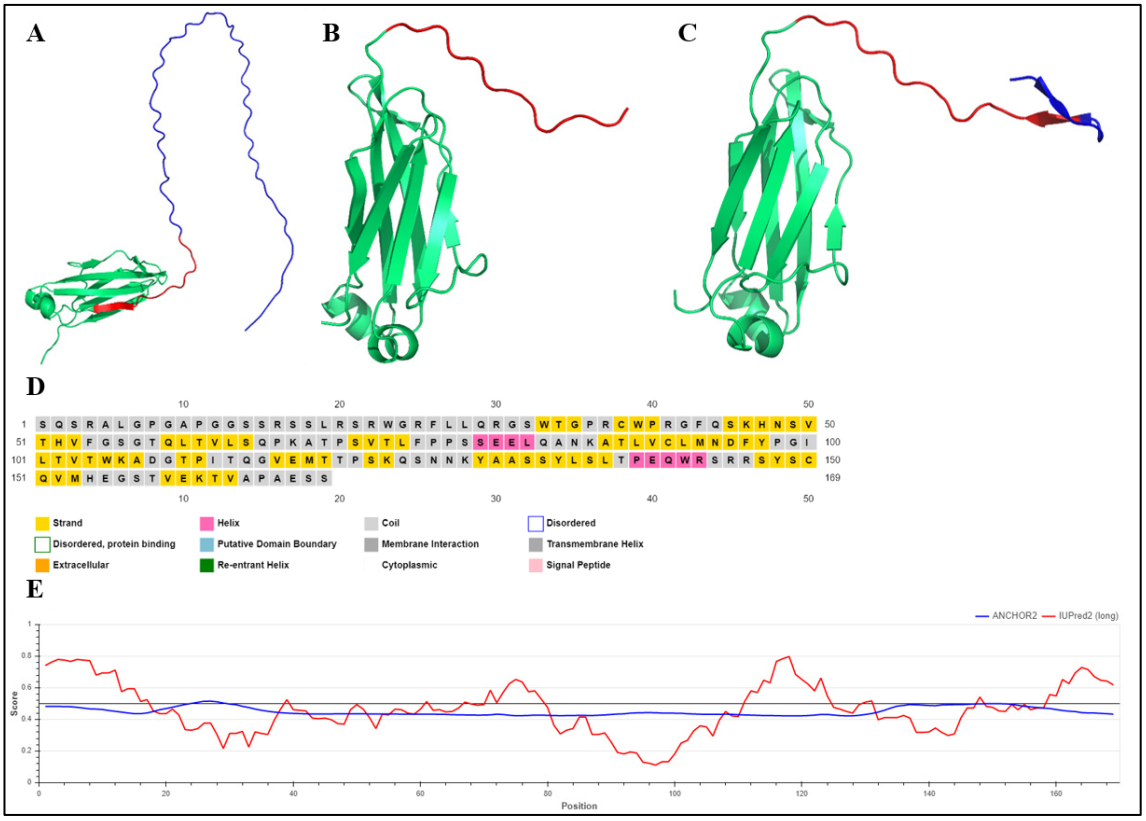

Figure 20: Secondary Structure Prediction for ʎ5 Using Different Prediction Tools.
The 3D structures are depicted in A-C by using AlphaFold (**A**) (Jumper et al., 2021; Varadi et al., 2022), Phyre2 (**B**) (Kelley et al., 2015) and SWISS-MODEL (**C**) (Guex et al., 2009; Bienert et al., 2016; Bertoni et al., 2017; Waterhouse et al., 2018; Studer et al., 2020). Secondary structure was predicted using Psipred (**D**) (Jones, 1999; McGuffin et al., 2000). For prediction of unfolded regions, IUPred was used (**E**) (Mészáros et al., 2018; Erdos and Dosztányi, 2020).

Psipred was also used to compare the number of polar, non-polar, hydrophobic as well as aromatic residues between ʎ5 and the two C_L domains, murine MAK33 and human 1GAF (Figure 21). The number of small non-polar amino acids is, contrary to VPREB, strikingly different between ʎ5 and the two C_L domains. There are 78 small nonpolar amino acids in ʎ5, 39 in C_L 1GAF and 42 in C_L MAK33. Also, the number of hydrophobic amino acids is other than in VPREB slightly different between the three proteins. There are 28 hydrophobic amino acids in ʎ5, 20 in C_L 1GAF,

and 17 in C_L MAK33. However, there is, in contrast to VPREB, only a minor difference in the number of polar as well as negatively charged amino acids between ʎ5, C_L 1GAF and C_L MAK33, but a major difference in the number of positively charged amino acids. ʎ5 possesses 45 polar amino acids of which 9 are negatively charged and 21 are positively charged, whereas C_L 1GAF only has 35 polar amino acids with 12 negatively and 12 positively charged amino acids and C_L MAK33 has 37 polar amino acids with 13 negatively and 13 positively charged amino acids. Remarkably, no negatively charged amino acids and 10 out of the 21 positively charged amino acids are in the UR. Last, the number of aromatic residues is roughly the same between the three proteins with ʎ5 having 14, C_L 1GAF having 9 and C_L MAK33 having 10. Furthermore, while ʎ5 contains 12 proline residues of which 4 are in the URs, C_L 1GAF only contains 5 prolines and C_L MAK33 as well. This also can be considered as a significant difference between the three proteins. Also interesting is the additional cysteine in the UR of ʎ5 compared to the two C_L domains that only have three cysteines (the C-terminal cysteine is not shown). Altogether, it should be mentioned that ʎ5 contains 50 amino acids more than C_L 1GAF and C_L MAK33. This is due to the UR and the additional β-strand.

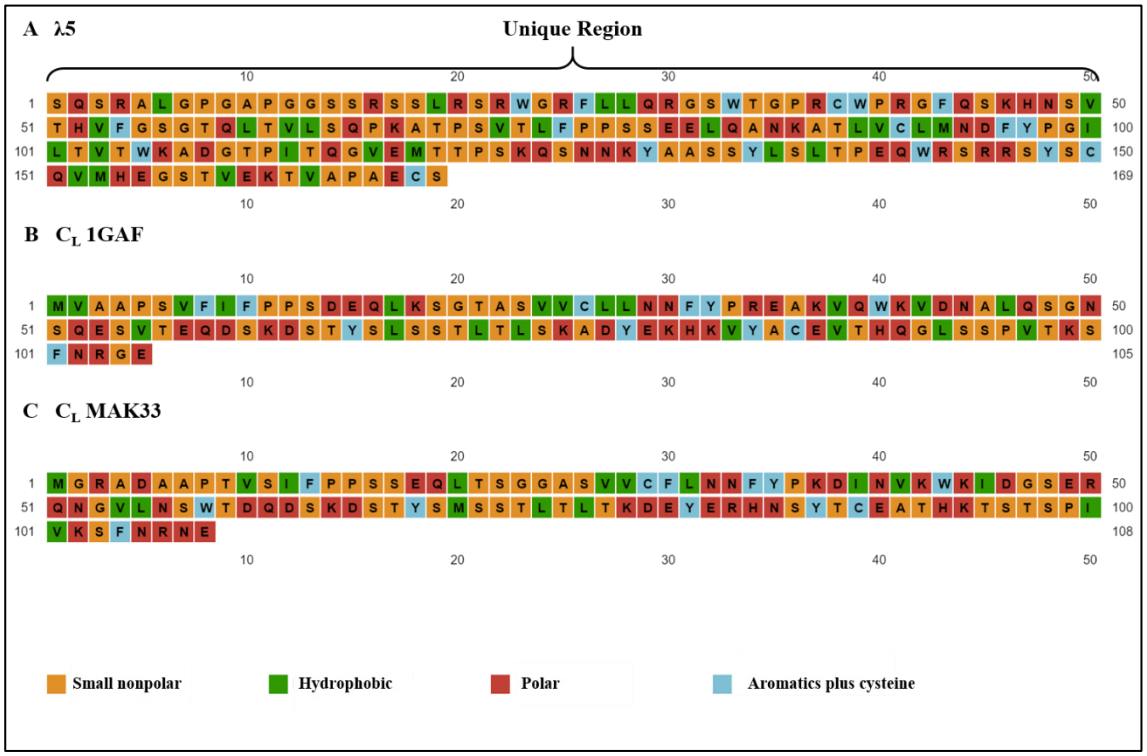

Figure 21: Amino Acid Types in ʎ5 (A) Compared to Human C_L 1GAF (B) and Murine C_L MAK33 (C).
The amino acid types were predicted by the use of Psipred (Jones, 1999; McGuffin et al., 2000). Small nonpolar amino acids are coloured in orange, hydrophobic amino acids in green, polar amino acids in red, aromatic amino acids and cysteines in blue. The UR in λ5 is marked with a brace.

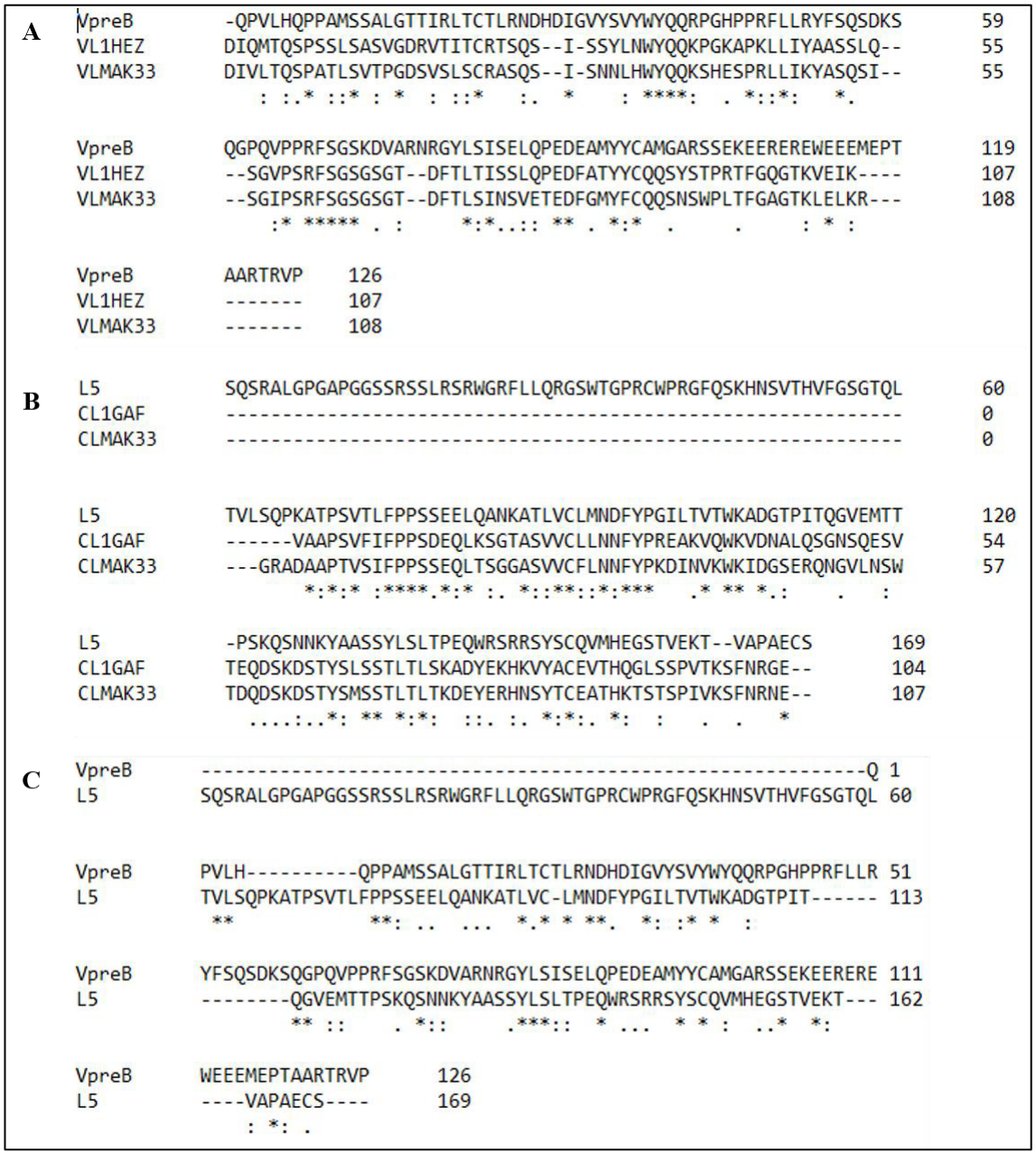

Figure 22: Sequence Alignments of VPREB, ƛ5, Murine and Human C_L and V_L Domains Using ClustalW (Madeira et al., 2019).
A Alignment of VPREB, V_L 1HEZ and V_L MAK33. **B** Alignment of ƛ5, C_L 1GAF and C_L MAK33. **C** Alignment of ƛ5 and VPREB.

Moreover, alignments of VPREB with V_L domains and of λ5 with C_L domains as well as of VPREB with λ5 were made by the use of Clustal Omega (Madeira et al., 2019). The alignment of VPREB with V_L 1HEZ (human origin) and V_L MAK33 (murine origin) is displayed in Figure 22A and it shows a surprising high degree of similarity. As expected, V_L 1HEZ and V_L MAK33 have a higher similarity than both compared to VPREB. The UR of VPREB shows little similarity with the V_L domains, only one glutamate is identical. Also, the WYQQ motif that is located directly after the first CDR is conserved in all three proteins. Furthermore, the P-RFSGS motif in the third framework region is conserved in all three proteins and comes after the second CDR

with two other amino acids in between. The PRFLLRY-motif in VPREB is also quite similar to the other two proteins. In V_L 1HEZ, it is PKLLIYA and in V_L MAK33, it is PRLLIKY. The first position is a proline in all three proteins, while the second position is a positively charged amino acid, arginine in VPREB and V_L MAK33 and lysine in V_L 1HEZ. The two consecutive leucines in all three proteins are also characteristic. Furthermore, the tyrosine at the end of the motif is conserved in all three.

The alignment of λ5 with C_L 1GAF (human origin) and C_L MAK33 (murine origin) shows similarity only for the core region of λ5 (Figure 22B). The UR and the additional β-strand have, as expected, no similarity at all with the other two proteins. The degree of similarity is overall higher compared to VPREB and the V_L domains. Outstanding is the conservation of 4 prolines in the three proteins.

Surprisingly, the alignment of VPREB and λ5 (Figure 22C) shows some similarity despite they are of complete different evolutionary origin. These are surprisingly 3 prolines. As expected, also the 2 cysteines that form intramolecular disulfide bonds are conserved.

2.2 Cloning, Expression and Purification of the SLC

To analyze the SLC structure and function, several protein purification protocols were developed in this thesis and an overview is given in the following chapters including detailed descriptions of the respective purification processes. The general information about the protein purifications mentioned in section 5.3.10 also applies to the purifications described in this section. Before expression and purification, all constructs were ordered from geneart and cloned into a pE-SUMOpro vector after the BsaI restriction site.

All VPREB and λ5 constructs as well as V_H MAK33-FLAG contained an N-terminal cleavable His_6-SUMO-Tag. The sequences were obtained from uniprot and PDB with the code 2H32 (Table 37) and are listed in section 5.1.11. The cloning and expression conditions that were established in this thesis are shown in sections 5.3.6 and 5.3.9.

All SLC variants that were cloned, expressed, and purified in this thesis are shown in Figure 23. It should be noted that all λ5 variants had a C-terminal cysteine, which forms a disulfide bridge with the C_H1 domain of the HC in the final assembled state. This cysteine was mutated to a serine in all λ5 variants. The mutants comprised constructs with deleted URs (VPREB ΔU and λ5 ΔU C212S), the deleted β-strand of λ5 (λ5 ΔU Δβ C212S and λ5 Δβ C212S), the inserted β-strand into VPREB (VPREB ΔU + β and VPREB βU), mutated tryptophanes to alanines in the URs (VPREB W131A and λ5 W67,77,83A C212S), and the mutation of all negatively charged glutamates in the UR of VPREB to uncharged glutamines (VPREB 9EurQ). It should be noted that in the VPREB βU mutant, the UR is located at the other side compared to WT VPREB. This results from the β-strand added C-terminally of the VPREB core region. The UR that is attached

C-terminal to this additional β-strand protrudes at the complete other side far away from the antigen interaction site and near the λ5 interaction site.

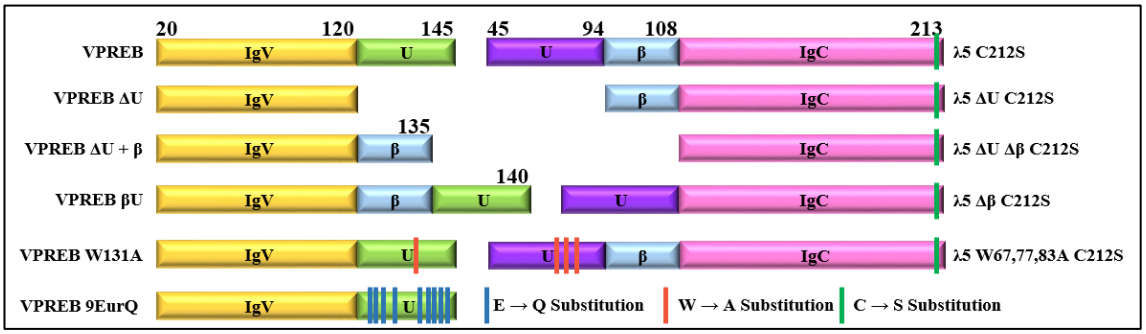

Figure 23: Schematic Representation of the Cloned and Purified SLC Variants.
The WT constructs are depicted on the top. WT VPREB is shown from amino acid 20 to 145 without the signal peptide. The core (IgV) region in yellow ranges from amino acid 20 to 120. Amino acids 121 to 145 show the UR of VPREB in green. λ5 is shown next to it without its signal squence from amino acid 45 to 213. The UR from amino acid 45 to 94 is coloured in violet, the additional β-strand from amino acid 95 to 108 in blue and the core region from amino acid 109 to 213 in magenta. VPREB ΔU and λ5 ΔU C212S are both lacking their URs. VPREB ΔU + β has the UR replaced by the β-strand and VPREB βU has the β-strand inserted between the core and the UR. λ5 ΔU Δβ C212S has both the UR and β-strand deleted, λ5 Δβ C212S has only the β-strand deleted. VPREB W131A has a tryptophane to alanine mutation at position 131 and λ5 W67,77,83A C212S three tryptophane to alanine mutations at positions 67, 77 and 83 (red lines). VPREB 9EurQ has all glutamates in the UR of VPREB mutated to glutamines (blue lines). All λ5 variants have a cysteine to serine mutation at position 212 at the C-terminal end (green line).

All VPREB and λ5 variants were purified according to the same purification protocol, which is described in the following. A schematic overview is shown in Figure 24. It should be noted that the establishment of the purification protocol required extensive optimization regarding the refolding buffer, the refolding temperature and time as well as the buffers used for HisTrap chromatography. Moreover, also the expression was optimized regarding its expression time and the amount of added IPTG. The single steps of the optimization are not shown here, only the final purification protocol is described.

The inclusion bodies obtained after inclusion body preparation (section 5.3.9.3) were solubilized in IB Dissolving Buffer SLC over night (O/N) at 4°C. After centrifugation, the cleared supernatant was applied to a HisTrap. The eluted protein was reduced with β-Mercaptoethanol. This was then drop-diluted to a concentration of 0.05 g L^{-1} for VPREB variants and 0.1 g L^{-1} for λ5 variants into 450 mL of Drop-Dilution Buffer. To this, Ulp1/SUMO-Protease was added to cleave off the His_6-SUMO-Tag and it was dialysed in Refolding Buffer SLC for 4 days at 10°C. The dialysate was afterwards applied to another pre-equilibrated HisTrap FF 5 mL. The protein of interest was collected from the flowthrough and the cleaved-off His_6-SUMO-Tag bound to the column.

The purification protocol for the SLC complex comprising VPREB and λ5 C212S was established in this thesis. The purification protocol is very similar to the protocol of the single domains, except for the drop dilution. The proteins were pooled together before drop-dilution. λ5 C212S was diluted to a concentration of 0.05 g L^{-1} and based on that an equimolar ratio of VPREB was added.

For the purification of the complex consisting of VPREB ΔU and λ5 ΔU C212S, a final SEC run was performed in HEPES buffer to get rid of residual monomers.

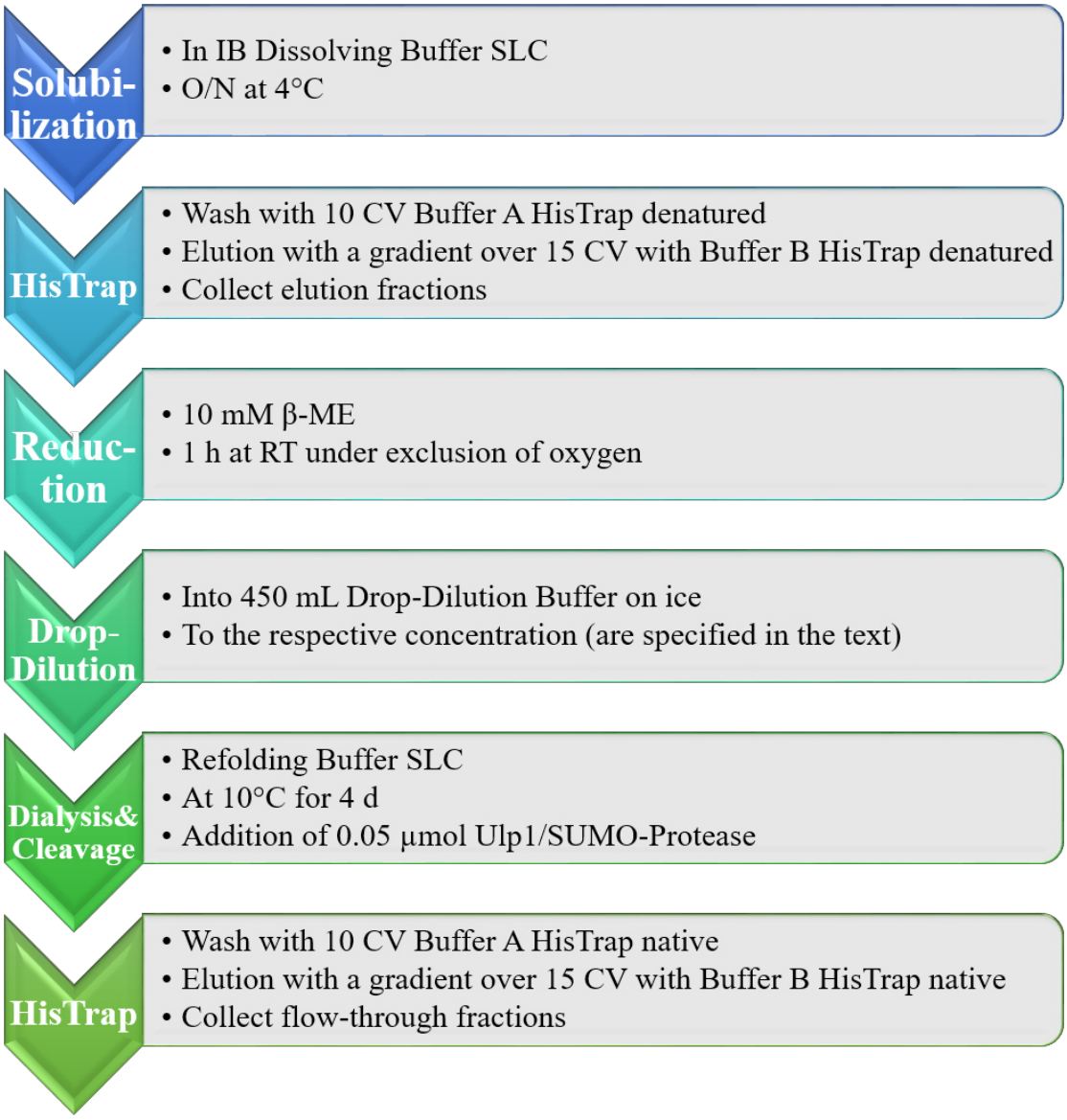

Figure 24: Purification Scheme of the Single SLC Proteins, ƛ5 C212S and VPREB, and Their Variants.
After solubilization of inclusion bodies in IB Dissolving Buffer SLC over night (O/N) at 4°C, the solubilized and centrifuged IBs were applied onto a His Trap FF 5 mL, washed with 10 CV of Buffer A HisTrap denatured and eluted with 15 CV of Buffer B HisTrap denatured. After reduction of disulfide bonds by incubation for 1 h at RT in 10 mM β-ME under exclusion of oxygen, reduced IBs were drop-diluted into 450 mL of Drop-Dilution Buffer to the respective concentration. After dialysis for 4 d at 10°C and simultaneous Ulp1/SUMO digestion (0.05 µmol added), the cleaved POI was collected in the flowthrough after applying to second His Trap FF 5 mL in Buffer A HisTrap native. The buffer recipes are listed in detail in Section 5.1.14.

The SLC was purified in complex with Fd MAK33-FLAG as a Fab domain. The purification protocol is like the protocol of the single VPREB and λ5 domains. It only varies in the drop-dilution step. Fd MAK33 with a C-terminal FLAG-Tag (sequence in section 5.1.11) was mixed

with the appropriate amount of λ5 and VPREB before drop-dilution. Fd MAK33-FLAG was diluted to a concentration of 0.06 g L^{-1} and mixed with equimolar ratios of λ5 C212S and VPREB, respectively.

2.3 Biophysical Characterization of the Human SLC

The SLC protein variants were biophysically characterized. The secondary and tertiary structures of the proteins and complexes were determined by far-UV and near-UV CD spectroscopy, respectively. AUC was used to assess the quaternary structure of the proteins. Glutaraldehyde crosslinking served as an orthogonal method to investigate the quaternary structures of the VPREB variants. The thermal stability was assessed by temperature-induced unfolding transitions followed by far-UV CD spectroscopy at 205 nm.

2.3.1 Characterization of the WT SLC

2.3.1.1 Secondary and Tertiary Structure of WT SLC

While large parts of the structure of the assembled SLC in complex with a HC fragment has been determined (Bankovich et al., 2007), we know little about the structure of the individual SLC proteins, the SLC heterodimer and the assembly reactions leading to the SLC and the SLC-HC complex. To address these questions, we studied the recombinantly produced proteins *in vitro*.
The proteins were analyzed by far- and near-UV CD spectroscopy to assess their secondary and tertiary structures, respectively. The spectra were recorded as described in section 5.3.13.2. The far-UV CD spectrum of ʎ5 C212S, which corresponds to the C_L domain of a regular LC, is dominated by β-strands, which can be observed by a minimum at roughly 215 nm. This is consistent with the immunoglobulin fold of ʎ5 (Figure 25A). The far-UV CD spectrum of ʎ5 also exhibits unfolded segments, as visualized by a broad minimum and a missing maximum at around 205 nm. This agrees with the structural predictions described in section 2.1.
VPREB, the second part of the SLC, which corresponds to the V_L domain in a regular LC, gave a far-UV CD spectrum that is indicative of an unfolded protein (Figure 25A). This contrasts with the folded state observed for isolated V_L domains (Herold et al., 2017), and with the structural predictions made in section 2.1. However, VPREB lacks a β-strand normally present in V_L domains. Of note, this strand is present in ʎ5 and is donated upon SLC assembly to complement the VPREB fold. Accordingly, the far-UV CD spectrum of SLC C212S revealed an almost same β-sheet content as for ʎ5 C212S with the characteristic minimum also at around 215 nm. However, upon addition of the single spectra of VPREB and λ5 C212S, the spectrum is characteristic of an unfolded protein, indicating that VPREB is folded upon complex formation with λ5 C212S.
The tertiary structure analysis of VPREB, ʎ5 C212S and SLC C212S by near-UV CD spectroscopy (Figure 25B) revealed large differences in the shape of the spectrum of the SLC

compared to the single proteins, which may reflect changes in the structure upon complex formation. While ʎ5 C212S and SLC C212S show near-UV CD spectra, which are indicative of a defined structure around the aromatic reporter groups, the spectrum of VPREB has no defined features, which is indicative of an unfolded protein. ʎ5 C212S and SLC C212S show a peak between 285 and 297 nm, which represents the structure around tryptophanes (Kelly et al., 2005). Also, between 275 and 282 nm, the tyrosine peaks exhibit a more defined structure for SLC C212S compared to ʎ5 C212S. The area between 261 and 268 nm, which is characteristic for phenylalanines, shows small peaks for SLC C212S but not for λ5 C212S. As expected, VPREB shows neither in the area around the tyrosines, nor phenylalanines, nor tryptophanes a defined structure. Also notable is, that λ5 C212S has higher negative values than SLC C212S.

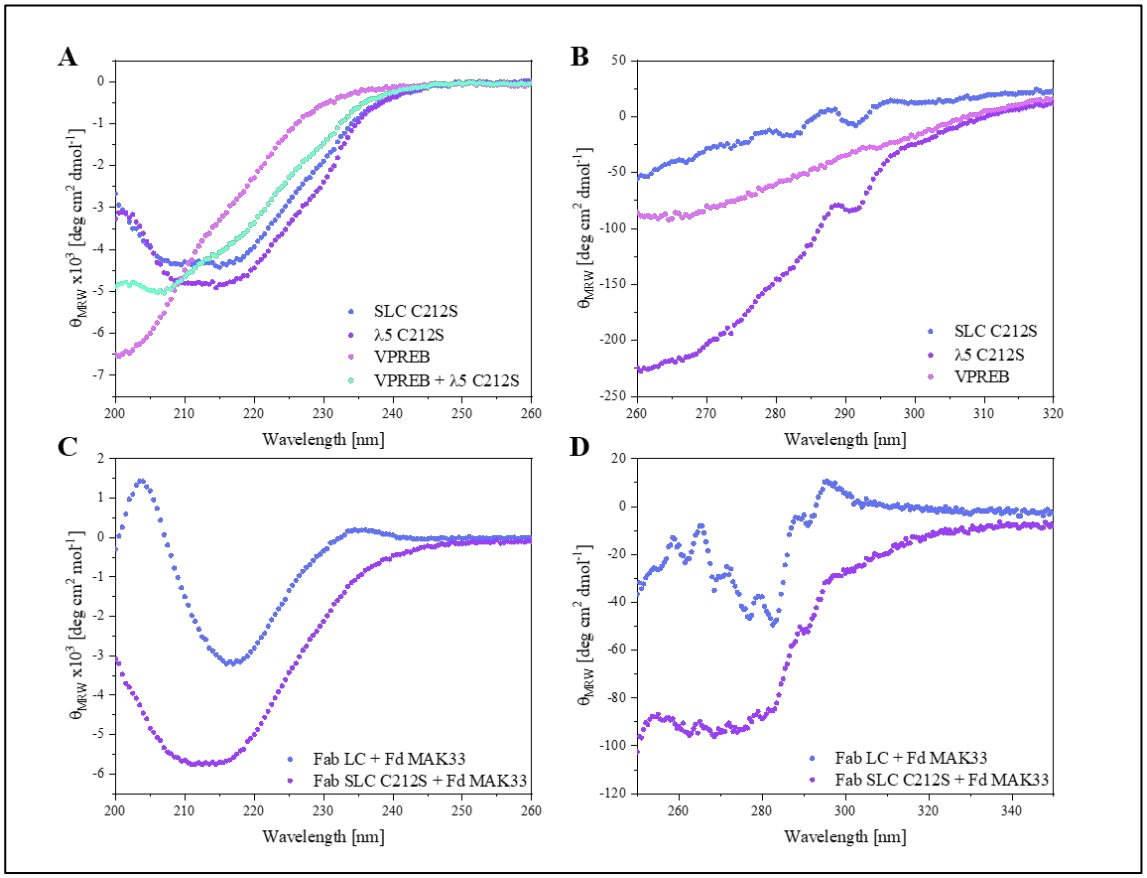

Figure 25: Secondary and Tertiary Structure Analysis of Single WT SLC Proteins and Complexes by Far- and Near-UV CD Spectroscopy.
Far- (**A**) and near-UV (**B**) CD spectra of VPREB, ʎ5 C212S and SLC C212S. Far- (**C**) and near-UV (**D**) CD spectra of Fab-SLC and Fab-LC.

Furthermore, the Fab complex consisting of Fd MAK33 and the SLC (Fab-SLC) as well as the Fab complex consisting of Fd MAK33 and LC MAK33 (Fab-LC) were analyzed by CD spectroscopy. As expected, Fab-LC showed a far-UV CD spectrum (Figure 25C) that is characteristic of a folded protein, dominated by β-strands. It has a minimum at around 216 nm and a maximum at around 205 nm. In contrast, Fab-SLC shows a far-UV CD spectrum (Figure

25B) that has some β-sheet content with a minimum at around 212 nm, but also contains unfolded segments as represented by a broad peak. This is to be expected since the URs of ʎ5 and VPREB are large, partially unfolded segments that have a large impact on the overall secondary structure. This spectrum is very similar to the spectra of SLC C212S and ʎ5 C212S alone.

Moreover, near-UV CD spectroscopy was performed to gain insight into the tertiary structure of the Fab complexes. As expected, Fab-SLC shows a near-UV CD spectrum (Figure 25D) with a well-defined structure around the aromatic residues, whereas the near-UV CD spectrum of Fab-LC (Figure 25D) exhibits a structure that seems to be masked by the URs, so that the characteristics can not be seen as pronounced as in Fab-LC.

2.3.1.2 Thermal Stability of WT SLC

To assess and compare the thermal stabilities of ʎ5 C212S alone, the SLC heterodimer as well as Fab-SLC and Fab-LC, loss of secondary structure during thermal unfolding was monitored by far-UV CD spectroscopy at 205 nm. ʎ5 C212S alone shows a higher thermal stability with a T_m, at which 50 % of the protein is unfolded, of 55.8 ± 0.7°C compared to SLC C212S, which has a T_m of 53.3 ± 0.4 °C (Figure 26A, Table 1). The stability is decreased by 2.5°C in the complex compared to ʎ5 C212S alone. Since VPREB alone is unfolded, no thermal transition could be observed, and no T_m could be determined.

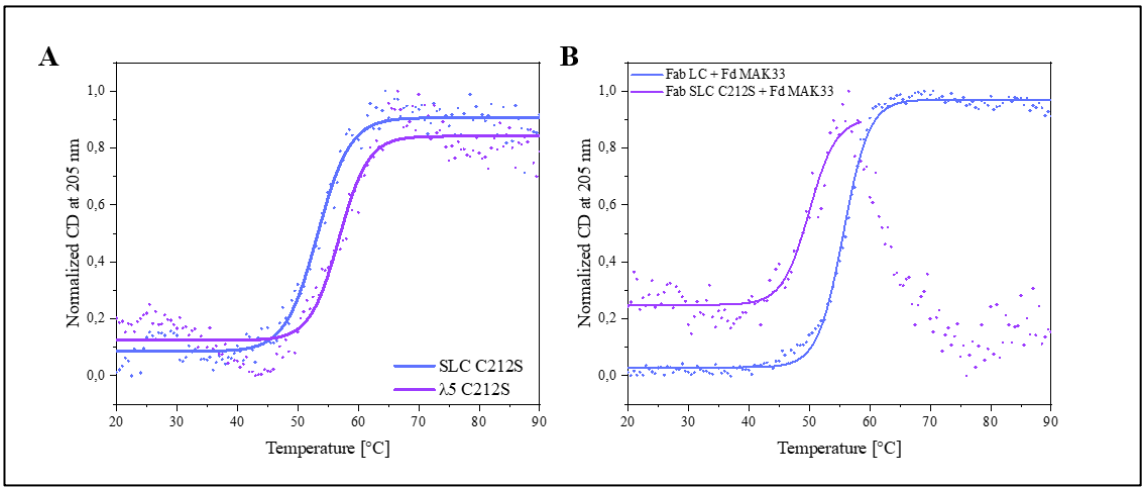

Figure 26: Conformational Stability of Single SLC Proteins and Complexes.
Temperature-induced unfolding transitions followed by far-UV CD spectroscopy at 205 nm of SLC C212S and ʎ5 C212S (**A**) as well as Fab-SLC and Fab-LC (**B**). Solid lines represent the Boltzmann fit of the recorded data to determine the turning point, which reflects the T_m at which 50 % of the protein is unfolded.

The thermal induced unfolding transition of Fab-SLC (Figure 26B) showed an even lower T_m of 49.2 ± 0.2°C (Table 1), which is decreased by 6.5°C compared to ʎ5 C212S alone and by 4°C compared to the SLC heterodimer. Furthermore, once the complex is fully unfolded, it aggregates, which is reflected in a decrease of the signal. Fab-LC (Figure 26B) shows the same stability as

ʎ5 C212S alone with a T_m of 55.8 ± 0.1°C (Table 1) and therefore an increased stability of 6.5°C compared to Fab-SLC. No aggregation was observed after unfolding. In conclusion, the complexes are more unstable than ʎ5 C212S alone. Especially, Fab-SLC is strikingly unstable.

Table 1: Melting Temperatures of Single SLC Proteins and Complexes.

Protein	**T_m [°C]**
SLC C212S	53.3 ± 0.4
ʎ5 C212S	55.8 ± 0.7
VPREB	n. d.
Fab LC + Fd MAK33	55.8 ± 0.1
Fab SLC C212S + Fd MAK33	49.2 ± 0.2

T_ms of the single SLC proteins, the SLC complex and the Fab complexes harboring the SLC and the LC. The indicated error is the standard deviation of three technical replicates. n. d.: not determined as VPREB is unfolded.

2.3.1.3 Quaternary Structure of WT SLC

To examine the quaternary structure of the single proteins and the complexes, AUC was used. It revealed SLC C212S to be predominantly a heterodimer consisting of ʎ5 C212S and VPREB with a sedimentation coefficient of ~2.8 S (Figure 27A).

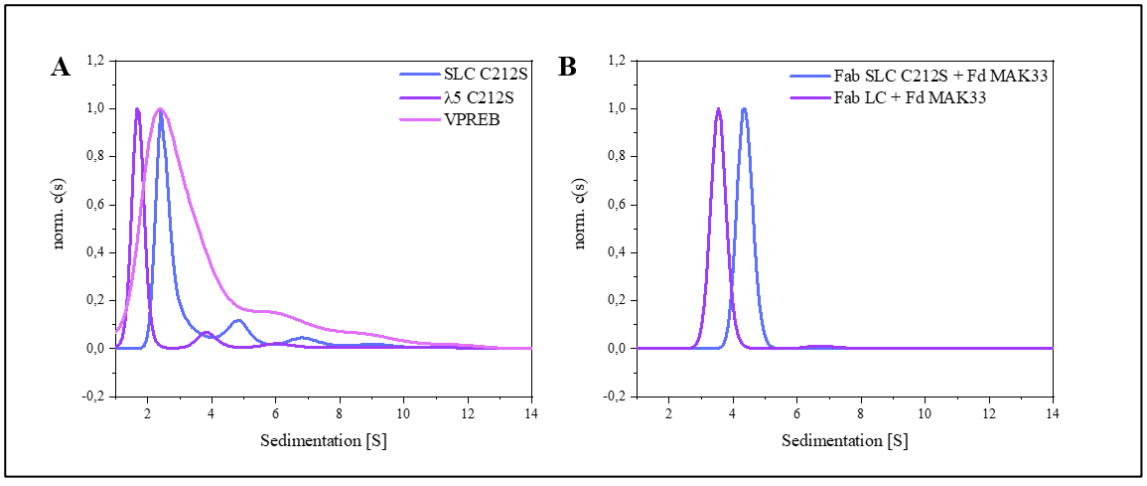

Figure 27: Quaternary Structure Analysis of Single SLC Proteins and Complexes by AUC.
AUC spectra of VPREB, ʎ5 C212S and SLC C212S are depicted in (**A**) and of Fab-SLC and Fab-LC in (**B**).

Interestingly, VPREB alone (Figure 27A) sedimented mainly with a sedimentation coefficient of ~2.8 S, indicating the presence of a homodimer. A minor fraction of tetramers was observed as

well at higher oligomers. Considering that unfolded proteins have a lower sedimentation coefficient as expected, this corroborates the assumption that VPREB alone forms a homodimer. ʎ5 C212S is predominantly monomeric with a sedimentation coefficient of ~1.8 S (Figure 27A). It tends to form dimers to a small extent.

The Fab-SLC (Figure 27B) complex forms a heterotrimer consisting of VPREB, ʎ5 C212S and the Fd MAK33 HC fragment and sediments at around 4.2 S. The Fab-LC heterodimer (Figure 27B) sediments at around 3.5. This is reasonable since Fab-SLC has a higher molecular weight of about 10 kDa compared to Fab-LC. No higher oligomers were observed for both complexes.

2.3.2 Characterization of the Mutants Lacking the URs

2.3.2.1 Secondary and Tertiary Structure of the ΔU-Mutants

While the core regions of ʎ5 and VPREB are resolved in the crystal structure (Bankovich et al., 2007), most of the URs are not resolved. Therefore, it is crucial to analyze the influence of the URs on the secondary and tertiary structure of the single SLC proteins as well as the complex. Far-UV CD spectroscopy of SLC ΔU C212S (Figure 28A) shows a spectrum of a protein that consists of β-strands with no random coil content with a characteristic minimum at 218 nm. Compared to SLC C212S, the minimum is shifted by about 3 nm. The shoulder at around 230 nm is characteristic of an internal disulfide bridge. The far-UV CD spectrum of ʎ5 ΔU C212S (Figure 28B) shows a minimum at 218 nm like SLC ΔU C212S and a maximum at around 203 nm. Compared to ʎ5 C212S, that has the minimum at 215 nm, it is shifted by 3 nm. Furthermore, the WT has no maximum. Also, ʎ5 ΔU C212S has a pronounced shoulder at around 230 nm, which is indicative of the intramolecular disulfide bridge. The far-UV CD spectrum of VPREB ΔU (Figure 28C) is like that of VPREB with some minor differences since it has a maximum at around 230 nm and a minimum at around 205 nm. VPREB ΔU is, like VPREB, also unfolded, which can be clearly seen in comparison with ʎ5 ΔU C212S and SLC ΔU C212S (Figure 28D).

The analysis of the tertiary structure of the ΔU-mutants by near-UV CD spectroscopy should serve to compare them to the WT spectra. The near-UV CD spectrum of SLC ΔU C212S (Figure 29A) shows, compared to the WT complex, a spectrum with a specific structure around the aromatic residues indicative of a folded protein. Because of the missing unfolded regions, the spectrum is more defined than that of the WT complex. Between 285 and 295 nm, there is a more pronounced local minimum indicating it to be more structured around the tryptophanes. At around 280 nm, which is the area where the tyrosines show up, there is also a higher peak in SLC ΔU C212S compared to SLC C212S, indicating a more structured complex for the ΔU-mutant, which is expected since the partially unfolded URs are missing.

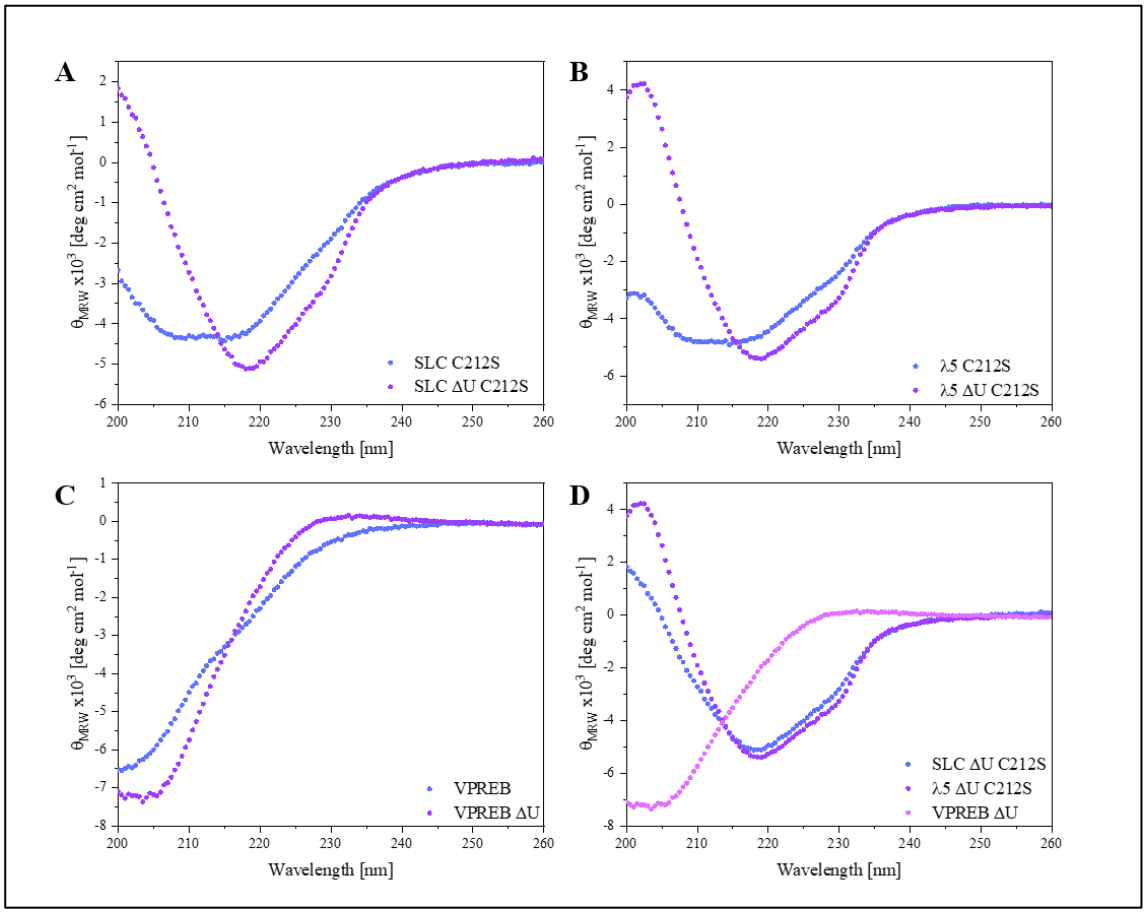

Figure 28: Secondary Structure Analysis of ΔU-Mutants of VPREB, ʎ5 C212S and SLC C212S by Far-UV CD Spectroscopy.
Far-UV CD spectra of SLC C212S and SLC ΔU C212S (**A**), ʎ5 C212S and ʎ5 ΔU C212S (**B**), VPREB and VPREB ΔU (C) and all three ΔU-mutants (**D**).

Also, ʎ5 ΔU C212S shows a spectrum with a more defined structure around the aromatic residues, whereas ʎ5 C212S is dominated by its unfolded UR (Figure 29B). Between 285 and 295 nm, there is a more pronounced local minimum in the spectrum of ʎ5 ΔU C212S compared to the spectrum of ʎ5 C212S. At 280 nm, there is a local maximum in ʎ5 ΔU C212S, whereas in ʎ5 C212S, this is missing. Both are indicative of a higher degree of structure in the ΔU-mutant. VPREB ΔU shows a near-UV CD spectrum of a protein that is unfolded (Figure 29C). The shape is like that of WT VPREB, however with more intensity. There is no defined structure nor peak in any of the three areas that are characteristic of the aromatic residues. Comparing the spectra of the three ΔU mutants (Figure 29D), one can clearly see that ʎ5 ΔU C212S and SLC ΔU C212S are very similar, whereas VPREB ΔU differs a lot. While ʎ5 ΔU C212S and SLC ΔU C212S show spectra characteristic of a folded protein, VPREB ΔU is completely unfolded.

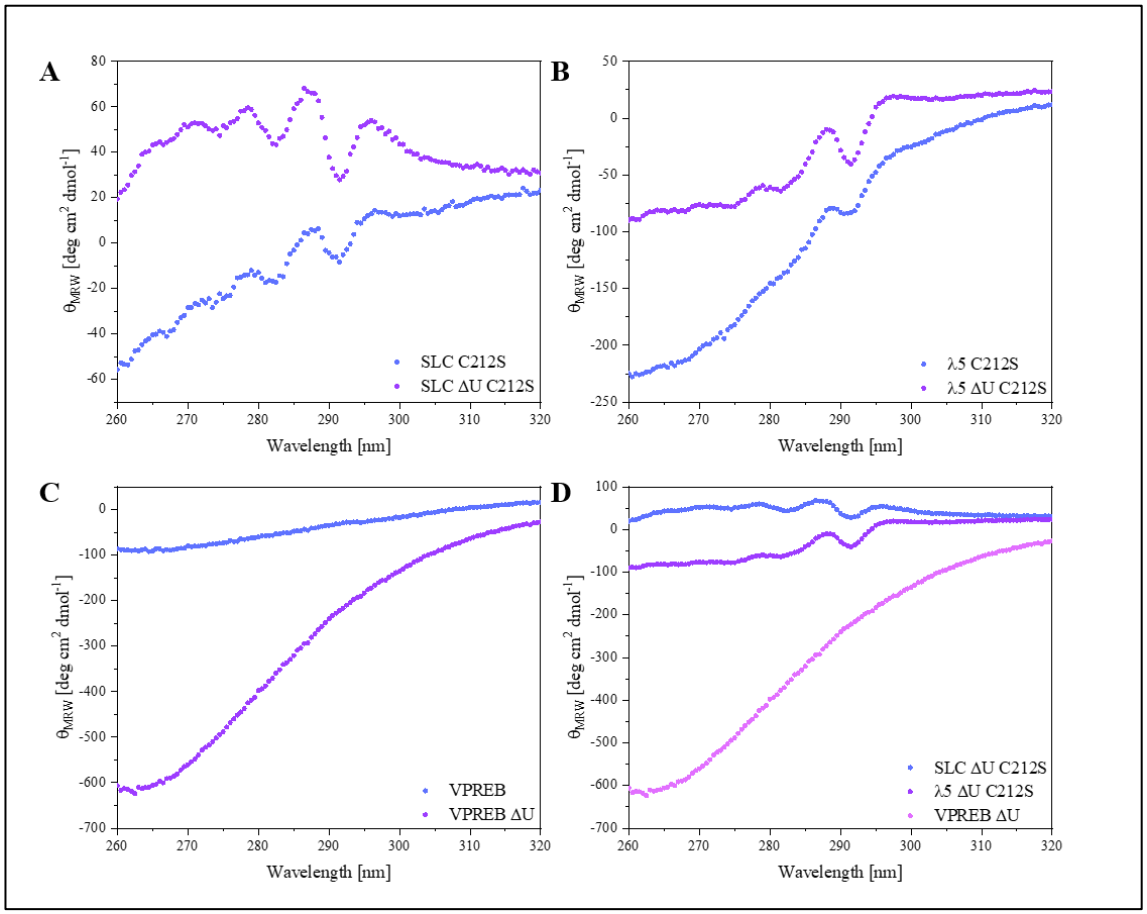

Figure 29: Tertiary Structure Analysis of the ΔU-Mutants of VPREB, ʎ5 C212S and SLC C212S by Near-UV CD Spectroscopy.
Near-UV CD spectra of SLC C212S and SLC ΔU C212S (**A**), ʎ5 C212S and ʎ5 ΔU C212S (**B**), VPREB and VPREB ΔU (**C**) and all three ΔU-mutants (**D**).

2.3.2.2 Thermal Stability of ΔU-Mutants

To assess the influence of the URs in the single proteins as well as in the complex on the thermal stability, temperature-induced unfolding transitions were followed by far-UV CD spectroscopy at 205 nm.

SLC ΔU C212S has a higher T_m than SLC C212S (56.1 ± 0.5°C vs. 53.3 ± 0.4) (Figure 30A, Table 2). ʎ5 ΔU C212S is characterized by a T_m of 58.5 ± 0.3°C (Figure 30B, Table 2). This is increased by about 3°C compared to ʎ5 C212S (55.8 ± 0.7°C), which indicates that the URs decrease the thermal stability not only in the complex but also in ʎ5 C212S alone. When comparing ʎ5 ΔU C212S alone with the complex SLC ΔU C212S (Figure 30C, Table 2), it confirms that the complexation does not stabilize it. The same is true for the WT complex as described in section 2.3.1.2.

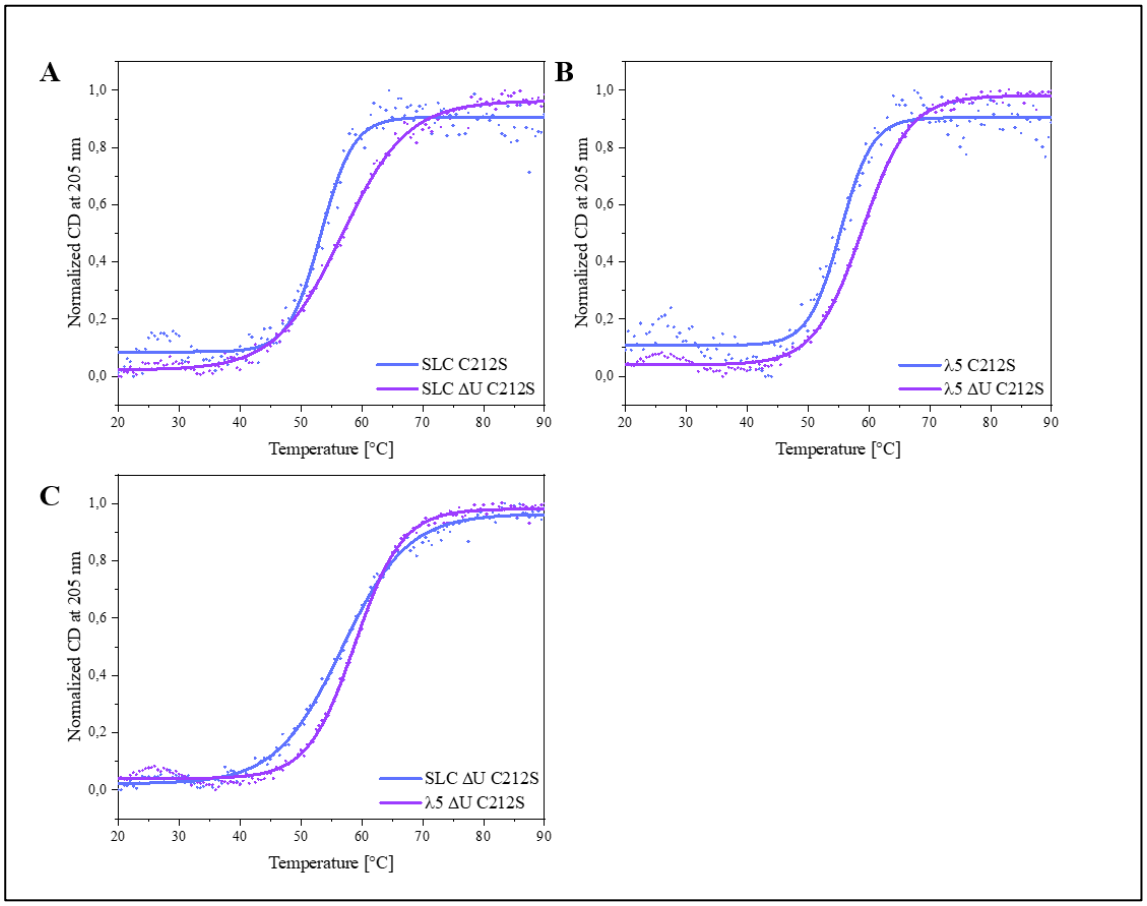

Figure 30: Conformational Stability of the ΔU-Mutants of VPREB, ʎ5 C212S and SLC C212S. Temperature-induced unfolding transitions followed by far-UV CD spectroscopy at 205 nm of SLC C212S and SLC ΔU C212S (**A**), ʎ5 C212S and ʎ5 ΔU C212S (**B**) as well as SLC ΔU C212S and ʎ5 ΔU C212S (**C**). Solid lines represent the Boltzmann fit of the recorded data to determine the turning point, which reflects the T_m at which 50 % of the protein is unfolded.

Table 2: Melting Temperatures of ΔU-Mutants of SLC C212S and ʎ5 C212S.

Protein	**T_m [°C]**
SLC ΔU C212S	56.1 ± 0.5
λ5 ΔU C212S	58.5 ± 0.3
VPREB ΔU	n. d.

T_ms of the ΔU-mutants of SLC and ʎ5. The indicated error is the standard deviation of three technical replicates. n. d.: not determined as VPREB ΔU is unfolded.

2.3.2.3 Quaternary Structure of ΔU-Mutants

Analysis of the ΔU-mutants by AUC was performed to determine, if the URs have an influence on the quaternary structure of the single proteins and the complex (Figure 31). As expected, ʎ5 ΔU C212S is a monomer regardless of its UR with a sedimentation coefficient of around 1.6 S. VPREB ΔU still forms a homodimer independent of its UR with a sedimentation coefficient of

around 2.8 S. The complex of ʎ5 ΔU C212S and VPREB ΔU forms a heterodimer at a sedimentation coefficient of around 3.0 S. These results indicate that the URs neither play a role in the quaternary structure of the single proteins nor in complex formation.

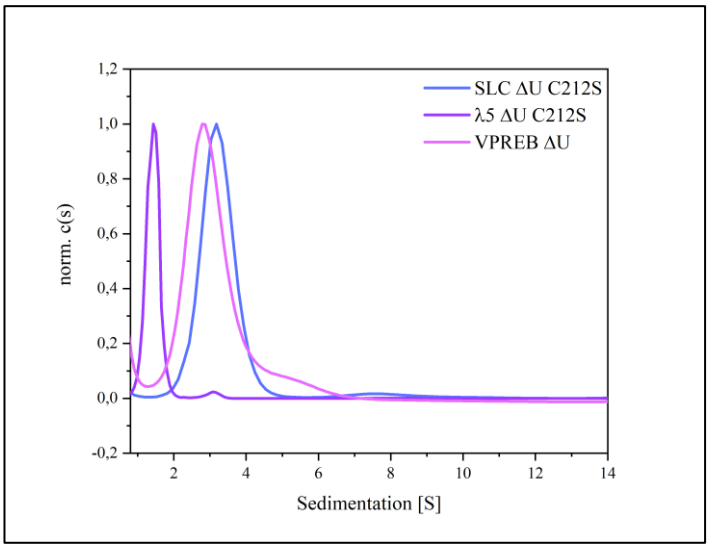

Figure 31: Quaternary Structure Analysis of the ΔU-Mutants of VPREB, ʎ5 C212S and SLC C212S by AUC.

2.3.3 Characterization of the β-Strand Swap Mutants

2.3.3.1 Secondary and Tertiary Structure of the β-Strand Swap Mutants

To assess the effect that the additional β-strand has on both, ʎ5 and VPREB, swap mutants were generated in which the β-strand was deleted from ʎ5 and added to VPREB (for further details see Figure 23). The far-UV CD spectrum of ʎ5 Δβ C212S (Figure 32A) shows that the protein has some β-sheet content with a minimum at around 216 nm. ʎ5 ΔU Δβ C212S shows a far-UV CD spectrum (Figure 32A) of a protein that consists of β-sheets with a characteristic minimum at 218 nm. The spectrum shows a shoulder at around 230 nm due to its intramolecular disulfide bond.
The near-UV CD spectra of both proteins, ʎ5 Δβ C212S and ʎ5 ΔU Δβ C212S (Figure 32B), show similar spectra compared to ʎ5 C212S regarding the shape and the area around the aromatic residues. They have a characteristic shape between 285 and 295 nm around the tryptophane residues, indicative of folded proteins. Only ʎ5 ΔU Δβ C212S shows a greater difference compared to the other two β variants of λ5, which may be attributed to the deletion of the UR that seems to have a larger impact on the tertiary structure of the protein than the β-strand. Neither at around 265 nor at around 280 nm, there are peaks for all three proteins.
The insertion of the β-strand into VPREB or VPREB ΔU results in folded proteins in both cases. In the VPREB βU mutant, the β-strand was inserted between the core region and the UR, whereas in the VPREB ΔU + β-mutant, it was inserted C-terminal to the core region without the UR. The far-UV CD spectrum of VPREB βU (Figure 32C) is dominated by β-strands with some random

coil content and a characteristic minimum at around 216 nm. This indicates that VPREB is folded upon insertion of the β-strand. The random coil content can be attributed to the UR. VPREB ΔU+β resembles VPREB βU but missing the UR. As such, it is similar to a conventional V_L domain. Its far-UV CD spectrum reflects its similar architecture compared to a V_L domain with its predominant content of β-strands with a minimum at around 217 nm. It also has the shoulder at around 230 nm that is characteristic for the intramolecular disulfide bond. The VPREB ΔU + β-mutant lacks random coil content because of the missing UR. That VPREB attains its native structure also is reflected in the near-UV CD spectra (Figure 32D). While VPREB shows a flat line, both VPREB βU and VPREB ΔU + β show spectra that are characteristic of folded proteins with a defined shape around their aromatic residues. They have defined peaks between 285 and 295 nm for the tryptophanes and at around 280 nm for the tyrosines.

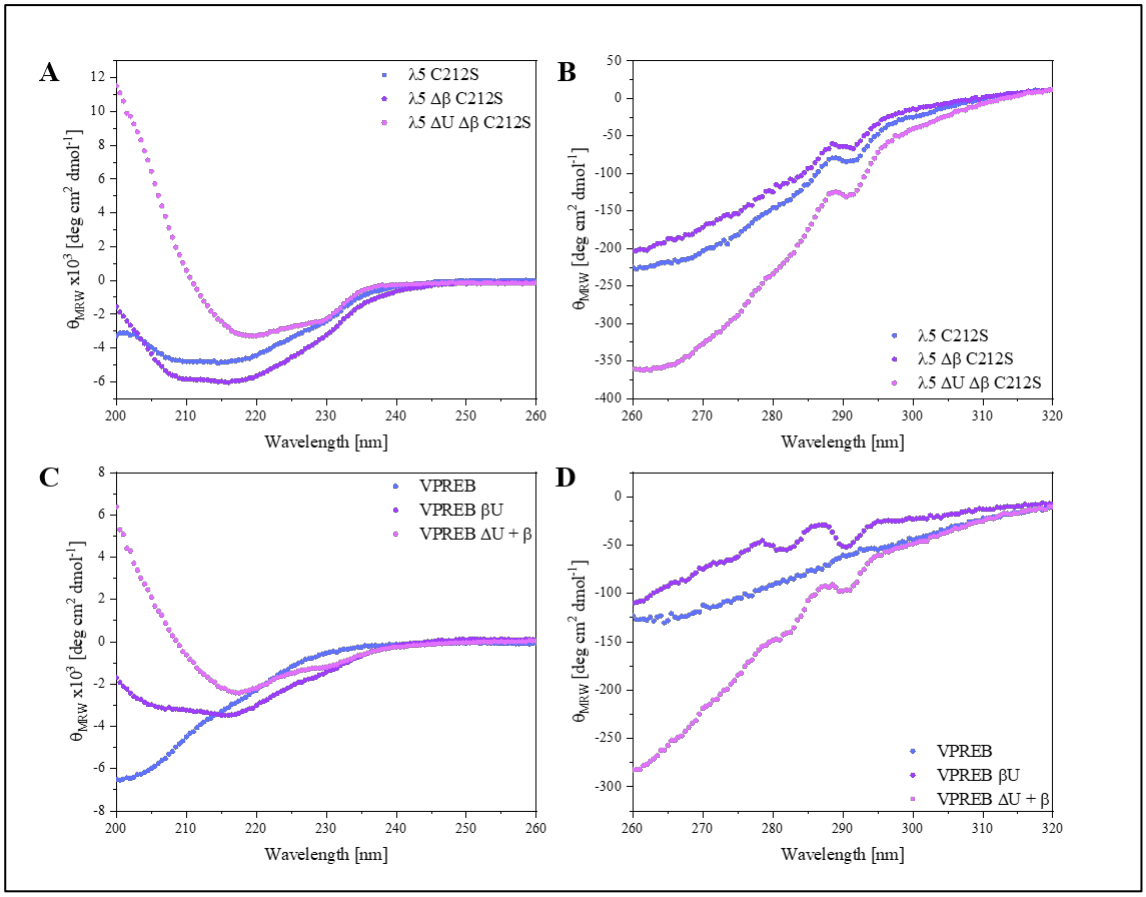

Figure 32: Secondary and Tertiary Structure Analysis of the β-Strand Swap Mutants of VPREB and λ5 C212S by Far- and Near-UV CD Spectroscopy.
Far- (**A**) and near-UV (**B**) CD spectra of λ5 C212S, λ5 Δβ C212S and λ5 ΔU Δβ C212S. Far- (**C**) and near-UV (**D**) CD spectra of VPREB, VPREB βU and VPREB ΔU + β.

2.3.3.2 Thermal Stability of β-Strand Swap Mutants

To evaluate wether the β-strand affects the thermal stabilities in both proteins, λ5 and VPREB, temperature-induced unfolding transitions were followed by far-UV CD spectroscopy at 205 nm.

Indeed, the additional β-strand of ʎ5 decreases its thermal stability (Figure 33A, Table 3). When deleted, the thermal stability is, compared to ʎ5 C212S, increased by about 3°C in the ʎ5 Δβ C212S mutant (59.0 ± 1.2°C) and by about 3.5 °C in the ʎ5 ΔU Δβ C212S mutant (59.5 ± 0.5°C). Compared to WT VPREB, VPREB βU and VPREB ΔU + β have a β-sheet-like structure according to their far-UV CD spectra and therefore it is possible to assess their thermal stabilities. Surprisingly, both mutants have high thermal stabilities with a T_m of 66.0 ± 1.3°C for VPREB βU and of 67.9 ± 2.0 °C for VPREB ΔU + β (Figure 33B, Table 3). This indicates that the additional β-strand of ʎ5 makes VPREB a stable protein when inserted directly into the amino acid sequence regardless of its UR.

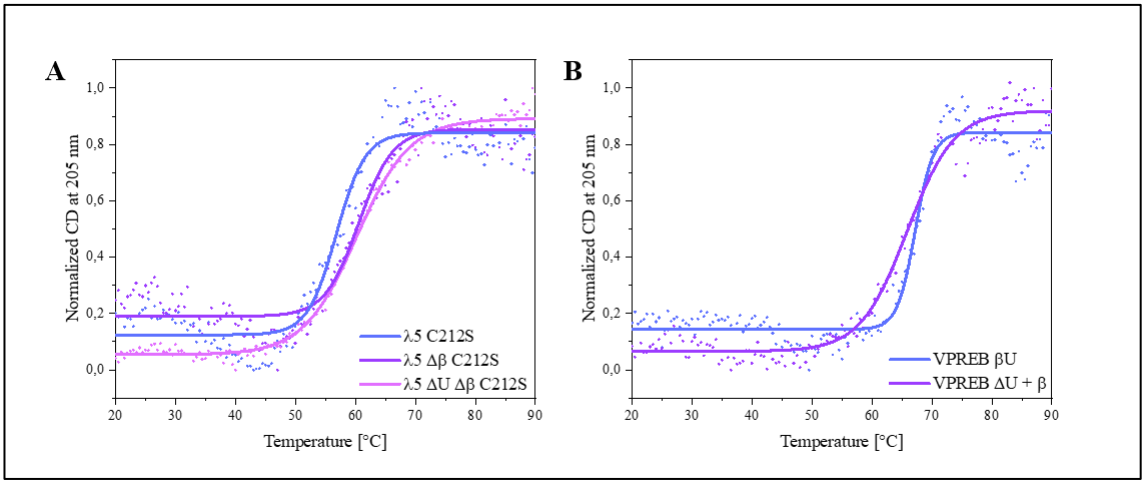

Figure 33: Conformational Stability of β-Strand Swap Mutants of VPREB and ʎ5 C212S.
Temperature-induced unfolding transitions followed by far-UV CD spectroscopy at 205 nm of ʎ5 C212S, ʎ5 Δβ C212S and ʎ5 ΔU Δβ C212S (**A**) and VPREB βU and VPREB ΔU + β (**C**). Solid lines represent the Boltzmann fit of the recorded data to determine the turning point, which reflects the T_m at which 50 % of the protein is unfolded.

Table 3: Melting Temperatures of β-Strand Swap Mutants of VPREB and ʎ5 C212S.

Protein	**T_m [°C]**
λ5 Δβ C212S	59.0 ± 1.2
λ5 ΔU Δβ C212S ΔU	59.5 ± 0.5
VPREB βU	66.0 ± 1.3
VPREB ΔU + β	67.9 ± 2.0

T_ms of the β-swap mutants of VPREB and ʎ5. The indicated error is the standard deviation of three technical replicates.

2.3.3.3 Quaternary Structure of β-Strand Swap Mutants

To determine, whether the β-strand affects the quaternary structure of ʎ5 and VPREB, AUC analysis was performed. As shown in Figure 34A, the β-strand has no influence on the quaternary structure of ʎ5 upon deletion. ʎ5 is predominantly a monomer regardless of its β-strand. Both, VPREB βU and VPREB ΔU + β, sedimented with a sedimentation coefficient of roughly 2 S (Figure 34B). The calculated molecular masses correspond to about 20 kDa. VPREB ΔU + β has a molecular weight of 13 kDa, which suggests a monomer-dimer equilibrium, as already reported in the literature (Morstadt et al., 2008). VPREB βU has a molecular weight of 16 kDa. So, the calculated mass of 20 kDa suggests a monomer-dimer equilibrium that is shifted to a monomeric species. This is also in accordance with the spectrum in Figure 34C. When the β-strand is added as a peptide to VPREB, the VPREB also exhibits a monomer-dimer equilibrium similar to VPREB ΔU + β with a calculated molecular weight of roughly 20 kDa and a sedimentation coefficient of 2 S.

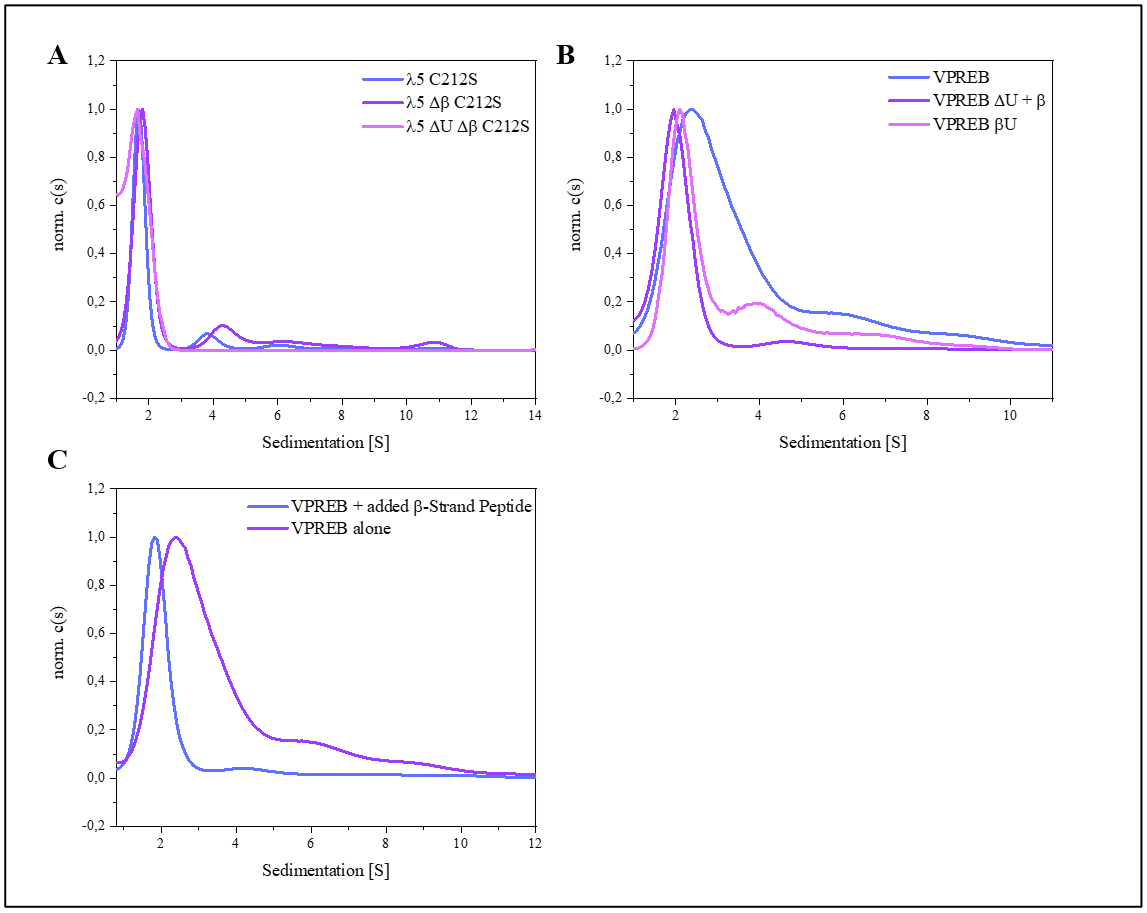

Figure 34: Quaternary Structure Analysis of the β-Strand Swap Mutants of VPREB and ʎ5 by AUC. AUC spectra of ʎ5 C212S, ʎ5 Δβ C212S and ʎ5 ΔU Δβ C212S are depicted in **A**, of VPREB, VPREB βU and VPREB ΔU + β in **B** and of VPREB alone and in complex with the β-strand as an added peptide in **C**.

In conclusion, VPREB alone is an unfolded homodimer. It forms a heterodimer dimer when it is folded with its missing β-strand supplemented from ʎ5 and it exhibits a monomer-dimer equilibrium. This also explains why VPREB and ʎ5 form a heterodimer and not a heterotrimer.

2.3.4 Characterization of the Tryptophane Mutants

2.3.4.1 Secondary and Tertiary Structure of Tryptophane Mutants

The URs of ʎ5 and VPREB contain several tryptophanes of which three are in the ʎ5-UR and one is in the VPREB-UR. These tryptophanes are interesting because normally tryptophanes are buried inside of proteins when they are folded. However, in the URs, they are potentially surface exposed in protruding segments. Thus, all UR-tryptophanes were mutated to alanines to see their influence on the secondary and tertiary structures, respectively.

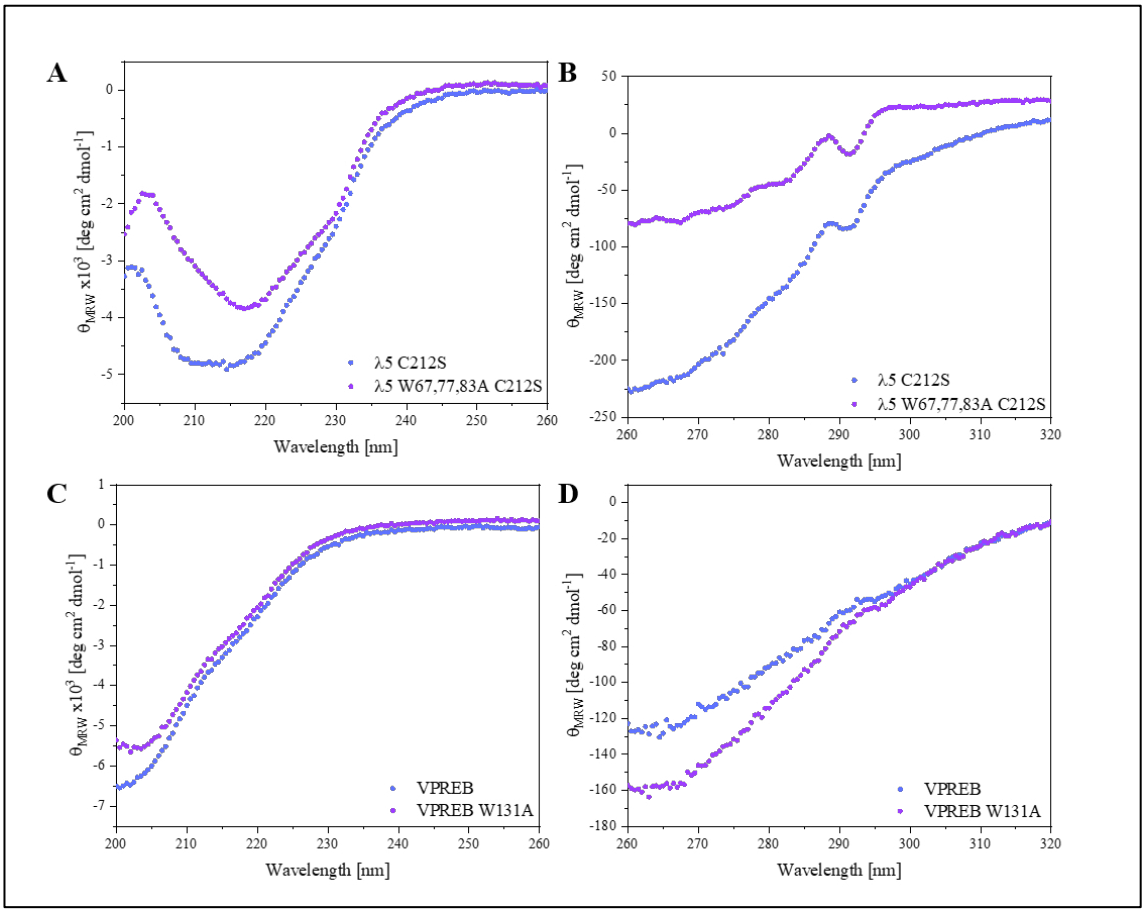

Figure 35: Secondary and Tertiary Structure Analysis of Tryptophane Mutants of VPREB and ʎ5 C212S by Far- and Near-UV CD Spectroscopy.
Far- (**A**) and near-UV (**B**) CD spectra of ʎ5 C212S and ʎ5 W67,77,83A C212S. Far- (**C**) and near-UV (**D**) CD spectra of VPREB and VPREB W131A.

The far-UV CD spectrum of ʎ5 W67,77,83A C212S (Figure 35A) shows a higher β-sheet content than ʎ5 C212S. It has a characteristic minimum at around 218 nm and a maximum at around 204 nm. It also shows the shoulder at around 230 nm for its intramolecular disulfide bridge.
The tertiary structure analysis of ʎ5 W67,77,83A C212S by near-UV CD spectroscopy shows a difference in the spectrum compared to that of ʎ5 C212S (Figure 35B). The shape is very similar showing structure around the aromatic residues, but the intensity is decreased in the tryptophane mutant with a more pronounced minimum indicating that it is more structured compared to ʎ5 C212S. Both, WT and mutant have a characteristic peak between 285 and 295 nm. In addition, λ5 W67,77,83A C212S also has small peaks at around 265 nm and 280 nm. This indicates a higher degree of structure in the mutant compared to the WT. In conclusion, according to the far- and near- UV CD data, the tryptophane mutant seems to be more folded.
The far-UV CD spectra of VPREB and VPREB W131A (Figure 35C) are very similar and characteristic of an unfolded protein consisting of random-coil like structures. Therefore, the tryptophane in the VPREB UR does not impact the secondary structure of VPREB. This is also reflected in the near-UV CD spectra, which are very similar for the two proteins (Figure 35D).

2.3.4.2 Thermal Stability of Tryptophane Mutants

Since the tryptophane mutations in the UR of ʎ5 C212S have an impact on the secondary structure of ʎ5, it was interesting to see, if this is also reflected in its thermal stability. The stability was assessed by thermal-induced unfolding transitions followed by CD spectroscopy at 205 nm.

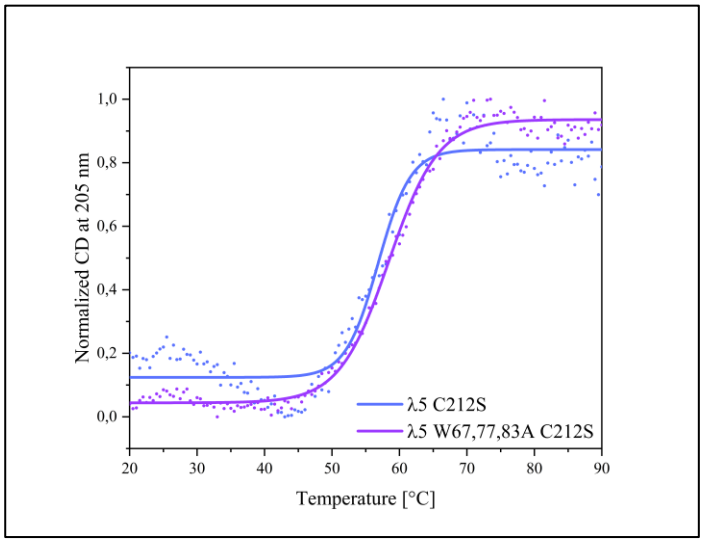

Figure 36: Conformational Stability of Tryptophane Mutant of ʎ5 C212S.
Temperature-induced unfolding transitions followed by CD spectroscopy at 205 nm of ʎ5 C212S and ʎ5 W67,77,83A C212S. Solid lines represent the Boltzmann fit of the recorded data to determine the turning point, which reflects the T_m at which 50 % of the protein is unfolded.

With a T_m of 57.5 ± 0.8°C, the thermal stability of λ5 W67,77,83A C212S was increased by about 2°C compared to λ5 C212S (55.8 ± 0.7°C) as shown in Figure 36 and Table 4. With VPREB W131A being unfolded, no thermal stability could be measured. Thus, the tryptophanes in the λ5-UR have an impact on the secondary and tertiary structure as well as on the thermal stability of λ5, which is interesting since the tryptophanes are in the protruding UR and were therefore supposed to have no impact on the overall structure of λ5.

Table 4: Melting Temperatures of Tryptophane Mutants of VPREB and λ5 C212S.

Protein	**T_m [°C]**
λ5 W67,77,83A C212S	57.5 ± 0.8
VPREB W131A	n. d.

T_ms of the tryptophane mutants of VPREB and λ5 C212S. The indicated error is the standard deviation of three technical replicates. n. d.: not determined as VPREB W131A is unfolded.

2.3.4.3 Quaternary Structure of Tryptophane Mutants

To determine, whether the tryptophanes in the URs of λ5 and VPREB affect the quaternary structure, AUC analysis was performed. As shown in Figure 37A, the tryptophanes in the λ5-UR have no influence on the quaternary structure of λ5. λ5 is predominantly a monomer independent of the tryptophanes. VPREB W131A showed a very similar AUC profile (Figure 37B) compared to that of VPREB. Therefore, the tryptophane mutation in the VPREB-UR has no influence on the quaternary structure.

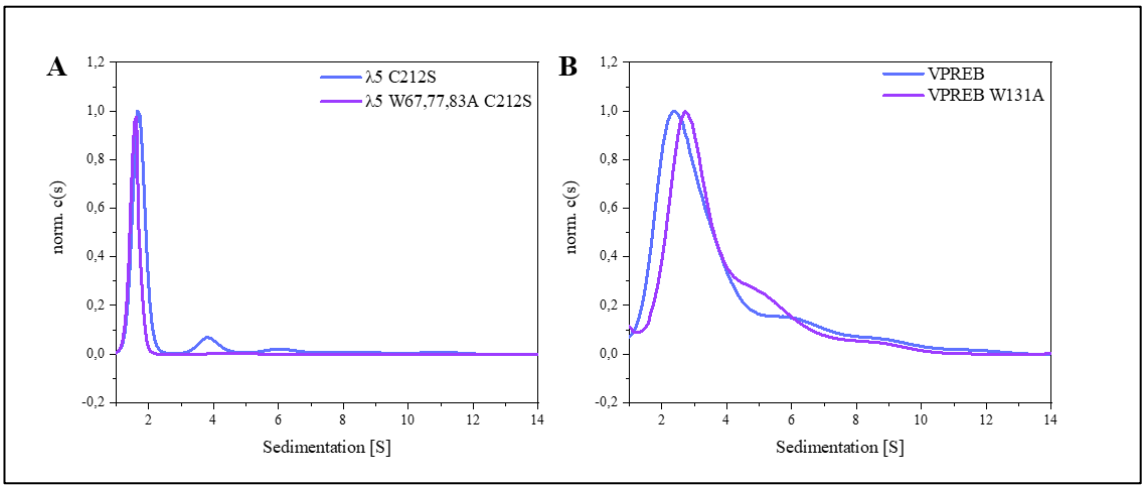

Figure 37: Quaternary Structure Analysis of the Tryptophane Mutants of VPREB and λ5 by AUC. AUC spectra of λ5 C212S and λ5 W67,77,83A C212S are depicted in (**A**), of VPREB and VPREB W131A in (**B**).

2.3.5 Characterization of the Glutamate Mutant of VPREB

2.3.5.1 Secondary and Tertiary Structure of the VPREB Glutamate Mutant

To figure out, whether the glutamates in the UR of VPREB have an impact on the secondary and tertiary structure, a mutant with all the glutamates mutated to glutamines was generated and far- and near-UV CD spectra were recorded. The far-UV CD spectrum of VPREB 9EurQ (Figure 38A) shows a spectrum typical of an unfolded protein that is dominated by random-coil like structures. However, its far-UV CD spectrum shows some deviation from the WT spectrum with a minimum at around 206 nm.

The near-UV CD spectrum of VPREB 9EurQ (Figure 38B) shows a difference to the spectrum of WT VPREB. Despite the unfolded nature of both proteins, the amplitude of the spectrum of VPREB 9EurQ is three times as high as that of the WT. A change in the structure compared to WT seems likely. However, in both proteins, there is neither a peak at 265, 280, nor at around 290 nm, which corroborates that WT and mutant are unfolded.

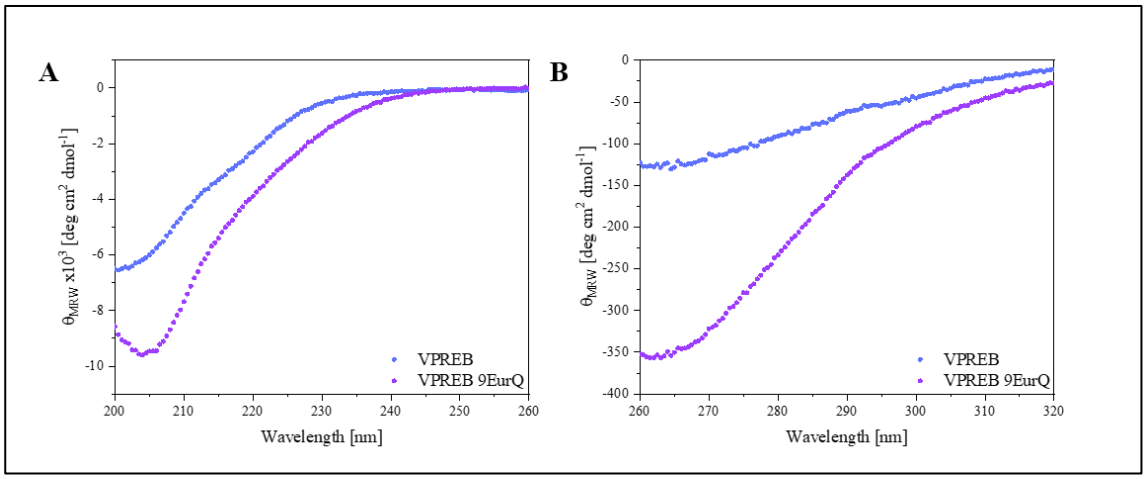

Figure 38: Secondary and Tertiary Structure Analysis of the Glutamate Mutant of VPREB by Far- and Near-UV CD Spectroscopy.
Far- (**A**) and near-UV (**B**) CD spectra of VPREB and VPREB 9EurQ.

2.3.5.2 Quaternary Structure of the VPREB Glutamate Mutant

The quaternary structure analysis of VPREB 9EurQ by AUC revealed it to be predominantly dimeric as WT VPREB (Figure 39).

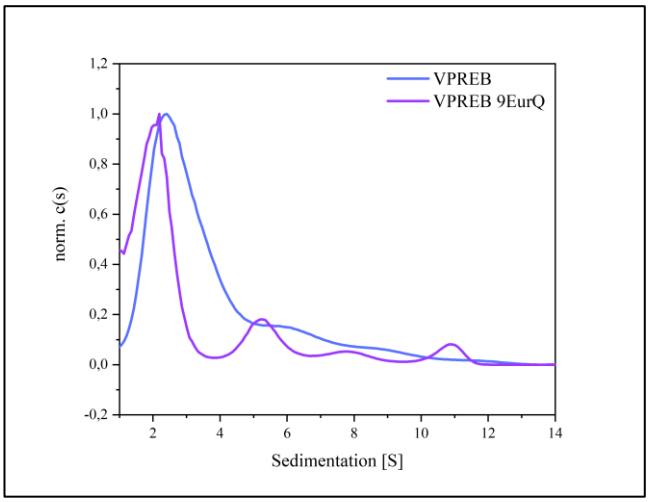

Figure 39: Quaternary Structure Analysis of the Glutamate Mutant of VPREB by AUC.

2.3.6 Glutaraldehyde Crosslinking of VPREB Variants

For verification of the AUC measurements, that showed VPREB, VPREB ΔU, VPREB W131A, VPREB 9EurQ to be homodimeric and VPREB βU as well as VPREB ΔU + β to be shifted towards a monomer in a monomer-dimer equilibrium, crosslinking with glutaraldehyde as a chemical crosslinker was performed (Figure 40). The crosslink covalently connects two lysine residues by one glutaraldehyde molecule. This interaction features a low specificity and only forms a bond between two proteins that are near to each other, which is the case in dimeric or oligomeric proteins. λ5 ΔU Δβ C212S and FOR005-PT (kindly provided by Georg Rottenaicher) served as negative controls that do not form a dimer and SLC C212S served as a positive control for a dimer. In addition, glutaraldehyde crosslinking was performed with λ5 C212S. As can be seen, there are clear monomer- as well as weak dimer-bands for VPREB, VPREB ΔU, VPREB W131A and VPREB 9EurQ. There are only monomer bands for VPREB βU and VPREB ΔU + β. Notably, the dimer band for VPREB ΔU is the weakest. From this, it can be concluded that VPREB forms a dimer regardless of its UR, the negatively charged glutamates as well as the tryptophane in its UR. Nonetheless, the UR seems to support the dimerization of VPREB. Therefore, both the UR and the core region are involved in dimer formation. Furthermore, it is notable that λ5 C212S is also able to form a dimer to a small extent. This coincides with the AUC data, which also shows λ5 C212S to be able to form dimers to a very small amount.

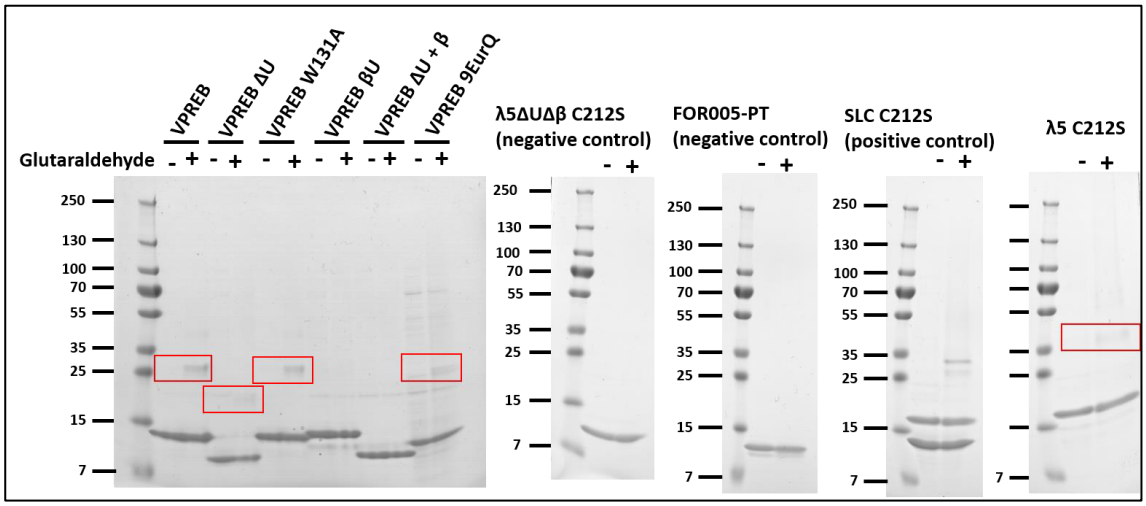

Figure 40: Glutaraldehyde Crosslinking of VPREB Variants.
Glutaraldehyde crosslinking was performed with the following VPREB variants: WT VPREB, VPREB ΔU, VPREB W131A, VPREB βU, VPREB ΔU + β and VPREB 9EurQ (left). ʎ5 ΔU Δβ C212S and FOR005-PT (kindly provided by Georg Rottenaicher) served as negative controls, while SLC C212S served as a positive control (middle). Glutaraldehyde crosslinking was also performed with ʎ5 C212S (right). "-" indicates no added glutaraldehyde, while "+" indicates added glutaralaldehyde.

2.4 Analysis of Conformational Dynamics by HDX-MS

2.4.1 VPREB Variants

To identify the possible interaction sites that are involved in the dimer interface of VPREB, VPREB ΔU, VPREB W131A and VPREB 9EurQ, the conformational dynamics, assessed by HDX-MS, throughout the variants were compared. The B value after 2 h of HDX was plotted on the residue number of the proteins (Figure 41). The B value represents the flexibility of the amino acids of the protein. The higher the B values, the higher is the flexibility of the respective amino acid (Sun et al., 2019). The residues that are involved in the interface with V_H are marked in green each, the URs in orange, the residues involved in interaction with λ5 are marked in violet and the β-strand in blue. While for VPREB, VPREB ΔU, VPREB W131A and VPREB 9EurQ, the B-values are fully displayed, VPREB βU and VPREB ΔU + β are only depicted with their core regions. Therefore, a separate plot (Figure 41B) was made to provide the data for β-strand and UR as well.

Overall, the variants show very diverse conformational dynamics. However, the UR exhibits similar conformational dynamics for all variants with a B value of roughly 0.55. The UR is one of the most flexible parts throughout the protein. This is not surprising because the UR is known to protrude. Remarkably, VPREB βU and especially VPREB ΔU + β have overall lower B values, i. e. decreased conformational dynamics, in their core domain and the additional β-strand, compared to the other variants, which might be attributed to their folding status. Upon folding, most segments are buried in the inside of proteins and a smaller portion is left to be surface-exposed, which can be also observed in the crystal structures of the respective proteins.

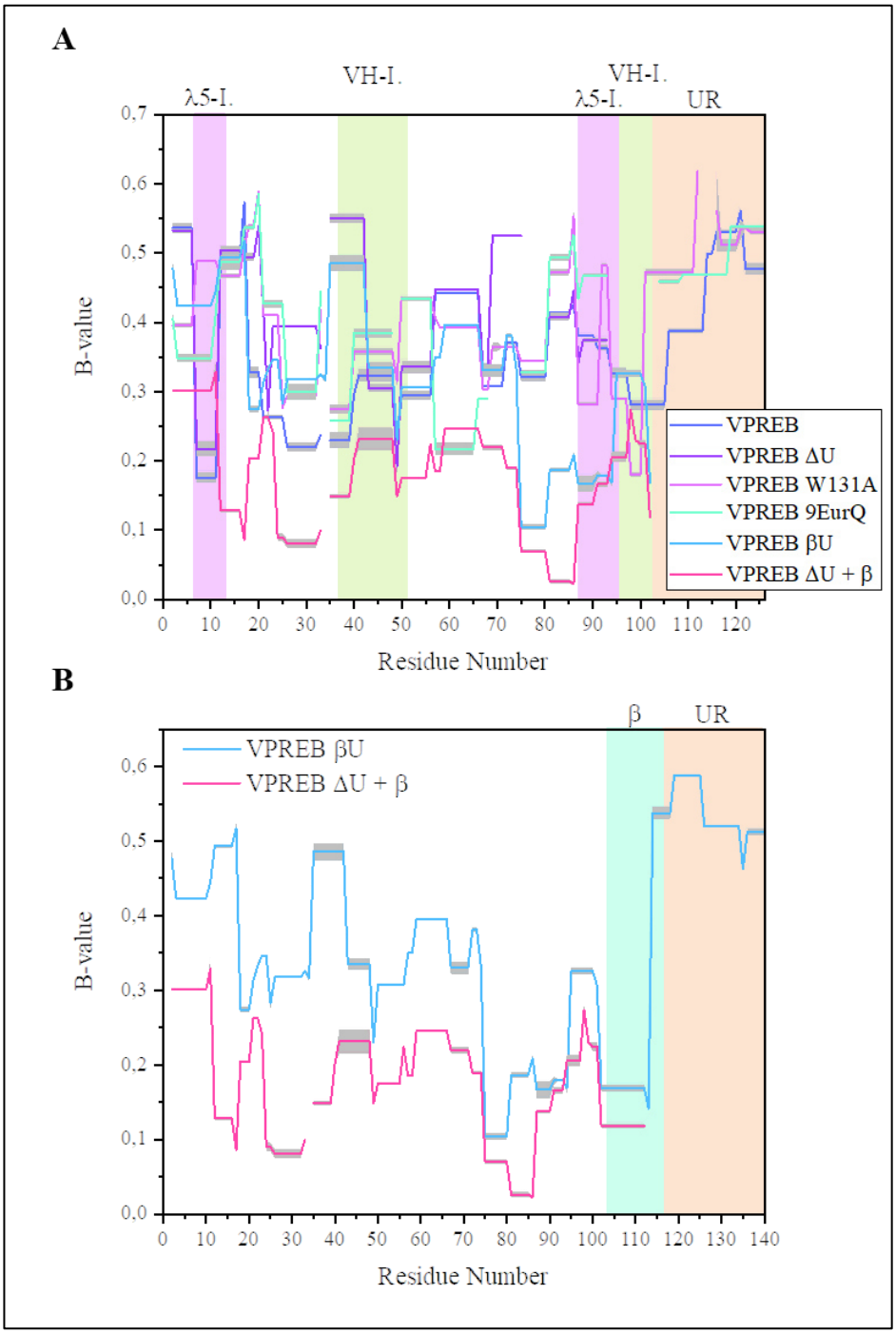

Figure 41: Conformational Dynamics of VPREB Variants by HDX-MS After 2 h of HDX.
B Values obtained from HDX-MS after 2 h of HDX are plotted against the residue number of the primary structure for each VPREB variant. VPREB, VPREB ΔU, VPREB W131A, VPREB 9EurQ, VPREB βU and VPREB ΔU + β are shown in (**A**). VPREB βU and VPREB ΔU + β are shown in (**B**). The URs are coloured in orange, the interface with ʎ5 in violet, the interface with V_H in green and the β-strand in turquoise. The colour assignments of the graphs are in the captions.

In the unfolded variants (VPREB, VPREB ΔU, VPREB W131A, VPREB 9EurQ), no pattern can be observed that shows low B values. Low B values and therefore parts with lower flexibility and lower conformational dynamics might represent segments that are involved in the dimer interface. This could mean that different portions in different mutants of the unfolded VPREB are involved

in dimerization. It is likely that VPREB forms a dimer at the interface with the V_H domain. Taken into account that the unfolded VPREB variants display B values in the range between 0.2 and 0.6, one can make the assumption that segments with B values lower than 0.3 or even 0.4 can be considered as less flexible areas. Segments, where all unfolded VPREB variants have B values lower than 0.4, are at amino acid positions 40 to 48 and again from positions 95 to 101. These two segments are involved in the interface with the V_H domain. Notably, in VPREB and VPREB ΔU, there is a very protected portion towards the N-terminus from amino acid 6 to 12 with B values of 0.17 and 0.21, respectively. The B value of VPREB 9EurQ is quite low with 0.35 in this segment. This segment is involved in the interaction with the additional β-strand of λ5. The same can be observed for the second interaction site with λ5 that displays, except for VPREB 9 EurQ, B values lower than 0.4. It seems that predominantly the V_H interfaces are also the dimer interfaces of VPREB, while the λ5 interaction sites play minor roles in the dimer formation of VPREB.

2.4.2 The SLC Complex

To gain insight into the conformational dynamics that change upon complex formation of λ5 and VPREB, differential HDX-MS analysis was used (Figure 42). The uptake of deuterium by VPREB and λ5 C212S was compared for the single proteins and the complex after 2 h of HDX. In the complex, especially the additional β-strand of ʎ5 is significantly more protected. This is reasonable because the β-strand is the main part that interacts with VPREB and is buried in the folded VPREB protein. Throughout ʎ5, in the UR as well as in the core region, most of the peptides are protected to a smaller extent. This may be due to some structural rearrangements upon interaction with VPREB. Interestingly, also segments in the UR are protected, which is surprising since the URs are thought to be unfolded and protruding from the complex. The Wood´s plot of complexed VPREB compared to single VPREB (Figure 42B) shows protected peptides for most of the protein. This is not surprising since the far- and near-UV CD data in section 2.3.1.1 showed VPREB alone to be unfolded. Not only the core region gets protected but also the UR. The protection is almost 3-fold compared to the protection of the UR in λ5 C212S. In conclusion, the folding of VPREB upon complex formation with λ5 C212S is reflected by the high number of protected peptides, not only in the core region but also in the UR. Also, λ5 C212S seems to experience some structural rearrangements, which can be seen in the protection of the peptides in core and UR, most prominently at the β-strand. The protection of the additional β-strand can be attributed to its interaction with VPREB that supplements its missing β-strand.

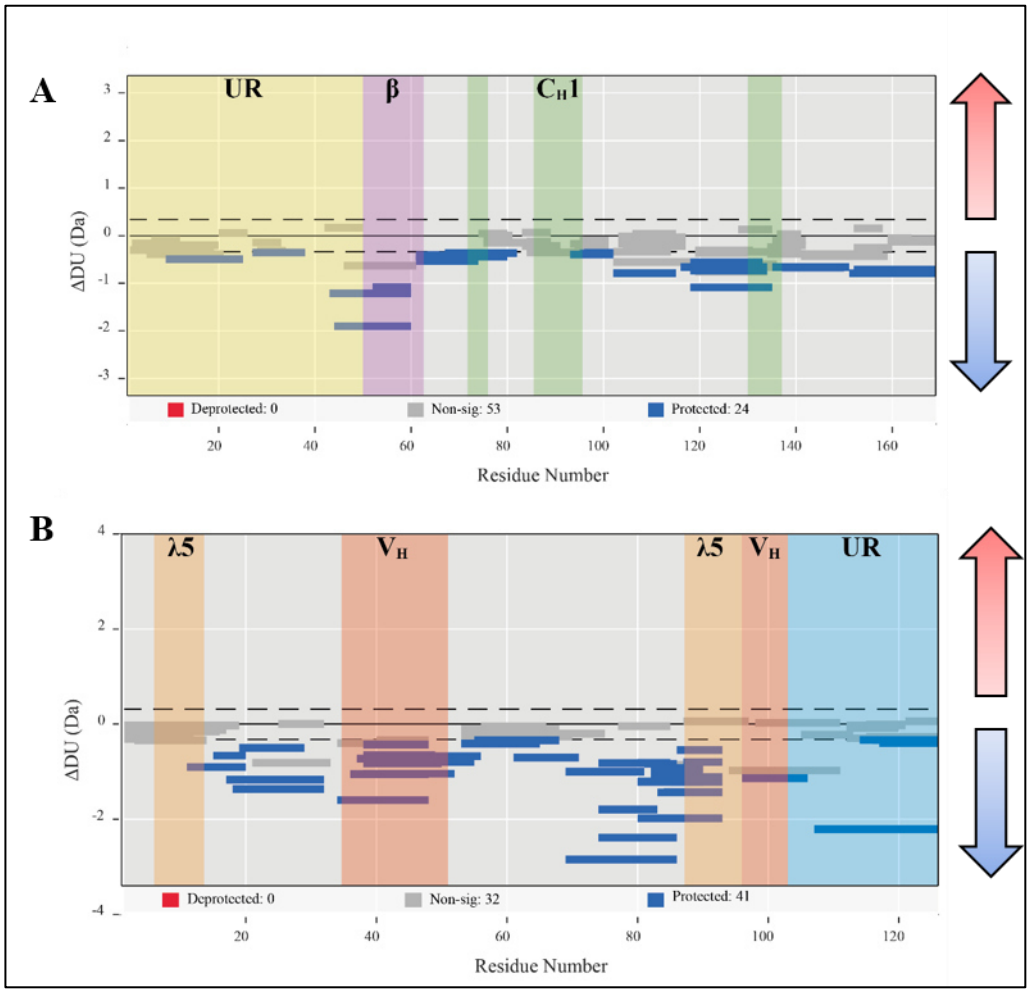

Figure 42: Conformational Dynamics of VPREB and ʎ5 C212S in the SLC Complex by Differential HDX-MS.
Wood´s plots showing the summed differences in deuterium uptake (ΔDU) in Dalton (Da) in VPREB and ʎ5 C212S after 2 h of HDX, comparing ʎ5 C212S alone with ʎ5 C212S in the presence of VPREB (**A**) and VPREB alone with VPREB in the presence of ʎ5 C212S (**B**). Wood´s plots were generated using Deuteros (Lau et al., 2020). Peptides coloured in blue or red, respectively, are protected or deprotected from exchange in the presence of the SLC counterpart protein each. Peptides with no significant difference between conditions, determined using a 99 % confidence interval (dotted line) and a p value < 0.1, are shown in grey. The VPREB-UR is coloured in blue, the λ5-UR in yellow, the λ5-interface in orange, the V_H-interface in red, the additional β-strand in magenta and the C_H1-interface in green.

2.4.3 λ5 ΔU C212S and VPREB ΔU

To compare the conformational dynamics between the single ΔU-mutants with λ5 C212S and WT VPREB, differential HDX-MS was performed after 2 h of HDX (Figure 44). The comparison of λ5 ΔU C212S with λ5 C212S revealed only a very significant change in the β-strand, which is deprotected to a high degree. In the core region, there are no big changes in conformational dynamics. In VPREB ΔU, there are no changes at all regarding the conformational dynamics compared to VPREB.

In conlusion, the deprotection of the β-strand may be attributed to the UR. It seems to influence the conformational dynamics by stabilizing the β-strand away from the surface. Moreover, since

VPREB and VPREB ΔU are both unfolded, as expected, no change in conformational dynamics was observed.

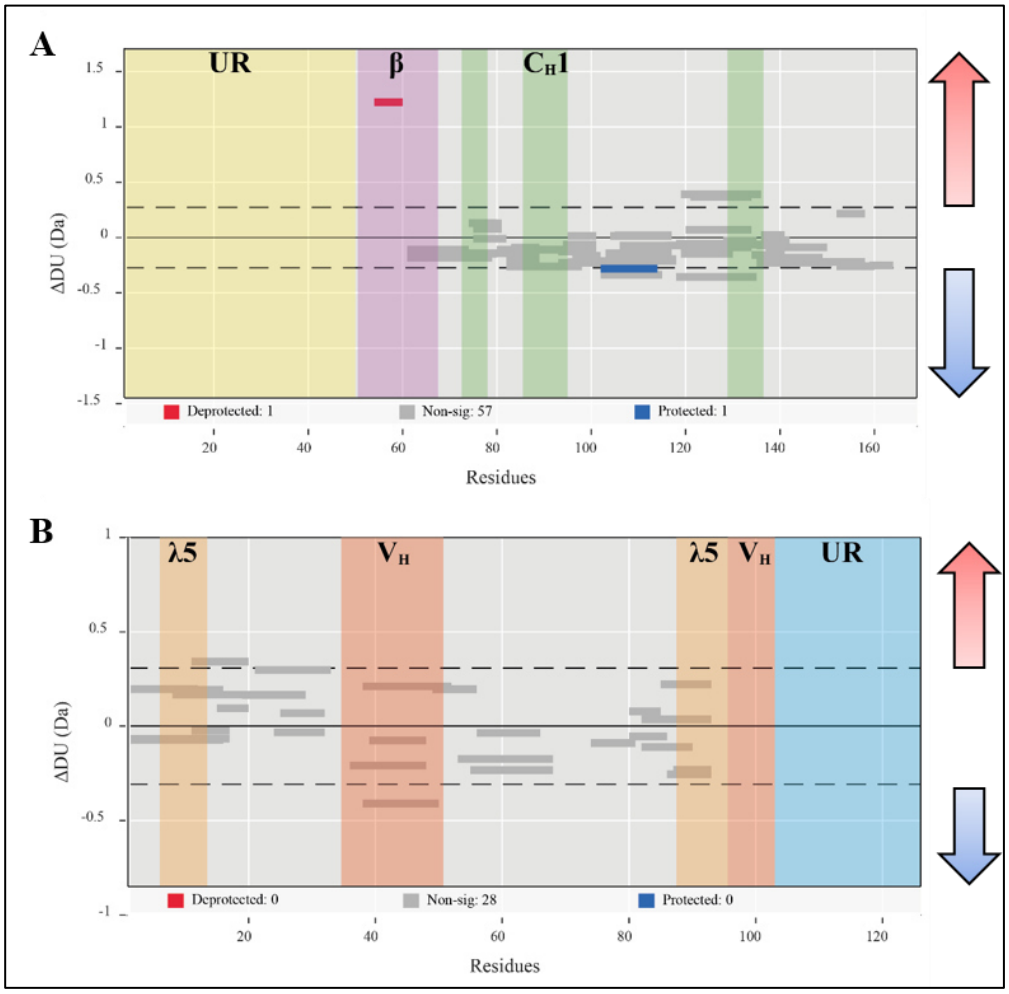

Figure 43: Comparison of Protection/Deprotection in the Single ΔU-Mutants Compared to the Single WT Proteins by Differential HDX-MS Analysis.
Wood´s plots showing the summed differences in deuterium uptake in ʎ5 ΔU C212S and VPREB ΔU after 2 h of HDX, comparing ʎ5 ΔU C212S with ʎ5 C212S (**A**) and VPREB ΔU with VPREB (**B**). Wood´s plots were generated using Deuteros (Lau et al., 2020). Peptides coloured in blue or red, respectively, are protected or deprotected from exchange in the ΔU-mutants compared to the WT SLC proteins. Peptides with no significant difference between conditions, determined using a 99 % confidence interval (dotted line) and a p value < 0.1, are shown in grey. The VPREB-UR is coloured in blue, the λ5-UR in yellow, the λ5-interface in orange, the V_H-interface in red, the additional β-strand in magenta and the C_H1-interface in green.

2.4.4 The SLC ΔU Complex

To gain insight into the influence of the UR on the conformational dynamics upon complex formation, the uptake of deuterium by VPREB ΔU and λ5 ΔU C212S was compared between the single proteins and the complex after 2 h of HDX (Figure 44). As depicted in Figure 44A, the additional β-strand in λ5 ΔU C212S is protected upon complex formation with VPREB ΔU to a much lesser extent than observed for λ5 C212S when it forms a heterodimer with VPREB. Also, in the core region, there is less protection in complexed λ5 ΔU C212S than it is the case for

complexed λ5 C212S, which indicates that λ5 ΔU C212S can attain its native structure quite alone. The lower degree of protection in the β-strand suggests that, because of the missing UR, λ5 ΔU C212S experiences less deprotection of the β-strand and rather be more included in the β-strand-fold of the single λ5 ΔU C212S protein. Therefore, no big changes can be observed upon complex formation with VPREB.

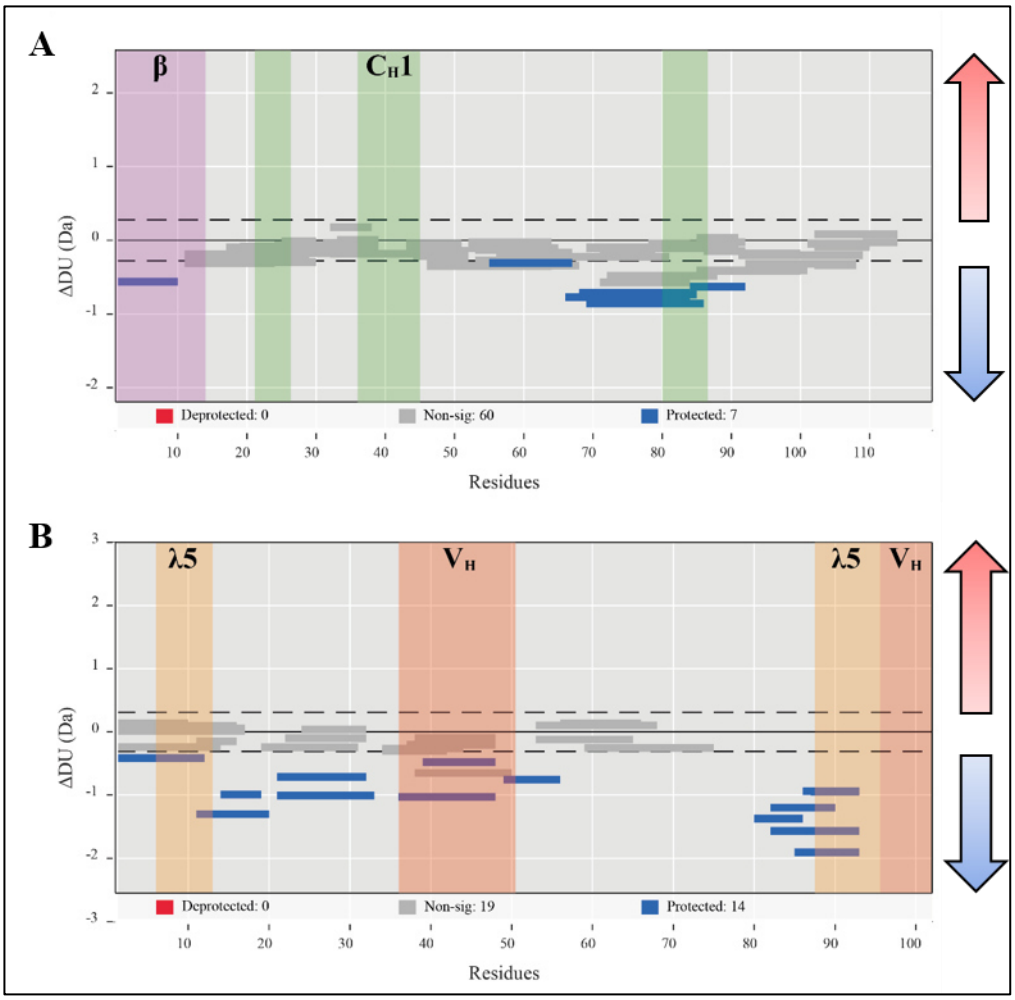

Figure 44: Complex Formation of VPREB ΔU and ʎ5 ΔU C212S Leads to Protection in Both Proteins by Differential HDX-MS Analysis.
Wood´s plots showing the summed differences in deuterium uptake in VPREB ΔU and ʎ5 ΔU C212S after 2 h of HDX, comparing ʎ5 ΔU C212S alone with ʎ5 ΔU C212S in the presence of VPREB ΔU (**A**) and VPREB ΔU alone with VPREB ΔU in the presence of ʎ5 ΔU C212S (**B**). Wood´s plots were generated using Deuteros (Lau et al., 2020). Peptides coloured in blue or red, respectively, are protected or deprotected from exchange in the presence of the counterpart protein each. Peptides with no significant difference between conditions, determined using a 99 % confidence interval (dotted line) and a p value < 0.1, are shown in grey. The VPREB-UR is coloured in blue, the λ5-UR in yellow, the λ5-interface in orange, the V_H-interface in red, the additional β-strand in magenta and the C_H1-interface in green.

Secondly, the protection in VPREB ΔU upon complex formation with λ5 ΔU C212S (Figure 44B) is less pronounced as it is in VPREB when complexed with λ5 C212S. There is also a region from amino acids 55 to 80, that is not protected. This region is neither involved in the interaction with λ5 nor with V_H. In WT VPREB, there is barely any region that is not protected.

λ5 ΔU C212S shows less protected peptides compared to λ5 C212S upon complex formation with VPREB ΔU and VPREB, respectively. Furthermore, the UR seems to have an impact on the conformational dynamics of the β-strand. However, VPREB ΔU shows less protection compared to VPREB upon SLC formation, which is surprising since both proteins are unfolded according to CD spectroscopy (Figure 28).

2.4.5 SLC ΔU C212S and SLC C212S

To gain understanding of how the URs affect the conformational dynamics in the SLC ΔU C212S-complex compared to the WT complex, differential HDX-MS was applied after two hours of HDX (Figure 45).

The differential HDX-MS of complexed λ5 ΔU C212S compared to complexed λ5 C212S (Figure 45A) revealed only a highly deprotected peptide in the β-strand region. The core region of ʎ5 ΔU C212S has no significant change in conformational dynamics except one minor protected peptide at the C-terminal end. When comparing complexed WT VPREB with complexed VPREB ΔU, the latter one has more protected protein segments.

Altogether, this suggests that the structure of the core region remains predominantly the same between λ5 ΔU C212S and λ5 C212S when in complex. The deprotected β-strand in complexed λ5 ΔU C212S can be attributed to the missing UR that seems to stabilize the β-strand when in complex with VPREB. The more protected protein segments in VPREB ΔU can be attributed to the missing UR that seems to have a negative influence on the stability of VPREB when in complex with λ5 C212S.

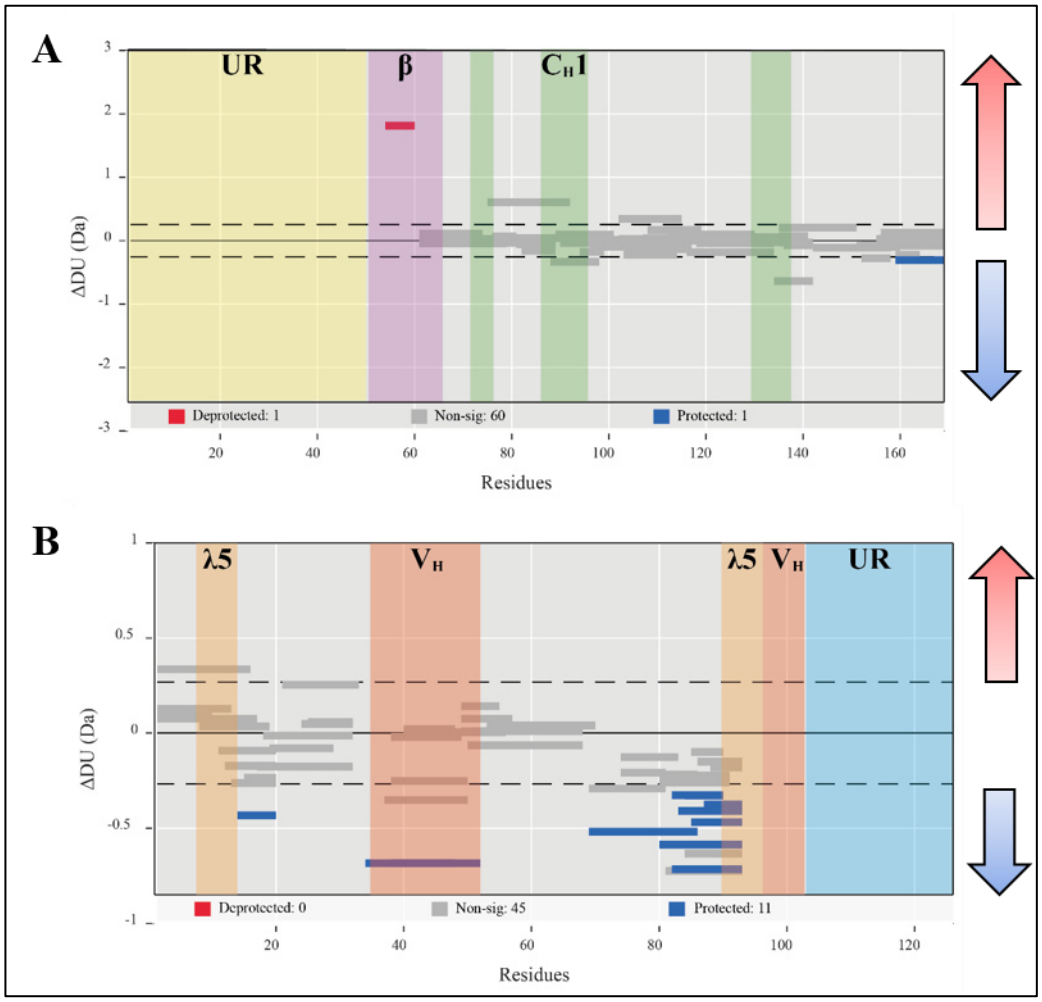

Figure 45: The Complex SLC ΔU C212S Shows Varying Patterns of Protection and Deprotection Compared to SLC C212S by Differential HDX-MS Analysis.
Wood´s plots showing the summed differences in deuterium uptake in SLC ΔU C212S and SLC C212S after 2 h of HDX, comparing ʎ5 ΔU C212S in the presence of VPREB ΔU with ʎ5 C212S in the presence of VPREB (**A**) and VPREB ΔU in the presence of ʎ5 ΔU C212S with VPREB in the presence of ʎ5 C212S (**B**). Wood´s plots were generated using Deuteros (Lau et al., 2020). Peptides coloured in blue or red, respectively, are protected or deprotected from exchange in the ΔU-mutants in complex compared to the WT complex. Peptides with no significant difference between conditions, determined using a 99 % confidence interval (dotted line) and a p value < 0.1, are shown in grey. The VPREB-UR is coloured in blue, the λ5-UR in yellow, the λ5-interface in orange, the V_H-interface in red, the additional β-strand in magenta and the C_H1-interface in green.

2.4.6 β-Strand Swap Mutants

To assess the influence that the additional β-strand has on conformational dynamics of λ5 Δβ C212S and ʎ5 ΔU Δβ C212S, differential HDX-MS after 2 h of HDX was performed and analyzed (Figure 46). When deleting the β-strand, but keeping the UR, peptides in the core region are deprotected, especially in the middle part between amino acid 100 and 140 and at the C-terminal end, starting at amino acid 150 (Figure 46A). There is also one peptide deprotected to a lower extent at the N-terminal end of the core region of λ5 between amino acid 65 and 80. With the β-strand, the UR seems to be covering the core region. The UR shows no difference in conformational dynamics. Comparing the λ5 ΔU Δβ C212S mutant with λ5 C212S by differential

HDX-MS after 2 h of HDX (Figure 46B), the effect is reverse, causing the core region to be more protected. This could be due to λ5 ΔU Δβ C212S resembling a conventional C_L domain and therefore attaining a more globular structure than the variants with the UR.

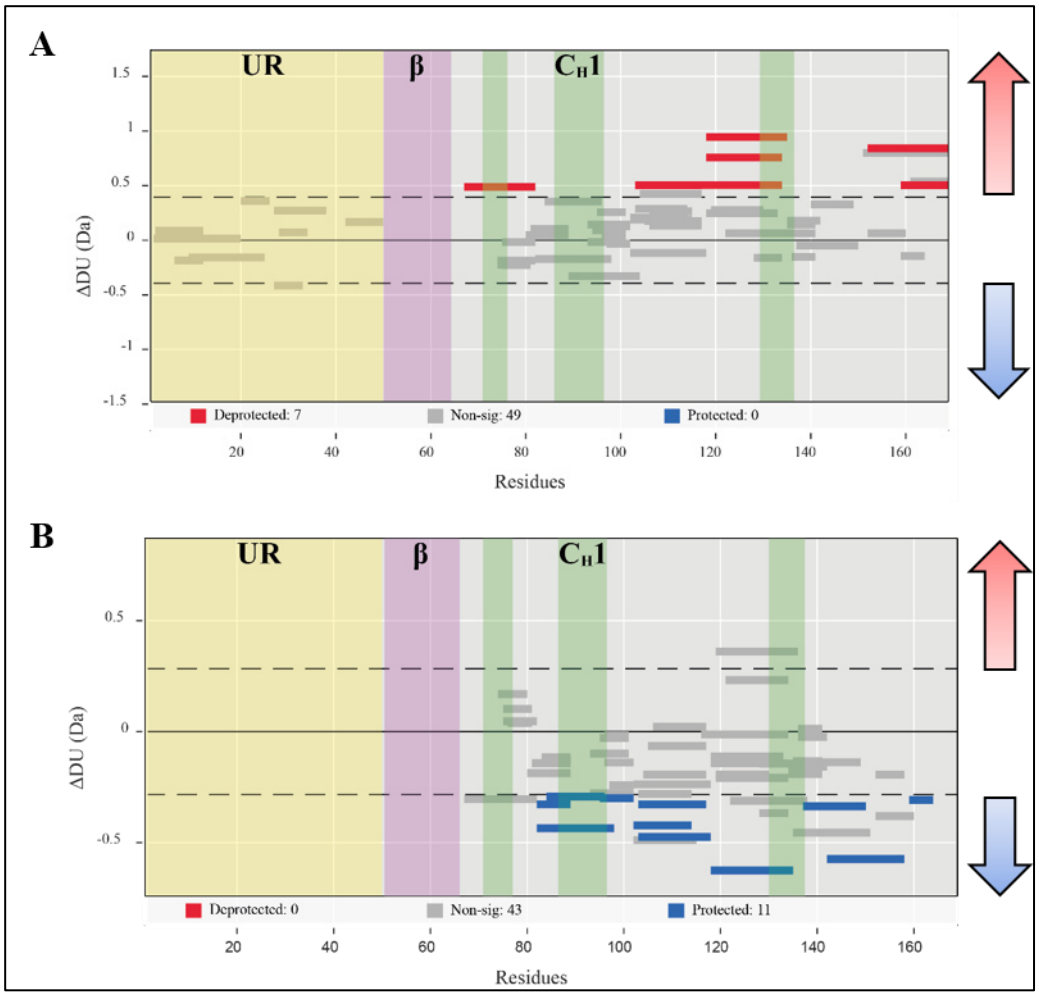

Figure 46: Comparison of Protection/Deprotection in the Δβ-Mutants of ʎ5 C212S with ʎ5 C212S by Differential HDX-MS Analysis.
Wood´s plots showing the summed differences in deuterium uptake in ʎ5 Δβ C212S and ʎ5 ΔU Δβ C212S after 2 h of HDX, comparing ʎ5 Δβ C212S with ʎ5 C212S (**A**) and ʎ5 ΔU Δβ C212S with ʎ5 C212S (**B**). Wood´s plots were generated using Deuteros (Lau et al., 2020). Peptides coloured in blue or red, respectively, are protected or deprotected from exchange in the Δβ-mutants compared to ʎ5 C212S. Peptides with no significant difference between conditions, determined using a 99 % confidence interval (dotted line) and a p value < 0.1, are shown in grey. The λ5-UR is coloured in yellow, the additional β-strand in maganta and the C_H1-interface in green.

Next, the influence of the β-strand on VPREB was investigated. Conformational dynamics between VPREB βU and VPREB was examined by differential HDX-MS after 2 h of HDX (Figure 47A). As expected, the peptides are more protected in the core region of VPREB βU compared to WT VPREB, especially between amino acids 70 and 90. The reason could be that VPREB βU attains its native structure compared to WT VPREB (section 2.3.3.1) because of the addition of the β-strand between the core region and the UR. However, the UR is more deprotected in VPREB βU compared to WT VPREB, which can be ascribed to the change in the

position of the UR. In the βU-mutant, VPREB has the UR protruding about 180° from the opposite side of the protein, as described in more detail in section 2.2. This may have an influence on how rigid the UR is protruding from the protein and on the secondary structure that the UR forms with itself.

Furthermore, the comparison of the conformational dynamics between VPREB βU and VPREB in complex with λ5 C212S is interesting (Figure 47B). Differential HDX-MS after 2 h of HDX revealed that the core region of VPREB βU is more protected compared to WT VPREB, whereas the UR is more deprotected. This is somewhat surprising since it was expected that VPREB is equally folded when the β-strand is present. Apparently, this is not the case, and it has an impact on the conformational dynamics, if the β-strand interacts intra- or intermolecularly with VPREB. It should be noted that the degree of protection is less pronounced when compared to WT VPREB alone, which is reasonable because VPREB alone is unfolded. The degree of deprotection of the UR is the same for VPREB alone and in complex with λ5 C212S.

Moreover, VPREB ΔU+β was compared to VPREB ΔU in terms of conformational dynamics by differential HDX-MS after 2 h of HDX (Figure 47C). As expected, also VPREB ΔU + β has more protected peptides in its core region compared to VPREB ΔU alone. The highest degree of protection was also between residues 80 and 90 as it was the case when comparing VPREB βU with VPREB alone. The protection is reasonable because VPREB ΔU + β, which is resembling a conventional V_L domain, attains its native structure because of the added β-strand which causes folding.

The comparison of the conformational dynamics between VPREB ΔU + β and VPREB ΔU in complex with λ5 ΔU C212S was performed by differential HDX-MS after 2 h of HDX (Figure 47D). Contrary to expectations, the core domain of VPREB ΔU + β is more protected than in complexed VPREB ΔU. Analogous to VPREB βU that shows a higher protection in the core domain compared to complexed VPREB, the reason could be that it makes a difference, if the β-strand interacts inter- or intramolecularly with VPREB. In the case of the intramolecular β-strand, it might cause the protein to attain a more globular fold compared to the intermolecular β-strand supplemented from λ5 C212S.

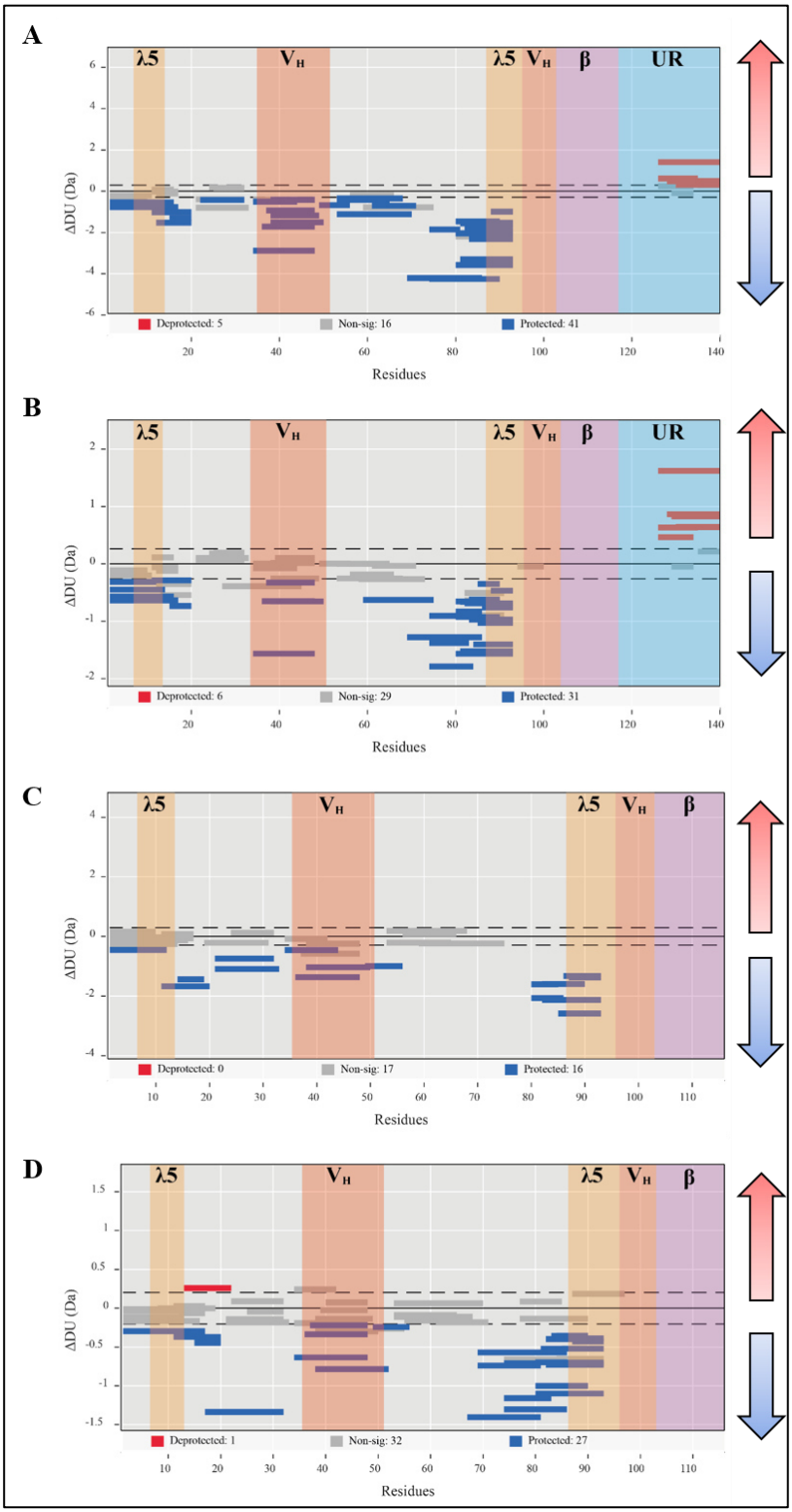

Figure 47: Comparison of Protection/Deprotection in the β-Insertion-Mutants of VPREB by Differential HDX-MS Analysis.
Wood´s plots showing the summed differences in deuterium uptake in VPREB βU and VPREB ΔU + β after 2 h of HDX, comparing VPREB βU with VPREB (**A**), VPREB βU with VPREB in complex with ʎ5 C212S (**B**), VPREB ΔU + β with VPREB ΔU (**C**) and VPREB ΔU+β with VPREB ΔU in complex with ʎ5 ΔU C212S (**D**). Wood´s plots were generated using Deuteros (Lau et al., 2020). Peptides coloured in blue or red, respectively, are protected or deprotected from exchange in the β-insertion mutants. Peptides with no significant difference between conditions, determined using a 99 % confidence interval (dotted line) and a p value < 0.1, are shown in grey. The VPREB-UR is coloured in blue, the λ5-interface in orange, the V_H-interface in red, the additional β-strand in magenta and the C_H1-interface in green.

2.4.7 λ5 W67,77,83A C212S and VPREB W131A

To compare the effects on the conformational dynamics of the tryptophane mutants of λ5 C212S and VPREB, respectively, with the WT SLC proteins, differential HDX-MS after 2 h of HDX was performed (Figure 48).

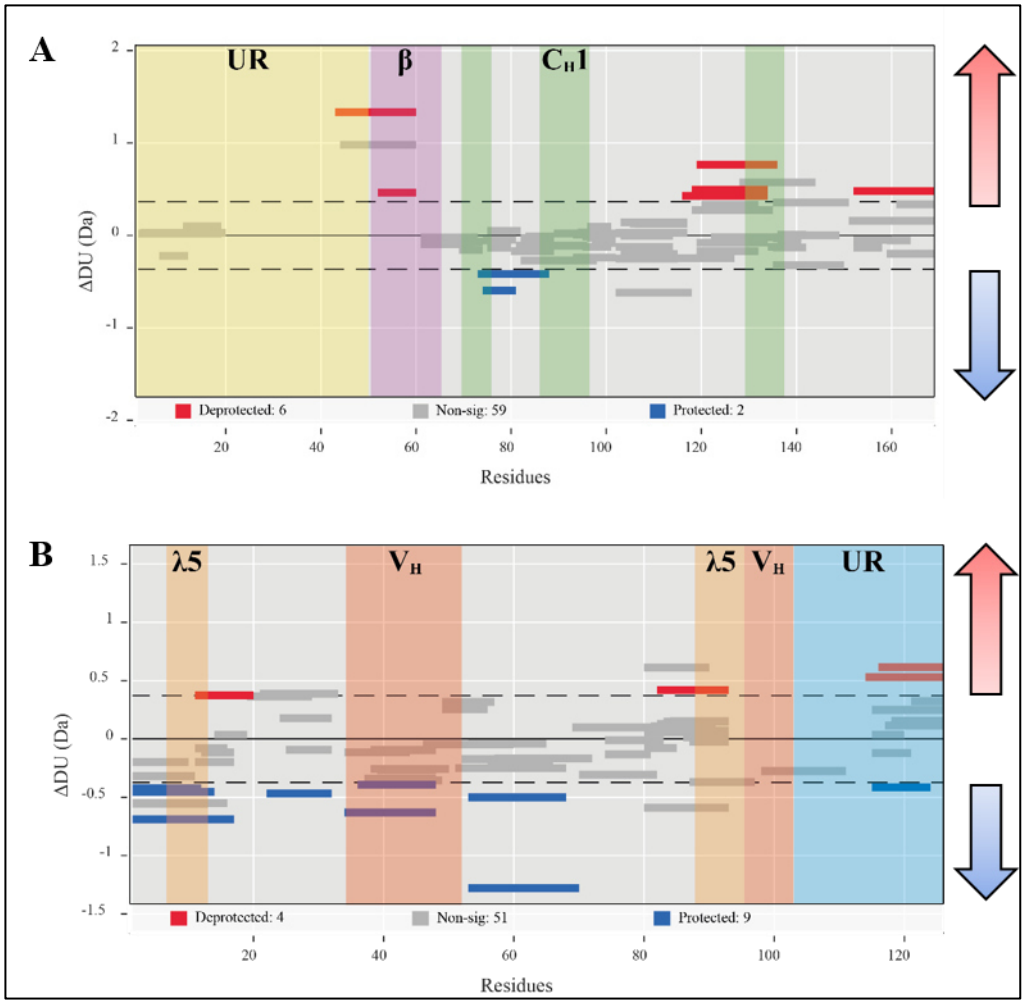

Figure 48: Comparison of Protection/Deprotection in the Tryptophane Mutants of VPREB and ʎ5 C212S by Differential HDX-MS Analysis.
Wood´s plots showing the summed differences in deuterium uptake in ʎ5 W67,77,83A C212S and VPREB W131A after 2 h of HDX, comparing ʎ5 W67,77,83A C212S with ʎ5 C212S (**A**) and VPREB βW131A with VPREB (**B**). Wood´s plots were generated using Deuteros (Lau et al., 2020). Peptides coloured in blue or red, respectively, are protected or deprotected from exchange in the tryptophane mutants. Peptides with no significant difference between conditions, determined using a 99 % confidence interval (dotted line) and a p value < 0.1, are shown in grey. The VPREB-UR is coloured in blue, the λ5-UR in yellow, the λ5-interface in orange, the V_H-interface in red, the additional β-strand in magenta and the C_H1-interface in green.

The differential HDX-MS between λ5 W67,77,83A C212S and λ5 C212S reveals that the β-strand is strongly deprotected in λ5 W67,77,83A C212S. This deprotection of the β-strand can also observed be in the λ5 ΔU C212S mutant. Additionally, few deprotected and protected peptides in the λ5 core region can be observed. This influence of the tryptophanes in the UR on the overall

conformational dynamics of λ5 C212S, not only in the additional β-strand but also in the core region, is surprising since the tryptophanes are in the protruding unfolded UR that is not supposed to have an impact on the structure of the protein. However, the tryptophanes impact the structure of λ5 C212S. Comparing it with the Wood´s plot of λ5 ΔU C212S and λ5 C212S, both, λ5 W67,77,83A and λ5 ΔU C212S show a similar deprotection of the additional β-strand.
Furthermore, the conformational dynamics between WT VPREB and VPREB W131A was compared by differential HDX-MS after 2 h of HDX (Figure 48B). That the mutation of one amino acid in an unfolded protein causes changes in the conformational dynamics of the whole protein is surprising. Not only protected segments but also deprotected segments can be observed.

2.4.8 VPREB 9EurQ

To gain insight into the influence of the negatively charged glutamates in the UR of VPREB on the conformational dynamics of the protein, differential HDX-MS was used after 2 h of HDX (Figure 49). It was expected that they have no influence on the overall dynamics and structure because they are in the protruding unfolded region and the unfolded protein. However, deprotected as well as protected peptides can be observed in the core region of the protein.

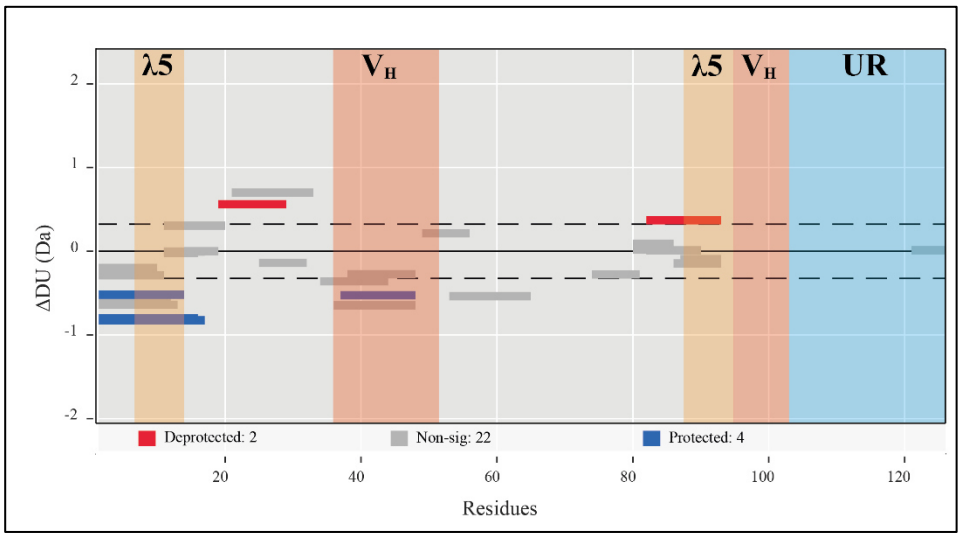

Figure 49: Comparison of Protection/Deprotection in the Glutamate Mutant of VPREB by Differential HDX-MS Analysis.
Wood´s plots showing the summed differences in deuterium uptake in VPREB 9EurQ after 2 h of HDX, comparing VPREB 9EurQ with VPREB. Wood´s plots were generated using Deuteros (Lau et al., 2020). Peptides coloured in blue or red, respectively, are protected or deprotected from exchange in the glutamate mutant. Peptides with no significant difference between conditions, determined using a 99 % confidence interval (dotted line) and a p value < 0.1, are shown in grey. The VPREB-UR is coloured in blue, the λ5-interface in orange, the V_H-interface in red, and the C_H1-interface in green.

2.5 Folding Kinetics, Affinities and Stabilities Between λ5 and VPREB Variants

2.5.1 Influence of λ5 Mutations on the Interaction with VPREB

The previous sections could show that VPREB alone is an unfolded dimer regardless of its UR and together with λ5 C212S, it forms a folded heterodimer. The mechanism of this interaction remains unclear. To analyze the ability of λ5 to induce folding in VPREB, kinetic measurements with several λ5 mutants were executed by CD (Figure 50, Table 5).

Table 5: Folding Time Constant τ, Thermal Stability T_m, Binding and Binding Rate Constants (K_D, k_a, k_d) and N-Sites of VPREB with ʎ5 Variants and β-Strand Peptide.

Construct	τ [min]	T_m [°C]	K_D [nM]	k_a [Ms^{-1}]	k_d [s^{-1}]	N-Value
λ5 C212S	51.0 ± 3.4	53.7 ± 0.7	17.7 ± 1.2	35795 ± 2445	0.0006 ± 0.0000007	-
λ5 ΔU C212S	113.5 ± 29.6	56.5 ± 0.8	13.5 ± 0.4	89615 ± 2025	0.001 ± 0.000009	-
λ5 W67,77,83 A C212S	28.9 ± 5.8	55.3 ± 0.1	5.2 ± 1.5	118340 ± 28760	0.0006 ± 0.00003	-
β-strand	23.6 ± 4.5	48.1 ± 0.9	164 ± 6	-	-	0.54 ± 0.01
λ5 Δβ C212S	No folding	-	-	-	-	-
λ5 ΔU Δβ C212S	No folding	-	-	-	-	-

The folding time constant τ in [min] of VPREB and ʎ5 variants was measured by far-UV CD spectroscopy at 205 nm. The thermal stability T_m in [°C] of the respective complexes was assessed by temperature-induced unfolding transitions followed by far-UV CD spectroscopy at 205 nm. The affinity of the complexes was measured by SPR to determine the K_D in [nM], k_a in [Ms^{-1}] and the k_d in [s^{-1}]. The affinity between VPREB and the β-strand peptide was measured by ITC to determine the K_D in [nM] and the N-value, which determine the ratio of how many analytes (syringe) bind to the ligand (cell).

The thermal stabilities of the complexes were assessed by temperature-induced unfolding transitions at 205 nm by CD spectroscopy and the affinities were measured by SPR to obain the dissociation constant (K_D), the association rate constant (k_a) and the dissociation rate constant (k_d) (Figure 51, Figure 52, and Table 5). The affinity of VPREB and the β-strand was measured by

ITC, which provided the K_D and the stoichiometry of the interaction, as represented by the N-value.

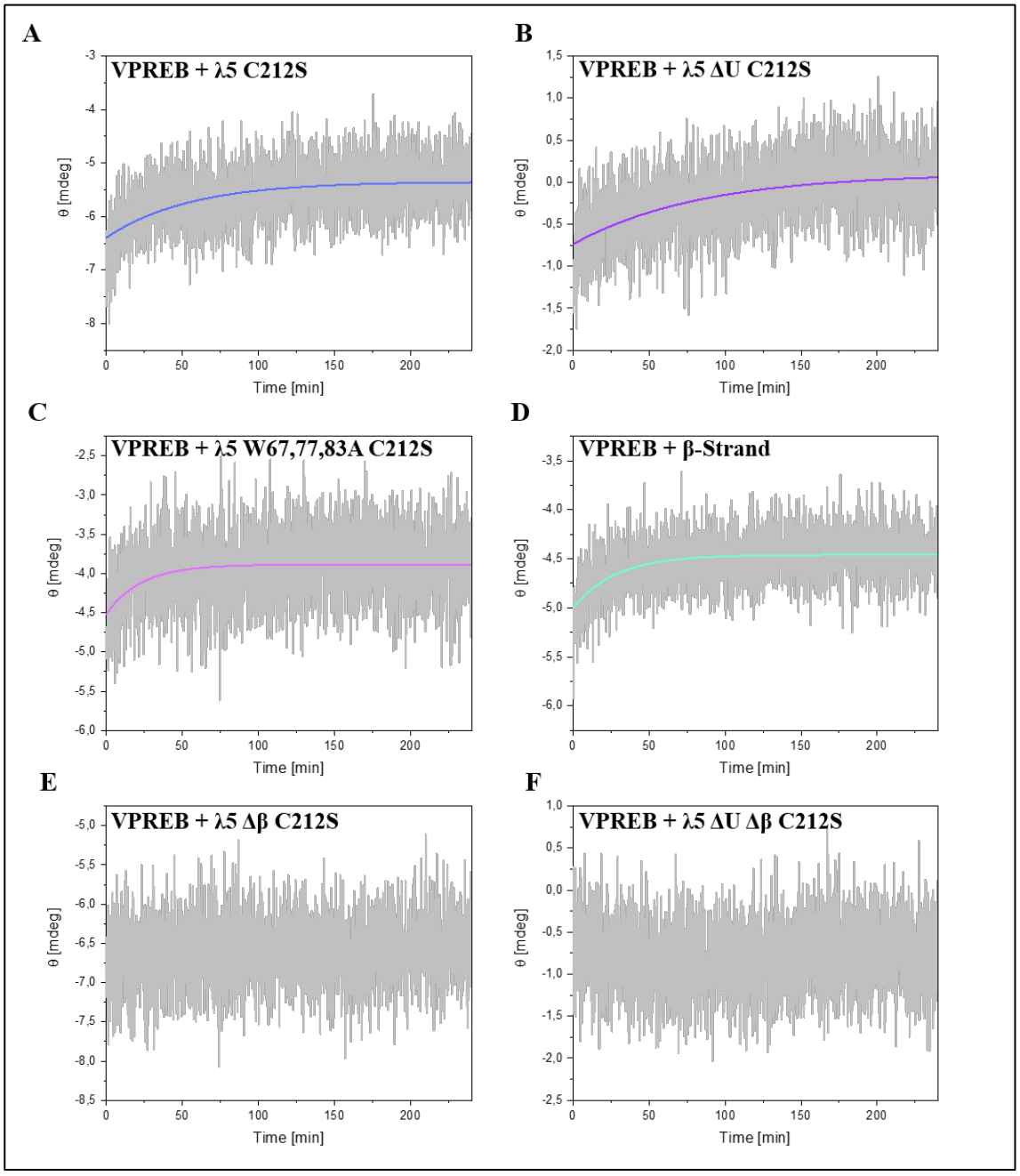

Figure 50: Folding Kinetics Measurements of VPREB with ʎ5 Variants and the β-Strand Peptide. Folding of VPREB was monitored by CD spectroscopy at a constant wavelength of 205 nm and 25°C for 4 h. VPREB alone was equilibrated for 10 min at 25°C before addition of the ʎ5 variants, respectively. Solid lines represent the exponential fit of the recorded data to determine τ, at which 63.2 % of the protein is folded. **A** VPREB and ʎ5 C212S. **B** VPREB and ʎ5 ΔU C212S. **C** VPREB and ʎ5 W67,77,83A C212S. **D** VPREB and β-strand peptide. **E** VPREB and ʎ5 Δβ C212S. **F** VPREB and ʎ5 ΔU Δβ C212S.

The kinetics of VPREB and λ5 C212S revealed a signal increase at 205 nm over time at 25°C with a τ, at which 63.2 % of the protein is folded, of 51.0 ± 3.4 min (Figure 50A, Table 5). It should be considered that all kinetics measurements by CD should be analyzed with care due to

a slight photobleaching effect. The same measurements were performed for several λ5 mutants with VPREB. For the combination of VPREB and λ5 ΔU C212S, τ was determined to be 113.5 ± 29.6 min (Figure 50B, Table 5), which is increased at least half compared to the complex of VPREB and λ5 C212S. This reveals the UR of λ5 to be a crucial part in the folding process of VPREB. Furthermore, the influence of the tryptophanes in the UR of λ5 were analyzed with respect to their influence on the folding of VPREB. Surprisingly, the λ5 W67,77,83A C212S mutant reduces τ to 28.9 ± 5.8 min (Figure 50C, Table 5), indicating a role for the tryptophanes in the λ5-UR in the folding pathway of VPREB. The β-strand alone causes VPREB to fold with a τ of 23.6 ± 4.5 min (Figure 50D, Table 5), identifying it as the crucial part for the folding reaction of VPREB.

As expected, neither λ5 Δβ C212S nor λ5 ΔU Δβ C212S cause folding in VPREB (Figure 50E and F), which is in accordance with the results above and the literature that identified the additional β-strand of λ5 to be indispensable for the interaction with VPREB (Minegishi et al., 1999).

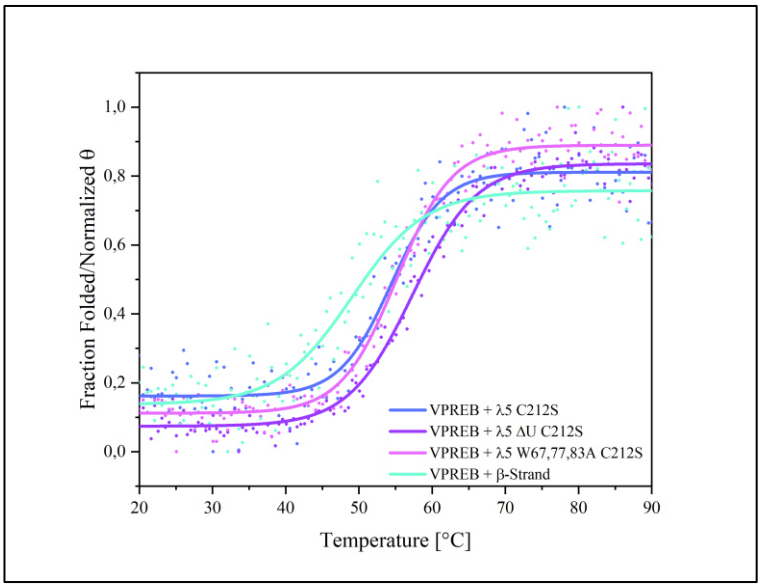

Figure 51: Conformational Stability of the Complexes of VPREB with λ5 Variants.
Temperature-induced unfolding transitions followed by far-UV CD spectroscopy at 205 nm of complexes of VPREB and various λ5 complexes. Solid lines represent the Boltzmann fit of the recorded data to determine the turning point, which reflects the T_m at which 50 % of the protein is unfolded.

The thermal stabilities of the formed complexes, which were assessed by temperature-induced unfolding transitions at 205 nm by CD spectroscopy, are illustrated in Figure 51 and listed in Table 5. The T_m of the WT complex of VPREB and λ5 C212S was determined to be 53.7 ± 0.7 °C, as already shown in section 2.3.1.2. λ5 ΔU C212S and λ5 W67,77,83A C212S increase the thermal stabilities, which can be observed by increased melting temperatures, T_m = 56.5 ± 0.8°C for λ5 ΔU C212S and T_m = 55.3 ± 0.1°C for λ5 W67,77,83A C212S. However, the thermal stability of the VPREB-β-strand complex is significantly decreased by about 5°C to T_m = 48.1 ±

0.9. Since the β-strand deletion mutants did not form any complex with VPREB, no thermal stabilities could be obtained. Altogether, λ5 stabilizes the interaction with VPREB compared to the β-strand. The UR and the UR-tryptophanes of λ5 seem to have an influence on the thermal stabilities of the complexes.

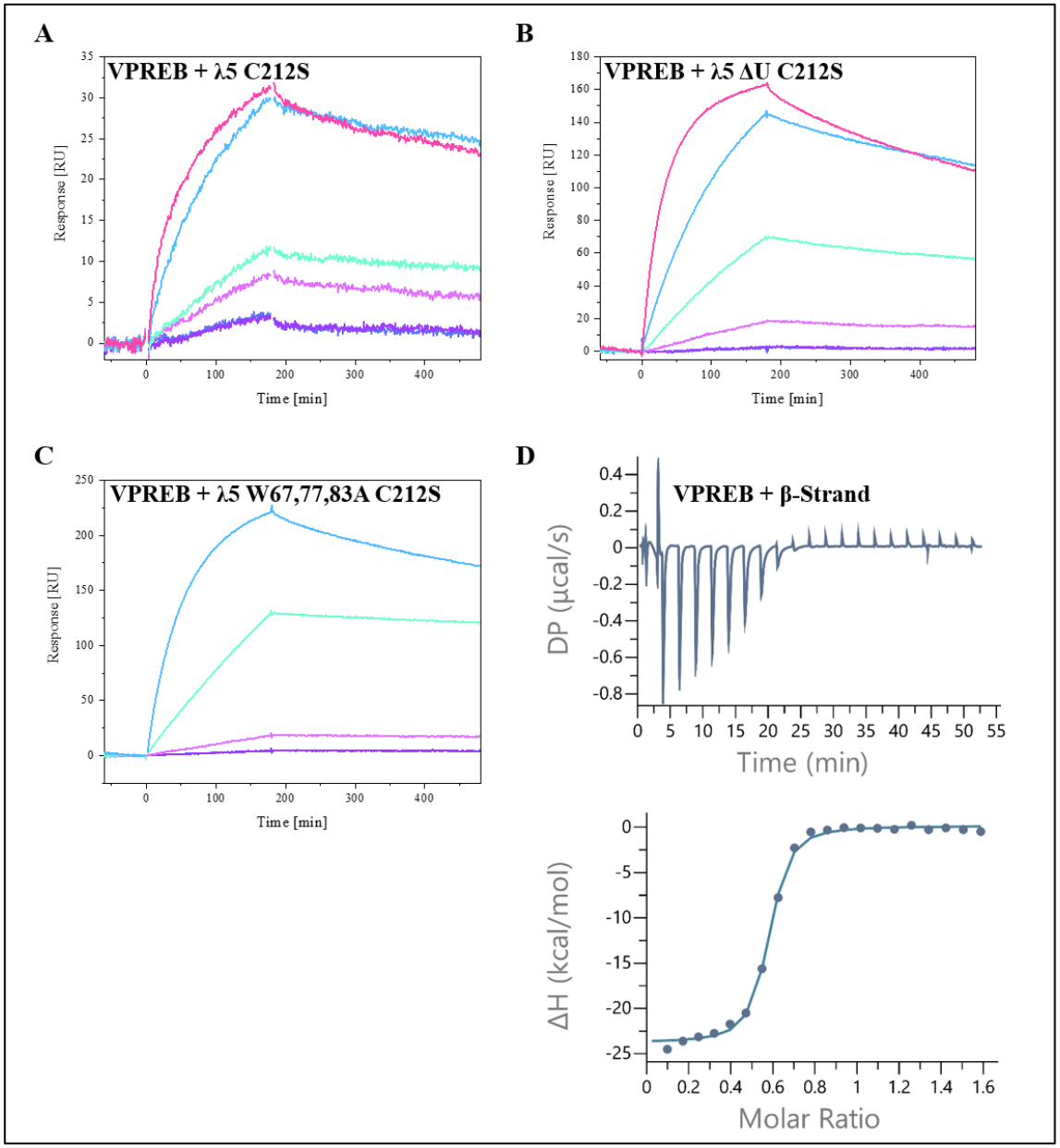

Figure 52: Affinities and Binding Kinetics of VPREB and λ5 Variants.
The affinities and binding kinetics of VPREB and λ5 C212S (**A**), VPREB and λ5 ΔU C212S (**B**) and VPREB and λ5 W67,77,83A C212S (**C**) were measured by SPR. The affinity of VPREB and the β-strand was measured by ITC.

The measurements of the affinities between the λ5 mutants and VPREB were performed by the use of either SPR or ITC (Figure 52, Table 5). A K_D of 17.7 ± 1.2 nM was determined for VPREB and λ5 C212S with k_a to be 35795 ± 2445 Ms^{-1} and k_d to be 0.0006 ± 0.0000007 s^{-1}. Both mutants, λ5 ΔU C212S and λ5 W67,77,83A C212S, show an increased affinity for VPREB with 13.5 ± 0.4

nM and 5.2 ± 1.5 nM, respectively. This is also reflected in the rate constants with k_a being 89615 ± 2025 Ms^{-1} and 118340 ± 28760 Ms^{-1}, respectively, and k_ds of 0.001 ± 0.000009 s^{-1} and 0.0006 ± 0.00003 s^{-1}. The increased affinity could be attributed to a more deprotected β-strand in these mutants compared to λ5 C212S, as shown by HDX measurements (sections 2.4.3 and 2.4.7), facilitating the access for VPREB.

The affinity of VPREB and the β-strand is decreased, which is reflected in an increased K_D of 164 ± 6 nM. The lower affinity could be explained by the impact that the λ5 C212S protein has on this interaction. The N-value was determined to be 0.54 ± 0.01. This means that one β-strand binds to two VPREB molecules. This confirms the AUC (section 2.3.1.3) and crosslinking data (section 2.3.6) that revealed VPREB to be a dimer.

2.5.2 Influence of VPREB Mutations on the Interaction with λ5 C212S

In the previous chapter, the influences of the λ5 mutations were analyzed in terms of folding, stability and affinity for VPREB (section 2.5.1). This chapter is about the influence of certain VPREB features on the interaction with λ5 C212S. To analyze the ability of λ5 C212S to fold or induce folding in VPREB mutants, kinetic measurements with several VPREB mutants were performed and monitored by CD (Figure 53, Table 6). Moreover, the thermal stabilities of the complexes were assessed by temperature-induced unfolding transitions at 205 nm and the affinities were measured by SPR to obain the dissociation constant (K_D), the association rate constant (k_a) and the dissociation rate constant (k_d) (Figure 54, Figure 55, and Table 6).

Table 6: Folding Time Constant τ, Thermal Stability T_m, Binding and Binding Rate Constants (K_D, k_a, k_d) of ʎ5 C212S and VPREB Variants.

Constructs		**τ [min]**	**T_m [°C]**	**K_D [nM]**	**k_a [Ms^{-1}]**	**k_d [s^{-1}]**
λ5 C212S	**VPREB ΔU**	40.9 ± 10.7	55.1 ± 0.1	3.0 ± 1.3	228450 ± 66850	0.0006 ± 0.0001
λ5 ΔU C212S	**VPREB ΔU**	-	-	5.0 ± 0.8	321000 ± 111600	0.002 ± 0.0003
λ5 C212S	**VPREB W131A**	33.9 ± 8.0	54.5 ± 0.01	16.8 ± 1.3	56475 ± 3385	0.0009 ± 0.00002
λ5 C212S	**VPREB 9EurQ**	27.1 ± 5.6	54.7 ± 0.7	1.7 ± 0.1	1014700 ± 99300	0.002 ± 0.0003

The folding time constant τ in [min] of ʎ5 and VPREB variants was measured by far-UV CD spectroscopy at 205 nm. The thermal stability T_m in [°C] of the respective complexes was assessed by temperature-induced unfolding transitions followed by far-UV CD spectroscopy at 205 nm. The affinity of the complexes was measured by SPR to determine the K_D in [nM], k_a in [Ms^{-1}] and the k_d in [s^{-1}].

In VPREB ΔU, τ is slightly reduced to 40.9 ± 10.7 min (Figure 53A, Table 6). For λ5 ΔU C212S and VPREB ΔU, no exponential curve could be observed (data not shown). Interestingly, the mutation of tryptophane at position 131 to alanine decreased τ by about 20 min to 33.9 ± 8.0 min (Figure 53B, Table 6). Also, for the combination of VPREB 9EurQ and λ5 C212S, τ was markedly decreased by about 25 min to 27.1 ± 5.6 min (Figure 53C, Table 6). From these observations, one can conclude that the UR of VPREB as well as the tryptophane and the glutamates influence its folding.

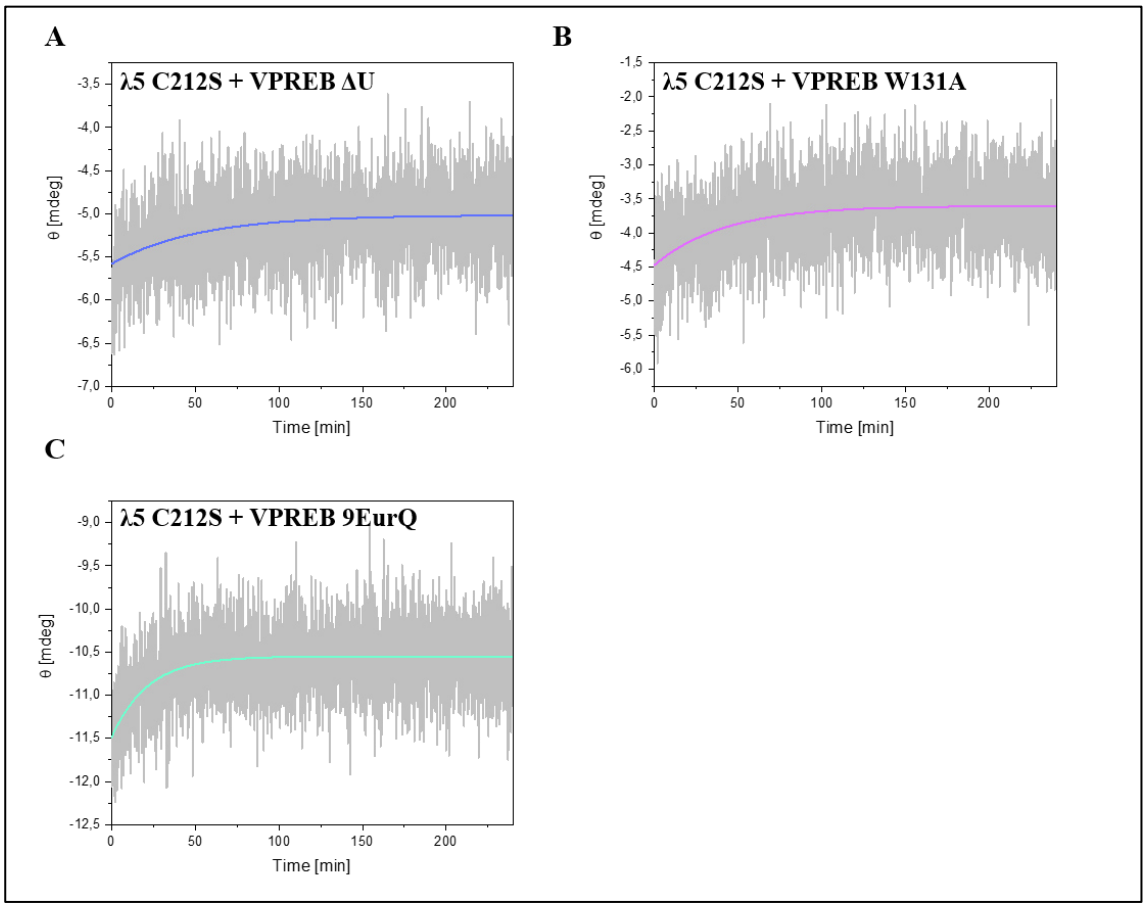

Figure 53: Folding Kinetics Measurements of ʎ5 C212S with VPREB Variants.
Folding of VPREB variants was monitored by CD spectroscopy at a constant wavelength of 205 nm and 25°C for 4 h. Each VPREB variant alone was equilibrated for 10 min at 25°C before the addition of ʎ5 C212S, respectively. Solid lines represent the exponential fit of the recorded data to determine τ, at which 63.2 % of the protein is folded. **A** ʎ5 C212S and VPREB ΔU. **B** ʎ5 C212S and VPREB W131A. **C** ʎ5 C212S and VPREB 9EurQ.

The thermal stabilities are roughly the same for all combinations (Figure 54, Table 6). The thermal stability of the complex consisting of λ5 ΔU C212S and VPREB ΔU is shown in an earlier chapter (section 2.3.2.2).

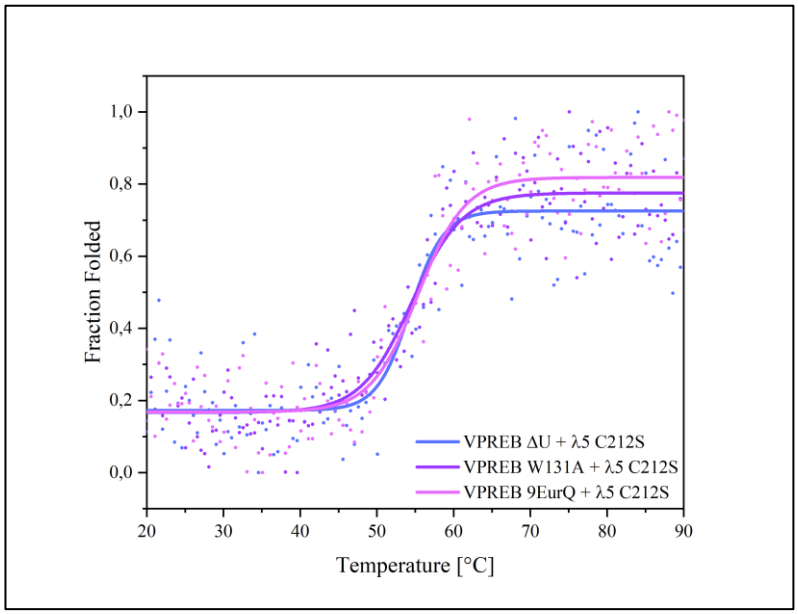

Figure 54: Conformational Stability of the Complexes of λ5 C212S with VPREB Variants.
Temperature-induced unfolding transitions followed by far-UV CD spectroscopy at 205 nm of complexes of VPREB variants and λ5 C212S. Solid lines represent the Boltzmann fit of the recorded data to determine the turning point, which reflects the T_m at which 50 % of the protein is unfolded.

When looking at the affinity measurements, it is interesting that except for VPREB W131A, all affinities are markedly increased. The K_D between λ5 C212S and VPREB ΔU was determined to be 3.0 ± 1.3 nM with k_a = 228450 ± 66850 Ms^{-1} and k_d = 0.0006 ± 0.0001 s^{-1} (Figure 55A, Table 6). Compared to the affinity of VPREB and λ5 C212S, the K_D and k_a were reduced about 6-fold with no change in the k_d. The K_D for the combination of λ5 ΔU C212S and VPREB ΔU was measured to be 5.0 ± 0.8 nM with k_a = 321000 ± 111600 Ms^{-1} and k_d = 0.002 ± 0.0003 s^{-1} (Figure 55D, Table 6). This result confirms the influence of the VPREB-UR on the affinity with λ5. It could already be shown before that also λ5 ΔU C212S has an increased affinity for VPREB (Figure 52, Table 5). It should be noted that the effect of both URs is not additive since the affinity between VPREB ΔU and λ5 ΔU C212S is not higher than between VPREB ΔU and λ5 C212S. However, the VPREB-UR seems to have a higher impact on the affinity compared to the λ5-UR. The mutation of tryptophane to alanine at position 131 in the VPREB-UR did not have a significant effect on the affinity with λ5 C212S. A K_D of 16.8 ± 1.3 nM was determined with k_a measured to be 56475 ± 3385 and k_d to be 0.0009 ± 0.00002 s^{-1} (Figure 55B, Table 6). The K_D, k_a and k_d are roughly the same as they were determined for λ5 C212S and VPREB, indicating that this mutation does not impact the λ5-VPREB affinity. Last, the affinity between VPREB 9EurQ was increased about 10-fold compared to the WT combination with a measured K_D of 1.7 ± 0.1 nM, a k_a of 1014700 ± 99300 Ms^{-1} and a k_d of 0.002 ± 0.0003 s^{-1} (Figure 55C, Table 6). The k_a is increased about 30-fold and the k_d around 10-fold. This result assigns the glutamates in the VPREB-UR an important function in the affinity and interaction with λ5 C212S.

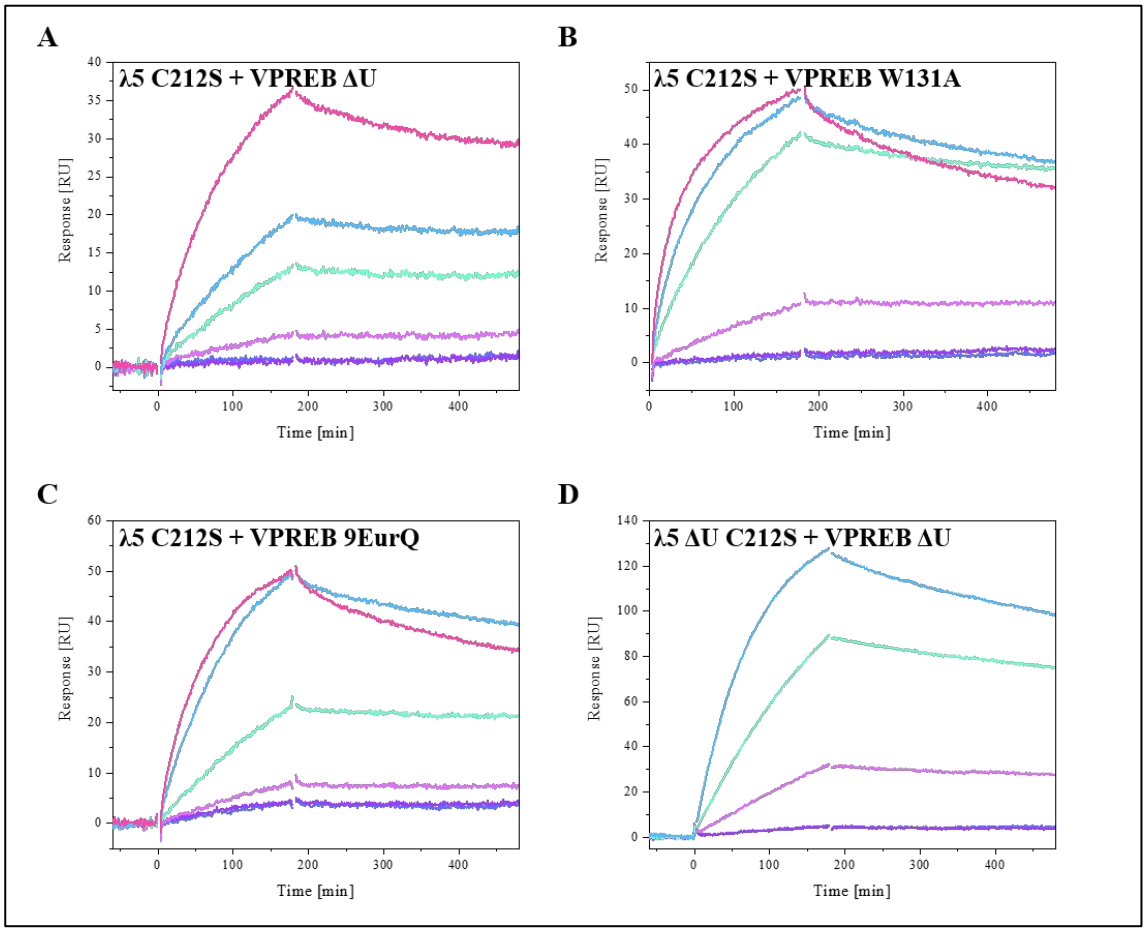

Figure 55: Affinities and Binding Kinetics of ʎ5 C212S with VPREB Variants.
The affinities and binding kinetics of ʎ5 C212S and VPREB ΔU (**A**), ʎ5 C212S and VPREB W131A (**B**), ʎ5 C212S and VPREB 9EurQ (**C**) and ʎ5 ΔU C212S and VPREB ΔU (**D**) were measured and fitted by SPR.

2.5.3 Folding of VPREB by NMR

To verify the unfolded state of intrinsically disordered VPREB alone and its folded state when it is complexed with the β-strand and λ5 C212S, NMR experiments were performed by Olga Sieluzyzka, a PhD student in the group of Prof. Bernd Reif (Figure 56). While the ^{15}N-^{1}H HSQC spectrum of isolated VPREB is characteristic of an unfolded protein (Figure 56A), which confirms the results described in section 2.3.1.1, the ^{13}C-^{15}N-^{1}H HSQC spectrum of isolated λ5 C212S (Figure 56B) is characteristic of a protein that is folded to a great part, which is in agreement with the results described in section 2.3.1.1.

Although VPREB alone is unfolded, it can attain its native structure upon interaction with the β-strand and λ5 C212S as shown by CD kinetic measurements in section 2.5.1. As shown in Figure 56C, after folding induced by the β-strand peptide, VPREB shows a well dispersed spectrum (blue spectrum). This result verifies that the additional β-strand in λ5 is sufficient for inducing the folding of VPREB. To corroborate this result further, the HSQC spectrum of labelled VPREB in complex with unlabelled λ5 C212S showed also a well-dispersed spectrum of a folded protein

(orange spectrum in Figure 56D). Because of the instability of the complex, it already starts aggregating and gives peaks that are typical of some aggregated parts of the protein in the bottom right part of the spectrum.

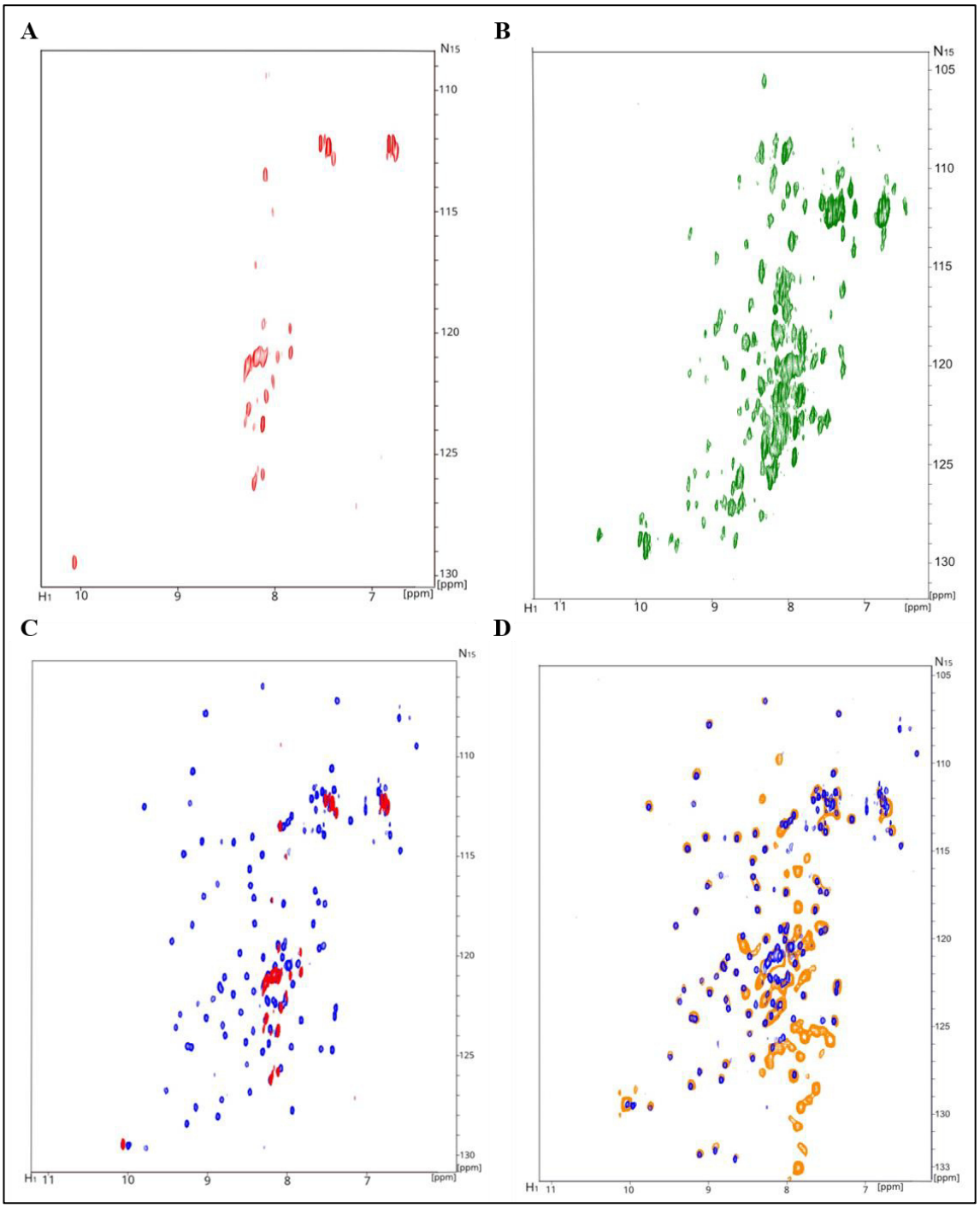

Figure 56: NMR Spectrometric Characterization of ʎ5 and β-Strand Induced Folding of VPREB. **A** ^{15}N-^{1}H HSQC spectrum of the isolated VPREB domain. **B** ^{15}N-^{13}C-^{1}H HSQC spectrum of isolated ʎ5 C212S. **C** ^{15}N-^{1}H HSQC spectrum of the isolated VPREB domain (red) and VPREB in complex with β-strand peptide (blue). **D** ^{15}N-^{1}H HSQC spectrum of VPREB in complex with β-strand peptide (blue) and ^{15}N-^{13}C-^{1}H HSQC spectrum of VPREB in complex with ʎ5 C212S (orange). The data was recorded by Olga Sieluzycka, a PhD student in the group of Prof. Bernd Reif.

2.6 Folding Kinetics and Affinities of C_H1 with SLC Variants

2.6.1 C_H1 with SLC Complex and Single Proteins

Since it could be shown before that a domain of the heavy chain, C_H1, is folded by its LC binding partner, C_L (Feige et al., 2009), it was assumed that λ5, a C_L analogous protein, is also able to induce the folding in C_H1. To further characterize this assumption, kinetic measurements of C_H1 MAK33 with the SLC proteins, λ5 and VPREB, and the SLC complex were performed and monitored by CD spectroscopy at 205 nm. Furthermore, affinity measurements by SPR were conducted.

Table 7: Time Constant τ, Binding and Binding Rate Constants (K_D, k_a, k_d) of C_H1 with the Single SLC Proteins and the Complex.

Protein	τ [min]	K_D [µM]	k_a [Ms^{-1}]	k_d [s^{-1}]
SLC C212S	53.9 ± 4.6	0.5 ± 0.3	12960 ± 7920	0.004 ± 0.00007
λ5 C212S	41.4 ± 2.0	2.1 ± 0.1	2106 ± 22	0.004 ± 0.0002
VPREB	No folding	1.3 ± 0.5	2938 ± 1301	0.003 ± 0.0003

The folding time constant τ in [min] of C_H1 and the SLC was measured by far-UV CD spectroscopy at 205 nm. The affinity of the complexes was measured by SPR to determine the K_D in [µM], k_a in [Ms^{-1}] and the k_d in [s^{-1}].

The interaction between SLC C212S and C_H1 was analyzed by CD kinetic measurements. The measurements show, as expected, that SLC C212S induces folding in and interacts with C_H1. τ, at which 63.2 % of the protein is folded, was determined to be 53.9 ± 4.6 min (Figure 57A, Table 7). To identify λ5 C212S as the important part in the interaction with C_H1, the CD kinetics for λ5 C212S and VPREB alone were measured, respectively. As expected, λ5 C212S alone induces the folding of C_H1 and not VPREB. For C_H1 and λ5 C212S, a τ of 41.4 ± 2.0 min was determined while VPREB together with C_H1 showed no change in the CD signal at 205 nm (Figure 57B and C, Table 7). It should be noted, that neither in λ5 C212S alone (Figure 57D) nor in VPREB alone (Figure 66C) a folding kinetic was detected by CD spectroscopy at 205 nm.

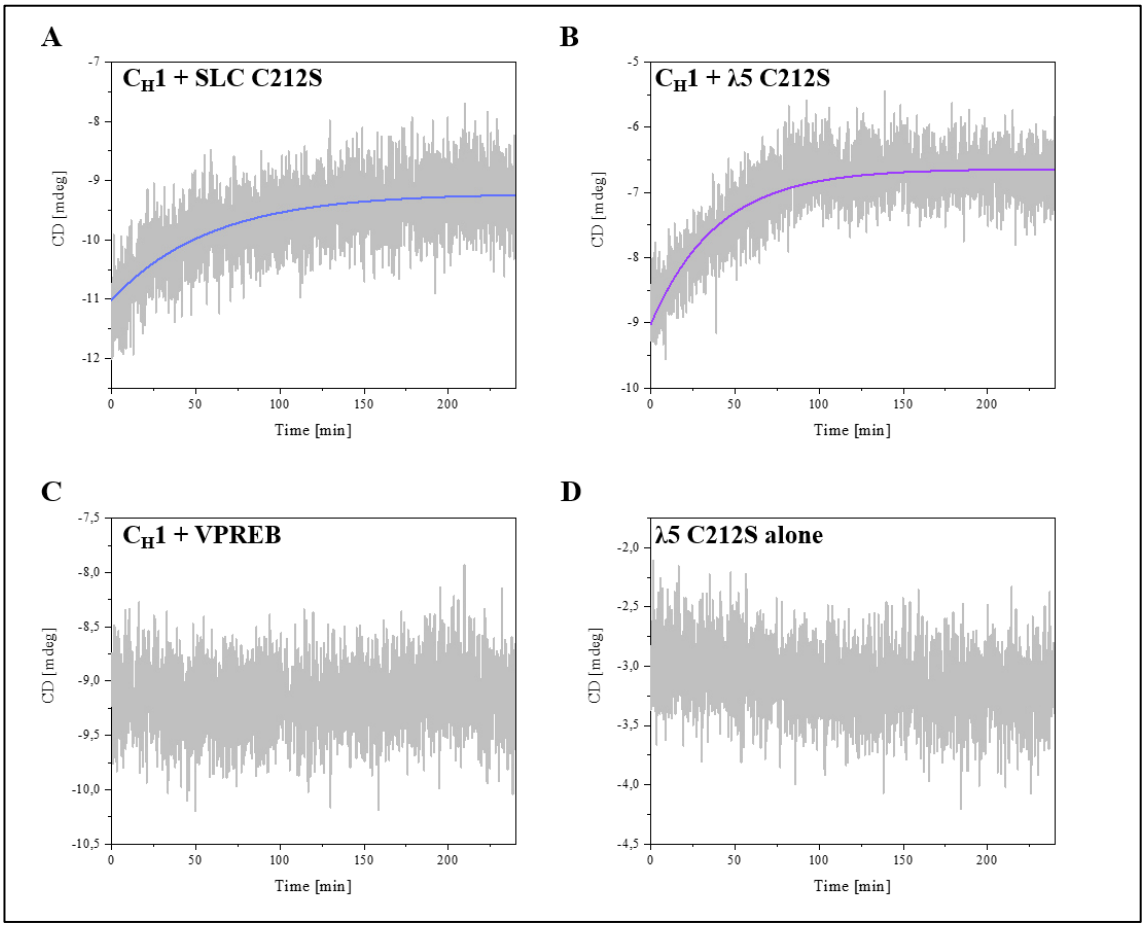

Figure 57: Folding Kinetics Measurements of C_H1 MAK33 and the SLC.
Folding of C_H1 was monitored by CD spectroscopy at a constant wavelength of 205 nm and 25°C for 4 h. C_H1 alone was equilibrated for 10 min at 25°C before the addition of the SLC proteins. Solid lines represent the exponential fit of the recorded data to determine τ, at which 63.2 % of the protein is folded. **A** C_H1 and SLC C212S. **B** C_H1 and ʎ5 C212S. **C** C_H1 and VPREB. **D** λ5 C212S alone.

To further characterize the interaction between C_H1 and the SLC, affinity measurements by SPR were performed (Figure 58, Table 7). For C_H1 and SLC C212S, a K_D of 0.5 ± 0.3 µM was determined with k_a to be 12960 ± 7920 Ms^{-1} and k_d to be 0.00364 ± 0.0000695 s^{-1} (Figure 58A, Table 7). The K_D between C_H1 and λ5 C212S is increased about 4-fold to 2.1 ± 0.1 µM with k_a to be 2106 ± 22 Ms^{-1} and k_d to be 0.00433 ± 0.0002195 s^{-1} (Figure 58B, Table 7). Suprisingly, although VPREB can not induce folding in C_H1, it can interact with it. The affinity is equally strong as it is for λ5 C212S and C_H1 with a K_D determined to be 1.3 ± 0.5 µM and k_a to be 2938 ± 1301 Ms^{-1} and k_d to be 0.00326 ± 0.00028 s^{-1} (Figure 58C, Table 7).

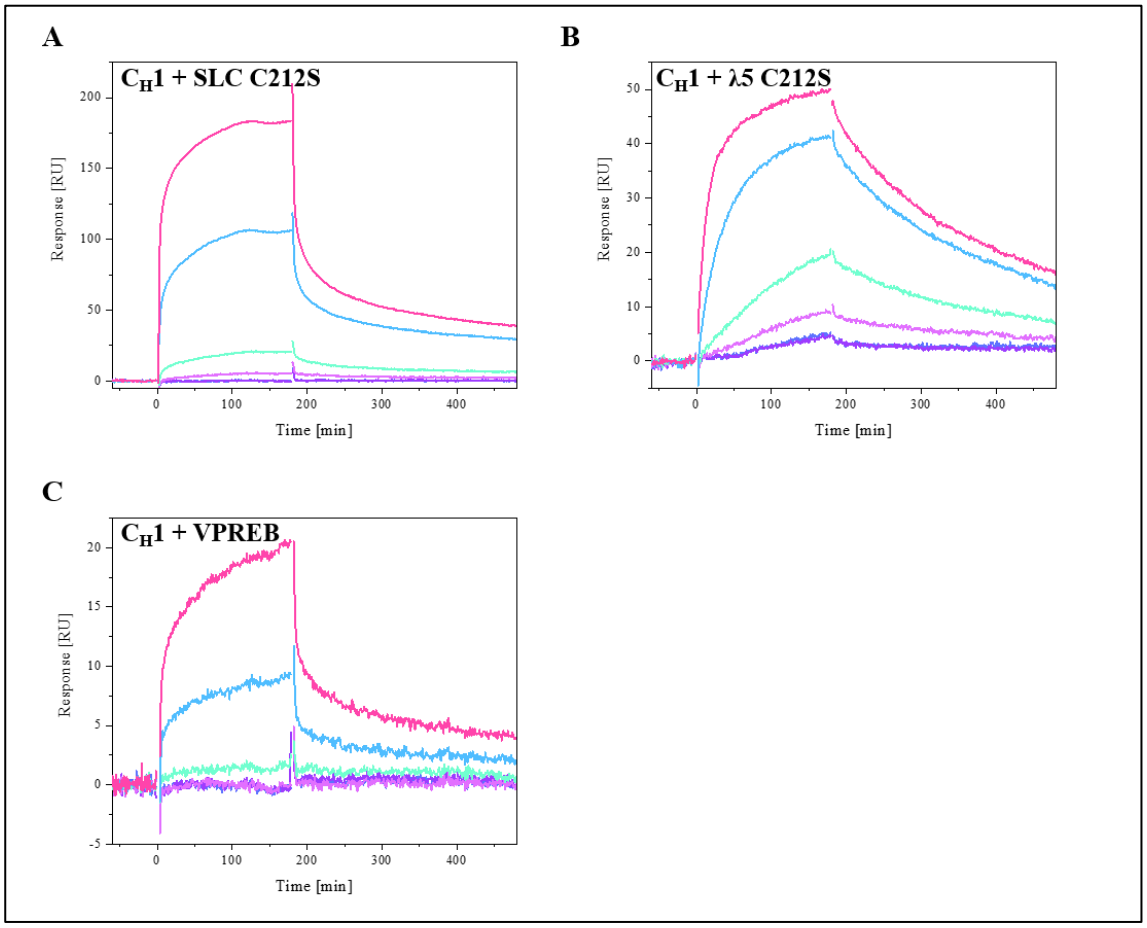

Figure 58: Affinities and Binding Kinetics of C_H1 MAK33 and SLC Proteins.
The affinities and binding kinetics of C_H1 and SLC C212S (**A**), C_H1 and ʎ5 C212S (**B**) and C_H1 and VPREB (**C**) were measured and fitted by SPR.

To further characterize the interaction of C_H1 and VPREB, AUC data of the complex was compared to AUC profiles of the single proteins (Figure 59). As already shown in sections 2.3.1.3 and 2.3.6, VPREB alone forms a homodimer. However, C_H1 alone forms a monomer and is also unfolded, while the complex of VPREB and C_H1 is shown to form a heterodimer. This means that upon interaction of VPREB and C_H1, the VPREB dimer collapses into a monomer. No heterotrimer is formed.

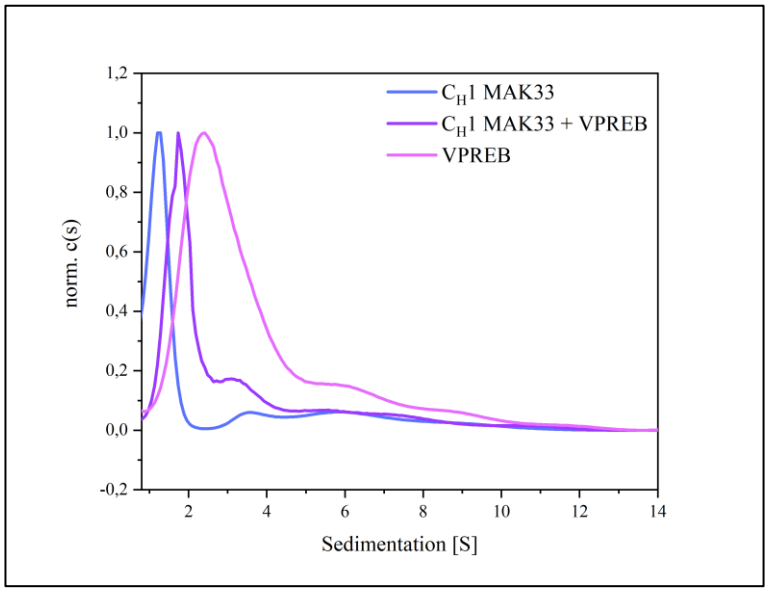

Figure 59: Quaternary Structure Analysis of the C_H1-VPREB Complex by AUC.

2.6.2 C_H1 with ƛ5 and VPREB Variants

To analyze whether the UR, the additional β-strand and the tryptophanes in the UR of λ5 have an impact on the folding of and affinity with C_H1, folding kinetics were followed by CD spectroscopy at 205 nm and affinities were measured by SPR. Furthermore, since VPREB is capable to interact with C_H1 without inducing its folding, the affinity of VPREB ΔU and C_H1 was determined by SPR.

Table 8: Time Constant τ, Binding and Binding Rate Constants (K_D, k_a, k_d) of C_H1 With SLC Variants.

Constructs	τ [min]	K_D [µM]	k_a [Ms^{-1}]	k_d [s^{-1}]
λ5 ΔU C212S	45.0 ± 1.7	1.4 ± 0.3	2330 ± 232	0.003 ± 0.0005
λ5 Δβ C212S	43.2 ± 3.7	1.1 ± 0.004	5010 ± 1740	0.005 ± 0.002
λ5 ΔU Δβ C212S	51.6 ± 1.4	1.7 ± 0.03	2866 ± 87	0.005 ± 0.00006
λ5 W67,77,83A C212S	45.8 ± 5.0	1.3 ± 0.06	1487 ± 21	0.002 ± 0.00006
VPREB ΔU	-	3.2 ± 0.1	760 ± 31	0.002 ± 0.00003

The folding time constant τ in [min] of C_H1 and SLC Variants was measured by far-UV CD spectroscopy at 205 nm. The affinity of the complexes was measured by SPR to determine the K_D in [µM], k_a in [Ms^{-1}] and the k_d in [s^{-1}].

The influence of the λ5 features on the folding of C_H1 was assessed by CD kinetics measurements to figure out which part of λ5 contributes to the induction of folding in C_H1 (Figure 60, Table 8).

For all λ5 mutants, τ was roughly the same in the range between 43 and 51 min. For the combination of C_H1 and λ5 ΔU C212S, a τ of 45.0 ± 1.7 min was measured (Figure 60A, Table 8). C_H1 and λ5 Δβ C212S achieved a time constant of 43.2 ± 3.7 min (Figure 60B, Table 8). C_H1 and λ5 ΔU Δβ C212S were determined to be 63.2 % folded after 51.6 ± 1.4 min (Figure 60C, Table 8). C_H1 and λ5 W67,77,83A C212S were showed a τ of 45.8 ± 5.0 min (Figure 60D, Table 8). As can be seen in the time constants, none of the examined structural features caused a significant change in folding kinetics and these were also in the same range as determined for C_H1 and λ5 C212S and SLC C212S.

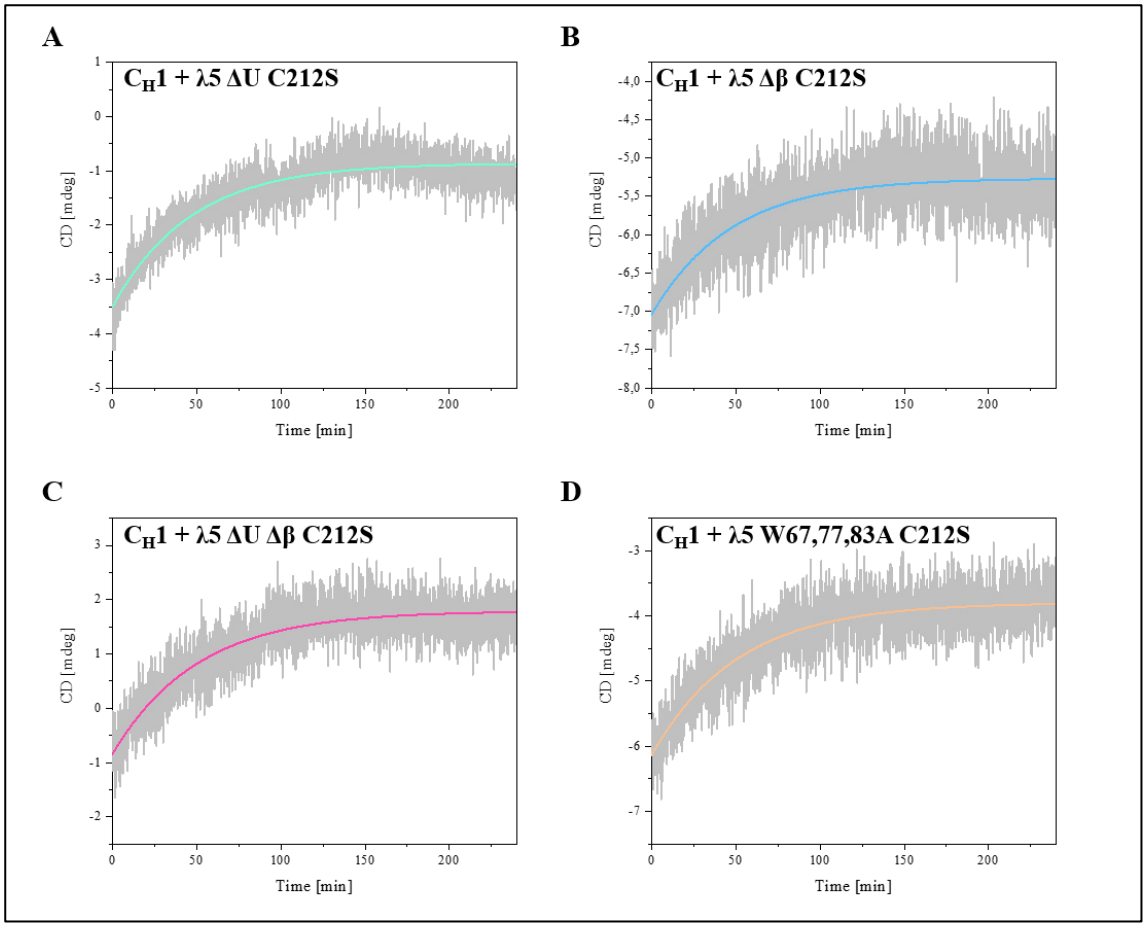

Figure 60: Folding Kinetics Measurements of C_H1 MAK33 and SLC Variants.
Folding of C_H1 was monitored by CD spectroscopy at a constant wavelength of 205 nm and 25°C for 4 h. C_H1 alone was equilibrated for 10 min at 25°C before the addition of the SLC proteins. Solid lines represent the exponential fit of the recorded data to determine τ, at which 63.2 % of the protein is folded. **A** C_H1 and λ5 ΔU C212S. **B** C_H1 and λ5 Δβ C212S. **C** C_H1 and λ5 ΔU Δβ C212S. **D** C_H1 and VPREB ΔU.

Next, the affinities of all λ5 mutants and the VPREB ΔU mutant with C_H1 were investigated. The results are depicted in Table 8 and Figure 61. The K_Ds of the λ5 mutants were all in a range from 1 to 1.7 µM. These K_Ds do not differ from the K_D of C_H1 and λ5 C212S. Notably, the K_D shows a correlation with τ for these mutants. The K_D of C_H1 and λ5 ΔU C212S was determined to be 1.4 ± 0.3 µM with k_a to be 2330 ± 232 Ms^{-1} and k_d to be 0.00312 ± 0.000455 s^{-1} (Figure 61A, Table

8). The determined K_D of C_H1 and λ5 Δβ C212S was 1.1 ± 0.004 µM, k_a was 5010 ± 1740 Ms^{-1}, and k_d was 0.005 ± 0.002 s^{-1}. For the combination of C_H1 and λ5 ΔU Δβ C212S, a K_D of 1.7 ± 0.03 µM was determined, a k_a of 2866 ± 87 Ms^{-1} and a k_d of 0.005 ± 0.00006 s^{-1}. The λ5 W67,77,83A C212S mutant showed a K_D of 1.3 ± 0.06 µM with k_a to be 1487 ± 21 Ms^{-1} and k_d to be 0.002 ± 0.00006 s^{-1}.

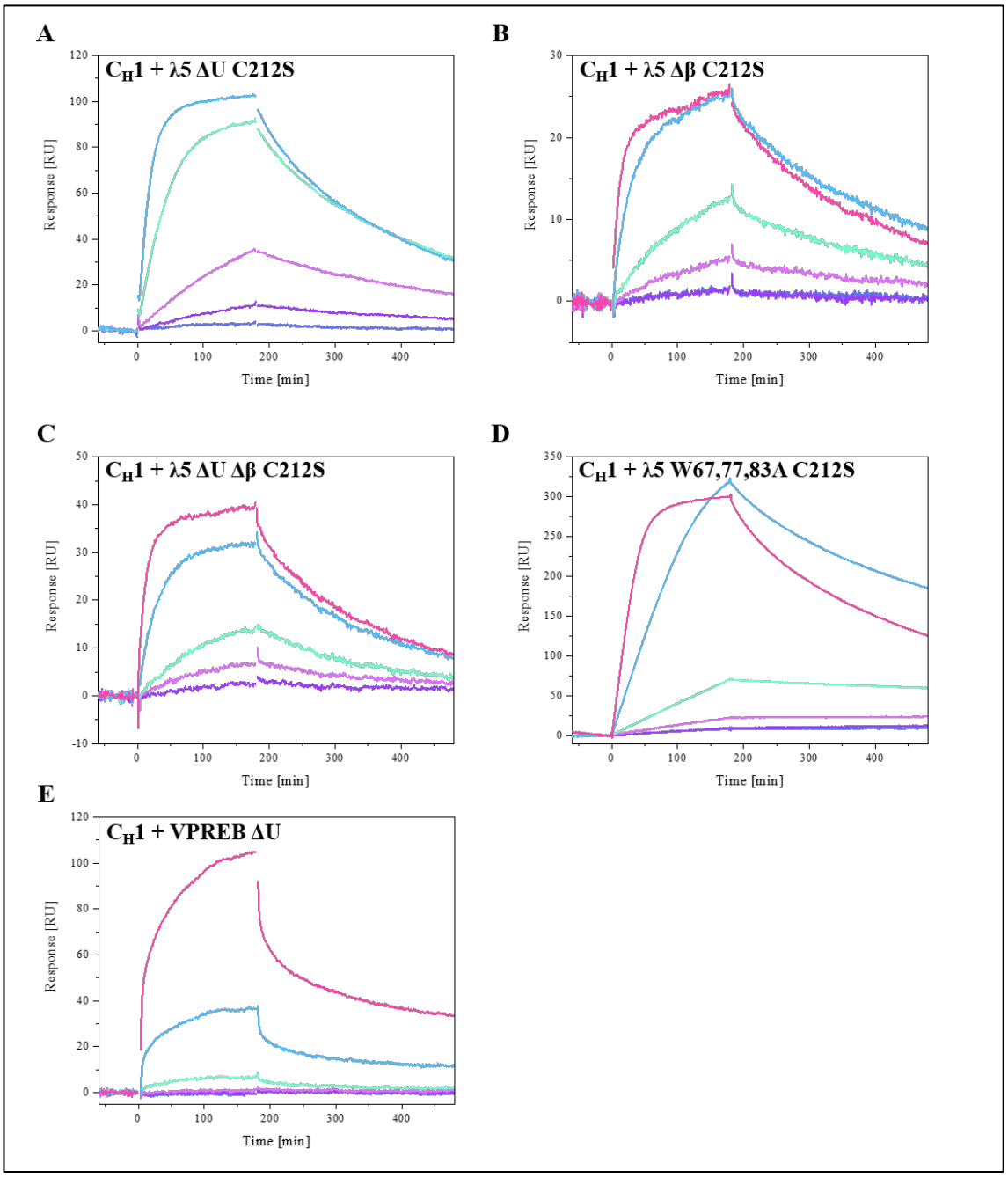

Figure 61: Affinities and Binding Kinetics of C_H1 MAK33 and SLC Variants.
The affinities and binding kinetics of C_H1 and ʎ5 ΔU C212S (**A**), C_H1 and ʎ5 Δβ C212S (**B**), C_H1 and ʎ5 ΔU Δβ C212S (**C**), C_H1 and ʎ5 W67,77,83A C212S (**D**) and C_H1 and VPREB ΔU (**E**) were measured and fitted by SPR.

The K_D of C_H1 and VPREB ΔU was determined to be 3.2 ± 0.1 µM with k_a to be 760 ± 31 Ms^{-1} and k_d to be 0.00246 ± 0.0000265 s^{-1} (Figure 61E, Table 8). Although the interaction is weaker as it is for C_H1 and VPREB, the UR of VPREB is dispensable for the interaction with C_H1.

2.7 Interaction Analysis of V_H and SLC

2.7.1 Changes in Conformational Dynamics in V_H and SLC Interaction

To discover possible interaction sites between V_H and the SLC proteins, VPREB and λ5, differential HDX-MS after 2 h of HDX was performed and analyzed (Figure 63). It revealed a significantly protected peptide in the third CDR of V_H upon interaction with VPREB (Figure 63A). This indicates that a part of VPREB interacts with the third CDR of V_H. It seems possible that the UR of VPREB is the part covering the CDR since it is protruding over the CDRs of V_H in the crystal structure of the SLC-Fd complex (Bankovich et al., 2007). The reason why there are no other protected peptides in V_H upon interaction with VPREB, since it is expected to have a buried interface, is that V_H alone forms a homodimer (section 2.7.2). VPREB and V_H seem to interact at this dimer interface as well.

There is no significant protected peptide in V_H upon interaction with λ5 C212S (Figure 63B). This could be explained also with V_H alone being a dimer and having the dimer interface as an interaction site with λ5 C212S.

When examining the conformational dynamics in VPREB in complex with V_H when compared to VPREB alone, many changes can be observed (Figure 63C). Complex formation leads to deprotected peptides in the whole protein. This might be regions that are also protected in the VPREB dimer, that get surface exposed upon interaction with V_H. There is a region of unprotected peptides towards the N-terminus of VPREB from amino acid position 1 to 18. A part of it is also the λ5 interaction site. It might be possible that the interaction of VPREB and V_H prepares VPREB for the interaction with λ5 by exposing the interface region. The next following deprotected segment is located roughly at amino acids 38 to 50. This is the part identified as the interface with V_H based on the crystal structure. A possible reason why this part shows higher conformational dynamics as in the VPREB dimer is that VPREB remains unfolded upon interaction with V_H and attains its tertiary structure only after interaction with λ5. A further reason might be that this part is more buried in the VPREB dimer than it is in the interaction with V_H, confirming the hypothesis that VPREB forms a dimer at its V_H interface. The amino acids 52 to 70 also show to be more deprotected in the VPREB-V_H heterodimer compared to the VPREB homodimer. Last, there is also an unprotected part in the UR of VPREB, which is surprising since it is believed to be unfolded, protruding and not involved in the VPREB dimer interface. However, this might confirm the hypothesis that it extends over the third CDR of V_H and thus being more surface-exposed and therefore exhibiting higher conformational dynamics.

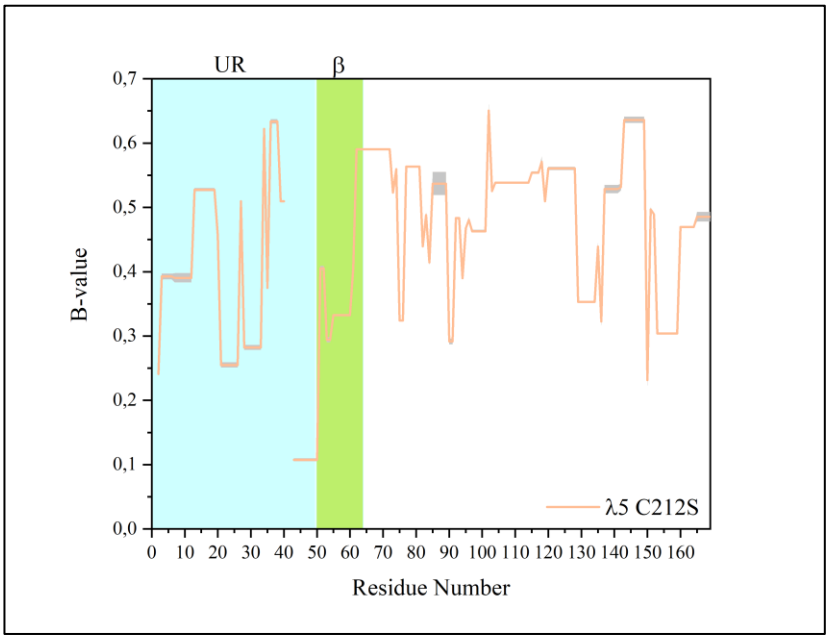

Figure 62: Conformational Dynamics by HDX-MS of ʎ5 C212S Alone after 2 h of HDX.
B Values obtained from HDX-MS after 2 h of HDX are plotted against the residue number of the primary structure for ʎ5 C212S. The UR is marked in blue and the additional β-strand in green.

The differential HDX-MS of λ5 C212S in complex with V_H (Figure 63D) revealed also only unprotected peptides compared to V_H alone. There are some parts in the UR of λ5 that are deprotected with a change in deuterium uptake of 0.3 to 1 Da. This agrees with the assumption with the λ5-UR to extend over the VPREB CDRs (Bankovich et al., 2007) and therefore causing the λ5-UR to be more surface-exposed. Secondly, it might be reasonable that the UR in the λ5 C212S monomer makes connections instead of protruding from the protein. This hypothesis is supported by HDX-MS of the single protein that shows, although it is folded as shown in section 2.3.1.1, that the UR has lower conformational dynamics compared to the core region. Moreover, the additional β-strand of λ5 and the flanking amino acids in the UR as well as in the core region show the highest degree of deprotection with a difference in deuterium uptake of about 2 Da. It could also be shown by HDX-MS analysis of λ5 C212S alone (Figure 62) that these are segments that display a low flexibility compared to the rest of the protein. The high conformational dynamics in the β-strand of λ5 C212S in complex with V_H might support its interaction with VPREB, which is determined exclusively by this β-strand. The rest of the core region shows not much pronounced changes in the conformational dynamics of the complexed λ5 C212S.

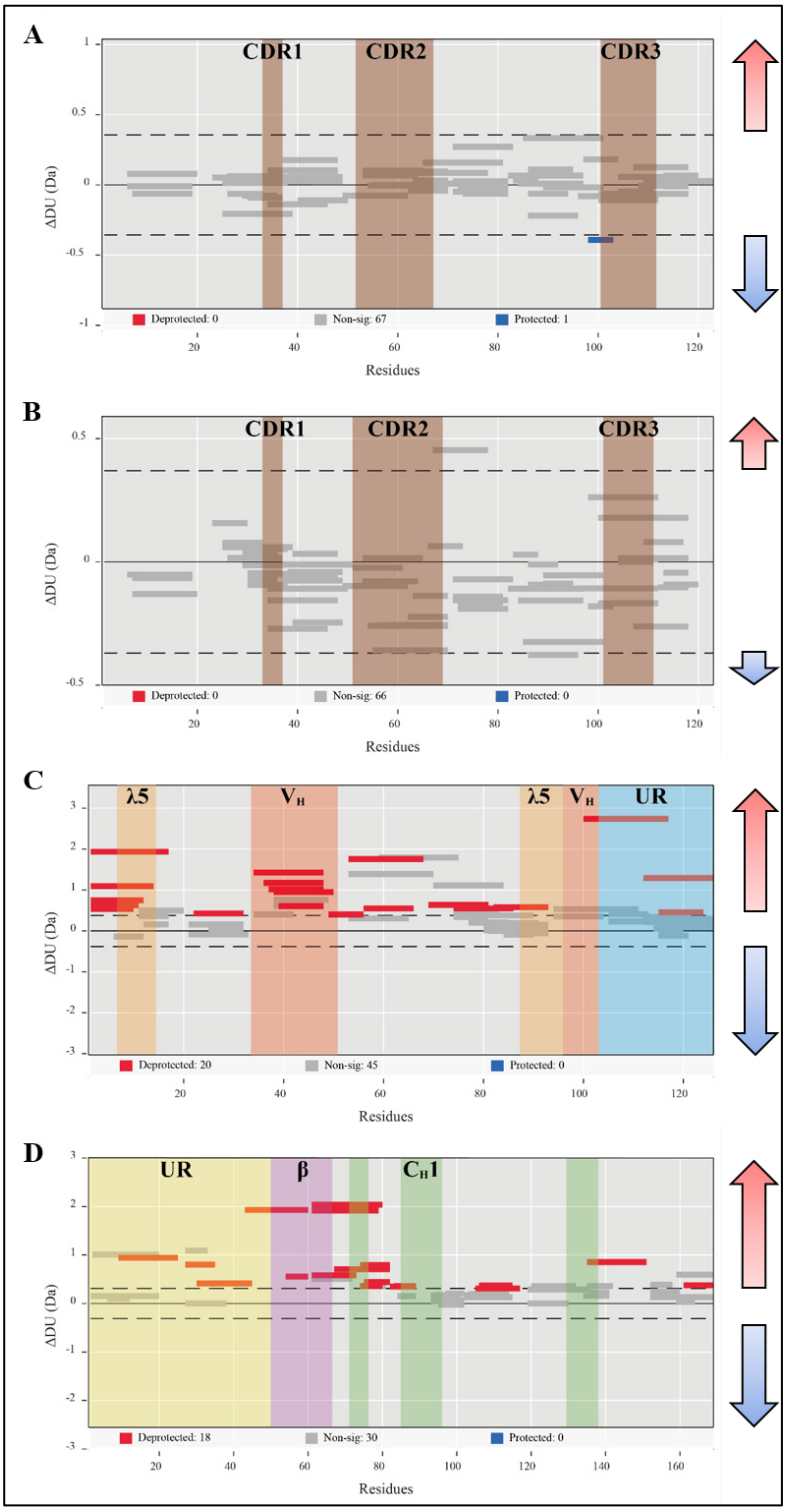

Figure 63: Complex Formation of VPREB and λ5 C212S with V_H 1HEZ Leads to Deprotection in the SLC Proteins and Protection in CDR3 of V_H 1HEZ by Differential HDX-MS Analysis.
Wood´s plots showing the summed differences in deuterium uptake in VPREB, λ5 C212S and V_H after 2 h of HDX, comparing V_H 1HEZ in the presence of VPREB alone with V_H 1HEZ alone (**A**), V_H 1HEZ in the presence of VPREB with V_H alone (**B**), VPREB in the presence of V_H 1HEZ with VPREB alone (**C**) and λ5 C212S in the presence of V_H 1HEZ with λ5 C212S alone (**D**). Wood´s plots were generated using Deuteros (Lau et al., 2020). Peptides coloured in blue or red, respectively, are protected or deprotected from exchange in presence of the interaction partner. Peptides with no significant difference between conditions, determined using a 99 % confidence interval (dotted line) and a p value < 0.1, are shown in grey. The VPREB-UR is coloured in blue, the λ5-UR in yellow, the λ5-interface in orange, the V_H-interface in red, the additional β-strand in magenta and the C_H1-interface in green. The CDRs in the V_H domain are coloured in brown.

2.7.2 Quaternary Structure Analysis of the SLC with V_H 1HEZ, V_L 1HEZ and V_L MAK33

To confirm the interaction of VPREB and λ5 C212S with V_H 1HEZ and to examine their quaternary structure upon interaction, AUC analysis was performed (Figure 64).

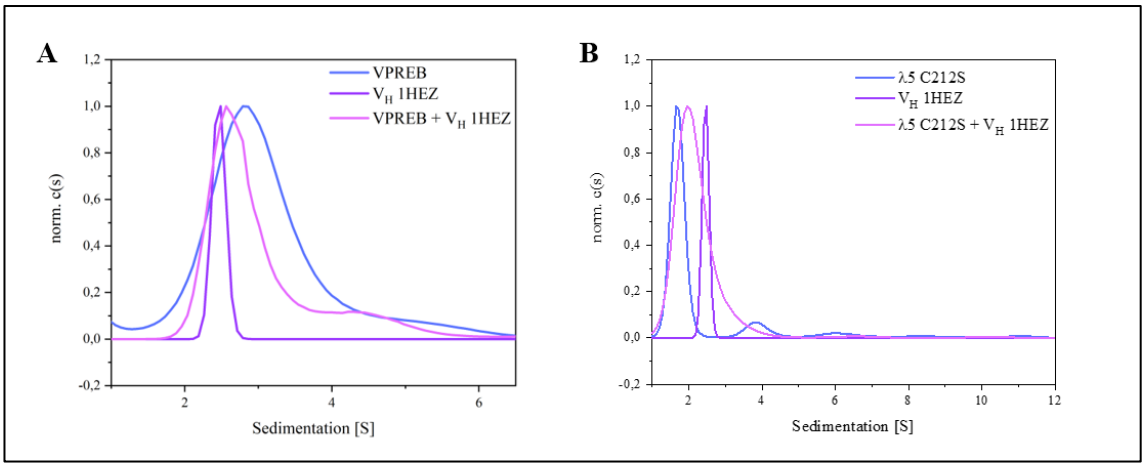

Figure 64: Quaternary Structure Analysis of V_H 1HEZ with VPREB (A) and with λ5 C212S (B) by AUC.

The analysis revealed that V_H 1HEZ alone forms a homodimer at about 2.5 S and that, upon interaction with VPREB, it collapses into a monomer that forms a heterodimer with VPREB at roughly 2.6 S (Figure 64A). Also, the interaction of λ5 C212S and V_H 1HEZ causes the dissociation of the V_H 1HEZ homodimer to form a heterodimer with λ5 C212S at around 2 S (Figure 64B).

Since VPREB, V_H and V_L domains share the same interface, it remained interesting, if VPREB can form a complex with V_L or with V_L and V_H at the same time. Therefore, it was tested if VPREB interacts with V_L MAK33 and V_L 1HEZ (Figure 65).

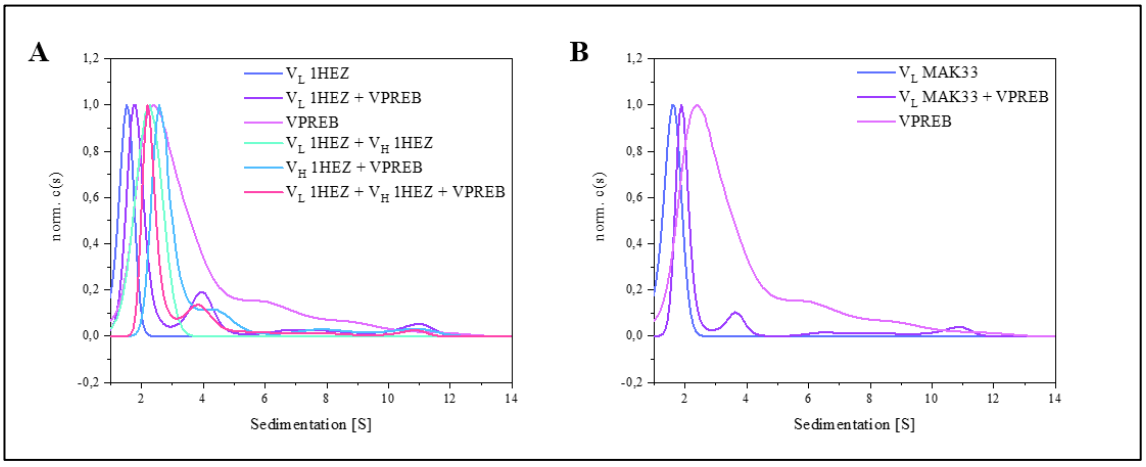

Figure 65: Quaternary Structure Analysis of VPREB with V_L 1HEZ (A) and with V_L MAK33 (B) by AUC.

As can be seen in Figure 65A, V_L 1HEZ and VPREB form a heterodimer at 1.9 S, as the peak is located between the V_L monomer and the VPREB homodimer. They are even able to form a heterotrimer to a minor fraction at 4 S. V_L 1HEZ alone is a monomer (1.6 S). The same can be observed for V_L MAK33 and VPREB. While V_L MAK33 alone is a monomer (1.8 S), the interaction with VPREB yielded a heterodimer at 2 S, with also a small fraction of trimers (VPREB homodimer + V_L MAK33) at roughly 3.8 S (Figure 65B).
V_L 1HEZ and V_H 1HEZ form a heterodimeric complex with a sedimentation coefficient of 2.2 S (Figure 65A). V_L 1HEZ, V_H 1HEZ and VPREB are even able to form a heterotrimeric complex at roughly 4 S indicating that the interface of VPREB and V_H is slightly distinct to the V_L-V_H interface.

2.7.3 CD Kinetics of V_H 1HEZ and VPREB

To investigate whether VPREB can get folded by V_H, CD kinetics were followed at 205 nm and 25°C (Figure 66).

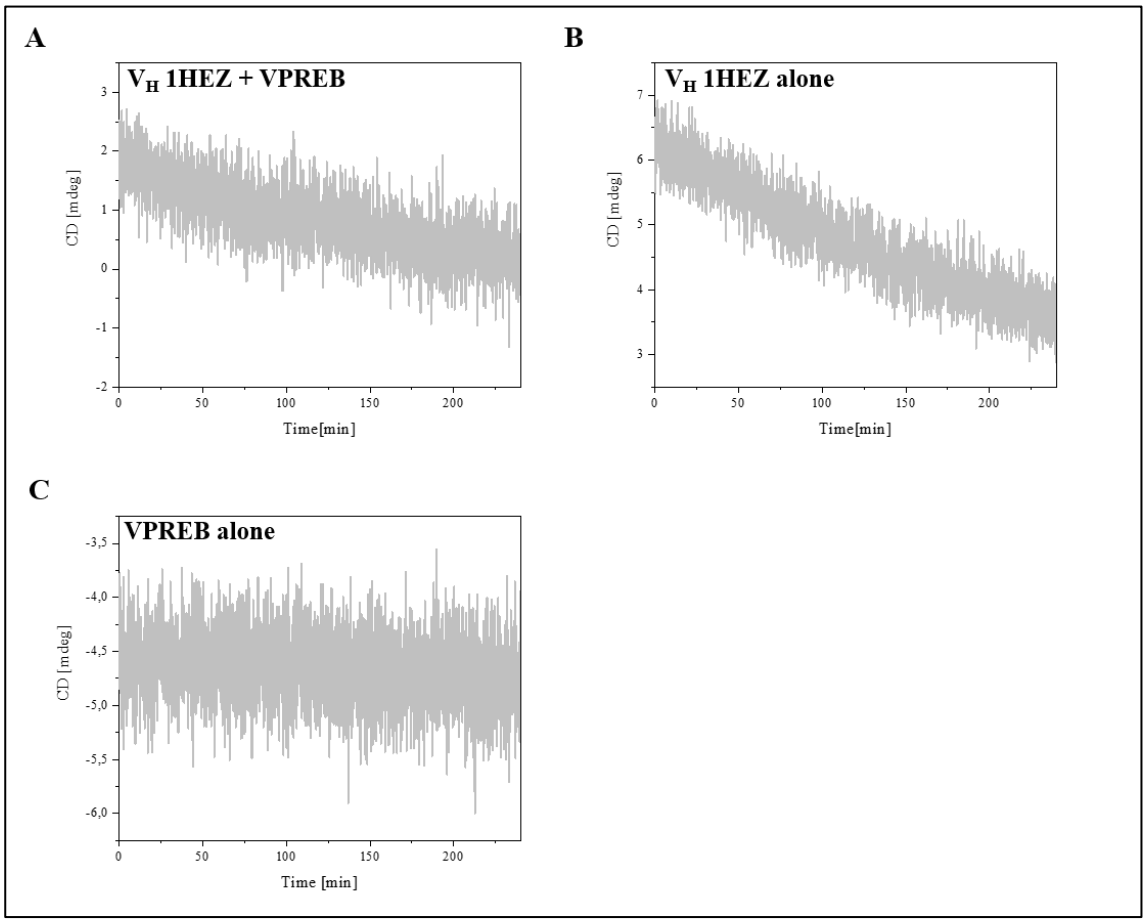

Figure 66: Folding Kinetics Measurements of V_H 1HEZ and VPREB.
Folding kinetics of V_H and VPREB (**A**), V_H 1HEZ alone (**B**) and VPREB alone (**C**) were monitored by CD spectroscopy at a constant wavelength of 205 nm at 25°C for 4 h. Each protein alone was equilibrated for 10 min at 25°C before the addition of the interaction partner.

As can be seen in Figure 66A, no increase in signal over time can be observed for V_H and VPREB, but rather a decrease of the signal over the time of 4 h. To examine whether this is a structural change because of interaction or can be ascribed to a photobleaching effect, V_H and VPREB each were measured alone over the same time of 4 h. While VPREB alone (Figure 66C) shows no decrease in signal and therefore no photobleaching, V_H alone (Figure 66B) shows a decrease in signal, which can be attributed to a potobleaching effect. Therefore, V_H doesn´t induce folding in VPREB.

2.7.4 Affinity of V_H with VPREB, λ5 C212S and Wildtype SLC

The understanding of the mechanism of how VPREB and λ5 interact with the V_H domain is still at an early stage. The affinities and binding kinetics were determined by SPR and should reveal the differences of the single proteins and the complex in interaction with V_H. To dissect these differences, two different V_H domains were utilized: V_H 1HEZ (human) and V_H MAK33 (murine). Their sequence alignment is depicted in Figure 67, which shows a high sequence similarity with only some minor variation and a bigger variation in the third CDR. These two sequences should serve to identify whether the mechanisms are conserved in mice and humans. The V_H domains were immobilized on a CM5 sensor chip by amine coupling via their lysines. This allows the V_H domains to be coupled in different orientations and therefore the probability that the binding site for the analytes is surface-exposed is higher.

```
VH1HEZ      AQVQLVESGGGVVQPGRSLRLSCAASGFTFSGYGMHWVRQAPGKGLEWVALISYDESNKY      60
VHMAK33     -EVQGVESGGGLVKPGGSLKLSCAASGFTFSDYYMYWVRQTPEKRLEWVATISDGGSYTY      59
             :** ******:*:** **:***********.* *:****:* * ***** ** . * .*

VH1HEZ      YADSVKGRFTISRDNSKNTLYLQMNSLRAEDTAVYYCAKVKFYDP--TAPNDYWGQGTLV      118
VHMAK33     YPDSVKGRFTISRDNAKNNLYLQMSSLKSEDTAMYYCARDKAYYGNYGDAMDYWGQGTSV      119
            * *************:**.*****.**::****:****: * *       ******* *

VH1HEZ      TVSS-      122
VHMAK33     TVSSA      124
            ****
```

Figure 67: Sequence Alignment of V_H 1HEZ and V_H MAK33 Using ClustalW (Madeira et al., 2019).

The sensorgrams are depicted in Figure 68 and show the titration of increasing analyte concentrations over the immobilized ligand. Their respective mean K_D, k_a and k_d values, which were obtained by fitting the data with the evaluation software of Biacore, are listed with their standard deviations in Table 9.

The association of V_H MAK33 and SLC C212S was observed with a K_D of 29.6 ± 5.5 nM with k_a to be determined as 42746 ± 7155 Ms^{-1} and k_d as 0.001 ± 0.00002 s^{-1} (Figure 68A, Table 9). It is lower than the K_D that was determined for V_H MAK33 and λ5 C212S, which was 43.1 ± 9.6 nM with k_a to be 44945 ± 12655 Ms^{-1} and k_d to be 0.002 ± 0.0001 s^{-1} (Figure 68B, Table 9). However,

the lowest K_D was determined for V_H MAK33 and VPREB to be 10.1 ± 3.7 nM with k_a = 65990 ± 25720 Ms^{-1} and k_d = 0.0006 ± 0.00002 s^{-1} (Figure 68C, Table 9).

Table 9: Binding and Binding Rate Constants (K_D, k_a, k_d) of V_H 1HEZ and V_H MAK33 with the Single SLC Proteins and the Complex.

Constructs		**K_D [nM]**	**k_a [Ms^{-1}]**	**k_d [s^{-1}]**
V_H MAK33	**SLC C212S**	29.6 ± 5.5	42745 ± 7155	0.001 ± 0.00002
	λ5 C212S	43.1 ± 9.6	44945 ± 12655	0.002 ± 0.0001
	VPREB	10.1 ± 3.7	65990 ± 25720	0.0006 ± 0.00002
V_H 1HEZ	**SLC C212S**	129.2 ± 26.8	19745 ± 305	0.003 ± 0.0005
	λ5 C212S	171.9 ± 77.0	12606 ± 6584	0.002 ± 0.0002
	VPREB	22.2 ± 9.0	41025 ± 10425	0.0008 ± 0.0001

The affinity of the complexes was measured by SPR to determine the K_D in [nM], k_a in [Ms^{-1}] and the k_d in [s^{-1}].

The same affinity pattern could be observed for the interaction with V_H 1HEZ. SLC C212S and V_H 1HEZ associate with a K_D of 129.2 ± 26.8 nM, a k_a of 19745 ± 305 Ms^{-1} and a k_d of 0.00254 ± 0.0004905 s^{-1} (Figure 68D, Table 9). The K_D is about 4-times higher than the K_D that was observed for SLC C212S and V_H MAK33. The K_D of λ5 C212S and V_H 1HEZ was measured to be 171.9 ± 77.0 nM with k_a to be 12606 ± 6584 Ms^{-1} and k_d to be 0.00166 ± 0.000162 s^{-1} (Figure 68E, Table 9), which is an about 4- fold higher K_D as it was determined for V_H MAK33. The affinity of λ5 C212S and V_H 1HEZ is decreased compared to SLC C212S and V_H 1HEZ. The association of VPREB and V_H 1HEZ was observed with a K_D of 22.245 ± 9.025 nM, a k_a of 41025 ± 10425 Ms^{-1} and a k_d of 0.000818 ± 0.0001384 s^{-1} (Figure 68F, Table 9). Altogether, K_Ds are about 2- to 4- fold higher than they were measured for V_H MAK33, which could be attributed to V_H 1HEZ forming a dimer when in isolation. The pattern is comparable to that observed for V_H MAK33. The affinity of VPREB and the V_H domains is remarkably higher than for λ5 C212S and SLC C212S. Furthermore, the affinity for SLC C212S is higher than for λ5 C212S alone. This might suggest, that VPREB alone binds first with the respective V_H domain, before λ5 C212S binds to VPREB, V_H and C_H1.

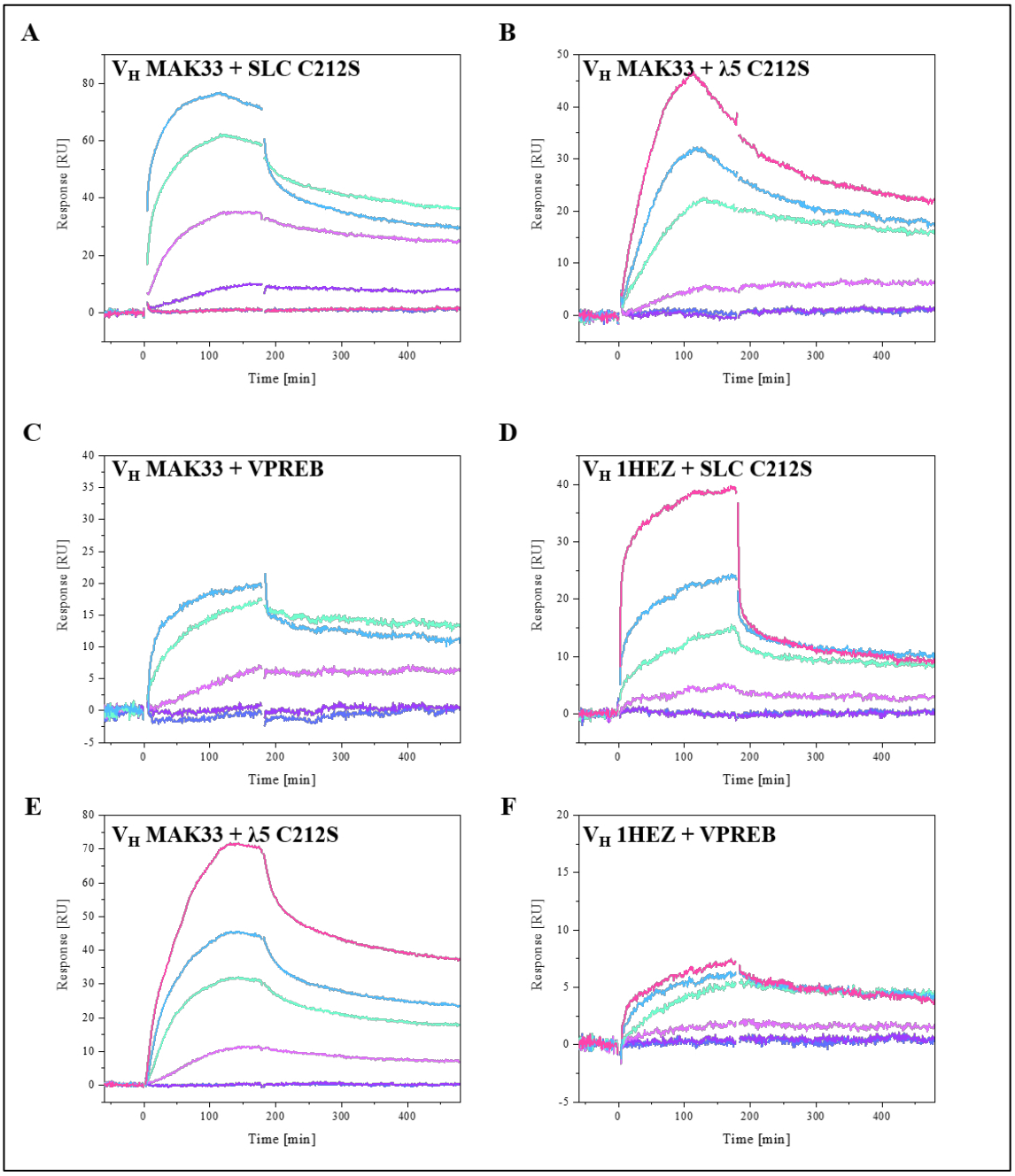

Figure 68: Affinities and Binding Kinetics of V_H 1HEZ and V_H MAK33 with the Single SLC Proteins and the Complex.
The affinities and binding kinetics of V_H MAK33 and SLC C212S (**A**), V_H MAK33 and ʎ5 C212S (**B**), V_H MAK33 and VPREB (**C**), V_H 1HEZ and SLC C212S (**D**), V_H 1HEZ and ʎ5 C212S (**E**) and V_H 1HEZ and VPREB (**F**) were measured and fitted by SPR.

2.7.5 Affinity of V_H with λ5 Variants

To analyze the roles that the additional β-strand, the UR and the tryptophanes in the UR of λ5 play in the interaction with V_H, the K_Ds, k_as and k_ds were determined between V_H 1HEZ and λ5 mutants lacking either the additional β-strand or the UR. V_H 1HEZ was immobilized as the ligand on the CM5 sensor chip via amine coupling and the λ5 mutants served as the analytes being

measured over the chip. The calculated K_Ds, k_as and k_ds are listed in Table 10 and the sensorgrams showing the titrations of increasing analyte concentrations are depicted in Figure 69.

Table 10: Binding and Binding Rate Constants (K_D, k_a, k_d) of V_H 1HEZ with ƛ5 Variants.

Protein	K_D [nM]	k_a [Ms^{-1}]	k_d [s^{-1}]
λ5 ΔU C212S	n. I.	n. I.	n. I.
λ5 Δβ C212S	121.7 ± 27.7	32175 ± 3735	0.004 ± 0.0004
λ5 W67,77,83A C212S	135.0 ± 25.6	16005 ± 4275	0.002 ± 0.0001

The affinity of the complexes was measured by SPR to determine the K_D in [nM], k_a in [Ms^{-1}] and the k_d in [s^{-1}].

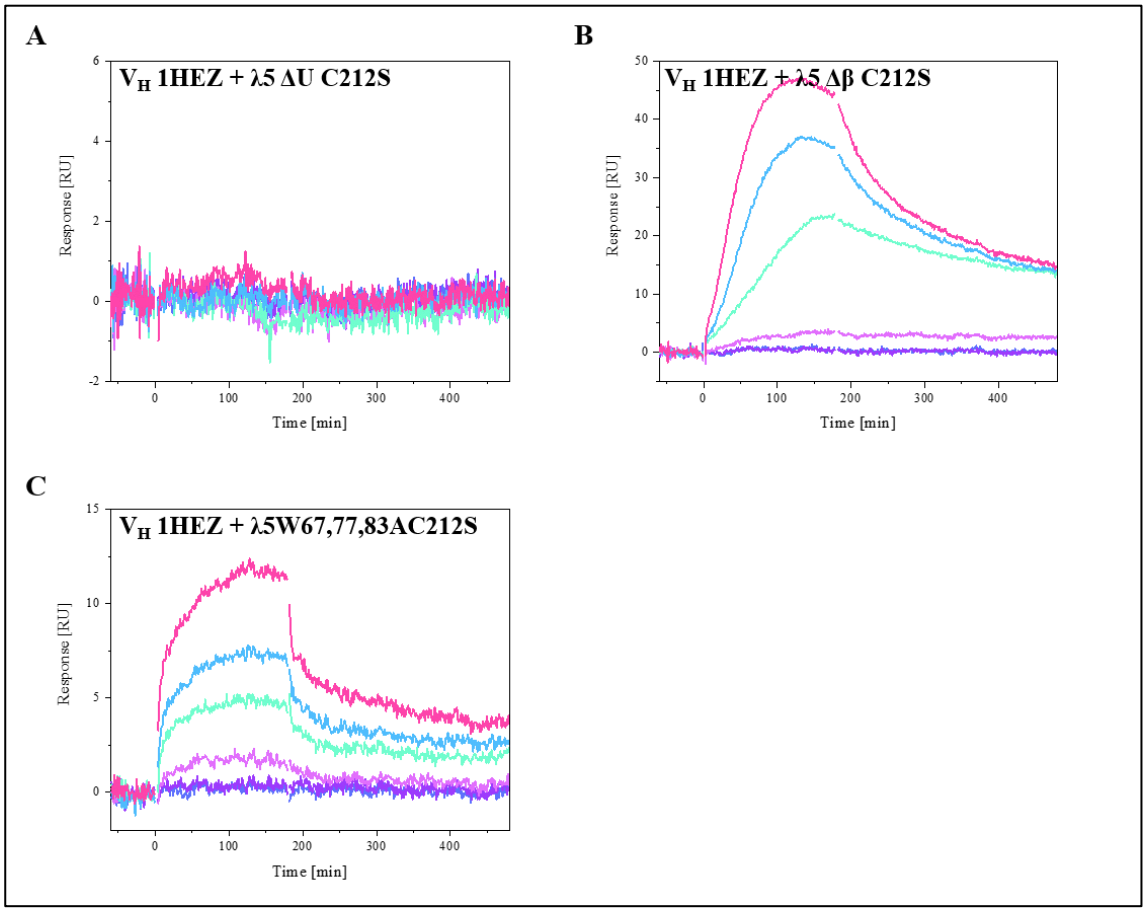

Figure 69: Affinities and Binding Kinetics of V_H 1HEZ With ƛ5 Variants.
The affinities and binding kinetics of V_H 1HEZ and ƛ5 ΔU C212S (**A**), V_H 1HEZ and ƛ5 Δβ C212S (**B**) and V_H 1HEZ and ƛ5 W67,77,83A C212S (**C**) were measured and fitted by SPR.

V_H 1HEZ and λ5 ΔU C212S showed no interaction as can be seen by the flat curves in the sensorgram (Figure 69A). This means that the interaction of λ5 C212S and V_H is conferred

uniquely by its UR. V_H 1HEZ and λ5 Δβ C212S can associate with a K_D measured to be 121.7 ± 27.7 nM, k_a to be 32175 ± 3735 Ms^{-1} and k_d to be 0.004 ± 0.0004 s^{-1} (Figure 69B, Table 10). This K_D is slightly lower as it was determined for λ5 C212S (K_D = 171.9 ± 77.0 nM) suggesting that the β-strand may play a role in the interaction of V_H and λ5 in impacting how the UR protrudes from λ5 and how accessible it is to interact with V_H. Furthermore, also the tryptophanes in the UR of λ5 might have an influence on its interaction with V_H because the K_D was slightly lower as it was observed for λ5 Δβ C212S. The association of V_H 1HEZ and λ5 W67,77,83A C212S could be measured with a K_D of 135.0 ± 25.6 nM, a k_d of 16005 ± 4275 Ms^{-1} and a k_d of 0.002 ± 0.0001 s^{-1} (Figure 69C, Table 10). In conclusion, both, the β-strand and the tryptophane-mutant of λ5, show a decreased affinity for V_H indicating a role in their interaction.

2.7.6 Affinity of V_H with VPREB Variants

The previous chapters could show the impact of the single SLC proteins and structural features of λ5 on the interaction with V_H. Not only the additional β-strand, but also the UR and its tryptophanes play a role. Moreover, VPREB alone was identified to bind with a remarkable high affinity to V_H. It remains elusive which part of VPREB is responsible for this high affinity. Therefore, several different mutants were tested that either lack the UR completely or have mutations in it like the tryptophane-to-alanine mutation at position 131 and the glutamate to glutamine mutations to delete all negative charges in the UR. To evaluate how the folding status impacts this interaction, VPREB mutants with the β-strand of λ5 and therefore being folded, were tested. The calculated K_Ds, k_as and k_ds are listed in Table 11 and the respective sensorgrams are depicted in Figure 70.

Table 11: Binding and Binding Rate Constants (K_D, k_a, k_d) of V_H with VPREB Variants.

Constructs		**K_D [nM]**	**k_a [Ms^{-1}]**	**k_d [s^{-1}]**
V_H MAK33	**VPREB ΔU**	31.5 ± 3.8	50185 ± 4105	0.002 ± 0.00006
V_H 1HEZ	**VPREB ΔU**	905.5 ± 278.5	1611 ± 656	0.001 ± 0.0001
	VPREB βU	1817.5 ± 707.5	1774 ± 653	0.003 ± 0.00007
	VPREB ΔU + β	700.4 ± 27.2	2261 ± 133	0.002 ± 0.0001
	VPREB W131A	69.7 ± 5.6	21350 ± 570	0.001 ± 0.0002
	VPREB 9EurQ	136.1 ± 5.4	15791 ± 7260	0.002 ± 0.0001

The affinity of the complexes was measured by SPR to determine the K_D in [nM], k_a in [Ms^{-1}] and the k_d in [s^{-1}].

Interestingly, VPREB ΔU and immobilized V_H 1HEZ associated with a roughly 40-fold higher K_D than VPREB and V_H 1HEZ. The K_D of VPREB ΔU and V_H 1HEZ was calculated to be 905.5 ± 278.5 nM with a k_a of 1611 ± 656 Ms^{-1} and a k_d of 0.001 ± 0.0001 s^{-1} (Figure 70B, Table 11). Because of this remarkable difference, VPREB ΔU and immobilized V_H MAK33 were measured. This affinity is only 3-fold lower than for VPREB and V_H MAK33 with a K_D of 31.5 ± 3.8 nM, a k_a of 50185 ± 4105 Ms^{-1} and a k_d of 0.002 ± 0.00006 s^{-1} (Figure 70A, Table 11). Considering that the overall affinity of V_H MAK33 and SLC proteins is higher, one can conclude that the UR of VPREB seems to be involved in the interaction with V_H.

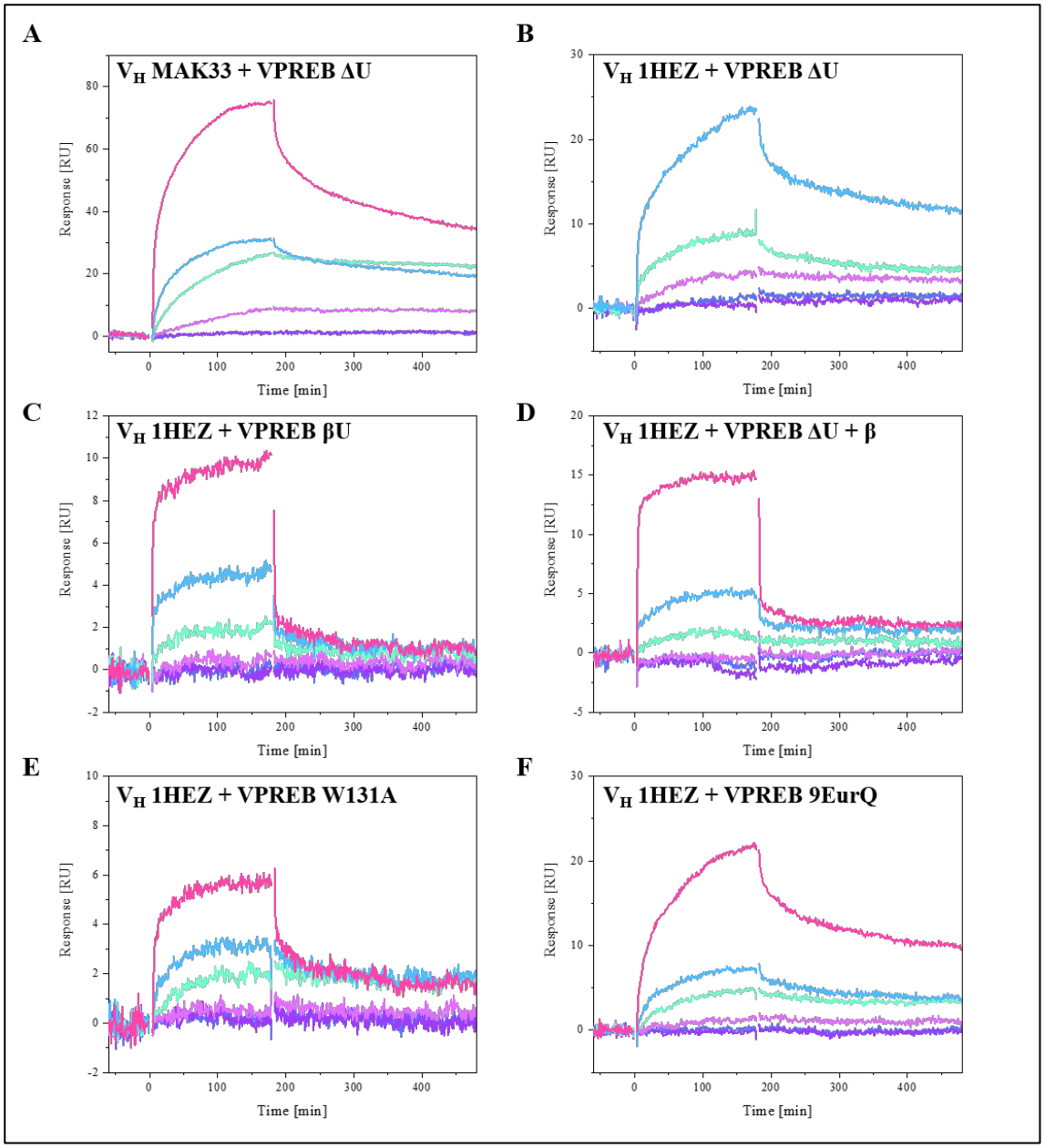

Figure 70: Affinities and Binding Kinetics of V_H with VPREB Variants.
The affinities and binding kinetics of V_H MAK33 and VPREB ΔU (**A**), V_H 1HEZ and VPREB ΔU (**B**), V_H 1HEZ and VPREB βU (**C**), V_H 1HEZ and VPREB ΔU + β (**D**), V_H 1HEZ and VPREB W131A (**E**) and V_H 1HEZ and VPREB 9EurQ (**F**) were measured and fitted by SPR.

To examine the influence of the folding status on V_H interaction, immobilized V_H 1HEZ was measured for its association with VPREB βU. The affinity was even 80-fold reduced compared to WT VPREB with a K_D calculated to be 1817.5 ± 707.5 nM, k_a to be 1774 ± 653 Ms^{-1} and k_d to be 0.003 ± 0.00007 s^{-1} (Figure 70C, Table 11). The affinity for the second folded mutant of VPREB, VPREB ΔU + β, was determined to have a K_D of 700.4 ± 27.2 nM, a k_a of 2261 ± 133 Ms^{-1} and a k_d of 0.002 ± 0.0001 s^{-1} (Figure 70D, Table 11). From this, it can be concluded that the association of unfolded VPREB with V_H 1HEZ is favorable over folded VPREB. One might expect that VPREB ΔU + β binds with lower affinity than VPREB βU because it is lacking the UR, which could be determined as a main interacting element with V_H. However, one should consider that in the VPREB βU mutant the UR is located on the other side of the protein as described in more detail in section 2.2 and might therefore have no point of contact with V_H 1HEZ.

V_H 1HEZ and VPREB W131A were able to associate with a calculated K_D of 69.7 ± 5.6 nM, a k_a of 21350 ± 570 Ms^{-1} and a k_d of 0.001 ± 0.0002 s^{-1} (Figure 70E, Table 11). This K_D is increased by about 3- fold compared to WT VPREB, indicating that the tryptophane in the UR of VPREB plays a role in interaction with V_H as do the tryptophanes in the UR of λ5. Moverover, the measurement of V_H 1HEZ and VPREB 9EurQ determined a K_D of 136.1 ± 5.4 nM, a k_a of 15791 ± 7260 Ms^{-1} and a k_d of 0.002 ± 0.0001 s^{-1} (Figure 70F, Table 11). The affinity is about 6-fold decreased compared to the WT, indicating the negatively charged glutamates in the UR of VPREB to be involved in V_H interaction.

2.8 Analysis of Antigen Affinity of SLC

It is known from the literature that the SLC in the context of a Fab complex is able to bind to GAL1 and Bill-Cadherin as antigens/ligands (Ohnishi et al., 2000; Elantak et al., 2012). Further antigens and binding partner of the pre-BCR are not known so far. Therefore, it is interesting how the SLC influences the antigen binding capacity of a Fab complex. In this context, the murine Fab MAK33 was investigated, which is known to bind human creatine kinase (muscle-type) as an antigen, and the MAK33 Fd fragment was combined with the SLC to create a SLC-Fab. Furthermore, V_H MAK33 was measured in different combinations with VPREB and λ5 variants and compared to V_L. To examine the influence of the SLC on antigen binding, enzyme-linked immune-sorbent assays (ELISAs) were set up with the biotinylated antigen to be immobilized via streptavidin binding in a 96-well plate. Both, the V_H MAK33 and the Fd MAK33 were C-terminally labelled with a FLAG-Tag, which was used to create a read-out of the assay (the ELISA is described in detail in section 5.3.13.7).

2.8.1 Antigen Affinity of the Fab-Fragments

To address whether the pre-BCR can recognize the antigen, the affinity of the Fab-SLC and Fab-LC complexes for human creatin kinase was determined by ELISA. The K_Ds that were obtained from the Hill1´s fitting of the data are listed in Table 12 and the respective diagrams are shown in Figure 71.

Table 12: K_D Values in [nM] of Fab-SLC and Fab-LC to the Antigen Determined by ELISA Assays.

	K_D [nM]
Fab - SLC	8.61 ± 1.89
Fab - LC	12.62 ± 3.11

Human creatin kinase (muscle type) was used as an antigen. The K_D values were determined by an Hill1 fit of the graphs.

As can be seen in Figure 71A, Fab-SLC is able to bind with a remarkable high affinity to the antigen creatin kinase. With a calculated K_D of 8.61 ± 1.89 nM, the affinity is almost double as high as the affinity of Fab-LC, which was caculated to be 12.63 ± 3.11 nM (Figure 71B, Table 12). This means that the SLC seems to enhance antigen binding instead of inhibiting it, contrary to expectations.

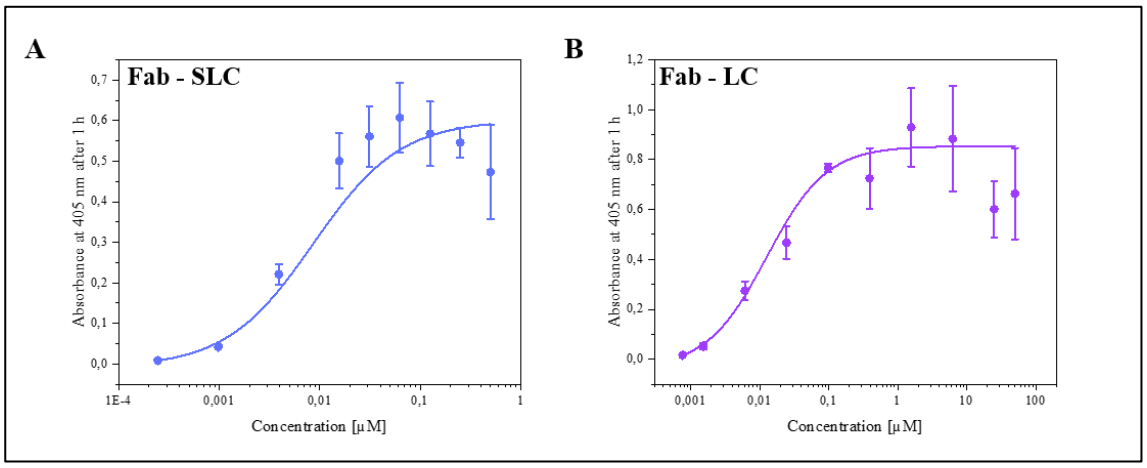

Figure 71: ELISA Revealed Higher Antigen Affinity of Fab-SLC (A) Over Fab-LC (B).
For comparison of the functionality of Fab-SLC (**A**) with Fab-LC (**B**) an ELISA was performed. Biotinylated human creatine kinase was coupled to a streptavidine-coated microwell plate. The Fd MAK33 was labelled with a C-terminal FLAG-Tag and could be detected with an anti-FLAG antibody coupled to horseradish peroxidase. The absorption was recorded after 1 h at 405 nm. Experiments were performed at 25°C.

2.8.2 Antigen Affinity of the SLC

To evaluate which SLC proteins and which part is involved in antigen interaction, different combinations of V_H MAK33 with the SLC proteins were measured. Moreover, their affinities

were compared with the affinity of V_H MAK33 alone and in complex with V_L MAK33. The calculated K_Ds are listed in Table 13 and the diagrams are shown in Figure 72.

V_H MAK33 binds to the antigen with a calculated K_D of 282.6 ± 0.06 nM (Figure 72A, Table 13). The K_D of the V_H-V_L MAK33 complex for the antigen was determined to be 155.9 ± 0.06 nM (Figure 72B, Table 13). The K_D is decreased by approximately half compared to V_H MAK33 alone and therefore the affinity is increased 2-fold. The complex of V_H MAK33 with SLC C212S was probed for its antigen interaction to evaluate the impact of the missing C_H1 domain. The K_D of V_H MAK33 and SLC C212S was determined to be 94.1 ± 0.02 nM (Figure 72C, Table 13). Compared to Fab-SLC, the K_D is increased about 10-fold, indicating that the affinity for the antigen is decreased. This should serve as a reference point for probing the single SLC proteins and its variants.

Table 13: K_D Values in [µM] of V_H with V_L or SLC Proteins to the Antigen Determined by ELISA Assays.

	K_D [nM]
V_H MAK33	282.6 ± 0.06
V_H MAK33 + V_L MAK33	155.9 ± 0.06
V_H MAK33 + SLC C212S	94.1 ± 0.02
V_H MAK33 + λ5 C212S	95.0 ± 0.03
V_H MAK33 + VPREB	260.1 ± 0.02

Human creatin kinase (muscle type) was used as an antigen. The K_D values were determined by an Hill1 fit of the graphs.

To determine which part of the SLC contributes to the antigen interaction, the single proteins, VPREB and λ5 C212S were measured each in complex with V_H MAK33. Surprisingly, the complex consisting of V_H MAK33 and λ5 C212S has a high affinity with a K_D determined as 95.0 ± 0.03 nM (Figure 72D, Table 13), whereas the complex of V_H MAK33 and VPREB has a lower affinity with a K_D of 260.1 ± 0.02 nM (Figure 72E, Table 13). This shows unambiguously that λ5 C212S is an important part of the SLC for antigen interaction. However, compared to V_H MAK33 alone, the complex of V_H MAK33 and VPREB has a similar affinity showing that VPREB does not interact significantly with the antigen.

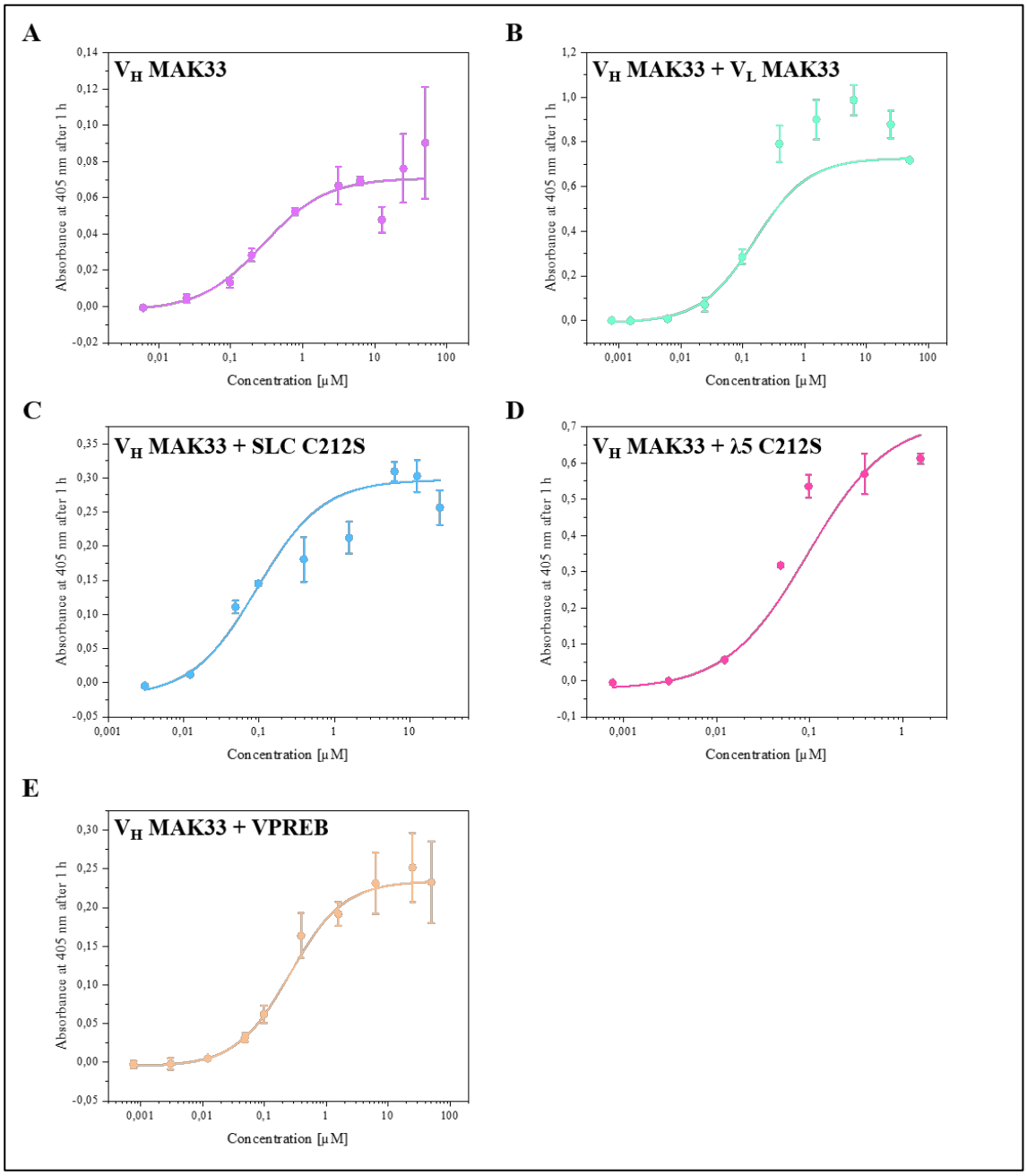

Figure 72: ELISA of V_H with V_L or SLC Proteins to the Antigen Determined by ELISA Assays. For comparison of the functionality of V_H-V_L and V_H-SLC an ELISA was performed. **A** V_H MAK33 alone, **B** V_H MAK33 + V_L MAK33, **C** V_H MAK33 + SLC C212S, **D** V_H MAK33 + ʎ5 C212S, **E** V_H MAK33 + VPREB. Biotinylated human creatine kinase was coupled to a streptavidine-coated microwell plate. The V_H MAK33 domain was each labelled with a C-terminal FLAG-Tag and could be detected with an anti-FLAG antibody coupled to horseradish peroxidase. The absorption was recorded after 1 h at 405 nm. Experiments were performed at 25°C.

2.8.3 Antigen Affinity of SLC Mutants

To dissect which parts of λ5 C212S and VPREB are important for antigen recognition and interaction, several mutants of both proteins were screened. These comprise mutants lacking the URs, mutations of the UR-tryptophanes to alanines and mutation of the negatively charged

glutamates in the UR of VPREB to uncharged glutamines. The diagrams are depicted in Figure 73 and the K_Ds obtained from their exponential fits are listed in Table 14.

Table 14: K_D Values in [µM] of V_H and SLC Variants to the Antigen Determined by ELISA Assays.

	K_D [µM]
V_H MAK33 + VPREB ΔU + β	140.9 ± 0.01
V_H MAK33 + VPREB ΔU	263.1 ± 0.03
V_H MAK33 + λ5 W67,77,83A C212S	130.7 ± 0.01
V_H MAK33 + VPREB W131A	157.6 ± 0.04
V_H MAK33 + VPREB 9EurQ	198.1 ± 0.03

Human creatin kinase (muscle type) was used as an antigen. The K_D values were determined by an Hill1 fit of the graphs.

V_H MAK33 and VPREB ΔU + β have an antigen affinity of 140.9 ± 0.01 µM (Figure 73), which is very similar to the affinity of V_H and V_L MAK33. This was to be expected because VPREB ΔU + β resembles a V_L domain and has also three CDRs. Obviously, they seem fully functional. V_H MAK33 and VPREB ΔU show a K_D of 263.1 ± 0.03 nM when interacting with the antigen (Figure 73B, Table 14). The K_D is roughly the same as for the complex of V_H MAK33 and WT VPREB and V_H MAK33 alone, indicating that the UR of VPREB doesn´t seem to be involved in antigen interaction. To identify a possible role of the tryptophanes in the UR of λ5 C212S, the complex of V_H MAK33 and λ5 W67,77,83A C212S was measured. A K_D of 130.7 ± 0.01 nM (Figure 73C, Table 14) was calculated for this combination, which is a bit higher than the K_D for λ5 C212S. This indicates a role for the tryptophanes in the UR of λ5 C212S in terms of antigen interaction. Moreover, the same question remained open for the tryptophanes in the UR of VPREB, which was determined to be 157.6 ± 0.04 µM (Figure 73D, Table 14). The K_D is decreased compared to WT VPREB. Finally, it was assessed if the glutamates in the UR of VPREB are involved in antigen interaction. V_H MAK33 and VPREB 9EurQ show association with the antigen with a calculated K_D of 198.1 ± 0.03 µM (Figure 73E, Table 14). This K_D is slightly lower than for WT VPREB.

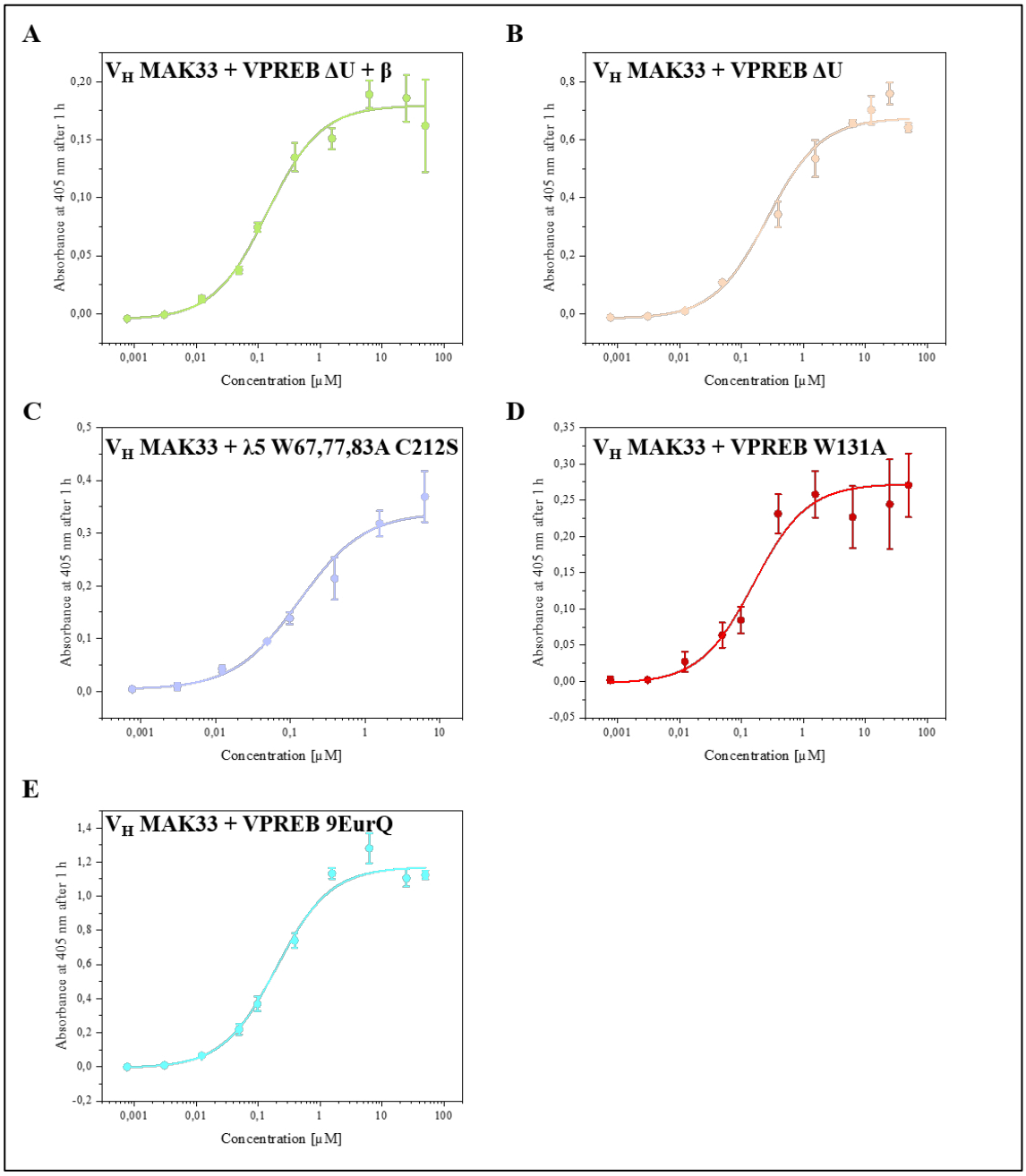

Figure 73: ELISA of V_H with SLC Variants to the Antigen Determined by ELISA Assays.
For comparison of the functionality of SLC Variants an ELISA was performed. **A** V_H MAK33 + VPREB ΔU + β. **B** V_H MAK33 + VPREB ΔU. **C** V_H MAK33 + ƛ5 W67,77,83A C212S. **D** V_H MAK33 + VPREB W131A. **E** V_H MAK33 + VPREB 9EurQ. Biotinylated human creatine kinase was coupled to a streptavidine-coated microwell plate. The V_H MAK33 domain was each labelled with a C-terminal FLAG-Tag and could be detected with an anti-FLAG antibody coupled to horseradish peroxidase. The absorption was recorded after 1 h at 405 nm. Experiments were performed at 25°C.

2.9 Analysis of BiP Binding Sites in VPREB and λ5 C212S

The BiP binding prediction algorithm (Schneider et al., 2016) predicted BiP binding sites in both, VPREB and λ5 C212S (Figure 74). The predicted BiP binding sites in VPREB are located near the interface with the V_H domain (Figure 74A), while the binding sites in λ5 C212S are in the UR (Figure 74B).

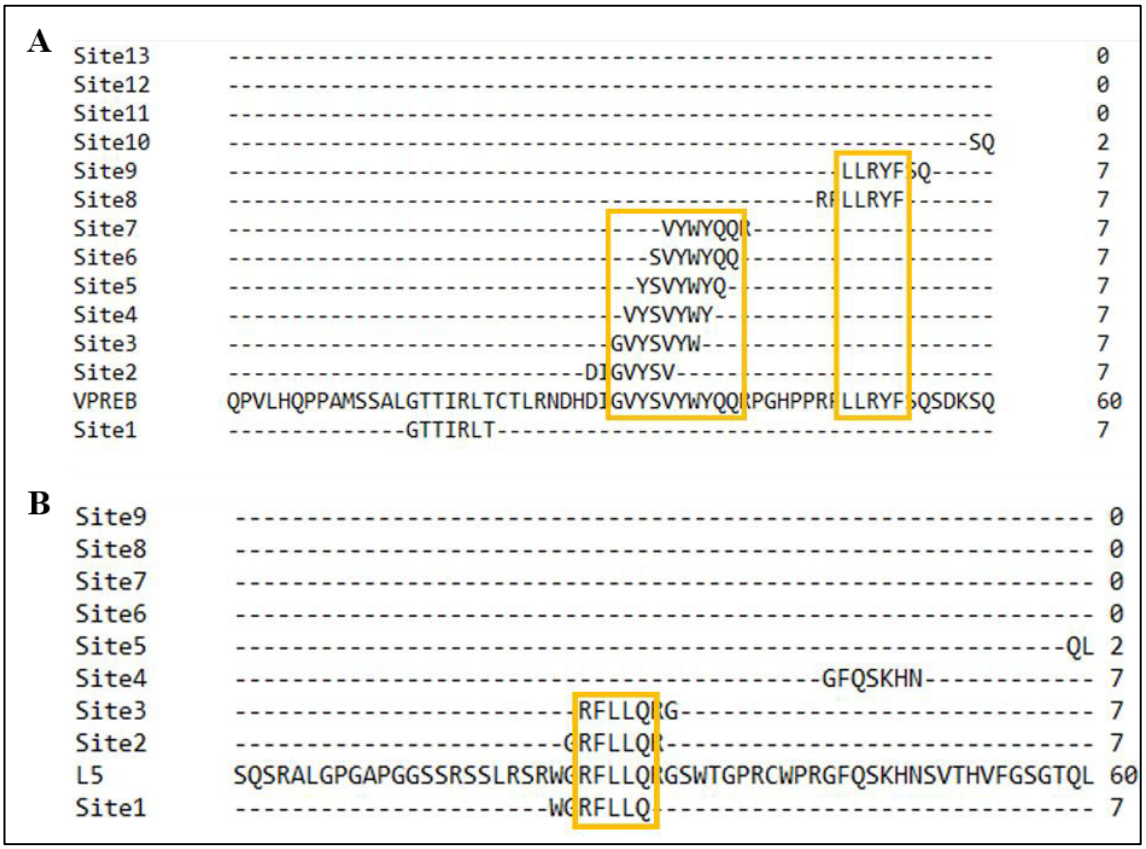

Figure 74: Predicted BiP Binding Sites in VPREB (A) and λ5 C212S (B).
The BiP binding sites were predicted by the algorithm of Schneider et al (Schneider et al., 2016). Residues identified in most sites are highlighted in orange. Only sites with a score >0.93 were taken.

3. DISCUSSION

The results produced in this thesis allow drawing several conclusions that are discussed in detail in the following chapters. Synoptical, one key finding was the existence of VPREB alone as an unfolded homodimer. This ratio is shifted in the presence of the β-strand, both, on an intra- and on an intermolecular level towards a monomer in a monomer-dimer equilibrium. Moreover, the additional β-strand of ʎ5 is sufficient for induction of the folding reaction in VPREB. Furthermore, VPREB and ʎ5 form a stable heterodimer but their association does not increase the stability. Additionally, it was found for the URs to both, destabilize the single SLC proteins and the complex. The Fab fragment, harboring the SLC instead of the LC, exhibits a strong antigen affinity, even higher than a conventional Fab fragment, which is mediated by the ʎ5-UR, specifically by the tryptophanes in the UR. This is surprising. Also, the ʎ5-UR is decisive for its interaction with V_H. Moreover, the VPREB-UR is implicated in the interaction with V_H by increasing the affinity. Unfolded VPREB and the V_H domain form a heterodimer with a high affinity and V_H does not induce any folding in VPREB. Surprisingly, VPREB and C_H1 form also a heterodimer without inducing a folding reaction in any of the two proteins. Additionally, ʎ5 alone induces the folding of C_H1 upon interaction and its core domain is sufficient and necessary in this interaction. In addition, the literature stated a possible role for the pre-BCR to cluster and aggregate ligand independently (Bankovich et al., 2007). However, the results showed that Fab-SLC is not able to form higher oligomers on its own but rather forms only a heterotrimer consisting of Fd, VPREB and λ5.

3.1 VPREB Alone Forms an Unfolded Homodimer

Several results indicate VPREB to form an unfolded homodimer in the absence of its binding partners, ʎ5 and the HC. This could be concluded from CD measurements as well as AUC analysis, glutaraldehyde crosslinking and ITC measurements. Also, NMR measurements confirmed the unfolded nature of VPREB. Notably, the two mutants with the intramolecularly inserted β-strand, VPREB βU and VPREB ΔU + β, are shifted towards a monomer in a monomer-dimer equilibrium. The same was observed for the intermolecularly added β-strand peptide to VPREB and for VPREB 9EurQ, the variant with all nine glutamates in its UR mutated to alanines. In the crosslinking experiments, no dimer was observed for VPREB βU and VPREB ΔU + β, which could be attributed to the used concentration. A concentration of 15 µM was used in the crosslinking experiments, which is lower than the calculated K_D for the dimer affinity. Morstadt et al. calculated a K_D of 34.3 ± 2.2 µM for the VPREB dimer by sedimentation equilibrium runs executed by AUC (Morstadt et al., 2008) and Hirabayashi et al. calculated a K_D of 508 nM by SPR experiments (Hirabayashi et al., 1995).

In Gauthier et al., it was also shown that VPREB interacts with itself with a K_D of 25.2 nM (Gauthier et al., 1999). Morstadt et al. also observed dimers in the crystal structure (Morstadt et al., 2008). The differences of the K_Ds between the three studies are quite outstanding with up to 30-fold differences. The K_D determined by Morstadt et al. seems the most reliable of the three because they performed the measurements in triplicates, whereas in the other two research papers only one replicate was measured. Furthermore, there is a limitation with the immobilization of dimeric proteins on the CM5 chip in SPR measurements. The proteins can only be immobilized as monomeric proteins because the acidic pH of the immobilization buffer disrupts non-covalent interactions in dimers. This may cause damage to the otherwise dimeric proteins and render them inactive or change their three-dimensional conformation. If the VPREB homodimer had such a high affinity, it would be not adavantegous for it to bind to λ5 or the Fd fragment. Therefore, the high affinity, especially the one measured by Gauthier et al. with a K_D of roughly 25 nM seems unreasonable. The sedimentation equilibrium runs by AUC seem to be the more suitable method for measuring the K_D of a dimer compared to SPR. The existence of a VPREB homodimer is consistent with the hydrophobic interface observed between subunits. This enables their dimerization in an aqueous solution (Morstadt et al., 2008).

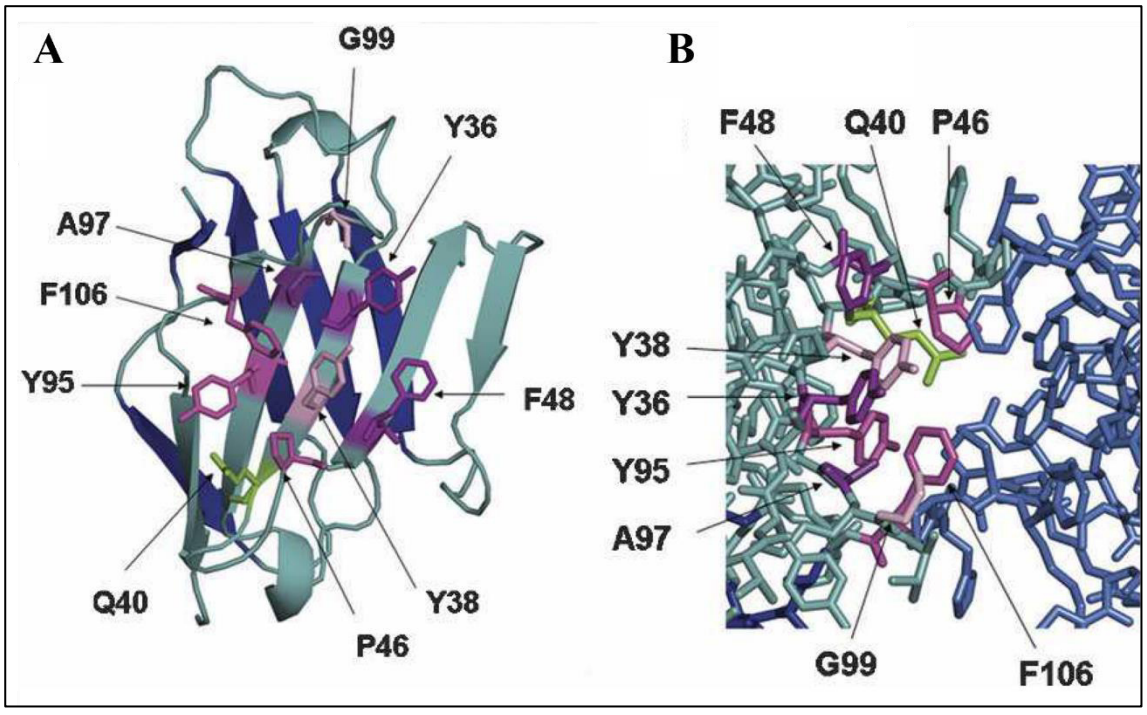

Figure 75: The Interface of the VPREBΔU+β Dimer.
A The interface residues of the VPREBΔU+β dimer are depicted, which are: Y36 (CDR1), Y38 (FR2), Q40 (FR2), P46 (FR2), F48 (FR2), Y95 (FR3), A97 (CDR3), G99 (CDR3), H104 (CDR3) and F106 (J region). Y38, Q40, P46, Y95 and F106 are conserved between VPREB and V_L domains. **B** Hydrophobic cavity of the interface of the VPREB ΔU+β dimer. The aromatic residues pack in a "herringbone" motif. Figure and legend were taken and modified from Morstadt et al., 2008 (Morstadt et al., 2008).

The interface for the VPREB ΔU + β (VPREBJ) homodimer was shown to be located at the VPREB-V_H interface by crystallography (Morstadt et al., 2008). They found the interface to be tilted forming a small cavity at the bottom, which ends with two hydrogen bonds being formed between the glutamines at position 40 in each monomer (Morstadt et al., 2008). This glutamine hydrogen bond was shown to be conserved in some V_H-V_L interfaces. As depicted in Figure 75, bulky residues contribute to the large non-polar dimer interface: Y36, Y38, P46, F48, Y95 and F106. Altogether, ten residues are important for the interface, one being not shown in Figure 75 (Morstadt et al., 2008). In addition to the already mentioned residues, also A97, G99, F106 and H104 play a role, the latter one not depicted (Morstadt et al., 2008). Compared to ten residues that are indispensable for V_L-V_H interaction (Chothia et al., 1985), Y38, Q40, P46, Y95 and F106 are conserved in mammalian VPREB and V_L. VPREB contributes with eight residues, while the β-strand of ʎ5 contribute two (Morstadt et al., 2008).

Gauthier et al. also showed that the single chain (sc) SLC can interact with itself with an even higher affinity (1.52 nM). The scSLC comprises the two SLC proteins, VPREB and λ5, that are covalently linked between their URs. The similar affinities between scSLC and scSLC+Fd point towards a similar type of interaction (Gauthier et al., 1999). Also, Bankovich et al. was able to observe a SLC homodimer in the crystal structure (Bankovich et al., 2007).

The affinity for the VPREB dimer was determined to be weaker than for the V_L-V_H interaction (K_D = 10 μM) (Klein et al., 1979). Morstadt et al. also performed 2D ^{15}N, ^{1}H HSQC NMR measurements, which further supported the existence of a monomer-dimer equilibrium of VPREB ΔU + β (Morstadt et al., 2008).

The reason for the lower affinity between the VPREB βU and VPREB ΔU + β dimers compared to the VPREB variants without the β-strand could be attributed to the VPREB-ʎ5 interface being involved in dimerization of unfolded VPREB. This is further substantiated by the shift to a monomer in a monomer-dimer equilibrium when the β-strand is added intermolecularly as a peptide to VPREB. Therefore, when the VPREB-ʎ5 interface is occupied by the β-strand, VPREB looses this site to form a homodimer. Another possible reason might be that the β-strand induces folding of VPREB, which causes the hydrophobic residues to be buried in the inside of the folded proteins, which are involved in the homodimerization of unfolded VPREB. Hydrophobic residues are surface-exposed in unfolded proteins.

The interface in the VPREB ΔU + β homodimer is a good reference point to study the interface in the VPREB homodimer. However, it seems obvious that the VPREB interface is deviating in the unfolded protein lacking the β-strand. Concluding from this, one can not assume that the VPREB and VPREB ΔU + β share completely the same residues in their interfaces. Therefore, it might be of further interest to identify the residues that are involved in the VPREB dimer interface. This could be facilitated by crosslinking coupled to MS experiments.

The URs seem to play a minor role in the homodimerization of VPREB. This could be on the one hand due to the localization of the UR in the VPREB βU mutant. In this variant, the UR is located opposite to where it is located in WT VPREB and therefore also far away from the hypothetical VPREB interface. This makes it impossible for the UR to contribute to the homodimerization, which is reflected by a monomer-dimer equilibrium with a shift to the monomer in AUC measurements, at least more than it is the case for the VPREB ΔU + β mutant. On the other hand, the importance of the UR is reflected in results of glutaraldehyde crosslinking experiments where the lack of the UR resulted in a weaker dimer band for VPREB ΔU indicating that the propensity for dimerization is lower in this mutant. The UR contains nine negatively charged glutamates and four positively charged residues (one histidine, three arginines), that might contribute to electrostatic interactions between the URs. Also, the VPREB 9EurQ mutant shows a shifted monomer-dimer equilibrium and a weaker dimer-band in the crosslinking experiments, which substantiates this hypothesis. In summary, the VPREB-UR seems to be involved, however to a smaller extent, in homodimerization via electrostatical interactions by oppositely charged amino acids.

The propensity of VPREB to dimerize could already be observed during purification. Oxidation of disulfide bonds by an introduced glutathione-system led also to the formation of intermolecular disulfide bridges in a small fraction, although the protein was diluted to a concentration of 0.05 g L^{-1}.

The HDX data could serve for identification and validation of the VPREB dimer interface. Regions with protected residues might reflect sites involved in dimer interaction. Indeed, the VPREB-V_H interface, that is assumed to also serve as the dimer interface in VPREB shows more protected amino acids compared to the rest of the protein. However, also a part of the VPREB-λ5 interface is considerably more protected in VPREB and VPREB ΔU. Of course, also in VPREB ΔU + β and VPREB βU, the VPREB-β interface is more protected but this is due to the added β-strand. However, also the VPREB-λ5 interface might therefore play a role in dimerization in the absence of the β-strand.

In mutants affecting the UR of VPREB, differences in conformational dynamics throughout the protein can be observed, also in the VPREB-V_H and VPREB-λ5 interface regions. For example, one can observe more deprotection in the VPREB-λ5 interface, most pronounced in the VPREB 9EurQ mutant. This mutant shows also a shifted monomer-dimer equilibrium with less dimers. Also, VPREB βU is deprotected in both, the VPREB-V_H and the VPREB-λ5 interfaces, reflected by its existence predominantly as a monomer. Furthermore, also VPREB ΔU displays a higher degree of deprotection in the VPREB-V_H interface, which might explain its weaker propensity to form dimers. One part of the VPREB-λ5 interface is directly adjacent to the VPREB-V_H interface in the primary sequence. The hypothesis that also some parts of the VPREB-λ5 interface are involved in the VPREB homodimer interface is supported by HDX measurements showing

deprotected peptides after interaction of VPREB and V_H. Since AUC measurements exhibit VPREB monomerization upon interaction with V_H, the interaction site with λ5 is free. Differences in the degree of protection of some peptides show, that the VPREB homodimer and the VPREB-V_H heterodimer do not completely share the same interface. Moreover, also tendency of VPREB to interact with the V_L domain to form a heterodimer of two VPREB molecules with one V_L and a heterotrimer of one VPREB with one V_L and one V_H domain, supports the hypothesis that the VPREB dimer interface varies from the VPREB-V_H interface.

The predicted structure for VPREB by AlphaFold shows, surprisingly, a folded VPREB protein on its own without λ5 or its additional β-strand. However, taking a closer look, one can observe that in the AlphaFold prediction, the VPREB-λ5 interface at the bottom of the protein is quite structureless whereas in the crystal structure from Bankovich et al., a β-strand and a alpha-helix can be observed. This supports the hypothesis that the VPREB-λ5 interface is involved also in the VPREB interface because in the VPREB homodimer, it has a changed random coil like structure being able to adopt other configurations. The rest of the predicted fold of VPREB shows a β-pleated structure similar to that of VPREB in the Fab complex.

The hypothesis that VPREB forms a homodimer mainly at its VPREB-V_H interface but to some extent also with the URs is supported by the observation that the SLC, VPREB and λ5 in complex, is able to form oligomers as observed in AUC. However, oligomers are not observed in the Fab complex, SLC and Fd, and not in SLC ΔU C212S. In the Fab-SLC fragment, large parts of the URs are involved in V_H interaction, while in the SLC ΔU C212S mutant, the URs are not present at all. This supports the hypothesis that the VPREB-UR is involved to a small extent in VPREB homodimerization and the absence of the V_H domain yields a homodimerization of VPREB.

The predicted binding sites for BiP in VPREB are located adjacent to the VPREB-V_H interface in the primary sequence (Schneider et al., 2016) and therefore also at the VPREB homodimer interface. Therefore, it is most likely that one BiP molecule binds to the VPREB homodimer at its dimer interface site. This is indicative of a VPREB homodimer and also supports a concerted binding of the SLC to the HC. BiP stays probably associated to VPREB, even when it is bound to V_H in the absence of λ5 causing its retention in the ER.

The tendency for the variable regions of antibodies to form dimers or even higher oligomers was observed quite often. On the one hand, the existence of LC dimers, that dimerize via their V_Ls, was observed in so called Bence Jones proteins (Bence Jones, 1850; Bernier and Putnam, 1963; Epp et al., 1975; Azuma et al., 1978). It could be shown that LC dimers associate in the same manner as V_H-V_L heterodimers (Schiffer et al., 1973) and the V_L dimer interface resembles pretty much the V_L-V_H interface (Novotný and Haber, 1985). This supports further the hypothesis of similar VPREB homodimer and VPREB-V_H heterodimer interfaces. On the other hand, also in AL amyloidosis, V_L domains were shown to form fibrils, starting from V_L dimers and oligomers (Kazman et al., 2021). The only difference is that VPREB forms a dimer in the unfolded state,

while Bence Jones proteins and amyloidogenic LCs and V_L domains are folded. It might be helpful in the future to investigate homologies between the mechanisms of dimerization in VPREB, Bence Jones proteins and amyloidogenic V_Ls. It also remains interesting, if VPREB can form fibrils.

Based on the results of this thesis and the discussed conclusions, a model of the VPREB homodimer was elaborated, which is shown in Figure 76. It is likely, that unfolded VPREB interacts with another unfolded VPREB monomer mainly at the VPREB-V_H interface site (depicted in red). BiP may probably bind very near to this dimer interface, which is only a hypotheis that needs to be confirmed by further experiments in the future. Also, some parts of the VPREB-λ5 interface seem to be involved in this dimerization, leaving a cavity for the interaction with the λ5 β-strand. The VPREB-URs are protruding from the homodimer. However, their opposite charges allow them to form electrostatic interactions and contribute to a smaller extent to the homodimerization of VPREB. Especially interesting, VPREB is the first protein identified to be a dimer in an unfolded state.

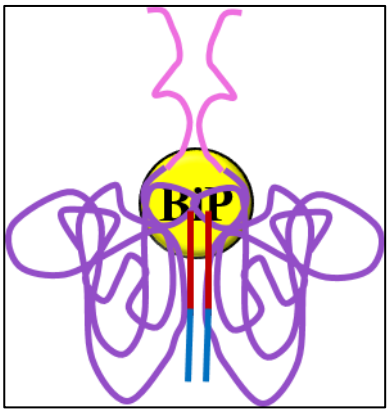

Figure 76: Hypothetic Model of a VPREB Homodimer.
The unfolded VPREB monomers are each depicted in violet. They seem to be interacting at the VPREB-V_H interface and at the VPREB-ƛ5 interface. The URs seem to be protruding on the top, while BiP is probably bound near the URs to the predicted BiP binding sites, which are predicted to be located at the VPREB-V_H interface (Schneider et al., 2016).

3.2 The Additional β-Strand of λ5 is Sufficient for Folding of VPREB

The additional β strand is not only necessary but also sufficient for inducing the folding in VPREB as shown by CD kinetics and NMR measurements. This is also observed in the two VPREB mutants, VPREB ΔU + β and VPREB βU, that are able to autonomously fold and attain their three dimensional conformation as shown by CD measurements in this thesis and NMR measurements in the literature (Morstadt et al., 2008). The β-strand alone is able to bind to a VPREB homodimer as proven by ITC measurements, while λ5 Δβ and λ5 ΔU Δβ are not able to bind to VPREB as shown by cell culture experiments (Minegishi et al., 1999). Furthermore, in this thesis, λ5 Δβ C212S and λ5 ΔU Δβ C212S are not able to induce folding in VPREB as proven by CD kinetics.

It is tempting to conclude that the additional β-strand can act as an intermolecular chaperone. The same could be oberserved in the case of C_H1 that is folded only in the presence of its native interaction partner C_L (Feige et al., 2009).

Since SLC complex formation and folding is still possible in the absence of URs, but not in the absence of the additional β-strand of λ5, as shown by CD kinetics measurements and the literature (Minegishi et al., 1999), one can conclude that the URs play minor roles in this process, whereas the β-strand is indispensable.

The integrity of the additional β-strand of λ5, also referred to as the J domain, was proven by the superimposition of the crystal structure from VPREB in the Fab complex and the crystal structure from VPREB ΔU + β as shown in Figure 77 (Morstadt et al., 2008). This proves that there is no structural difference in the final Fab-complex, when the β-strand inserts intermolecularly into VPREB by λ5 compared to the intramolecular β-strand in the VPREB ΔU + β variant.

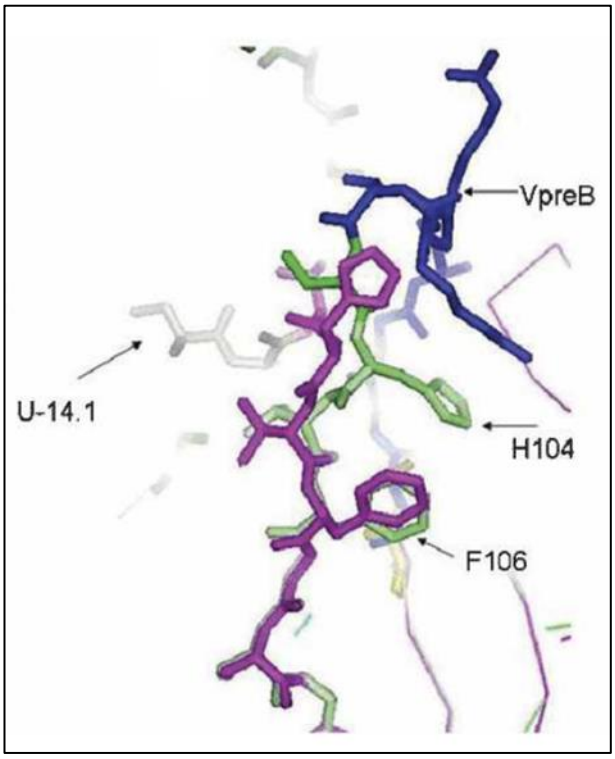

Figure 77: Integrity of the Additional β-Strand of λ5.
Superimposition of the additional β-strand of λ5 in 2H32 (magenta) with VPREB ΔU + β (green). F106 of VPREB ΔU + β overlaps with F61 from 2H32, while H104 of VPREB ΔU + β is different from H59 in 2H32. Figure and legend were taken and modified from Morstadt et al., 2008 (Morstadt et al., 2008).

If there is no "structural" reason to split the Ig fold of VPREB into two proteins, there must be a "functional" reason of this separation. If VPREB and λ5 would be covalently linked, then there would be no unfolded VPREB homodimer. In this state, VPREB can bind to V_H as part of the HC, but this complex can not be secreted because of the unfolded nature of VPREB without its native counterpart λ5. This wouldn´t allow the SLC to perform a proof-reading process of the HC.

Every SLC-HC pair would be secreted immediately without the exclusion of HC that did not pass the quality control by the SLC. Therefore, it is obvious that mostly VPREB is responsible for proof-reading of the HC. It seems that VPREB performs an initial "pre-scan" process of the V_H domain to proof its "correctness" mainly at the CDR3 as it was shown by HDX measurements that VPREB-V_H binding causes one single peptide in the CDR3 of V_H to be protected. This is in accordance with the literature, where it was shown that V_H domains are selected by their CDR3s (Martin et al., 2003; Kawano et al., 2005). If the HC does not pass the quality control checkpoint performed by VPREB, this heterodimeric complex induce the UPR. It could be transported into the cytosol for proteasomal degradation in the context of ERAD or degraded via ER-phagy. After this first step of proof-reading of the HC is mastered by VPREB, λ5 binds by its UR to V_H and simultaneously by its β-strand to VPREB. It should be noted that most of the part of the λ5-UR is protruding as it is known to be implicated in signaling processes by interaction with ligands (Elantak et al., 2012). VPREB is folded upon λ5 interaction. As soon as the simultaneous binding of λ5 to VPREB and λ5 to V_H is established, BiP that is predicted to bind to the λ5-UR (Schneider et al., 2016) dissociates and the core region of λ5 forms an interaction with the unfolded C_H1. This starts the folding reaction of C_H1 and the dissociation of BiP. The reason for the unfolded λ5-UR to be so long and harboring a cysteine might be that it is a recognition site for BiP as it binds to unfolded reduced proteins. Furthermore, the hypothesis of a concerted binding of VPREB and λ5 is supported by the modulating effect of C_H1 glycosylation and fucosylation on λ5 binding as it is summarized in Sun et al., 2022 (Sun et al., 2022). A lack of fucosylation, which is facilitated only in the trans-Golgi, diminishes the binding of λ5 and C_H1 *in vivo* (Sun et al., 2022). Therefore, it is assumed that only after the HC is scrutinized by both VPREB and λ5, the pre-BCR gets secreted. During the secretion pathway, the pre-BCR seems to be "finalized" in its complex formation.

3.3 The URs Decrease the Thermal Stability and Affinity of the SLC Proteins

The URs of the SLC proteins, VPREB and λ5, were shown to have a destabilizing effect on the SLC complex as well as on λ5 C212S alone by temperature-induced unfolding transitions followed by CD spectroscopy at 205 nm. Moreover, SPR measurements revealed that the URs decrease the affinity of VPREB and λ5 proving that the SLC-URs not only play a role in association with V_H, but also in SLC complex formation. This hypothesis is even further supported by CD kinetics measurements that followed the folding reaction of VPREB at 205 nm, which showed different folding times for the ΔU-mutants.

SLC and λ5 C212S have a T_m of 53.3 ± 0.4°C and 55.8 ± 0.7°C, respectively, as determined by temperature-induced unfolding transitions followed by CD spectroscopy at 205 nm. The thermal stability is comparable to other antibody domains (Feige et al., 2010b). Complex formation of

VPREB and λ5 C212S did not yield a gain in stability, but in the contrary led to a decreased stability by roughly 2.5°C as reflected by the T_m. The URs destabilize both, the SLC complex and λ5 C212S alone. The VPREB-UR can not have any influence on its thermal stability since VPREB is anyway unfolded. The thermal stabilities are with a T_m of 56.1 ± 0.5°C for SLC ΔU C212S and a T_m of 58.5 ± 0.3°C for λ5 ΔU C212S increased by about 3°C compared to the WT. Also, complex formation of the VPREB ΔU and λ5 ΔU C212S does not result in an increased stability, but rather a decrease by about 2.5°C similar as it was for the WT proteins.

The absence of the URs in VPREB and λ5 C212S results in an increased affinity of the two SLC proteins. The K_D was determined by SPR to be 17.7 ± 1.2 nM of λ5 C212S and VPREB, which is higher as for λ5 ΔU C212S and VPREB (13.5 ± 0.4 nM). The absence of the VPREB-UR increases its affinity for λ5 C212S even more by roughly 6-fold (3.0 ± 1.3 nM) compared to the WT complex. The increased affinity is pertained in the λ5 ΔU C212S-VPREB ΔU complex with a K_D of 5.0 ± 0.8 µM. Therefore, the VPREB-UR seems to have a higher impact on SLC complex formation than the λ5-UR. This suggests that both URs, the VPREB-UR a bit more, hinder the binding of λ5 to VPREB. This finding is also reflected in the stability of the respective complexes. The increased affinity of λ5 ΔU C212S for VPREB could be explained by the better accessibility of the J domain in λ5 upon deletion of the UR, which is reflected in HDX data. The high affinity of VPREB and ʎ5 is surprising because a moderate affinity is expected since ʎ5 must induce folding of VPREB. Furthermore, taking into account that the antibody concentrations are much lower in cells (Cenci and Sitia, 2007), association of VPREB and ʎ5 as well as VPREB and V_H must occur readily *in vivo*.

The λ5 ΔU C212S-VPREB complex has a thermal stability of 56.5 ± 0.8°C, which is increased by 3°C compared to WT complex. The λ5 C212S-VPREB ΔU complex has a thermal stability of 55.1 ± 0.1°C, which is decresed by about 1.5°C compared to the λ5ΔU C212S-VPREB complex. This suggests that the λ5-UR adds more instability to the complex than the VPREB-UR. Comparing it with the T_m of the λ5 ΔU C212S-VPREB ΔU complex (56.1 ± 0.5°C), it is further substantiated that the λ5-UR contributes more to the instability of the SLC complex that VPREB-UR.

Comparing the time needed for folding of VPREB in the respective combinations of UR-lacking proteins, one can also observe significant differences. While the WT complex, VPREB and λ5 C212S, needs 51.0 ± 3.4 min until 63.2 % of VPREB is folded (τ), the complex of VPREB and λ5 ΔU C212S has a τ of 113.5 ± 29.6 min, which is increased 2-fold compared to the WT. Consequently, the λ5-UR seems to be involved in the induction of folding in VPREB. On the other hand VPREB ΔU needs 40.9 ± 10.7 min until 63.2 % of the protein is folded by λ5 C212S. This is only slightly decreased compared to the WT indicating that the VPREB-UR has a minor impact on folding of VPREB.

The impact of the URs on folding, complex formation and thermal stability of complexes and single proteins could be further supported by mutants with only a few mutated residues in their URs. For example, the variants with the tryptophanes in the URs are of special interest. Two variants were generated: λ5 W67,77,83A C212S and VPREB W131A. λ5 W67,77,83A C212S on its own shows a thermal stability of 57.5 ± 0.8. This is an increase by 2°C compared to the thermal stability of λ5 C212S (T_m = 55.8 ± 0.7°C). VPREB W131A shows no temperature-induced unfolding transition because it is unfolded like WT VPREB. The change in thermal stability of λ5 W67,77,83A C212S alone is also reflected in a change in affinity. It is increased by about 3-fold to a K_D of 5.2 ± 1.5 nM compared to the WT complex (17.7 ± 1.2 nM), while the affinity of λ5 C212S and VPREB W131A stays roughly at the same level (16.8 ± 1.3). This indicates that the three tryptophanes in the UR of λ5 play crucial roles in thermal stability and interaction with VPREB. The structural changes in the λ5 W67,77,83A C212S mutant are reflected in the HDX data, that revealed the additional β-strand, to be very deprotected. This might explain the higher affinity for VPREB because of the increased accessibility of the main interacting element between VPREB and λ5. Furthermore, the folding times are both drastically decreased: For VPREB and λ5 W67,77,83A C212S, τ was determined to be 28.9 ± 5.8 min. This is surprising since deletion of λ5-UR markedly increased τ. Also, VPREB W131A and λ5 C212S showed a decreased τ of 33.9 ± 8.0 compared to the WT complex (51.0 ± 3.4 min). This leads to the conclusion that the tryptophanes in both URs play a role in the folding of VPREB. The fact that only one mutation in the UR of VPREB has such a big impact on its folding might be explained by structural differences that this mutation causes in the protein. It is somewhat surprising that this mutation causes many regions to be protected and deprotected throughout the protein. However, the thermal stability of the respective complexes was affected. The T_m of the VPREB-λ5 W67,77,83A C212S complex was determined to be 55.3 ± 0.1°C, which is increased by 2°C compared to the WT complex (53.7 ± 0.7°C). The thermal stability of the VPREB W131A-λ5 C212S showed an increase by roughly 1°C (54.5 ± 0.01°C).

Also, the decreased τ (27.1 ± 5.6 min) of VPREB 9EurQ and λ5 C212S could be traced back to overall structural changes in the protein leading to an increased folding time. A minor effect was seen in the thermal stability of the complex (54.7 ± 0.7°C vs. 53.7 ± 0.7°C). The about 10-fold increase in affinity of VPREB 9EurQ for λ5 C212S, as reflected by a K_D of 1.7 ± 0.1 nM, could be explained by a more exposed λ5 binding site. This is reflected in the HDX measurements, which show indeed more deprotection in the λ5 binding site.

Overall, these findings suggest that the function of the URs is not only limited to signaling (Ohnishi and Melchers, 2003; Knoll et al., 2012) and V_H interaction as well as CDR H3 proof-reading (Martin et al., 2003; Kawano et al., 2005). They also seem to influence the VPREB folding and SLC affinity and stability.

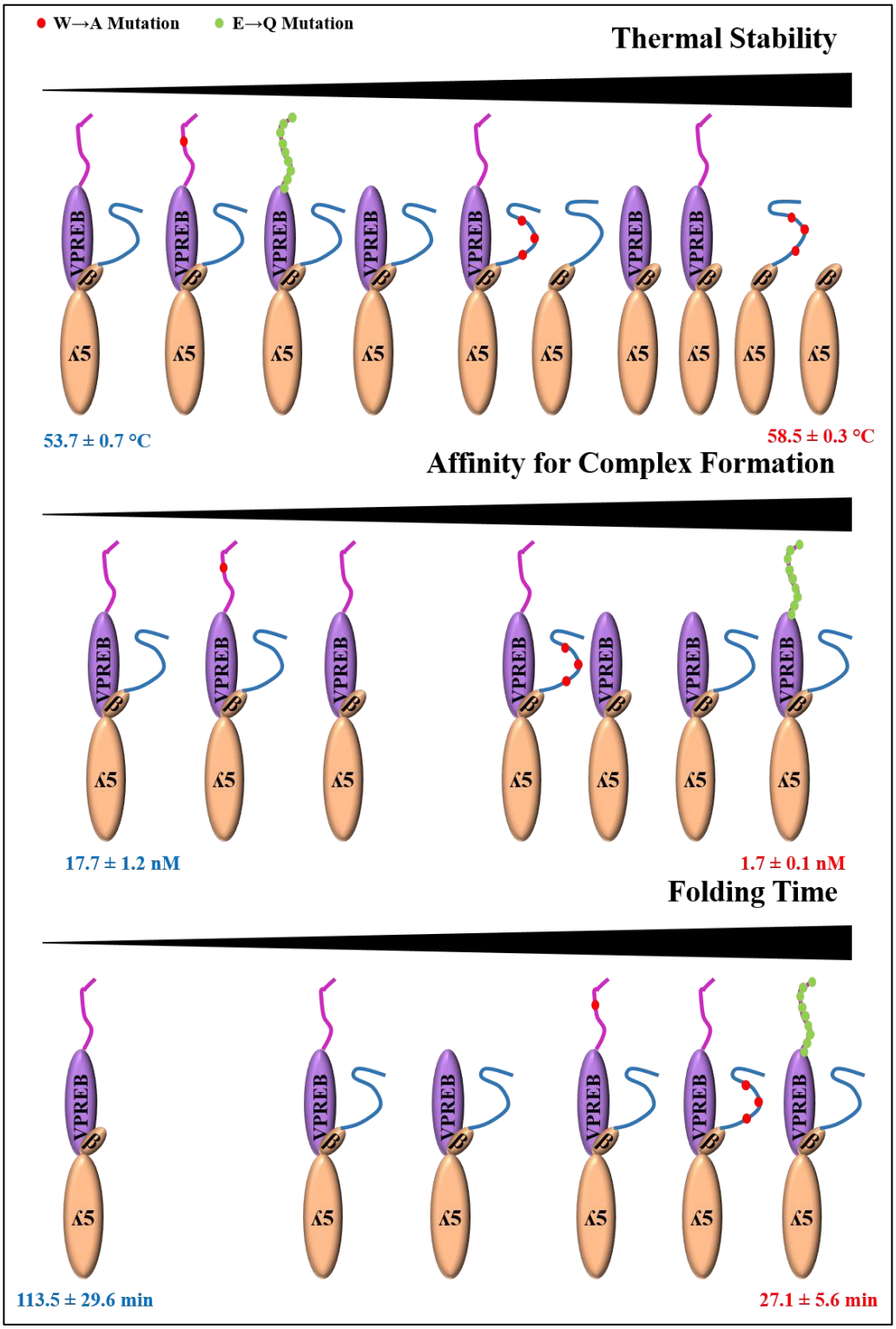

Figure 78: Overview of the Different Variants and their Combinatorial Effects on SLC Affinity, Thermal Stability and Folding Time.
The variants and their combinations are shown in an ascending order, from left to right, with regard to their thermal stabilities, affinities for complex formation and folding time.

A schematic overview of all mutants and mutant complexes discussed in this chapter is given in Figure 78, where the proteins are ordered in an ascending manner regarding their thermal stability, affinity for complex formation and time needed for folding. It is outstanding that the most stable

complex is completely lacking the URs, while the WT complex is the most unstable. The WT complex is also the complex with the lowest affinity of VPREB and λ5.

3.4 The URs of the SLC Are Important for Interaction with V_H

The UR of λ5 was identified as the only element that is important for its V_H interaction as it could be shown by a complete abolished binding of λ5 ΔU C212S in SPR experiments. This is not surprising because in conventional Fab fragments, C_L, the LC analogue of λ5, is only interacting with C_H1 and not with V_H. Furthermore, the SPR experiments showed a significant decrease in affinity for the VPREB ΔU variant with both, the murine (31.525 ± 3.825 nM) and the human V_H domain (905.5 ± 278.5 nM), compared to WT VPREB (10.1295 ± 3.6605 nM with murine V_H and 22.245 ± 9.025 nM with human V_H). While VPREB ΔU is still able to interact with V_H, λ5 ΔU C212S can not bind.

Bankovich et al. showed that the VPREB-UR protrudes from VPREB and extends over the top of CDR3 of the V_H domain and obscures it (Figure 79) (Bankovich et al., 2007). A salt bridge is formed between VPREB E106 and HC R59 (asterisk in Figure 79 A). The crystal structure with the rough localization of the URs, since only parts of it could be resolved, is shown in Figure 11 (Bankovich et al., 2007). They also could show that there is a net loss of interface contacts (hydrogen bonds and van der Waals interactions), but an increase of the overall SLC/HC interface due to the URs interactiong with CDR H3 as indicated by the contact residues in Figure 79 A. This goes along with a higher number of contacts between SLC UR residues and CDR-H3 compared to CDR-L3 and CDR-H3 (Bankovich et al., 2007). This is in accordance with our results that show a deleted VPREB-UR accounting for a decreased affinity and a complete abrogated interaction of λ5 ΔU C212S and V_H. SLC-URs have a plasticity that may permit them to adapt to diverse CDR3s (Martin et al., 2003). The extended CDR-H3 loop in the pre-BCR was shown to interact with the VPREB CDR2, too. This is attributed to a long CDR2 loop, which was also observed in human germline V ʎ chain subgroup 5 and in non-mammalian species such as horned shark and frog (Solomon et al., 1997). This has been proposed to extend the SLC interface with the VH domain (Solomon et al., 1997). The authors could also show that several amino acids are involved in CDR-H3 interaction: S59 and S103 in VPREB (not in the UR) as well as H59 in the UR of λ5 (Figure 79B) (Bankovich et al., 2007).

That the site of HC scrutiny is most likely localized to the CDR-H3 fits the HDX data that showed a protected peptide in the CDR H3 of V_H 1HEZ upon interaction with VPREB. Thus, it is most likely that VPREB plays a superior role in CDR3 discrimination of HCs since in the V_H-λ5 C212S complex no change in conformational dynamics was detected. This suggests that the λ5-UR interacts with V_H rather at the V_H dimer interface and not at the antigen binding surface of V_H. This is supported by the AUC measurements that showed λ5 C212S and V_H to form a heterodimer.

Moreover, since the λ5-UR was identified as the only interacting element with V_H and not its J domain, the SLC-V_H interface appears to deviate from the VPREB ΔU + β dimer interface. Morstadt et al. showed two residues of the inserted J-domain to be involved (Morstadt et al., 2008). Also, Bence Jones proteins associate like V_L-V_H dimers (Schiffer et al., 1973) and their side chain arrangements in the V_L-V_L interface are similar to that of the V_L-V_H interface (Novotný and Haber, 1985). Futhermore, it was to be expected that the core domain of λ5 is not involved in V_H interaction, but, as a C_L analogue, only interacts with C_H1 (discussed in more detail in section 3.5). Also Minegishi et al. could show that stable association of SLC with the V_H domain requires the core domain of VPREB, but neither the constant domain of λ5 nor the UR of VPREB (Minegishi et al., 1999). This is in accordance with the literature where it was demonstrated that the λ5-UR is indispensable for signaling through the pre-BCR (Ohnishi and Melchers, 2003). Thus, it is unlikely for the λ5-UR to be not interacting with V_H, where its surface exposure leads to an interaction with possible ligands and antigens. This is further supported by a deletion of the λ5-UR in mice that resulted in an increased cell-surface representation, a diminished rate of aggregation and internalization, abolished tyrosine phosphorylation, and thus indicating a lack of signal transduction (Ohnishi and Melchers, 2003). In the literature, it was shown that in mice functional HCs are selected via the CDR H3 and the capacity to form a pre-BCR (Hayden et al., 2002).

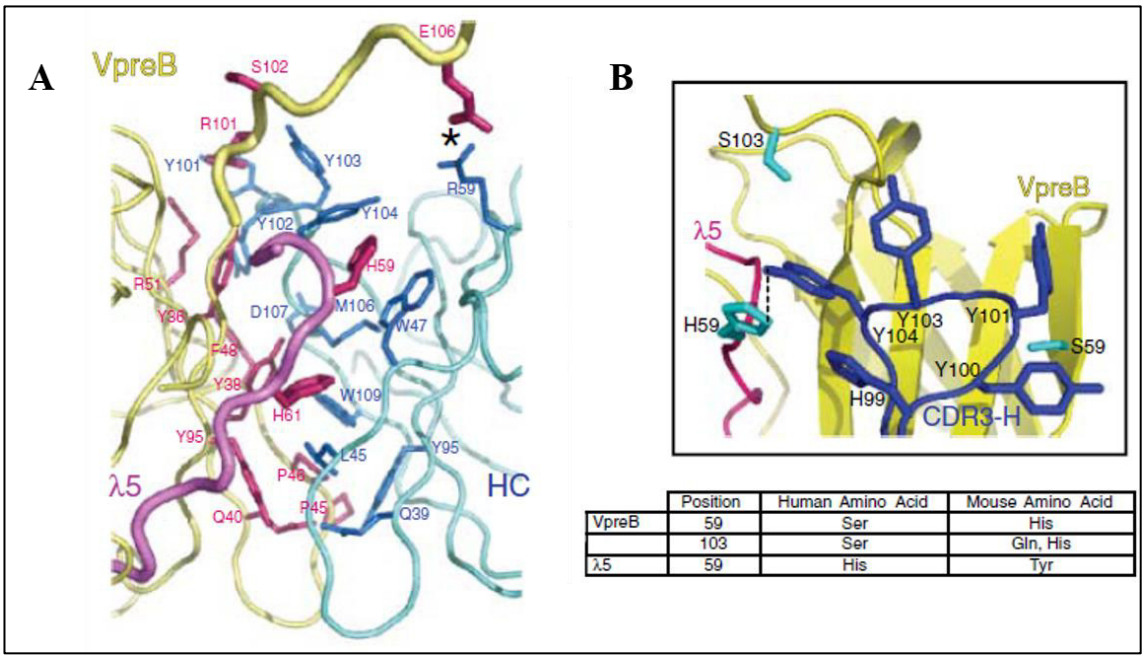

	Position	Human Amino Acid	Mouse Amino Acid
VpreB	59	Ser	His
	103	Ser	Gln, His
λ5	59	His	Tyr

Figure 79: The Interface of the SLC and the CDR3 in V_H.
A Contact residues within the SLC/HC interface. Contact residue side chains from SLC are marked in red and from HC in blue. Asterisk highlights the salt bridge between VPREB and HC. **B** The human pre-BCR CDR3-H sensing site. Variable side chains between human and mice are marked in cyan, which are listed in the table below the figure. The dashed line designates a hydrogen bond. Figure and legend were taken from Bankovich et al., 2007 (Bankovich et al., 2007).

High affinity was shown of VPREB alone with V_H compared to the SLC complex by SPR measurements. In the literature, affinities with K_D values of about 500 nM were reported (Hirabayashi et al., 1995), which is up to 50-fold higher than observed in this thesis. This could be due to the V_H domain to be SPA-tagged in their study and the V_H domains that are used in this thesis are untagged. They proved that there is no binding of VPREB and the SPA-tag but it might still be the case that the SPA-tag sterically or conformationally hinders or impacts VPREB-V_H binding, which might result in a lower affinity. They observed the formation of a heterotrimeric complex of VL, VH and VPREB and a VPREB-V_L heterotrimer. This indicates a different site of interaction in VPREB-V_H compared to V_L-V_H (Hirabayashi et al., 1995). The limitation of their study are missing replicate measurements. The K_D between VPREB and V_H was determined to be lower than the K_D between V_H and V_L, which is in the µM range (Hochman et al., 1976; Klein et al., 1979; Horne et al., 1982; Glockshuber et al., 1990; Anthony et al., 1992; Hirabayashi et al., 1995; Herold et al., 2017). Taken together, based on the data and the literature, the increased affinity of SLC and V_H can be attributed to the URs, especially the VPREB-UR.

The K_Ds, which were measured in this thesis, for VPREB-V_H binding fit to the data from Gauthier et al. They showed that VPREB binds to V_H-C_H1 from Nalm6 cells with a K_D of 31.6 nM and to V_H-C_H1 from 1E8 cells with a K_D of 25.1 nM as measured by SPR as well (Gauthier et al., 1999). The K_D of SLC binding to V_H as determined in this thesis to be 29.585 ± 5.515 nM for murine V_H and 129.2 ± 26.8 nM for human V_H is different to the literature for the human V_H domain. This might be attributed to the human V_H homodimer. Gauthier et al. demonstrated that single chain SLC (scSLC) binds to VH-CH1 from Nalm6 with a KD of 1.19 nM and from 1E8 with a K_D of 0.268 nM (Gauthier et al., 1999). Again, they did not measure in replicates and moreover, they used a single chain SLC construct. This might have differences in structure compared to the non-covalently linked SLC used in this thesis.

Hirabayashi et al. states that VPREB associates with human and murine V_H with a similar K_D (Hirabayashi et al., 1995). This was not observed for this thesis, where VPREB binds to murine V_H with a higher affinity compared to human V_H because of the human V_H being homdimeric.

The affinity between V_H 1HEZ and ʎ5 Δβ C212S is increased (121.7 ± 27.7 nM) compared to ʎ5 C212S (171.9 ± 77.0 nM). This was expected because the β-strand and the ʎ5-UR might form local secondary structures in the absence of VPREB that might cover the residues in the UR and prevent it from interacting with V_H. The deletion of the β-strand might cause a full exposure and therefore accessibility of the UR. An increased affinity could also be observed between ʎ5 W67,77,83A C212S and V_H (135.0 ± 25.6 nM). This could mean that the tryptophanes in the ʎ5-UR might influence local structures in the UR as it was shown that the UR harbors an α-helix at residues 22-45 (Elantak et al., 2012). The mutation of the URs might also increase the accessibility of the ʎ5-UR for V_H interaction. It could also mean that the tryptophanes are involved in proof-reading of the V_H and especially the CDR3. For this, a lower affinity interaction might

be needed, so that in case the V_H domain does not pass the quality control by the SLC, the dissociation is more easily conferred.

The affinity of VPREB ΔU + β (700.4 ± 27.2 nM) and VPREB βU (1817.5 ± 707.5 nM) is drastically decreased compared to WT VPREB (22.2 ± 9.0 nM). This can be attributed to the missing UR in VPREB ΔU + β, as the affinity is quite like VPREB ΔU (905.5 ± 278.5 nM). Furthermore, the opposite location of the UR in VPREB βU might be the reason for its significantly decreased affinity for V_H. In VPREB βU, the UR has no interface at all with V_H. Moreover, this mutant might have a very different structure compared to VPREB ΔU + β, although Morstadt et al. showed with overlaying ^{1}H ^{15}N NMR spectra of VPREB ΔU + β and VPREB Uβ that the structure is quite similar except for the UR that is present in VPREB Uβ (Figure 80) (Morstadt et al., 2008).

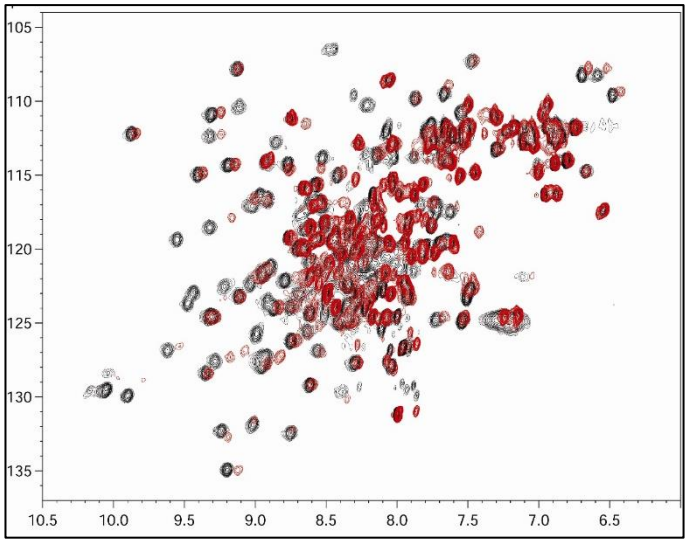

Figure 80: Superimposition of the HSQC spectra of ^{15}N-labelled VPREB Uβ (black) and ^{15}N-labelled VPREB ΔU + β (red).
Figure and legend were taken from Morstadt et al., 2008, the legend was modified (Morstadt et al., 2008).

Furthermore, VPREB W131A (69.7 ± 5.6 nM) and VPREB 9EurQ (136.1 ± 5.4 nM) have both a reduced affinity to V_H compared to WT VPREB. This could be attributed to the mutations in the UR of VPREB. They have an influence on structural organization of both the UR and whole VPREB as proven by differential HDX MS, which might influence its affinity for V_H.

3.5 The Core Region of λ5 is Sufficient for Folding of C_H1

Secretion of antibody molecules is controlled by the assembly of C_L and C_H1 in order for C_H1 to adopt the Ig fold in presence of C_L (Feige et al., 2009). This association-coupled folding reaction of C_H1 in the presence of C_L requires both, disulfide bridge formation and peptidyl-prolyl-isomerization, which is supported by the ER chaperone machinery (Lilie et al., 1993; Lee et al., 1999; Feige et al., 2009). The intrinsically unfolded C_H1 domain is an essential part to control

antibody secretion (Feige et al., 2009). By correlation, it is assumed, that the C_H1 domains also is involved in the control of the pre-BCR transport to the cell surface.

To understand the interplay of binding and folding of λ5 and C_H1, the thermodynamic and kinetic paramteers for this reaction were assessed. The K_D for λ5 C212S and C_H1 was determined to be 2.055 ± 0.083 µM by SPR analysis. This value is quite similar to the K_D that was measured for the C_L-C_H1 interaction (6.2 ± 0.4 µM) (Feige et al., 2009). The folding process of C_H1 as induced by λ5 C212S occur with a time constant of τ = 41.4 ± 2.0 min as assesed by kinetics analysis using far-UV CD spectroscopy. This is similar to the value determined for the folding of C_H1 by C_L (τ = 60 ± 10 min) (Feige et al., 2009). This and the K_D suggests a similar mode of interaction. The increased affinity of SLC and C_H1 (K_D = 0.453 ± 0.282 µM) compared to λ5 alone and C_H1 supports the hypothesis that VPREB binds first and scrutinizes V_H before λ5 binds to VPREB, V_H and C_H1. This is also supported by the outstanding high affinity of VPREB with V_H compared to SLC and λ5 with C_H1.

To figure out, which part of λ5 interacts and induces folding of C_H1, several mutants were tested, which show that only the core domain of λ5 interacts with and folds C_H1, which was also shown in the literature (Gauthier et al., 1999). The core domain of λ5 is homologous to the C_L domain, which can fold autonomously to a stable protein in a monomeric state (Goto et al., 1979). Therefore, it is not surpising that λ5 C212S is able to attain a folded structure despite its UR. The C_L homologue is the λ5 ΔU Δβ C212S variant because it only comprises the core domain. Both Δβ-variants, λ5 Δβ C212S and λ5 ΔU Δβ C212S, show a higher thermal stability with T_ms of 59.0 ± 1.2°C and 59.5 ± 0.5°C, respectively, which is an increase of more than 3°C compared to λ5 C212S. This suggests that both, the β-strand and the UR, destabilize the protein.

Secretion of antibody molecules is controlled by the assembly of C_L and C_H1 in order for C_H1 to adopt the Ig fold in presence of C_L (Feige et al., 2009). This association-coupled folding reaction of C_H1 in the presence of C_L requires disulfide bridge formation and peptidyl-prolyl-isomerization, which is supported by the ER chaperone machinery (Lilie et al., 1993; Lee et al., 1999; Feige et al., 2009). The intrinsically unfolded C_H1 domain is an essential part to control antibody secretion, and by correlation also the transport of the pre-BCR to the cell surface.

An interesting finding of this thesis is that VPREB also associates with C_H1 in absence of λ5 and regardless of its UR. Neither VPREB nor C_H1 are folded upon this interaction according to the CD data, but they form a stable heterodimer as shown by AUC analysis. This implies that the VPREB dimer interface might also very much resemble the VPREB-C_H1 interface. This interaction may be attributed to unspecific interactions between two unfolded proteins that have exposed hydrophobic residues and therefore form a hydrophobic core. It might be interesting to test whether this is an artefact *in vitro* or this interaction also occurs *in vivo*.

A murine C_H1 domain was used in combination with a human SLC. The fact that folding and interaction was observed indicates that these mechanisms are conserved in mice and men.

The interplay of the λ5-C_H1 interaction with BiP is still unclear, but it seems obvious that λ5, like C_L releases C_H1 from its interaction with BiP (Melchers, 1999; Feige et al., 2009).

3.6 Fab-SLC Does Not Form Oligomers *In Vitro*

The AUC data show that Fab-SLC forms a stable heterotrimer but not higher oligomers. This implicates that pre-BCR clustering on the cell surface of pre-B-cells does not occur without any ligands. In the literature, it is controversially discussed whether the pre-BCR can oligomerize and cluster autonomously or ligand dependent.

Gauthier et al. showed that neither in FACS, nor in SPR, a self-interaction of the pre-BCR was possible (Gauthier et al., 1999). This in accordance with the data observed in this thesis that also showed no self-oligomerization on its own. This is supported by studies that showed that the deletion of the UR of λ5 showed abolished clustering of surface pre-BCRs and phosphorylation of Igα (Ohnishi and Melchers, 2003). Furthermore, the growth of primary B-cells *in vitro* was diminished (Guloglu et al., 2005). The UR of λ5 is the major binding element, whereas VPREB is not involved in the Galectin-1 interaction at all (Gauthier et al., 2002).

It might be interesting to observe oligomerization *in vitro* by adding Galectin-1 to Fab-SLC and see if oligomerization occurs readily *in vitro*. Based on this, one could go ahead and test the oligomerization with Fab-SLC variants lacking the UR of λ5 or VPREB or both.

3.7 Strong Antigen Affinity of Fab-SLC is Mediated by λ5-UR

The ELISA experiments with the human biotinylated creatin kinase (muscle type) revealed a high antigen affinity for the Fab-SLC (8.61 ± 1.89 nM), even slightly increased compared to the Fab-LC (12.62 ± 3.11 nM). The ʎ5-UR was identified as the main part in antigen interaction while the VPREB plays a minor role, which is not surprising because in the literature, the ʎ5-UR, and not VPREB, was shown to be the crucial part in interaction with ligands, e. g. GAL1 (Gauthier et al., 2002; Smith and Roman, 2010). Therefore, the strong antigen interaction of Fab-SLC is reasonable since it interacts with ligands to induce signaling pathways (Elantak et al., 2012).

The structural characterization of Fab-SLC by CD spectroscopy reveals a β-pleated structure with a random coil content because of the unfolded URs. This is also reflected in the tertiary structure, where the UR seem to cover the folded nature of the Fab-SLC. However, this is indicative of a structurally and functionally intact Fab-SLC fragment. AUC runs confirmed the presence of a heterotrimeric complex as the only species, consisting of VPREB, λ5C212S and Fd MAK33. λ5 and Fd, both were lacking their C-terminal cysteine, which is otherwise important for intermolecular disulfide bridge formation. However, the complexes were formed based on the hydrophobic interface between SLC and Fd, as it was described for LC and Fd (Azuma and Hamaguchi, 1976; Lilie and Buchner, 1995; Lappalainen et al., 2008).

SLC C212S in a heterotrimeric complex with V_H showed a K_D of 94.1 ± 0.02 nM for the antigen, and the heterodimeric complex of ʎ5 C212S and V_H MAK33 had an almost identical amtigen affinity (95.0 ± 0.03 nM). Thus, it seems obvious that ʎ5, especially its UR, confers mainly the interaction with the antigen. This is even more corroborated when observing the antigen affinity of VPREB and V_H MAK33 in a heterodimeric complex. VPREB and V_H MAK33 (260.1 ± 0.02 nM) did not yield in an improvement on antigen binding compared to V_H MAK33 alone (282.6 ± 0.06 nM), while the V_H-V_L heterodimer achieved an affinity almost double as high (155.9 ± 0.06 nM). This could be due to the unfolded nature of VPREB when ʎ5 is absent. If this was the case, then the K_D of SLC C212S and V_H MAK33 for the antigen should be even more decreased as the K_D determined for the ʎ5 C212S-V_H heterodimer.

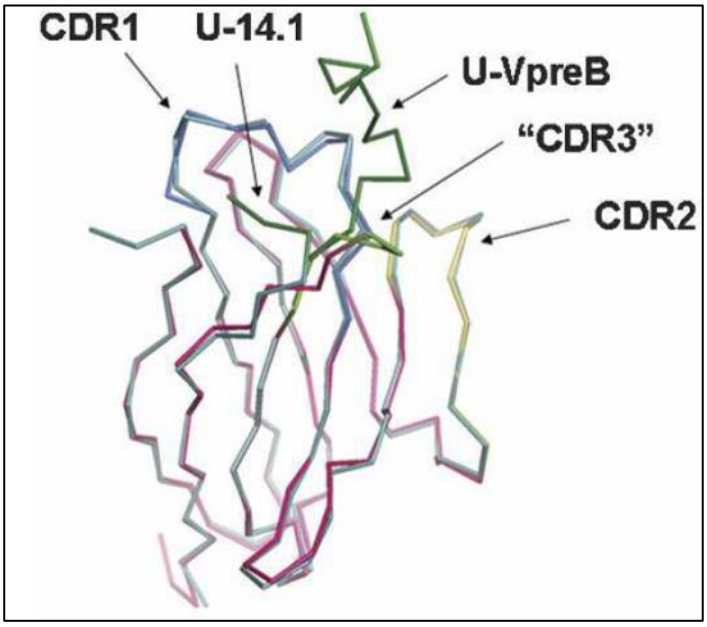

Figure 81: Preserved Integrity in VPREB in absence of UR.
Superimposition of VPREBΔU+β (magenta; CDR1 in blue; CDR2 in yellow, "CDR3" in light green) to VPREB of the pre-BCR from PDB 2H32 (cyan; UR in dark green). Figure and legend were taken and modified from Morstadt et al., 2008 (Morstadt et al., 2008).

VPREB ΔU and V_H MAK33 (263.1 ± 0.03 nM) did not show an increased antigen affinity compared to VPREB-V_H. In the ELISA experiments, VPREB, VPREB ΔU, VPREB W131A and VPREB 9EurQ were used as heterodimeric complexes with C-terminally FLAG-tagged V_H MAK33. This interaction does not induce folding in the VPREB variants. Although VPREB does not have a CDR3, it has CDR1 and CDR2. However, when it is unfolded, the CDRs are probably not fully functional or covered in the random coil like structure. Nevertheless, both, VPREB W131A (157.6 ± 0.04 nM) and VPREB 9EurQ (198.1 ± 0.03 nM) in complex with V_H MAK33 have decreased K_D for the antigen compared to VPREB-V_H and thus a slightly higher antigen affinity. Since these mutations are located in the URs of VPREB, they might change the structure of the VPREB-UR and therefore increase the affinity of the antigen.

The VPREB ΔU + β mutant was also tested for its ability to bind antigens in complex with V_H MAK33. This mutant completely resembles a V_L domain. Indeed, it showed a similar affinity (140.9 ± 0.01 nM) compared to V_H-V_L (155.9 ± 0.06 µM). Abysis showed a slightly different pattern of the three CDRs in VPREB ΔU + β (Figure 19D) compared to murine and human V_L. However, a third CDR was generated in this mutant, which may contribute to the higher antigen affinity. Nevertheless, the antigen affinity was increased compared to VPREB-V_H (260.1 ± 0.02 µM). This may be attributed to the unfolded nature of VPREB in the absence of the β-strand from λ5. This might cause CDR1 and CDR2, which are present in VPREB, to not be fully functional and accessible for antigen binding. This and the presence of the third CDR may both contribute in equal amounts to the increased antigen affinity. The superimposition of VPREBΔU+β from Morstadt et al. with VPREB from the pre-BCR from Bankovich et al. showed that the integrity of the Ig domain was preserved in the absence of the UR (Figure 81) (Morstadt et al., 2008). Morstadt et al. showed that the superimposition of VPREB ΔU + β and VPREB from PDB 2H32 was almost identical except for five residues near the covalent linkage of VPREB and the β-strand (Morstadt et al., 2008). These amino acids include H104 oriented towards the antigen-binding site in VPREB 2H32, which is tilted towards the V_H interface in VPREB ΔU + β. The loop that links VPREB and the additional β-strand in VPREB ΔU + β corresponds to the CDR3 in V_L domains. It is directed towards the antigen-binding site, for which there is no space in the SLC dimer from PDB 2H32.

The limitation of the antigen affinity experiments by ELISA is that only one antigen was tested with one HC. It might be necessary to extend the antigen interaction study to further antigens and HCs.

3.8 Proposed Model for SLC and Pre-BCR Assembly

Based on the data of this thesis, a hypothetic model for the assembly mechanism of the SLC and the Fab fragment of the pre-BCR and the potential role of BiP was elaborated (Figure 82). In the beginning, there exists VPREB alone as an unfolded homodimer, which is considered to associate with BiP at its predicted BiP binding site near the VPREB dimer interface (section 2.9). It might be possible that BiP causes the monomerization of VPREB. λ5 alone is a monomer, also considered to associate with BiP at its predicted BiP binding site in the unfolded UR near the cysteine. It should be mentioned that both, VPREB and λ5 C212S, do not possess a KDEL retention motif, which is reasonable since they get transported to the cell surface of pre-B cells as the pre-BCR. So far, there is no experimental data about the role of BiP in pre-BCR receptor assembly, only the predicition of its binding site. Therefore, the hypothetical statements of BiP in this chapter need to be verified by experiments.

There are two possible association mechanisms. One possibility is the association of VPREB and ʎ5 completely independent of a HC. Since the additional β-strand of ʎ5 induces folding in VPREB, the dissociation of BiP from VPREB upon SLC complex formation seems likely. Whether BiP also dissociates from the ʎ5 during SLC association is unclear. However, upon SLC formation, VPREB becomes a monomer that interacts with ʎ5 to form a heterodimer. It is conceivable, that BiP stays bound to both, VPREB and λ5, until their association with the HC.
The second possibility includes the interplay of the SLC with the HC. Based on the findings in this thesis, the VPREB homodimer seems to bind first to the V_H domain with the UR having a large interface with V_H. During binding, VPREB becomes monomeric to form a heterodimer with V_H. The VPREB dimer interface seems to be replaced by the VPREB-V_H interface. BiP probably remains bound to VPREB because V_H does not induce any folding reaction in VPREB. The VPREB-UR most likely scrutinizes the CDR3 of V_H as a first "control check point" in pre-BCR assembly. The interaction of VPREB with V_H prepares the interaction site with ʎ5 to be exposed to facilite VPREB-ʎ5 interaction. The binding of ʎ5 to the VPREB-V_H heterodimer is mediated by its UR and the additional β-strand. While the UR interacts with V_H, the β-strand binds to VPREB and induces its folding. BiP dissociation from VPREB and ʎ5 is driven serially: First, BiP dissociates from ʎ5-UR upon association with V_H, then BiP dissociation is initiated from VPREB while it is folded by the β-strand. In this complex, the CDR2 of VPREB also interacts with the CDR3 of the V_H domain. The binding of ʎ5-UR to V_H represents the second "control check point" in pre-BCR assembly.
Only if the proof-reading process of the HC, especially of the CDR3 of the V_H domain, is completed and BiP dissociated from ʎ5-UR, the ʎ5 core domain associates with C_H1, induces folding of C_H1 and dissociation of BiP. The intermolecular disulfide bond between the C-terminal cysteines of ʎ5 and C_H1 is formed. A cell would not invest energy to induce the folding of C_H1 by ʎ5 if the quality of the HC is not completely ensured before. The UR of ʎ5 is most likely protruding because of its greater length compared to VPREB (50 to 25 aa) and its functions in signaling. The fully assembled pre-BCR can be transported to the cell surface, where it can exert its function in signaling to induce cell proliferation and cell cycle progression. It is noteworthy, that it was shown in the literature that λ5 association with C_H1 is mediated by glucosylation and especially fucosylation in the trans-Golgi (Sun et al., 2022). This supports the hypothesis of concerted binding of VPREB and λ5 to the HC.
Taken together, the results in this thesis provide a first approach to describe the underlying mechanisms of SLC and pre-BCR assembly. Expansion of the elaborated model in this thesis and examination of the role of BiP may help to understand the HC selection by the SLC in the future.

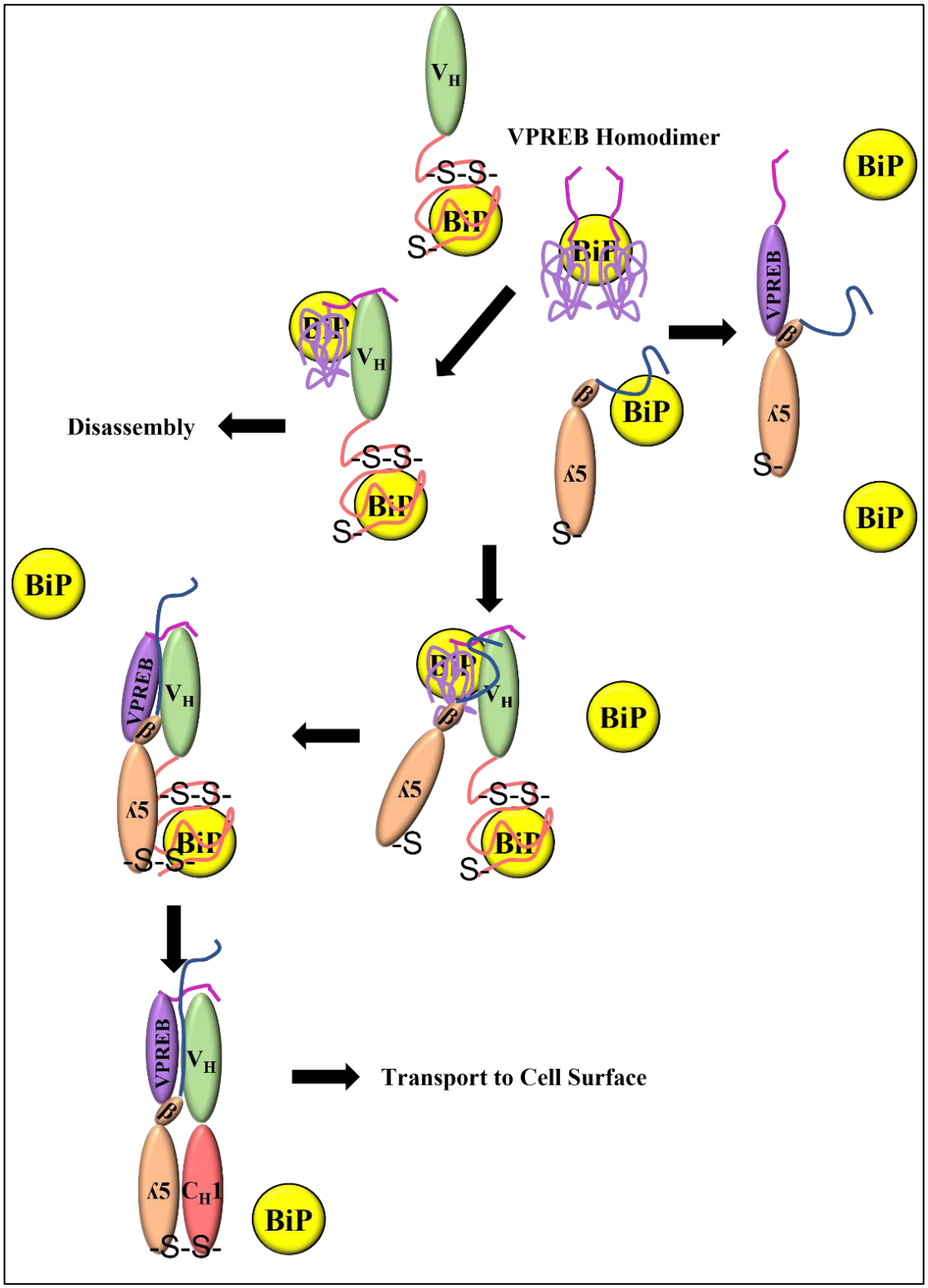

Figure 82: Proposed Model for SLC and Pre-BCR Assembly.
VPREB alone is an unfolded homodimer bound to BiP. The homodimer interacts at the V_H- and to a small part also at the λ5-VPREB interface. BiP is associated near the VPREB-V_H interface. VPREB can either bind to λ5, which induces its folding and collapse into a monomer with simultaneous BiP dissociation. Whether the SLC gets secreted independent of the HC remains unclear. The second fate of the VPREB homodimer is the interaction with the V_H domain of a HC. This interaction doesn´t induce its folding but the collapse into a monomer. The VPREB-UR is interacting with CDR H3. BiP probably remains bound to the unfolded VPREB monomer. λ5 can interact via its additional β-strand with VPREB and induce its folding. BiP dissociates from VPREB. λ5 forms an intermolecular disulfide bridge with C_H1 and induce its folding. BiP dissociates from C_H1 as well. The assembled pre-BCR is ready for transport to the cell surface.

4. FUTURE PERSPECTIVES

While previous studies on the SLC mostly focused on its functions by *in vivo* studies in mice or cell lines, the results of this doctoral thesis provided an insight into the structure and function of the SLC with the focus on the structure-function relationship and it conveys a holistic picture by *in vitro* studies. This thesis allows to draw several conclusions about mechanistic aspects of pre-BCR assembly and for the first time, a model could be developed based on the key findings in this research work.

For the future, the focus on SLC ligands and interaction partners other than the HC is interesting. To clarify, if pre-BCR clustering is dependent on ligands, it is interesting to see the change in oligomerization status of Fab-SLC in the presence of GAL1. This can be investigated by AUC measurements, EM, DLS *in vitro* or FACS measurements in cell culture. Identifying further binding partners in the environment of the bone marrow that might act as ligands to induce clustering or intracellular signaling pathways might be of special interest. This could be facilitated by pull down assays with cell lysates from murine bone marrow or stromal cells.

The interaction of the SLC with BILL-cadherin (cadherin-17) to form the pro-B-cell receptor on the cell surface of pro-B-cells also is an interesting point of research. Very little is known about this receptor, both on a functional and on a structural level. Therefore, it is highly interesting how the SLC associates with BILL-cadherin. This could be investigated by crystallizing the complex and examining its structure. Furthermore, it would be interesting how and if the URs are implicated in this interaction. This could be analysed using human cell lines transfected with SLC variants and BILL-cadherin to monitor their expression, surface exposure and secretion levels. These experiments could be supplemented by interaction studies e. g. by SPR. It would be interesting to see if the pro-B-cell receptor interacts with GAL1, if it has further interaction partners and if antigen interaction is conferred.

Since BiP is known to bind to unfolded proteins to retain them in the ER via its ER-retention motif, KDEL, its interaction with the SLC, especially with VPREB because it is unfolded without its SLC binding partner ʎ5 should be analyzed in more detail. Both, VPREB and ʎ5 have predicted BiP binding sites. In VPREB, they are located near the VPREB-V_H interface, which was shown in this thesis to be probably also the interface site for the VPREB dimer. This could mean that one BiP molecule directly can bind to the VPREB homodimer to retain it in the ER when the HC or ʎ5 are not bound. The predicted BiP binding site of ʎ5 is in its unfolded UR. Without a HC, BiP is probably binding to the SLC. BiP gets released upon assembly of the SLC to the HC. This could be analyzed with fluorescently labelled proteins in different nucleotide states via anisotropy or microscale thermophoresis. Another option is the analysis in human cell lines. In this context, also the binding of fluorescently labelled VPREB ΔU + β and VPREB βU could be tested for binding to BiP via anisotropy measurements.

The high antigen affinity of the SLC poses an extraordinary result. To further substantiate this, further antigens together with other HCs should be tested. Since it was shown that the λ5-UR is responsible for this high affinity, an alanine scanning approach could be applied to identify the residues involved in this interaction. Since the three tryptophanes could be possible interaction sites, it might be interesting to have single tryptophane to alanine mutants to possibly figure out if any of the three has more impact. It would be also interesting to find out if the same amino acids or amino acid patterns are important to bind to other antigens as well. Furthermore, it would be interesting to include another mutant of λ5 that has its arginines mutated to alanines to scan their impact on antigen affinity.

The effects that the tryptophanes in both URs and the negatively charged glutamates in the VPREB-UR have *in vivo*, are also interesting. For this, gene inactivation and mutation in mice could be performed by CRISPR/Cas9 or RNAi to get an insight in its functions. Furthermore, dissecting the role of the evolutionary conserved cysteine in the UR of λ5 is of special interest. Other interesting amino acids are the two serines at positions 59 and 103 in VPREB and the histidine at position 59 in λ5 as they were shown to be involved in CDR H3 interaction (Bankovich et al., 2007).

Because the stabilities of the mutants investigated in this thesis are quite different, limited proteolysis experiments might also be interesting. This could give an insight in which roles the URs have in regard of proteolysis in the ER. Because an assembled pre-BCR with a HC that failed to pass the SLC proof-reading must be degraded. Maybe this is done by proteolysis and the protruding unfolded URs might provide a possible target for the proteases.

Furthermore, it is still not fully understood how the URs interact with the V_H domain. To get a better mechanistic insight, NMR experiments could be performed to see the mode and the site of interaction. For this, the single SLC proteins as well as the SLC in complex with V_H should be analyzed in further detail. In this context, the mutants lacking the URs, the tryptophane mutants as well as the VPREB 9EurQ variant are of special interest. Furthermore, also λ5 that has the arginines in its UR mutated to alanines might be an interesting variant. In this context, also SAXS measurements of Fab-SLC and Fab-LC might be interesting to see where the URs are located.

Another open question is how VPREB and λ5 scrutinize the V_H domain. This could be tested with V_H domains that were previously shown to not bind to the SLC (Smith and Roman, 2010). Testing VPREB lacking the UR for its interaction with these V_H domains might be a starting point to see if they can interact and if the UR is the determining factor. Further, other mutants of both, VPREB and λ5, can be tested. This includes the tryptophane mutants of both, the glutamate mutant of VPREB and the arginine mutant of λ5. Also, other mutants that have not been investigated are conceivable. This could be executed by SPR measurements.

A further surprising finding in this thesis is the interaction of VPREB and C_H1 without inducing any folding reaction. To solve this question, immunoprecipitations in human cell lines transfected

with VPREB and C_H1 could be performed to test if this is also the case in the cellular context. HDX measurements of the VPREB-C_H1 complex might reveal the interaction site at protected amino acid residues. It would be interesting to investigate, if the VPREB-C_H1 interface is near the predicted BiP binding site in both proteins.

So far, crystallography was only performed on the Fab-SLC complex and the VPREB ΔU + β mutant. It should be tested if the core domains are structurally altered in the SLC complex without the HC and how ʎ5 behaves without VPREB, since in HDX, it showed several changes in peptide protection upon interaction with VPREB. Also, NMR of ʎ5 alone and in complex with VPREB could be a possible method to solve this question.

Another aspect to analyze might be the CDR2 of VPREB because it is longer than CDR2s in regular V_L domains. It could be interesting to create several different short CDR2s based on the original CDR2. Further, it could be tried to replace the CDR2 completely with CDR2s from V_L domains. These mutants could be scanned for their differences in interaction with V_H domains and with antigens.

Two things that should be considered in the future: repeat the experiments of this thesis with murine SLC; and investigate the possible interplay of the SLC and Calmodulin since there was shown to be a possible connection (Hauser et al., 2010).

Overall, a lot of open questions on the structure and function on the SLC remain, which can not be all covered in this section. Research on the SLC is still at an early age, especially at the structural level. In the next decades, we will hopefully gain a deeper understanding about the structural implications on the SLC function.

5. MATERIALS AND METHODS

5.1 Materials

5.1.1 Chemicals

The chemicals, which were used for the experiments in this dissertation, are listed in Table 15 with their respective suppliers and countries. For the preparation of buffers and solutions, double-distilled water was used from an Arium® pro water system (Sartorius, Göttingen, Germany).

Table 15: Chemicals with Their Suppliers and Countries.

Chemical	Supplier	Country
1,4-Dithiothreit	Carl Roth GmbH + Co. KG	Karlsruhe, Germany
^{15}N Ammonium chloride	Cambridge Isotope Laboratories, Inc.	Andover, US-MA
2-Mercaptoethanol	Sigma-Aldrich Chemie GmbH	Steinheim, Germany
2-Propanol	Carl Roth GmbH + Co. KG	Karlsruhe, Germany
2-Propanol ULC/MS-CC/SFC	Biosolve BV	Valkenswaard, Netherlands
ABTS Tablets	Roche Diagnostics GmbH	Mannheim, Germany
Acetic acid	Carl Roth GmbH + Co. KG	Karlsruhe, Germany
Acetonitrile ULC/MS-CC/SFC	Biosolve BV	Valkenswaard, Netherlands
Acrylamide/Bis Solution, 19:1 (40% w/v), 5% C	SERVA Electrophoresis GmbH	Heidelberg, Germany
Agar Agar SERVA Kobe I	SERVA Electrophoresis GmbH	Heidelberg, Germany
Agarose SERVA Wide Range	SERVA Electrophoresis GmbH	Heidelberg, Germany
Ammonium chloride	Merck KGaA	Darmstadt, Germany

Chemical	**Supplier**	**Country**
Ammonium peroxodisulfate	Carl Roth GmbH + Co. KG	Karlsruhe, Germany
Bacto™ Tryptone	Life Technologies Corporation	Detroit, US-MI
Biotin	Sigma-Aldrich Chemie GmbH	Steinheim, Germany
Biotinylated Creatinekinase	Roche Diagnostics GmbH	Mannheim, Germany
Blocking Reagent for ELISA	Roche Diagnostics GmbH	Mannheim, Germany
Boric acid	Merck KGaA	Darmstadt, Germany
Bromophenol blue sodium salt	Merck KGaA	Darmstadt, Germany
Buffer for ABTS	Roche Diagnostics GmbH	Mannheim, Germany
Buffer solution pH 10.00 (20°C)	Merck KGaA	Darmstadt, Germany
Buffer solution pH 4.00 (20°C)	Merck KGaA	Darmstadt, Germany
Buffer solution pH 7.00 (20°C)	Merck KGaA	Darmstadt, Germany
Calcium chloride dihydrate	Carl Roth GmbH + Co. KG	Karlsruhe, Germany
Cobalt (II) chloride hexahydrate	Merck KGaA	Darmstadt, Germany
cOmplete Tablets, EDTA-free, EASYpack	Roche Diagnostics GmbH	Mannheim, Germany
Coomassie Brilliant Blue G 250	SERVA Electrophoresis GmbH	Heidelberg, Germany
Coomassie® Blue R	SERVA Electrophoresis GmbH	Heidelberg, Germany

Chemical	**Supplier**	**Country**
Copper (II) chloride dihydrate	Merck KGaA	Darmstadt, Germany
D (+)-Glucose monohydrate	Merck KGaA	Darmstadt, Germany
Deuterium oxide (D_2O)	Cambridge Isotope Laboratories, Inc.	Andover, US-MA
Deuterium oxide 99.9 atom % D	Sigma-Aldrich Chemie GmbH	Steinheim, Germany
Dimethyl sulfoxide	Sigma-Aldrich Chemie GmbH	Steinheim, Germany
di-Sodium hydrogen phosphate	Merck KGaA	Darmstadt, Germany
di-Sodium hydrogen phosphate	Merck KGaA	Darmstadt, Germany
di-Sodium hydrogen phosphate dihydrate	Merck KGaA	Darmstadt, Germany
DNAse I	PanReac Applichem	Darmstadt, Germany
Dodeylsulfate-Na-Salt in pellets	SERVA Electrophoresis GmbH	Heidelberg, Germany
Dulbeccos´s Phosphate Buffered Saline	Sigma-Aldrich Chemie GmbH	Steinheim, Germany
Ethanol	Merck KGaA	Darmstadt, Germany
Extran® MA01	Merck KGaA	Darmstadt, Germany
Formic acid 99 % ULC/MS-CC/SFC	Biosolve BV	Valkenswaard, Netherlands
Glass Beads	Carl Roth GmbH + Co. KG	Karlsruhe, Germany
Glutaraldehyde solution	Sigma-Aldrich Chemie GmbH	Steinheim, Germany

Chemical	**Supplier**	**Country**
Glycerol	Carl Roth GmbH + Co. KG	Karlsruhe, Germany
Glycin	Carl Roth GmbH + Co. KG	Karlsruhe, Germany
Guanidine hydrochloride	Sigma-Aldrich Chemie GmbH	Steinheim, Germany
HEPES PUFFERAN® ≥ 99.5 %, p. a.	Carl Roth GmbH + Co. KG	Karlsruhe, Germany
HEPES, analytical grade, for cell culture	SERVA Electrophoresis GmbH	Heidelberg, Germany
Hydrochloric acid 32 %	Merck KGaA	Darmstadt, Germany
Imidazole	Sigma-Aldrich Chemie GmbH	Steinheim, Germany
Iron (III) chloride tetrahydrate	Merck KGaA	Darmstadt, Germany
Isopropyl-β-D-thiogalactopyranoside (IPTG)	SERVA Electrophoresis GmbH	Heidelberg, Germany
Kanamycin sulphate	Carl Roth GmbH + Co. KG	Karlsruhe, Germany
L-Arginine	Sigma-Aldrich Chemie GmbH	Steinheim, Germany
LB Medium powder	SERVA Electrophoresis GmbH	Heidelberg, Germany
L-Glutathione oxidized	Sigma-Aldrich Chemie GmbH	Steinheim, Germany
L-Glutathione reduced	Sigma-Aldrich Chemie GmbH	Steinheim, Germany
Magnesium chloride hexahydrate	Merck KGaA	Darmstadt, Germany

Chemical	Supplier	Country
Magnesium sulfate heptahydrate	Merck KGaA	Darmstadt, Germany
Manganese (II) chloride tetrahydrate	Merck KGaA	Darmstadt, Germany
Methanol	Carl Roth GmbH + Co. KG	Karlsruhe, Germany
Methanol absolute ULS/MS-CC/SFC	Biosolve BV	Valkenswaard, Netherlands
Natriumacetat – Trihydrat	Carl Roth GmbH + Co. KG	Karlsruhe, Germany
Nonidet P-40 Substitute	Sigma-Aldrich Chemie GmbH	Steinheim, Germany
Ortho-Phosphoric acid 85 %	Carl Roth GmbH + Co. KG	Karlsruhe, Germany
Potassium chloride BioUltra, for molecular biology, ≥ 99.5 % (AT)	Sigma-Aldrich Chemie GmbH	Steinheim, Germany
Potassium chloride, ≥ 99.5 %, p. a., ACS, ISO	Carl Roth GmbH + Co. KG	Karlsruhe, Germany
Potassium dihydrogen phosphate	Merck KGaA	Darmstadt, Germany
Potassium hydroxide	Carl Roth GmbH + Co. KG	Karlsruhe, Germany
Powdered milk	Carl Roth GmbH + Co. KG	Karlsruhe, Germany
Protease Inhibitor Mix HP	SERVA Electrophoresis GmbH	Heidelberg, Germany
SERVA HiSens Stain G	SERVA Electrophoresis GmbH	Heidelberg, Germany
Sodium azide	Merck KGaA	Darmstadt, Germany
Sodium chloride	Merck KGaA	Darmstadt, Germany

Chemical	**Supplier**	**Country**
Sodium deoxycholate	Sigma-Aldrich Chemie GmbH	Steinheim, Germany
Sodium deuteroxide 40 wt. % in D_2O, 99.5 atom % D	Sigma-Aldrich Chemie GmbH	Steinheim, Germany
Sodium dihydrogen phosphate monohydrate	Merck KGaA	Darmstadt, Germany
Sodium hydroxide	Carl Roth GmbH + Co. KG	Karlsruhe, Germany
Sodium hypochlorite, 10-15% freies Chlor	Acros Organics	Geel, Belgium
TEMED	Carl Roth GmbH + Co. KG	Karlsruhe, Germany
Thiamin-HCl	Sigma-Aldrich Chemie GmbH	Steinheim, Germany
Titriplex® III (ethylenedinitrilotetraacetic acid disodium salt dihydrate)	Merck KGaA	Darmstadt, Germany
TOF Instruments Service Sample Kit ([Glu1]-Fibrinopeptide B)	Waters Corporation	Milford, US-MA
TRICINE	Carl Roth GmbH + Co. KG	Karlsruhe, Germany
Tris-EDTA buffer solution pH 8.0	Sigma-Aldrich Chemie GmbH	Steinheim, Germany
Trizma® base	Sigma-Aldrich Chemie GmbH	Steinheim, Germany
TWEEN® 20 Detergent	EMD Millipore Corp.	Billerica, US-MA
U-^{13}C D-Glucose	Cambridge Isotope Laboratories, Inc.	Andover, US-MA
Urea	Merck KGaA	Darmstadt, Germany

Chemical	Supplier	Country
Water ULC/MS-CC/SFC	Biosolve BV	Valkenswaard, Netherlands
Yeast extract SERVABACTER® powder	SERVA Electrophoresis GmbH	Heidelberg, Germany
Zeocin™ Selection Reagent	Thermo Fisher Scientific	Waltham, US-MA
Zinc chloride	Merck KGaA	Darmstadt, Germany

5.1.2 Electrical Equipment

The technical devices used in this dissertation are listed in Table 16 with their respective suppliers and countries.

Table 16: Electrical Devices with Their Suppliers and Countries.

Electrical Device	Supplier	Country
10-mL Loop	Cytiva Sweden AB	Uppsala, Sweden
150-mL Superloop	Cytiva Sweden AB	Uppsala, Sweden
5-mL Loop	Cytiva Sweden AB	Uppsala, Sweden
ACQ-ASM	Waters Corporation	Milford, US-MA
ACQ-HDX	Waters Corporation	Milford, US-MA
ACQ-nBSM	Waters Corporation	Milford, US-MA
ÄKTA FPLC	Amersham Pharmacia Biotech, Inc.	Amersham, UK
ÄKTA pure	Cytiva Sweden AB	Uppsala, Sweden
Arium® pro	Sartorius	Göttingen, Germany
Avanti JX-26 Centrifuge	Beckman Coulter	Brea, US-CA
Biacore X100	Cytiva Sweden AB	Uppsala, Sweden
Biometra Thermoblock	Biometra	Göttingen, Germany

Electrical Device	**Supplier**	**Country**
Bruker AVANCE600	Bruker	Rheinstetten,Germany
Canon ET-67B	Canon Inc., Japan	Tokio, Japan
Cell Disruption Disruptor	Constant Cell Disruption Systems	Northants, UK
Centrifuge 5418	eppendorf	Hamburg, Germany
Centrifuge 5418 R	eppendorf	Hamburg, Germany
Chirascan plus	Applied Photophysics	Leatherhead, UK
Criterion™ Blotter	Bio-Rad Laboratories, Inc.	Hercules, US-CA
Electrophoresis Power Supply – EPS 601	Amersham Pharmacia Biotech, Inc.	Amersham, UK
Ice maker	ZIEGRA Eismaschinen GmbH	Isernhagen, Germany
ImageScanner III	GE Healthcare	Uppsala, Sweden
Incubator	Mytron Bio- und Solartechnik GmbH	Heilbad Heiligenstadt, Germany
Infinite M Nano	Tecan Group	Männedorf, Switzerland
Jasco J-1500 CD Spectrometer	JASCO Deutschland GmbH	Pfungstadt, Germany
Jasco V-630 Spectrophotometer	JASCO Deutschland GmbH	Pfungstadt, Germany
Laminar flow hood	Thermo Fisher Scientific	Waltham, US-MA
LCQ-FLEET	Thermo Fisher Scientific	Waltham, US-MA
LP 6200 S	Sartorius	Göttingen, Germany
MicroCal ITC200	Malvern Panalytical GmbH	Kassel, Germany

Electrical Device	**Supplier**	**Country**
Mighty Small™ SE245 Dual Gel Caster	Hoefer	Holliston, US-MA
MM 400 ball mill	Retsch	Haan, Germany
MR Hei-Standard	Heidolph Instruments GmbH & Co. KG	Schwabach, Germany
NanoDrop 2000 Spectrophotometer	Thermo Fisher Scientific	Waltham, US-MA
Optima AUC I	Beckman	Krefeld, Germany
pH Meter pH 538	WTW	Weilheim, Germany
PP 121 S	Sartorius	Göttingen, Germany
ROTINA 420 R	Hettich	Tuttlingen, Germany
Silent Crusher M	Heidolph Instruments GmbH & Co. KG	Schwabach, Germany
Sonopuls	BANDELIN electronic GmbH & Co. KG	Berlin, Germany
SYNAPT XS	Waters Corporation	Milford, US-MA
SYNAPT-G2S ESI-TOF mass spectrometer	Waters Corporation	Milford, US-MA
Systec DX-150	Systec GmbH	Linden, Germany
T100™ Thermal Cycler	Bio-Rad Laboratories, Inc.	Hercules, US-CA
Thermomixer comfort	eppendorf	Hamburg, Germany
Thermomixer compact	eppendorf	Hamburg, Germany
Transilluminator	VWR International	Radnor, US-PA
Vacuum System ME 4 NT + 2 AK	Vacuubrand GmbH + Co. KG	Olching, Germany

5.1.3 Consumables

The consumables that were used for the experiments in this dissertation are listed in Table 17 with their respective suppliers and countries.

Table 17: Consumables with Their Suppliers and Countries.

Consumable	Supplier	Country
1,5 mL tubes	Nerbe plus GmbH	Winsen/Luhe, Germany
2 mL tubes	Nerbe plus GmbH	Winsen/Luhe, Germany
50 mL Reagent Reservoir	Corning Incorporated	Corning, US-NY
Adhesive sealing film, for PCR, ELISA and EIA, 60 µm, -40°C up to +120°C, PE, clear, np pcr ready	Nerbe plus GmbH	Winsen/Luhe, Germany
Amicon® Ultra-15 30K MWCO	Merck KGaA	Darmstadt, Germany
Amicon® Ultra-15 3K MWCO	Merck KGaA	Darmstadt, Germany
Amicon® Ultra-15 50K MWCO	Merck KGaA	Darmstadt, Germany
CD cuvettes	Hellma GmbH & Co. KG	Müllheim, Germany
Cell Scraper 25 cm	Sarstedt AG & Co. KG	Nümbrecht, Germany
Falcon Tubes 15 mL	Greiner AG	Kremsmünster, Österreich
Falcon Tubes 20,000 RPM	VWR International	Radnor, US-PA
Falcon Tubes 50 mL	Greiner AG	Kremsmünster, Österreich
Low Protein Binding Durapore® (PVDF) Membrane	Merck KGaA	Darmstadt, Germany
MF-Millipore™ Membrane	Merck KGaA	Darmstadt, Germany

Consumable	**Supplier**	**Country**
PCR microcentrifuge tube, 0.2 mL	Nerbe plus GmbH	Winsen/Luhe, Germany
Petri dishes	Nerbe plus GmbH	Winsen/Luhe, Germany
pH-indicator paper	Merck KGaA	Darmstadt, Germany
Pierce™ Streptavidin Coated Clear 96-Well Plate with SuperBlock™ Blocking Buffer	Thermo Fisher Scientific	Rockford, US-IL
Pipette Tips	Sarstedt AG & Co. KG	Nümbrecht, Germany
Plastic Cuvettes	Sarstedt AG & Co. KG	Nümbrecht, Germany
Roti®-Fluoro PVDF, pore size 0.2 µm	Carl Roth GmbH + Co. KG	Karlsruhe, Germany
Sensor Chip CM5	Cytiva Sweden AB	Uppsala, Sweden
Serological pipettes	Sarstedt AG & Co. KG	Nümbrecht, Germany
SERVAGel™ TG PRiME™ 4-20 %	SERVA Electrophoresis GmbH	Heidelberg, Germany
Spectra/Por® 1 Dialysis Membrane MWCO 3.5 kDa	Spectrum Laboratories, Inc.	Rancho Dominguez, US-CA
Spectra/Por® 1 Dialysis Membrane MWCO 6-8 kDa	Spectrum Laboratories, Inc.	Rancho Dominguez, US-CA
Whatman™	GE Healthcare UK Limited	Buckinghamshire, UK
Xpress Micro Dialyzer MD100 & 300, 3.5 kDa MWCO	SERVA Electrophoresis GmbH	Heidelberg, Germany

5.1.4 Enzymes and Solutions

Enzymes and their respective buffers are listed in Table 18 and were all purchased from New England Biolabs GmbH (Frankfurt am Main, Germany).

Table 18: Enzymes and Buffers with Their Suppliers and Countries.

Enzyme	Supplier	Country
CutSmart® Buffer	New England Biolabs GmbH	Frankfurt am Main, Germany
Deoxynucleotide (dNTP) Solution Mix	New England Biolabs GmbH	Frankfurt am Main, Germany
DMSO, sterile	New England Biolabs GmbH	Frankfurt am Main, Germany
Gel Loading Dye Purple (6X)	New England Biolabs GmbH	Frankfurt am Main, Germany
KLD Enzyme Mix	New England Biolabs GmbH	Frankfurt am Main, Germany
KLD Reaction Buffer	New England Biolabs GmbH	Frankfurt am Main, Germany
Magnesium Chloride Solution	New England Biolabs GmbH	Frankfurt am Main, Germany
NEBuffer 2.1	New England Biolabs GmbH	Frankfurt am Main, Germany
Phusion® GC Buffer	New England Biolabs GmbH	Frankfurt am Main, Germany
Phusion® HF Buffer	New England Biolabs GmbH	Frankfurt am Main, Germany
Phusion® High-Fidelity DNA Polymerase	New England Biolabs GmbH	Frankfurt am Main, Germany
Q5® Hot Start High-Fidelity 2X Master Mix	New England Biolabs GmbH	Frankfurt am Main, Germany
Restriction Enzymes	New England Biolabs GmbH	Frankfurt am Main, Germany
T4 DNA-Polymerase	New England Biolabs GmbH	Frankfurt am Main, Germany

5.1.5 Standards

The protein and DNA standards that were used in this dissertation are listed in Table 19 with their respective suppliers and countries.

Table 19: Protein and DNA Standards with Their Suppliers and Countries.

Name	Supplier	Country
PageRuler™ Plus Prestained Protein Ladder	Thermo Fisher Scientific	Rockford, US-IL
SERVA Dual Color Protein Standard III	SERVA Electrophoresis GmbH	Heidelberg, Germany
SERVA FastLoad 1kb DNA Ladder	SERVA Electrophoresis GmbH	Heidelberg, Germany

5.1.6 Kits

The kits that were used in this thesis are listed in Table 20 with their respective suppliers and countries.

Table 20: Kits with Their Suppliers and Countries.

Name	Supplier	Country
Amine Coupling Kit	Cytiva Sweden AB	Uppsala, Sweden
BIAmaintenance Kit	Cytiva Sweden AB	Uppsala, Sweden
PureYield™ Plasmid Midiprep System	Promega Corporation	Madison, US-WI
QIAGEN® Plasmid MaxiKit (25)	QIAGEN GmbH	Hilden, Germany
Western Bright™ ECL-Spray	advansta	San Jose, US-CA
Wizard® Plus SV Minipreps DNA Purification System	Promega Corporation	Madison, US-WI
Wizard® SV Gel and PCR Clean-Up System	Promega Corporation	Madison, US-WI

5.1.7 Chromatography Columns and Materials

Chromatography columns and materials are listed in Table 21 with their respective suppliers and countries.

Table 21: Columns with Their Suppliers and Countries.

Column	Supplier	Country
HiLoad™ 26/60 Superdex™ 75 prep grade	GE Healthcare Bio-Sciences AB	Uppsala, Schweden
HisTrap™ Fast Flow 5 mL	GE Healthcare Bio-Sciences AB	Uppsala, Schweden
Q Sepharose™ Fast Flow	GE Healthcare Bio-Sciences AB	Uppsala, Schweden
SP Sepharose™ Fast Flow	GE Healthcare Bio-Sciences AB	Uppsala, Schweden
WATERS® ENZYMATE™ BEH PEPSIN COLUMN 2.1 x 30 mm	Waters Corporation	Milford, US-MA
ACQUITY UPLC® BEH C18 1.7 µm VanGuard™ Pre-Column 3/Pk 2.1 x 5 mm Column	Waters Corporation	Milford, US-MA
ACQUITY UPLC® BEH C18 1.7 µm 1.0 x 100 mm Column	Waters Corporation	Milford, US-MA

5.1.8 Oligonucleotides

The oligonucleotides used for PCRs are listed in Table 22 and were purchased from eurofins genomics (Ebersberg, Germany).

Table 22: Primer Sequences in 5'→3' Direction with Their Names.

Name	**Sequence (5' → 3')**
SUMOBsaI_L5DU_fwd	GAACAGATTGGAGGTACCCATGTTTTTGGT
SUMOBsaI_L5DU_rev	ATTCGGATCCTCTAGCTAGCTACATTCTGC
SUMOBsaI_VpreBDU_fwd	GAACAGATTGGAGGTCAGCCGGTTCTGCAT
SUMOBsaI_VpreBDU_rev	ATTCGGATCCTCTAGTTAGCTACGTGCACC
SUMOBsaI_L5DUDβ_fwd	GAACAGATTGGAGGTCAGCCGAAAGCAACC
SUMOBsaI_L5DUDβ_rev	ATTCGGATCCTCTAGCTAGCTACATTCTGC
SUMOBsaI_VpreBDU+β_fwd	GAACAGATTGGAGGTCAGCCGGTTCTGCAT
SUMOBsaI_VpreBDU+β_rev	ATTCGGATCCTCTAGTTAGCTCAGAACGGT
SUMOBsaI_L5_C212S_fwd	ACCGGCAGAAAGCAGCTAGAGCC
SUMOBsaI_L5_C212S_rev	GCAACGGTTTTTTCAACGG
SUMOBsaI_L5_W67A_fwd	GCGTAGCCGTGCGGGTCGTTTTC
SUMOBsaI_L5_W67A_rev	AGACTGCTACGGCTGCTA
SUMOBsaI_L5_W77A_fwd	GCGTGGTAGCGCGACCGGACCGC

Name	**Sequence (5‘ → 3‘)**
SUMOBsaI_L5_W77A_rev	TGCAGCAGAAAACGACCC
SUMOBsaI_L5_W83A_fwd	ACCGCGTTGTGCGCCTCGTGGTTTTC
SUMOBsaI_L5_W83A_rev	CCGGTCCAGCTACCACGC
SUMOBsaI_VpreB_W131A_fwd	TGAACGTGAAGCGGAAGAAGAAATGG
SUMOBsaI_VpreB_W131A_rev	CGTTCTTCTTTTTCGCTG
SUMOBsaI_C212STAA_fwd	ACCGGCAGAAAGCAGCTAAAGCC
SUMOBsa_C212STAA_rev	GCAACGGTTTTTTCAACGG
SUMOBsaI_L5DBC212S_fwd	AACAGATTGGAGGTAGCCAGAGCCGT
SUMOBsaI_L5DBC212S_rev	ATTCGGATCCTCTAGTTAGCTGCTTTCTGC
SUMOBsaI_VpreBEurQ_fwd	AACAGATTGGAGGTCAGCCGGTTCTG
SUMOBsaI_VpreBEurQ_rev	ATTCGGATCCTCTAGTTACGGAACACGGGT
SUMOBsaI_VpreBBetaU_fwd	AACAGATTGGAGGTCAGCCGGTTCTG
SUMOBsaI_VpreBBetaU_rev	ATT CGGATCCTCTAGTTACGGAACACGGGTAC

Name	**Sequence (5‘ → 3‘)**
pBUD_L5_L_V5-tag_Q5_f	CCCCCTGCTGGGCCTGGACAGCACCTAGTAAGGATCCGAACAAAAACTCATCTCAG
pBUD_L5_L_V5-tag_Q5_r	TTGGGGATGGGCTTGCCGCCGCCGGCGCCGCCGCTACACTCGGCAGGAGC
pBUD_L5DU_L_V5-tag_Q5_f	CCCCCTGCTGGGCCTGGACAGCACCTAGTAAGGATCCGAACAAAAACTCATCTCAG
pBUD_L5DU_L_V5-tag_Q5_r	TTGGGGATGGGCTTGCCGCCGCCGGCGCCGCCGCTACACTCGGCAGGAGC
pBUD_VpreB_L_Flag-tag_Q5_f	GGACGACGACGACAAGTAGTAACTCGAGAGATCTGGCCGG
pBUD_VpreB_L_Flag-tag_Q5_r	TTGTAGTCGCCGCCGGCGCCGCCAGGAACTCTGGTTCTGGC
pBUD_VpreBDU_L_Flag-tag_Q5_f	GGACGACGACGACAAGTAGTAACTCGAGAGATCTGGCCGGC
pBUD_VpreBDU_L_Flag-tag_Q5_r	TTGTAGTCGCCGCCGGCGCCGCCGCTTCTGGCGCCCATGGC
pBUD_VpreBFlagtoL5V5_NotIXhoI_f	AACACGTGGTCGCGCCACCATGTCTT
pBUD_VpreBFlagtoL5V5_NotIXhoI_r	GGCCAGATCTCTCGAGTTACTACTTGTCGTC
pBUD_VpreBW131A_f	CGAGCGCGAGGCCGAAGAAGAGATG
pBUD_VpreBW131A_r	CGTTCCTCTTTCTCGCTG
pBUD_L5WA-V5_HindBamh_f	TAGGGAGACCCAAGCTTGCCACCATGAG
pBUD_L5WA-V5_HindBamh_r	GAGTTTTTGTTCGGATCCTTACTAGGTGCTGTC

Name	Sequence (5‘ → 3‘)
pBUD_VpBEurQ-Flag_NotXho_f	AACACGTGGTCGCGCCACCATGT
pBUD_VpBEurQ-Flag_NotXho_r	GCCAGATCTCTCGAGTTACTACTTGTCGTC

5.1.9 Antibodies

The antibodiy that was used for ELISAs is listed in Table 23 with its respective host animal, dilution, supplier and country.

Table 23: Antibody Used for ELISAs with its Respective Host Animal, Dilution, Supplier and Country.

Name	Host Animal	Dilution	Supplier	Country
Monoclonal ANTI-FLAG® M2-Peroxidase (HRP) antibody produced in mouse	Mouse	1/15,000	Sigma-Aldrich Chemie GmbH	Steinheim, Germany

5.1.10 Bacterial and Human Cell Lines

The bacterial and human cells that were used in this thesis are listed in Table 24 and with their respective genotype and origin.

Table 24: Bacterial and Human Cell Lines with Their Genotypes and Origins.

Strain	Genotype	Origin
E.coli BL21-CodonPlus(DE3)-RIL	F^- *ompT hsdS*(r_B^- m_B^-) *dcm*$^+$ Tet^r *gal* λ(DE3) *end*A Hte [*arg*U *ile*Y *leu*W (Cam^r)]	Stratagene (La Jolla, USA)
E.coli XL1 Blue	*rec*A1 *end*A1 *gyr*A96 *thi* *hsd*R17(r_k^- m_k^+) *sup*E44 *rel*A1 *lac* [F´ *pro*AB$^+$ *lac*I^{q}ZΔM15 ::Tn10 (Tet^r)]	Stratagene (La Jolla, USA)

5.1.11 Sequences of Used Constructs

The amino acid sequences of the proteins used in this thesis are listed in the following.

ʎ5:
SQSRALGPGAPGGSSRSSLRSRWGRFLLQRGSWTGPRCWPRGFQSKHNSVTHVFGSGT
QLTVLSQPKATPSVTLFPPSSEELQANKATLVCLMNDFYPGILTVTWKADGTPITQGVE
MTTPSKQSNNKYAASSYLSLTPEQWRSRRSYSCQVMHEGSTVEKTVAPAECS

VPREB:
QPVLHQPPAMSSALGTTIRLTCTLRNDHDIGVYSVYWYQQRPGHPPRFLLRYFSQSDKS
QGPQVPPRFSGSKDVARNRGYLSISELQPEDEAMYYCAMGARSSEKEERERERWEEEME
PTAARTRVP

The UR of ʎ5 is marked in blue, the UR of VPREB in green and the additional β-strand of ʎ5 in orange.

C_H1 without the C-terminal cysteine:
MTTPPSVYPLAPGSAAQTNSMVTLGCLVKGYFPEPVTVTWNSGSLSSGVHTFPAVLQS
DLYTLSSSVTVPSSTWPSETVTCNVAHPASSTKVDKKIVPR

C_L without the C-terminal cysteine:
MGRADAAPTVSIFPPSSEQLTSGGASVVCFLNNFYPKDINVKWKIDGSERQNGVLNSW
TDQDSKDSTYSMSSTLTLTKDEYERHNSYTCEATHKTSTSPIVKSFNRNE

Fd MAK33 with and without FLAG-tag and without the C-terminal cysteine:
(M)EVQGVESGGGLVKPGGSLKLSCAASGFTFSDYYMYWVRQTPEKRLEWVATISDGG
SYTYYPDSVKGRFTISRDNAKNNLYLQMSSLKSEDTAMYYCARDKAYYGNYGDAMD
YWGQGTSVTVSSAKTTPPSVYPLAPGSAAQTNSMVTLGCLVKGYFPEPVTVTWNSGSL
SSGVHTFPAVLQSDLYTLSSSVTVPSSTWPSETVTCNVAHPASSTKVDKKIVPR(DYKDD
DDK)

V_H MAK33 with and without FLAG-tag:
(M)EVQGVESGGGLVKPGGSLKLSCAASGFTFSDYYMYWVRQTPEKRLEWVATISDGG
SYTYYPDSVKGRFTISRDNAKNNLYLQMSSLKSEDTAMYYCARDKAYYGNYGDAMD
YWGQGTSVTVSSA(DYKDDDDK)

V_L MAK33:

MDIVLTQSPATLSVTPGDSVSLSCRASQSISNNLHWYQQKSHESPRLLIKYASQSISGIPS
RFSGSGSGTDFTLSINSVETEDFGMYFCQQSNSWPLTFGAGTKLELKR

V_H 1HEZ:

MAQVQLVESGGGVVQPGRSLRLSCAASGFTFSGYGMHWVRQAPGKGLEWVALISYD
ESNKYYADSVKGRFTISRDNSKNTLYLQMNSLRAEDTAVYYCAKVKFYDPTAPNDYW
GQGTLVTVSS

Ulp1/SUMO-Protease (AA403-621):

MGSSHHHHHHSSGLVPRGSHAICLVPELNEKDDDQVQKALASRENTQLMNRDNIEITV
RDFKTLAPRRWLNDTIIEFFMKYIEKSTPNTVAFNSFFYTNLSERGYQGVRRWMKRKK
TQIDKLDKIFTPINLNQSHWALGIIDLKKKTIGYVDSLSNGPNAMSFAILTDLQKYVMEE
SKHTIGEDFDLIHLDCPQQPNGYDCGIYVCMNTLYGSADAPLDFDYKDAIRMRRFIAHL
ILTDALK

5.1.12 Peptide

The peptide used in this thesis is displayed with its sequence and origin in Table 25. The purity was at least 95 %. The N- and C-termini were not modified.

Table 25: Sequence of the β-Strand Peptide.

Name	Sequence	Origin
λ5 β-strand	THVFGSGTQLTVLS	Biozol Diagnostika Vertrieb GmbH, Eching, Germany

5.1.13 Media

Media and their relevant solutions with their récipes are displayed in Table 26.

Table 26: Media and Their Relevant Solution Récipes.

Medium	**Récipe**
100x Trace Elements Solution	5 g/L EDTA pH 7.5 (13.4 mM) 0.83 g/L $FeCl_3$-$6H_2O$ (3.1 mM) 84 mg/L $ZnCl_2$ (0.62 mM) 13 mg/L $CuCl_2$-$2H_2O$ (76 µM) 10 mg/L $CoCl_2$-$2H_2O$ (42 µM) 10 mg/L H_3BO_3 (162 µM) 1.6 mg/L $MnCl_2$-$4H_2O$ (8.1 µM) Dissolve 5 g EDTA in 800 mL of water and adjust pH to 7.5 with NaOH. Then add the other components in the quantities mentioned below and add water to a final volume of 1 L. Sterilize the solution over a 0.22-µm filter. 498 mg $FeCl_3$ (anhydrous) 84 mg $ZnCl_2$ 765 µL 0.1 M $CuCl_2$-$2H_2O$ (1.7 g/100 mL) 210 µL 0.2 M $CoCl_2$-$6H_2O$ (4.76 g/100 mL) 1.6 mL 0.1 M H_3BO_3 (0.62 g/100 mL) 8.1 µL 1 M $MnCl_2$-$4H_2O$ (19.8 g/100mL)
20% (w/v) Glucose	200 g/L Glucose
Kanamycin	35 µg/mL Working Concentration
Low Salt LB Medium	10 g/L Tryptone 5 g/L NaCl 5 g/L Yeast extract Adjust pH to 7.5 with 5 M NaOH 15 g/L Agar for Plates
Luria Bertani (LB) Broth	20g/L in Water 15 g/L Agar Agar to LB Medium for Plates
M9 Mineral Medium	100 mL M9 Salt Solution (10X)

Medium	Récipe
	20 mL 20% Glucose 1 mL 1 M $MgSO_4$ 0.3 mL 1 M $CaCl_2$ 1 mL Biotin (1 mg/mL) 1 mL Thiamin (1 mg/mL) 10 mL 100x Trace Elements Solution
M9 Salt Solution (10X)	75.2 g/L Na_2HPO_4-$2H_2O$ 30 g/L KH_2PO_4 5 g/L NaCL 5 g/L NH_4Cl
SOB Medium	2% Bacto tryptone 0.5 % Yeast extract 8.56 mM NaCl 2.5 mM KCl 10 mM $MgCl_2$ 10 mM $MgSO_4$
Zeocin	25 µg/mL Working Concentration

5.1.14 Buffers and Solutions

5.1.15.1 Protein Purification

The buffers and their respective récipes used for protein purification are shown in Table 27.

Table 27: Buffer Récipes for Protein Purification.

Name	Récipe
5x IB Lyse & Wash Buffer	250 mM Tris/HCl pH 7.5 50 mM NaCl
IB Dissolving Buffer SLC	6 M Gdn/HCl 50 mM NaP pH 7.5 10 mM Imidazole
Buffer A HisTrap denatured	5 M Gdn/HCl

Name	**Récipe**
	50 mM NaP pH 7.5 10 mM Imidazole
Buffer B HisTrap denatured	5 M Gdn/HCl 50 mM NaP pH 7.5 500 mM Imidazole
Drop-Dilution Buffer SLC	100 mM Tris/HCl (pH 8.2) 150 mM NaCl 350 mM L-Arginine 10 mM β-Mercaptoethanol
Refolding Buffer SLC	100 mM Tris/HCl pH 8.2 150 mM NaCl 350 mM L-Arginine 4 mM GSSG 0.5 mM GSH
Drop-Dilution Buffer His-SUMO-VHMAK33 Flag	100 mM Tris/HCl (pH 8.2) 350 mM L-Arginine 10 mM β-Mercaptoethanol
Refolding Buffer His-SUMO-VHMAK33 Flag	100 mM Tris/HCl pH 8.2 350 mM L-Arginine 4 mM GSSG 0.5 mM GSH
Buffer A HisTrap native	50 mM HEPES pH 7.4 150 mM KCl 20 mM Imidazole
Buffer B HisTrap native	50 mM HEPES pH 7.4 150 mM KCl 500 mM Imidazole
HEPES Storage Buffer	50 mM HEPES pH 7.4 150 mM KCl
10x PBS Buffer	100 mM $Na_2HPO_4x2H_2O$ or Na_2HPO_4

Name	**Récipe**
	18 mM KH_2PO_4 27 mM KCl 1.37 M NaCl
IB Dissolving Buffer	50 mM Tris/HCl pH 7.5 8 M Urea 10 mM β-Mercaptoethanol
Q-Seph Buffer A	50 mM Tris/HCl pH 7.5 5 M Urea
Q-Seph Buffer B	50 mM Tris/HCl pH 7.5 5 M Urea 1 M NaCl
C_H1 Refolding Buffer	250 mM Tris/HCl pH 9
VH & VL Refolding Buffer	250 mM Tris/HCl pH 8.0 100 mM L-Arginine 2 mM GSSG 0.5 mM GSH
Refolding Buffer Fab-SLC	100 mM Tris/HCl (pH 8.2) 150 mM NaCl 500 mM L-Arginine 4 mM GSSG 0.5 mM GSH
Drop-Dilution Buffer Fab-SLC	100 mM Tris/HCl (pH 8.2) 150 mM NaCl 500 mM L-Arginine 10 mM β-Mercaptoethanol
Refolding Buffer Fab-LC	100 mM Tris/HCl (pH 8.2) 500 mM L-Arginine 4 mM GSSG 0.5 mM GSH

Name	Récipe
Buffer A SUMO-Protease	40 mM Sodium phosphate pH 7.4 300 mM NaCl 40 mM Imidazole
Buffer B SUMO-Protease	40 mM Sodium phosphate pH 7.4 300 mM NaCl 300 mM Imidazole
SEC Buffer SUMO Protease	50 mM Tris/HCl pH 8.0 500 mM NaCl 1 mM DTT

5.1.15.2 Laemmli SDS-PAGE

The solutions and buffers that were used for Laemmli SDS-PAGE are listed in Table 28 with their respective récipes.

Table 28: Récipes of Buffers and Solutions Used for Laemmli SDS-PAGE.

Name	Récipe
10x SDS-PAGE Running Buffer	250 mM Tris/HCl pH 8.3 1.92 M Glycine 1 % SDS
5x Laemmli Buffer	0.3125 M Tris/HCl pH 6.8 10 % (w/v) SDS 50 % (v/v) Glycerol 5 % (v/v) 2-Mercaptoethanol 0.05 % (w/v) Bromophenol blue 10 % β-Bromophenol blue
Fairbanks A	25 % (v/v) 2-Propanol 10 % (v/v) Acetic acid 0.05 % (w/v) Coomassie Blue R
Fairbanks D	10 % (v/v) Acetic Acid
Separation Gel Buffer	1.5 M Tris/HCl 8.8

Name	Récipe
Stacking Gel Buffer	1 M Tris/HCl 6.8

5.1.15.3 Tris-Tricine SDS-PAGE

The solutions and buffers that were used for Tris-Tricine SDS-PAGE are listed in Table 29 with their respective récipes.

Table 29: Récipes of Buffers and Solutions Used for Tris-Tricine SDS-PAGE.

Name	Récipe
10x Anode Buffer (lower buffer)	2 M Tris/HCl pH 9.0
10x Cathode Buffer (upper buffer)	1 M Tris/HCl pH 8.25 10 M Tricine 1 % SDS
1x Gel loading buffer (non-reducing)	50 mM Tris/HCl pH 8 12 % glycerol 4 % SDS 0.01 % Coomassie blue G-250
1x Gel Loading Buffer (reducing)	50 mM Tris/HCl pH 8 12 % glycerol 4 % SDS 0.01 % Coomassie blue G-250 10 % 2-Mercaptoethanol
Gel Buffer	3 M Tris/HCl pH 8.45 3 % SDS *adjust pH before adding SDS

5.1.15.4 Agarosegel

The buffer used for agarose gel electrophoreses is listed with its récipe in Table 30.

Table 30: Récipe of Buffer Used for Agarose Gel Electrophoresis.

Name	Récipe
TAE Buffer	40 mM Tris/Acetic Acid pH 8.2

	1 mM EDTA

5.1.15.5 Chemically Competent Cells

The buffer used for preparation of chemically competent *E. coli* cells, is listed with its récipe in Table 31.

Table 31: Récipe of Buffer Used for Preparation of Chemical Competent Cells.

Name	**Récipe**
TB buffer	10 mM Pipes pH 6.7 55 mM $MnCl_2$ 15 mM $CaCl_2$ 250 mM KCl

5.1.15.6 Hydrogen/Deuterium Exchange Mass Spectrometry

The buffers used for HDX-MS are listed in Table 32 with their respective récipes.

Table 32: Buffer Récipes for HDX-MS.

Name	**Récipe**
Quench Buffer	200 mM Na_2HPO_4 pH 2.2 200 mM KH_2PO_4 4 M Gdn/HCl MS-H_2O
Deuterated Buffer	50 mM HEPES pH 7.4 150 mL KCl
Pepsin Wash Solution	1.5 M Gdn/HCl 4 % ACN 0.8 % Fa
Glufib solution	100 fmol Glufib in 30 mL MS-H_2O+0.1 % FA/ACN (1/1)
Solution A	ddH_2O + 0.1 % FA
Solution B	ACN + 0.1 % FA

Name	Récipe
Solution C	10 % ACN
Solution D	4 % MeOH + 0.1 % FA
Solution E	25 % Isopropanol 25 % ACN 25 % MeOH 0.1 % FA MS-H_2O

5.1.15.7 Surface Plasmon Resonance

The buffers and solutions used for SPR experiments are listed in Table 33 with their respective récipes.

Table 33: Buffer and Solution Récipes for SPR.

Name	Récipe
Biacore Running Buffer	50 mM HEPES 150 mM KCl 3 mM EDTA 0.05 % Tween 20
CM5 Chip Coupling Buffer	10 mM Sodium Acetate – 3 H_2O pH 4, 4.5, 5, 5.5, 6
Regeneration Solution	1.5 M KCl
Sodium Hydroxide	50 mM NaOH

5.1.15.8 Enzyme-Linked Immunosorbent Assay

The buffers and solutions used for ELISA experiments are listed in Table 34 with their respective récipes.

Table 34: Buffer and Solution Récipes for ELISAs.

Name	Récipe
Blocking Buffer	50 mM NaCl 0.5 mM EDTA 0.1 % Tween 20 0.5 g/50 mL blocking reagent 100 mM NaP pH 7.5
ABTS solution	1 ABTS pill (5 mg) 5 mL ABTS buffer
NaCl solution	1 M NaCl
EDTA solution	0.5 M EDTA pH 8.0
Antigen solution	25 µg biotinylated Creatinkinase 5 % blocking reagent 2 mL ddH_2O
Antibody solution	Anti-Flag 1/15,000 in Blocking buffer

5.2 Software, Databases and Web-based Tools

5.2.1 Software

The software relevant for this thesis is listed with its respective developer in Table 35.

Table 35: Used Software and Their Developers.

Software	Developer
Adobe Photoshop CS5 12.0 x64	Adobe Inc.
Affinity Designer	Serif Europe
Biacore X100 Control Software	Cytiva Sweden AB
Biacore X100 Evaluation Software	Cytiva Sweden AB

Software	**Developer**
CCPN V3.0.4	University of Leicester, United Kingdom
Chirascan Software & Pro-Data Viewer	Applied Photophysics
Deuteros 2.0 (cite paper)	Paper zitieren
DynamX 3.0	Waters Corporation
EndNote X9	Clarivate Analytics
EOS Utility 2	Canon
GENtle	Magnus Maske, University of Cologne, Germany
LabScan 6.0	GE Healthcare
MassLynx V4.1	Waters Corporation
MicroCal ITC200 Software	Malvern Instruments
Microsoft Office 2016	Microsoft Corporation
NanoDrop2000	Thermo Fisher Scientific
Origin 2018b	Electronic Arts
ProteinLynx Global Server 3.0.3	Waters Corporation
Pymol V2.4	DeLano Scientific LLC, Schrödinger
SedFit (version?)	Peter Schuck (Paper?)
SnapGeneViewer	GSL Biotech LLC
Spectra Manager Ver 2	JASCO Deutschland GmbH
TOPSPIn 4.0.3	Bruker Biospin
UNICORN	Cytiva Sweden AB

5.2.2 Web-based Tools

The web-based tools that were used in this doctoral thesis are depicted in Table 36 with their respective URLs.

Table 36: Web-Based Tools with Their URLs.

Tool	**URL**
AlphaFold Protein Structure Database – EMBL-EBI	https://alphafold.ebi.ac.uk
Bestsel	https://bestsel.elte.hu
BLAST: Basic Local Alignment Search Tool	https://blast.ncbi.nlm.nih.gov/Blast.cgi
Clustal Omega < Multiple Sequence Alignment < EMBL-EBI	https://www.ebi.ac.uk/Tools/msa/clustalo
E. coli codon usage analyzer	http://www.faculty.ucr.edu/~mmaduro/codonusage/usage.htm
E. coli codon usage optimizer	http://genomes.urv.es/OPTIMIZER/
EMBOSS Backtranseq – Sequence Translation – EMBL-EBI	https://www.ebi.ac.uk/Tools/st/emboss-backtranseq/
IgBlast tool - NCBI	https://www.ncbi.nlm.nih.gov/igblast/
Interactive Tools – NEB	https://www.neb.com/tools-and-resources/interactive-tools
iTOL: Interactive Tree Of Life	https://itol.embl.de
IUPred2A	https://iupred2a.elte.hu/
NetNGlyc – 1.0 – Services – DTU Health Tech	https://services.healthtech.dtu.dk/service.php?NetNGlyc-1.0
NetOGlyc – 4.0 – Services – DTU Health Tech	https://services.healthtech.dtu.dk/service.php?NetOGlyc-4.0

Tool	**URL**
PeptideCutter – Expasy	https://web.expasy.org/peptide_cutter/
PHYRE2 Protein Fold Recognition Server	http://www.sbg.bio.ic.ac.uk/phyre2/html/page.cgi?id=index
PrimerX – Bioinformatics.org	https://www.bioinformatics.org/primerx/
PROSITE – Expasy	https://prosite.expasy.org
ProtParam tool - Expasy	https://web.expasy.org/protparam/
PSIPRED Workbench – Bioinformatics Group	http://bioinf.cs.ucl.ac.uk/psipred/
QuickChange Primer Design - Agilent	https://www.agilent.com/store/primerDesignProgram.jsp
REFOLDdb	https://pford.info/refolddb/
Reverse Translate – Bioinformatics.org	https://www.bioinformatics.org/sms2/rev-trans.html
SignalP – 5.0 – Services – DTU Health Tech	https://services.healthtech.dtu.dk/service.php?SignalP-5.0
SWISS-MODEL	https://swissmodel.expasy.org
TCB Tools	https://www.bioinformatics.wzw.tum.de/bippred/submit/
T-COFFEE Multiple Sequence Alignment Server - CRG	http://tcoffee.crg.cat
Translate tool - Expasy	https://web.expasy.org/translate/

5.2.3 Databases

The databases that were used in this thesis are listed with their respective URLs in Table 37.

Table 37: Databases with Their URLs.

Databases	**URL**
AbYsis	http://www.abysis.org
MobiDB	https://mobidb.bio.unipd.it
PubMed	https://pubmed.ncbi.nlm.nih.gov
RCSB PDB	https://www.rcsb.org
UniProt.Org	https://www.uniprot.org

5.3 Methods

5.3.1 Generation of Chemically Competent *Escherichia coli (E. coli)* Cells

For the generation of chemically competent *E. coli* cells, 25 mL of SOB medium were inoculated with fresh colonies from an O/N cultured plate, and this was incubated at 37°C for 6 – 8 h while shaking. From this culture, 10 mL were used to inoculate 250 mL of SOB medium, which was then incubated O/N at 18°C until an optical density at 600 nm (OD_{600}) of 0.55 to 0.6 was reached. After giving the cells a cold shock of 10 minutes on ice, they were centrifuged at 2,500 xg for 10 min at 4°C. The cell pellet was resuspended in 50 mL of ice-cold TB buffer and incubated for 10 min on ice. Another centrifugation step as described above followed to pellet the cells. The pelleted cells were thereafter resuspended in 20 mL of TB buffer supplemented with 7% of DMSO. The cells were then aliquoted, frozen in liquid nitrogen and stored at -80°C.

5.3.2 Plasmid Transformation into Chemically Competent *E. coli* Cells

For the retransformation of plasmid DNA into chemically competent *E. coli* cells, 60 µL of cells were added to 100 ng of plasmid DNA without mixing to not harm the cells. To transform a newly cloned plasmid into chemically competent *E. coli* cells, 100 µL of cells were added to the entire sequence and ligation independent cloning (SLIC) reaction batch (10 µL). Both were incubated on ice for 15 minutes and then heat-shocked at 42°C for 45 seconds. Thereafter, the cells were immediately put on ice and incubated for 5 minutes. Then, 700 µL of LB^0 medium was added and incubated at 37°C, while shaking for 1 h. Subsequently, the suspension was pelleted at 8,000 xg for 5 minutes and plated on selective LB agar plates.

5.3.3 Plasmid Digestion and Purification

For the digestion of plasmid DNA by restriction enzymes, 1 µg of DNA was mixed with the recommended number of units of restriction enzymes in the recommended buffer in a final reaction volume of 50 µL. This was calculated with a web-based tool called NEBcloner (Table 36). The reaction was performed at 37°C for 1 h. The digested plasmid was purified using the Wizard SV Gel and PCR Clean-Up System according to the manufacturer´s protocol.

5.3.4 Polymerase Chain Reaction

Polymerase Chain Reaction (PCR) was used to amplify insert DNA for SLIC (section 5.3.6). The PCR conditions for standard PCRs are shown in Table 38.

Table 38: Pipetting Scheme for SLIC PCR Reactions.

Component	**Final Concentration**
Template DNA	10 ng
dNTPs (10 mM per dNTP)	200 µM
Forward Primer (10 µM)	500 µM
Reverse Primer (10 µM)	500 µM
DMSO	3%
5x HF/GC Phusion Buffer	1x
Phusion® High-Fidelity DNA Polymerase (2000 units/mL)	20 units/mL
ddH_2O	to 50 µL

The standard temperature cycle program used for the PCRs in this thesis is displayed in Table 39. It was performed in a T100™ Thermal Cycler (Bio-Rad Laboratories, Inc., Hercules, US-CA).
X indicates the primer-specific annealing temperature as determined by NEB Tm Calculator. After the reaction, the PCR product was purified using the Wizard SV Gel and PCR Clean-Up System according to the manufacturer´s protocol.

Table 39: Temperature Cycle Program for SLIC PCR Reactions.

Step	Temperature	Time
Initial Denaturation	98°C	30 sec
35 cycles		
Denaturation	98°C	10 sec
Annealing	X°C	30 sec
Extension	72°C	30 sec per kb
Final Extension	72°C	10 min

5.3.5 Agarose Gel Electrophoresis for DNA Analysis

For verification of the correct size and purity of the PCR product, agarose gel electrophoresis was applied to a small amount of the PCR product. To perform agarose gel electrophoresis, 1% agarose gels in TAE buffer were prepared. The agarose was dissolved by heating the suspension up and afterwards, Serva DNA Stain G in a ratio of 1:50,000 was added. The solution was then poured into a corresponding chamber and incubated until it was fully polymerized. The gels were then run at a constant voltage of 120 V for 20 min and DNA was visualized by UV irradiation. Thereafter, the remaining PCR product was purified using the Wizard SV Gel and PCR Clean-Up System.

5.3.6 Sequence and Ligation Independent Cloning

To clone the construct of interest into its desired vector, sequence, and ligation independent cloning (SLIC) was performed. The primers were designed according to Jeong et al. (Jeong et al., 2012). One SLIC reaction batch consisted of: 100 ng of digested vector, insert DNA in a ratio of 2:1 to the vector, 1x Buffer 2.1, 1mM DTT, 0.6 U T4 DNA Polymerase in a 20 µL reaction volume in ddH_2O. The reaction was performed at RT for 2.5 min and then immediately placed on ice, incubated for 10 min. After this incubation step, 10 µL of the reaction batch were transformed into *E. coli* XL1 blue cells (section 5.3.2).

5.3.7 Site-Directed Mutagenesis

To substitute up to 10 nucleotides and perform insertions or deletions of nucleotides, the site-directed mutagenesis protocol from NEB was used (Chiu et al., 2004). PCR primers were designed using the NEBaseChanger tool. Step 1 of this protocol comprised exponential amplification of the plasmid DNA (Table 40) with standard cycling conditions (Table 41) in a T100™ Thermal Cycler (Bio-Rad Laboratories, Inc., Hercules, US-CA).

Table 40: Pipetting Scheme for Site-Directed Mutagenesis PCR from NEB.

Component	25 µL RXN	Final concentration
Q5 HotStart High-Fidelity 2X Master Mix	12.5 µL	1X
10 µM Forward Primer	1.25 µL	0.5 µM
10 µM Reverse Primer	1.25 µL	0.5 µM
Template DNA (25 ng/µL)	1 µL	25 ng
Nuclease-free water	9.0 µL	

Table 41: Temperature Cycle Program for Site-Directed Mutagenesis PCR from NEB.

Step	Temp	Time
Initial Denaturation	98°C	30 sec
25 Cycles	98°C X°C 72°C	10 sec 30 sec 30 sec/kb
Final Extension	72°C	2 min
Hold	4-10°C	

The exponential amplification was followed by the KLD reaction. The pipetting scheme of this reaction is displayed in Table 42. It was incubated for 5 min at RT and placed immediately on ice for at least 10 min. Afterwards, the whole reaction mix was transformed into *E. coli* XL1 blue cells (section 5.3.2).

Table 42: Pipetting Scheme for KLD Digestion Following Site-Directed Mutagenesis.

Component	Volume	Final concentration
PCR Product	1 µL	
2X KLD Reaction Buffer	5 µL	1X
10X KLD Enzyme Mix	1 µL	1X
Nuclease-free water	3 µL	

5.3.8 Determination of Nucleic Acid Concentration and Quality

The DNA concentration was determined by UV/Vis spectroscopy with a NanoDrop 2000 Spectrophotometer (Thermo Fisher Scientific, Waltham, US-MA). The determination of nucleic acid concentration depends on the specific UV absorption characteristics of the biomolecules. Nucleic acids show a maximum UV absorption at 260 nm, which depends on the nucleo bases. The concentration can therefore be calculated using the Lambert-Beer´s law (Equation 2).
DNA purity was determined by ensuring the A_{260}/A_{280} ratio was between 1.8 and 2.0. H_2O was measured to correct for background absorption.

$$A_{260\,nm} = c * \varepsilon * d$$

Equation 2: Lambert-Beer´s Law for Nucleic Acid Concentration Determination.
A_{260}: Absorption at 260 nm; ε: Extinction coefficient for DNA (0.02 mL μg^{-1} cm^{-1}); *c*: DNA concentration [ng μL^{-1}]; *d*: Layer thickness [cm].

5.3.9 Heterologous Protein Expression and Inclusion Body Preparation

5.3.9.1 Test Expression of Proteins

After the constructs were cloned, an expression test in *E. coli* BL21 CodonPlus (DE3) (Table 24) was performed to find the optimal expression conditions for large scale expression. A pre-culture of 5 mL selective LB medium was inoculated with one fresh colony of the respective construct from a selective LB agar plate and incubated O/N at 37°C. This colony served for inoculation of 50 mL selective medium to an OD_{600} of 0.1. The cell suspension was incubated at 37°C up to an OD_{600} of 0.7 – 0.9, where the expression was induced with 1 mM IPTG. Before induction, a 1-mL sample was taken for analysis on the gel. The cells were continued to be incubated after induction at 37°C and a sample was taken every hour up to 4 hours post-induction. The amount of taken sample was calculated accordingly. Last, an O/N sample was taken. The scheme is depicted in Figure 83.
All samples were centrifuged at 5,510 xg for 10 min at 4°C. The supernatant was discarded, and the cell pellet was resuspended in 200 µL of 1x IB Lyse & Wash Buffer. Glass beads were added and and the samples were shaken 4 times for 2 min at a frequency of 30 s^{-1} in a ball mill. The lysed cells were centrifuged at 16,873 xg at 4°C for 10 min. Then, 48 µL of supernatant, representing the soluble fraction, was mixed with 12 µL of 5x reducing Laemmli buffer. After removing the remaining supernatant from the beads, 25 µL of 5x reducing Laemmli buffer was added to the beads, representing the insoluble fraction. After boiling the samples at 95°C for 5 min, they were applied to a gel (section 5.3.11).

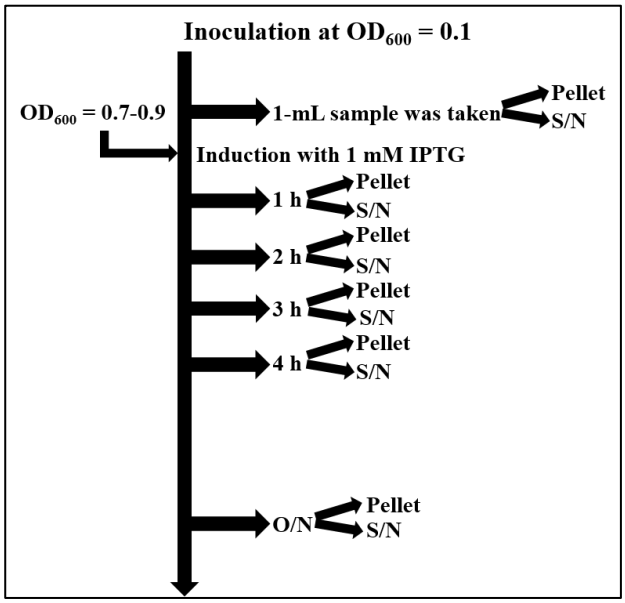

Figure 83: Schematic Workflow for the Test Expression of Successful Cloned Constructs.
After the inoculation of 50 mL medium to an OD_{600} of 0.1, the cells were grown at 37°C to an OD_{600} of roughly 0.7-0.9. Before induction with 1 mM IPTG, a 1-mL sample was taken. Samples with corresponding amounts of cells were taken after 1 h, 2 h, 3 h, 4 h and O/N expression.

5.3.9.2 Heterologous Protein Expression

All proteins used for this thesis were expressed in *E. coli* BL21-Codon Plus (DE3)-RIL cells (Table 24). First, a 50 mL preculture of selective LB medium was inoculated with a fresh colony from an O/N cultured selective LB agar plate and incubated O/N at 37°C while shaking. This culture was then used to inoculate 2x 2 L culture of selective LB medium in a baffled 5 L flask each to an OD_{600} of 0.1. This culture was incubated at 37°C until an OD_{600} of 0.8 – 1.0 was reached. The expression was induced by the addition of 1 mM IPTG fresh powder. The proteins were expressed at 37°C for 3 h while shaking. For Ulp1/SUMO-Protease (403-621), the protocol slightly varied. It was incubated until an OD_{600} of 0.6 – 0.8 was reached. The protein was expressed for 4 h at 37°C while shaking.

For NMR experiments, expression of ^{15}N-labelled or ^{13}C-^{15}N-labelled VPREB and ^{13}C-^{15}N-labelled λ5 C212S was performed in selective M9 minimal medium containing $^{15}NH_4Cl$ and glucose or ^{13}C-glucose (Table 26), respectively.

Cells were harvested by centrifugation at 7,562 xg in a JA-10 rotor for 15 min at 4°C in an Avanti JX-26 Centrifuge (Beckman Coulter, Brea, US-CA). The pellet was resuspended in IB Lyse & Wash Buffer supplemented with DNase I and Protease Inhibitor Mix HP and lysed either by pressure at 2 kbar in a cell disruption machine or in a sonicator for seven times at 50 % power, 8 pulses for 30 sec each.

The cell pellet of Ulp1/SUMO-Protease (403-621) was resuspended in Buffer A SUMO-Protease supplemented with DNase I and Protease Inhibitor Mix HP and lysed by pressure at 2 kbar in a

cell disruption machine. The lysate was cleared by centrifugation at 32,928 xg in a JA-25.50 rotor in an Avanti JX-26 Centrifuge (Beckman Coulter, Brea, US-CA) at 4°C for 1 h.

5.3.9.3 Inclusion Body Preparation

The lysate from section 5.3.9.2 was centrifuged at 12,197 xg in a J-LITE JLA-16.250 rotor in an Avanti JX-26 Centrifuge (Beckman Coulter, Brea, US-CA) for 40 min at 4°C to obtain the inclusion bodies in the pellet, which were washed twice with 1x IB Lyse & Wash Buffer and centrifuged again after each washing step as above-mentioned. The pellet contained the pure inclusion bodies, which were stored at -20°C until purification.

5.3.10 Protein Purification

The purification protocol for all SLC variants and complexes as well as V_H MAK33-Flag were established in this thesis and can be found in the results section (section 2.2). For all other proteins that were purified during this doctoral thesis, the purification protocols are described below. Generally, all proteins were flash-frozen in liquid N_2 and stored at -80°C after purification. All purification steps were monitored by Laemmli SDS-PAGE to identify protein-containing fractions. All purified proteins had at least a purity of 95 %. Protein identity and purity were identified by Tris-Tricine SDS-PAGE and MALDI-TOF for fingerprint analysis and LCQ-FLEET for its correct molecular mass. Purified proteins were concentrated by ultracentrifugation in amicon filters, and the protein concentration was determined by UV/Vis spectrophotometry at 280 nm (section 5.3.13.1) after baseline correction of the respective buffer. The extinction coefficients were determined with the use of the Expasy Protparam tool (Table 36). The proteins were either purified with the help of an ÄKTA pure (Cytiva Sweden AB, Uppsala, Sweden) or an ÄKTA FPLC (Amersham Pharmacia Biotech, Inc., Amersham, UK).

5.3.10.1 Purification of C_H1 MAK33

The inclusion bodies obtained after expression and preparation (sections 5.3.9.2 & 5.3.9.3) were solubilized in 50 mL of IB dissolving buffer O/N at 4°C, gently stirring. The solubilized inclusion bodies were centrifuged at 32,928 xg in a JA-25.50 rotor in an Avanti JX-26 Centrifuge (Beckman Coulter, Brea, US-CA) for 1 h at 4°C prior to loading onto a pre-equilibrated Q-Sepharose column. The protein was collected from the flowthrough, diluted to a concentration of 0.1 g/L in Q-Seph Buffer A and dialyzed O/N in C_H1 Refolding Buffer at 10°C, gently stirring. The concentrated dialysate with a final volume of 5 mL was purified using a Superdex 75 26/60 gel filtration column in PBS buffer. Protein containing fractions were pooled and concentrated.

5.3.10.2 Purification of V_H 1HEZ and V_H MAK33, and V_L MAK33

The inclusion bodies obtained after expression and preparation sections 5.3.9.2 & 5.3.9.3) were each solubilized in 50 mL of IB dissolving buffer O/N at 4°C, gently stirring. The solubilized inclusion bodies were centrifuged at 32,928 xg in a JA-25.50 rotor in an Avanti JX-26 Centrifuge (Beckman Coulter, Brea, US-CA) for 1 h at 4°C prior to loading onto a pre-equilibrated Q-Sepharose column. The protein was collected from the flowthrough each and subsequently loaded onto a pre-equilibrated SP-Sepharose column for V_H 1HEZ and V_H MAK33 with the same buffers as for Q-Sepharose. The bound protein was washed with 5 CV Q-Seph Buffer A and eluted eluted with a 0-100% gradient with Buffer B SUMO-Protease over 5 CV. The protein containing fractions were pooled and diluted to a concentration of 0.1 g/L in Q-Seph Buffer A and dialyzed O/N in VH&VL Refolding Buffer at 10°C, gently stirring. The concentrated dialysates with a final volume of 5 mL each were purified using a Superdex 75 26/60 gel filtration column in PBS buffer. Protein containing fractions were pooled and concentrated.

5.3.10.3 Purification of the F_{ab} MAK33 with a C-terminal FLAG-Tag

The inclusion bodies obtained after expression and preparation (sections 5.3.9.2 & 5.3.9.3) were each solubilized in 50 mL of IB dissolving buffer O/N at 4°C, gently stirring. The solubilized inclusion bodies were centrifuged at at 32,928 xg in a JA-25.50 rotor in an Avanti JX-26 Centrifuge (Beckman Coulter, Brea, US-CA) for 1 h at 4°C prior to loading onto a pre-equilibrated Q-Sepharose column. The proteins were each collected from the flowthrough, pooled together, and the cysteines were reduced with 10 mM β-Mercaptoethanol for 1 h at 4°C under exclusion of oxygen. Thereafter, they were drop-diluted on ice to a concentration of 0.05 g/L of LC in an equimolar ratio with Fd MAK33-FLAG into Refolding Buffer Fab-LC and dialyzed for seven days in Refolding Buffer Fab-LC at 10°C, gently stirring. The concentrated dialysate with a final volume of 5 mL was purified using a Superdex 75 26/60 gel filtration column in HEPES Storage buffer. Protein containing fractions were pooled and concentrated. The protocol was obtained from Buchner et al. (Buchner and Rudolph, 1991).

5.3.10.4 Purification of Ulp1 SUMO Protease

Lysate in Buffer A SUMO-Protease (section 5.3.9.2) was loaded onto a pre-equilibrated HisTrap column and the bound protein was washed with at least 5 column volumes (CV) of Buffer A SUMO-Protease. The bound protein was eluted with a 0-100% gradient with Buffer B SUMO-Protease over 15 CV. The concentrated protein-containing fractions with a final volume of 5 mL were subjected to a pre-equilibrated Superdex 75 26/60 gel filtration column in SEC Buffer SUMO Protease. To the final protein, 50 % Glycerol and 1 % NP-40 were added.

5.3.11 Laemmli SDS-PAGE and Tris-Tricine SDS-PAGE

Sodium Dodecyl Sulfate Polyacrylamide Gel Electrophoresis (SDS-PAGE) and Tris-Tricine SDS-PAGE were used to separate proteins based on differences in their molecular weight. While proteins with lower molecular weight migrate longer through the gel, proteins with higher molecular weight have a quite short migration path. Hereby, Tris-Tricine SDS-PAGE varies from Laemmli SDS-PAGE by replacing Glycine (pK 9.6) with Tricine (pK 8.15). While Laemmli SDS-PAGE gel can separate high molecular weight proteins ranging from 20 to 200 kDa, Tris-Tricine SDS-PAGE is used to separate proteins with less than 20 kDa, which was crucial since the proteins that were worked with in this thesis were all below 20 kDa.

Table 43: Pipetting Scheme for a 5 % Stacking Gel and a 14 % Separating Gel for Laemmli SDS-PAGE.

Gel Type	Récipe
Stacking Gel	1.85 mL ddH_2O 0.325 mL 1.0 M Tris/HCl pH 6.8 0.275 mL 40% Acrylamide 25 µL 10 % SDS 25 µL APS 2.5 µL TEMED
14 % Separating Gel	1.9 mL ddH_2O 1.25 mL 1.5 M Tris/HCl pH 8.8 1.75 mL 40 % Acrylamide 50 µL 10 % SDS 50 µL APS 4 µL TEMED

For Laemmli SDS-PAGE, separation gels that contained 14 % (w/v) acrylamide were used. The stacking gel had a fixed concentration of 5 % (w/v) acrylamide. The pipetting scheme are shown in Table 43. Protein samples were mixed with 1x Laemmli Buffer and boiled at 95°C for 5 min. They were spinned down before loading them onto the gel. The gels were run at a current of 35 mA for 40 minutes.

Table 44: Pipetting Scheme for Stacking and Separating Gels of Tris-Tricine SDS PAGE.

Gel Type	Récipe
Stacking Gel	1 mL Acrylamide 3.1 mL Gel Buffer Up to 12.5 mL with ddH_2O
Separating Gel	6.1 mL Acrylamide 10 mL Gel Buffer 4 g Glycerol Up to 30 mL with ddH_2O

For Tris-Tricine SDS-PAGE, separation gels with 10 % (w/v) acrylamide and stacking gels with 4 % acrylamide were used according to the scheme in Table 44. Protein samples were mixed with 1x Gel Loading Buffer and boiled at 95°C for 5 min. They were spinned down before loading 2 µg of protein per lane onto the gel. The gels were run in the cold room at a voltage of 30 V for 1 h initially and continued to run at 180 V thereafter. Both, the Laemmli and Tris-Tricine SDS PAGE were run until the loading front disappeared and the protein standard was properly separated.

5.3.12 Coomassie Staining of Gels

For visualisation of the protein bands on a Laemmli or Tris-Tricine SDS-PAGE gel, they were stained with the help of Coomassie Staining. For this, gels were first incubated for 5 min in Fairbanks A after heating them up. Afterwards, the gels were destained by incubation in Fairbanks D after heating them up until they are destained.

5.3.13 *In Vitro* Protein Analysis

5.3.13.1 UV Spectroscopy

UV spectroscopy was used to estimate the concentration of proteins by utilizing their respective extinction coefficient as determined by ProtParam (Table 36). The UV absorbance of proteins is based on the ability of the aromatic amino acids tryptophane and tyrosine, which comprise the chromophores of the molecule, to absorb light in the near UV range between 260 and 280 nm. Moreover, also phenylalanines and disulfide bonds contribute to a smaller extent to this absorption. The absorption of UV light is associated with the electronic transitions in the molecules from lower to higher energy states.

For determination of the concentration of a protein solution, the extinction (E) is measured at 280 nm due to very high absorption of tryptophane and tyrosine at this wavelength using the Lambert Beer law (Equation 3).

$$A_{280\,nm} = \varepsilon * c * d$$

Equation 3: Lambert Beer´s Law for Protein Concentration Determination.
A_{260}: Absorption at 260 nm; ε: Molar extinction coefficient in [M^{-1} cm^{-1}]; d: Pathlength of the cuvette in [cm]; c: Concentration of the protein in [M].

The linear range of absorption is between roughly 0.2 and 1.0. Therefore, the concentrations of the proteins were initially estimated using a NanoDrop2000. For measurement in the Jasco V-630 Spectrophotometer (JASCO Deutschland GmbH, Pfungstadt, Germany), the proteins were diluted to an extinction in the above-mentioned range and their concentration was calculated by applying the Lambert Beer law at 280 nm.

5.3.13.2 CD Spectroscopy

CD spectroscopy is a powerful method to study the secondary and tertiary structure of proteins (Kelly et al., 2005). It is based on the ability to measure the differences in absorbance of right- and left-circularly polarized light of chiral molecules. Far-UV CD ranges from roughly 190 to 260 nm and it can be analyzed for the different secondary structural types comprising the alpha helix, parallel and anti-parallel beta sheet, turn, and random coil. Near-UV CD ranges roughly from 250 to 400 nm and it detects the tertiary structure of a protein. The near-UV CD signal is defined by the asymmetric environment of aromatic residues and to a small extent of disulfide bonds. This generates an individual tertiary structure fingerprint CD spectrum for each protein.
All CD measurements conducted in this work were made in PBS buffer. Far-UV and near-UV CD spectra were performed in a Chirascan plus (Applied Photophysics, Leatherhead, UK) and the used parameters are displayed in Table 45.
All spectra were buffer subtracted and normalized to the mean residue weight ellipticity at a wavelength λ ($\theta_{MRW,\lambda}$) in [deg cm^2 $dmol^{-1}$] and it was calculated following Equation 4:

$$\theta_{MRW,\lambda} = \frac{\theta_\lambda * (\frac{M_r}{n-1})}{c * d}$$

Equation 4: Mean Residue Molar Ellipticity.
θ_λ: Observed ellipticity at wavelength λ in [mdeg]; M_r: Molecular mass in [Da = g mol^{-1}]; n: Number of amino acids; c: Concentration of protein in [g L^{-1}]; d: pathlength in [mm].

Table 45: Parameters Used for Far- and Near-UV CD Spectroscopy.

Parameters	Far-UV CD Spectra	Near-UV CD Spectra
Wavelength [nm]	200-260	260-320
Time per point [s]	0.5	0.5
Data pitch [nm]	0.5	0.5
Bandwidth [nm]	1	1
Sample period [µs]	25	25
Default number of samples	20,000	20,000
Temperature [°C]	25	25
Accumulations	15	15
Concentration [g L^{-1}]	0.12	0.5
Cuvette path length [mm]	1	5

To assess the stability of single proteins or complexes, temperature-induced unfolding transitions followed by far-UV CD were performed in a Chirascan plus (Applied Photophysics, Leatherhead, UK). The transitions after folding kinetics of two proteins were made in a Jasco J-1500 CD Spectrometer (JASCO Deutschland GmbH, Pfungstadt, Germany). The settings are shown in Table 46, respectively.

Thermal unfolding transitions are normalized according to the following formula (Equation 5):

$$f_U = \frac{\theta_\lambda - A1}{A2 - A1}$$

Equation 5: Normalization of Thermal Transitions.
f_u: Fraction unfolded; θ_λ: Observed ellipticity at wavelength λ in [mdeg]; $A1$: Initial value of transition in [mdeg]; $A2$: Final value of transition in [mdeg].

Table 46: Parameters Used for Temperature-Induced Unfolding Transitions in Chirascan plus and Jasco J-1500 CD Spectrometer.

Parameters	**Temperature-Induced Unfolding Transition in Chirascan plus**	**Temperature-Induced Unfolding Transition after Folding Kinetics in Jasco J-1500 CD Spectrometer**
Wavelength [nm]	205	205
Data pitch [°C]	0.5	0.5
Band width [nm]	1	1
Sample period [µs]/D. I. T. [s]	25	4
Default number of samples	20,000	/
Starting Temperature [°C]	20	20
End Temperature [°C]	90	90
Heating Rate [°C min^{-1}]	1	1
Concentration	0.12 g L^{-1}	5 µM per protein
Cuvette pathlength [mm]	1	1

After normalization, unfolding transitions were fitted to a Boltzmann fit (Equation 6) to obtain x_0, at which half of the protein is unfolded, also referred to as T_m:

$$y(x) = A_2 + (A_1 + A_2)/(1 + \exp\left(\frac{x - x_0}{dx}\right))$$

Equation 6: Boltzmann Fit.
A_1: Initial value; A_2: Final value; x_0: Center; dx: Time constant.

The folding kinetics of two proteins were performed in a Jasco J-1500 CD Spectrometer (JASCO Deutschland GmbH, Pfungstadt, Germany) and the settings are shown in Table 47. The folding kinetics were buffer corrected.

Folding Kinetics were fitted to an ExpDec1 fit () to obtain t_1, at which 62.3 % of the protein is folded, also referred to as τ:

$$y(x) = A_1 * \exp\left(-\frac{x}{t_1}\right) + y_0$$

Equation 7: ExpDec1 Fit.
A_1: Amplitude; y_0: Offset; t_1: Time constant.

Table 47: Parameters Used for Folding Kinetics.

Parameters	**Folding Kinetics**
Wavelength [nm]	205
Data pitch [sec]	5
Band width [nm]	1
D. I. T. [sec]	4
Temperature [°C]	25
Time [h]	4
Concentration	5 µM per Protein
Cuvette pathlength [mm]	1

5.3.13.3 Analytical Ultracentrifugation

AUC was applied to assess the quaternary structure of the proteins. AUC enables the real-time observation of the sedimentation of macromolecules, e. g. proteins, in the centrifugal field together with the application of centrifugal force (Laue and Stafford III, 1999). The advantage of this method is that it is not influenced by any interaction with a matrix or a surface because the studied proteins in this thesis are very sticky and interact with several different matrices. In this thesis, sedimentation velocity experiments were performed. Sedimentation velocity experiments use the hydrodynamic theory for interpretation of the movement of solutes in high centrifugal fields to define the size, shape, and interactions of macromolecules. Three factors define the sedimentation process: the gravitational force, the buoyancy, and the hydrodynamic friction. The gravitational force is proportional to the square of the rotor speed.

The Svedberg equation (Equation 8) accounts for the balance of all three forces:

$$s(M) = D(M) * \frac{M(1 - v_M \rho)}{RT}$$

Equation 8: Svedberg Equation.
ρ: Solvent density in [g cm^3]; R: Gas constant (8.314472 J K^{-1} mol^{-1}); T: Rotor temperature in [K]; ν_M: Partial specific volume in [cm^3 g^{-1}]; s(M): Sedimentation coefficient in [S]; D(M): Diffusion coefficient in [m^2 s^{-1}]; M: Macromolecular size in [g mol^{-1}].

All AUC experiments were performed in HEPES Storage Buffer. All proteins were measured at 20 µM at 20°C at 42,000 RPM in an Optima AUC I (Beckman, Krefeld, Germany) equipped with absorbance optics. The absorption was measured at 280 nm. Data Analysis was carried out with SedFit using the continuous c(S) distribution mode (Schuck, 2000; Brown and Schuck, 2006).

5.3.13.4 Glutaraldehyde Crosslinking

For analysis of oligomeric species, a fresh solution of 0.1 % Glutaraldehyde in 50 mM HEPES, 150 mM KCl, pH 7.4 was prepared. 5 µL of the solution was added to 100 µL of a 15 µM protein sample and incubated for 20 min at RT. The reaction was quenched by the addition of 10 µL of 1 M Tris/HCl (pH 8.0). Finally, reducing Laemmli Buffer was added, and the samples were boiled at 95°C for 5 min before running a precast gradient gel with 4-20 % acrylamide.

5.3.13.5 Hydrogen/Deuterium Exchange Mass Spectrometry

HDX-MS is a biochemical method, which facilitates to gain information about the dynamics, structure and interactions of proteins. The principle is that surface-exposed and therefore accessible hydrogen atoms are exchanged by deuterium upon incubation in a deuterium-containing buffer. This is coupled to a proteolytic digest and a mass spectrometry device to monitor the peptide fragments of a protein, which where able to exchange hydrogen with deuterium. A schematic overview of the method is shown in Figure 84.
HDX was performed on a fully automated robotic system (HTS PAL; LEAP Technologies, Ft Lauderdale, US-FL) coupled to an Acquity M-Class UPLC and a HDX manager (Waters Corp., Milford, USA) as described elsewhere (Zhang et al., 2014).
3 µL of a 30 µM protein sample was added to 57 µL deuterated buffer (50 mM HEPES/KOH, 150 mM KCl, pH 7.4) and incubated at 20°C for 0.17, 1, 10, 30 and 120 min. Three replicate measurements were performed for each protein and each time point. The exchange was stopped by adding 50 µL of quench buffer (200 mM Na_2HPO_4, 200 mM KH_2PO_4, 4 M GdmCl, pH 2.2) to 50 µL of labelled protein at 1˚C. Digestion was performed on-line using an immobilized Waters® Enzymate™ BEH Pepsin Column (2.1 x 30 mm; Waters Corporation, Milford, US-MA) at 20˚C. Peptides were trapped at 0˚C on a VanGuard Pre-column [Acquity UPLC BEH C18 (1.7

µm, 2.1 x 5 mm, Waters Corporation, Milford, US-MA)] for 5 min. The peptides were separated using a C18 column [Acquity UPLC BEH C18 (1.0 x 100 mm, Waters Corporation, Milford, US-MA)] at 0°C by gradient elution of 0-35% (v/v) acetonitrile (0.1% v/v formic acid) in H_2O (0.1 % v/v formic acid) over 6 min followed by a gradient elution of 35-40% (v/v) acetonitrile (0.1% v/v formic acid) in H_2O (0.1 % v/v formic acid) over 7 min, both gradients at a flow rate of 40 µL min^{-1}.

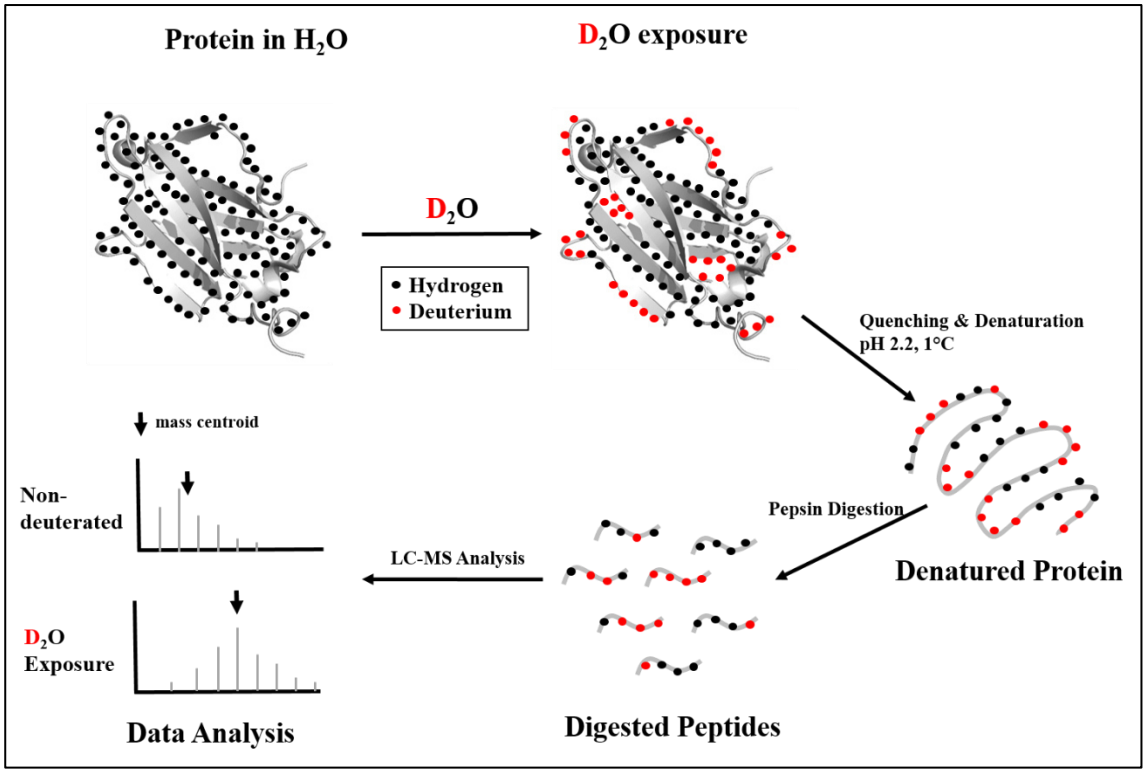

Figure 84: Schematic Overview of the Workflow of HDX-MS Experiments.
The protein is exposed to a D_2O containing buffer. The hydrogen atoms on the surface of the protein are exchanged by deuterium atoms. After a certain time of incubation, the exchange is quenched and the protein gets denatured at a pH of 2.2 at 1°C. The denatured protein is applied on a pepsin column for digestion of the protein. The digested peptides are then analyzed by LC-MS analysis. The chromatograms of non-neuterated and deuterated samples are compared to obtain surface-regions susceptible to HD exchange.

Eluting peptides were detected using a Synapt G2S mass spectrometer (Waters Corporation, Milford, US-MA). The mass spectrometer was operated in $HDMS^E$ mode, with dynamic range enabled (data independent analysis (DIA) coupled with IMS separation) were used to separate peptides prior to CID fragmentation in the transfer cell. CID data were used for peptide identification, and uptake quantification was performed at peptide level (as CID results in deuterium scrambling).

Data were analysed using Protein Lynx Global Server PLGS (v3.0.3) and DynamX (v3.0.0) software (Waters Corporation, Milford, US-MA). Search parameters in DynamX were as follows: peptide and fragment tolerances = automatic, min fragment ion matches = 1, digest reagent = non-specific, false discovery rate = 100. Restrictions for peptide in DynamX were as follows:

minimum intensity = 5000, minimum products per amino acid = 0, max sequence length = 20, min sequence length = 5, max ppm error = 0, file threshold = 0. The software Deuteros (Lau et al., 2020) was used to identify peptides with statistically significant increases/decreases in deuterium uptake (applying a 99% confidence interval) and to prepare Wood´s plots.

5.3.13.6 Nuclear Magnetic Resonance Spectroscopy

NMR is a method used in structural biology, which relies on the quantum mechanical properties of the nuclei of atoms depending on their microenvironment. It provides information about a protein´s structure and dynamics. NMR experiments in this work were performed in collaboration with the group of Prof. Bernd Reif (TUM). Measurements were performed by Olga Sieluzycka.
All spectra were acquired at 25°C on a Bruker AVANCE600 (Bruker, Rheinstetten, Germany). All proteins were measured in 50 mM HEPES, 150 mM KCl, pH 7.4 supplemented with 10% D_2O.
For the measurement of VPREB in association with the β-strand peptide, 2-fold excess of unlabelled β-strand peptide was added to ^{15}N-labelled VPREB. Prior to steady-state measurement, the VPREB-β-strand complex was incubated for at least 2 h at RT to ensure complete folding of the VPREB.
The structure of VPREB and ʎ5 association was obtained by purifying ^{13}C- and ^{15}N-double-labelled VPREB and unlabelled ʎ5 as a complex. Spectral measurements of ^{15}N-labelled VPREB alone and ^{15}N-^{13}C-double-labelled ʎ5 alone were also performed.
To probe the structure of VPREB in presence or absence of folding agents such as β-strand peptide and ʎ5, ^{15}N-HSQC spectra were recorded of VPREB alone at 25°C by using selective proton flip back techniques for fast pulsing. Identical processing of all spectra was performed in TOPSPIn 4.0.3 (Bruker Biospin). The data was further processed and visualized in CCPN V3.0.4 (University of Leicester, United Kingdom). The figures were created in Affinity Designer (Serif Europe).

5.3.13.7 Enzyme-linked Immunosorbent Assay

To assess the influence of the URs on antigen binding, an enzyme-linked immunosorbent assay (ELISA) was applied, which was established by Eva Herold. An overview of the experimental setup is shown in Figure 85.
First, the streptavidin-coated 96-well plate was incubated with 90 µL of antigen solution per well at 25°C for 45 min, rotating on a Thermomixer compact (eppendorf, Hamburg, Germany) at 350 RPM. This serves for immobilization of the antigen, which is a human biotinylated creatin kinase. The antigen solution was discarded afterwards, and each well was washed 3 times with 150 µL of ddH_2O.

Next, a serial dilution of the proteins and protein complexes in a stoichiometric ratio of 1:1 was prepared in triplicates and, 50 µL of each protein concentration of the serial dilution was added to the 96-well plate and again incubated at 25°C for 45 min, rotating on a Thermomixer compact (eppendorf, Hamburg, Germany) at 350 RPM. Another washing step of 3 times with 150 µL of ddH_2O followed. Thereafter, each well was incubated with 100 µL of antibody solution in a dilution of 1:15,000 at 25°C for 45 min, rotating on a Thermomixer compact (eppendorf, Hamburg, Germany) at 350 RPM, covered from light. The antibody solution contained horseradish peroxidase (HRP) conjugated anti-FLAG antibody. After it was discarded, the third and last washing step with 3 times of 150 µL ddH_2O followed.

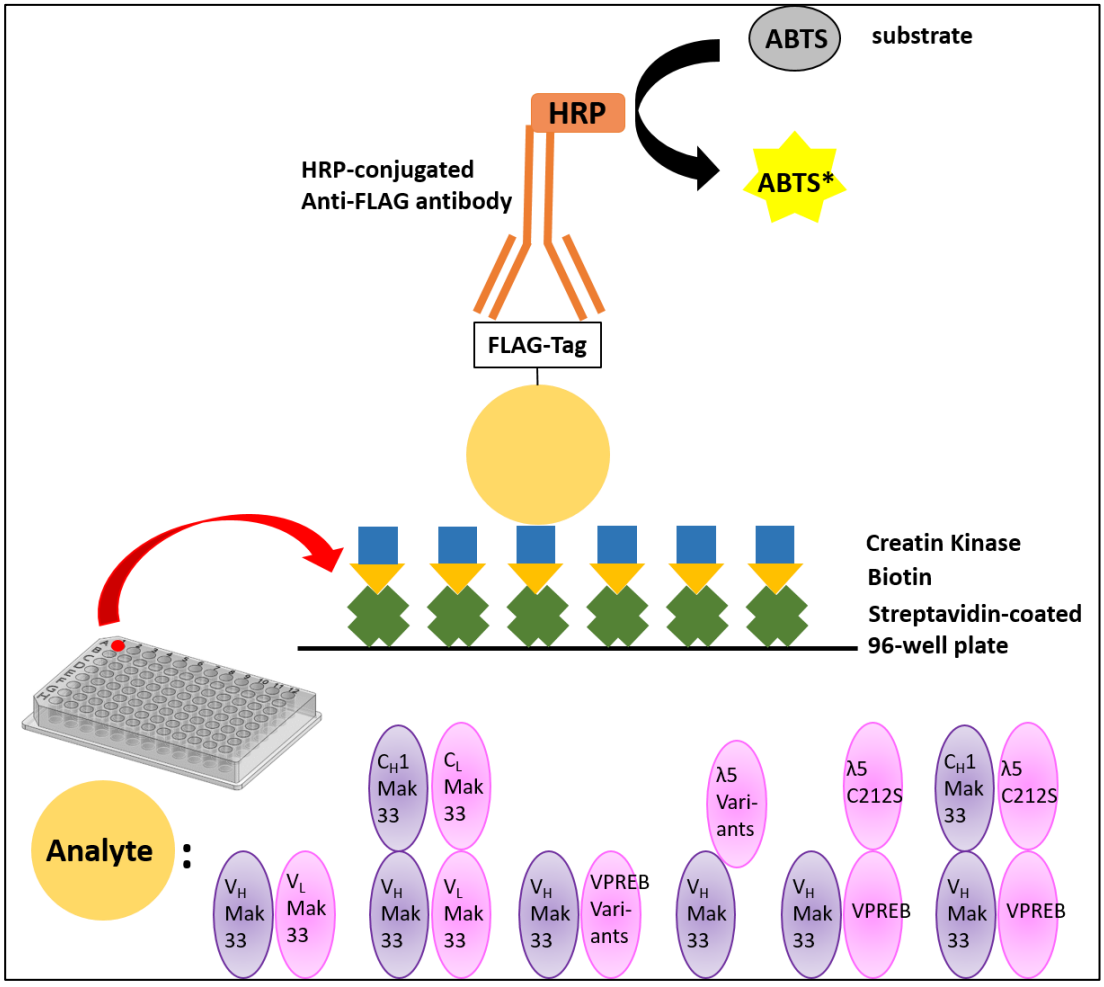

Figure 85: Schematic Overview of the ELISA Workflow.
The biotinylated antigen human creating kinase (muscle type) gets immobilized on a streptavidin-coated 96-well plate. After the immobilization, the FLAG-tagged analyte is incubated and detected by HRP-coupled anti-FLAG antibody. HRP converts its substrate ABTS, which can be detected at a wavelength of 405 nm.

Finally, 100 µL of ABTS solution was added per well and the plate was covered with a sealing foil. ABTS is a substrate of HRP, and its enzymatic conversion leads to an increase in absorption at a wavelength of 405 nm. Immediately, the absorption was measured without shaking in an

Infinite M Nano (Tecan Group, Männedorf, Switzerland) with the following settings: at a wavelength of 405 nm and 25°C. The measurement was conducted for a total time of 8 h with data intervals of 5 min. The intensities after 1 h of measurement were taken for the analysis. The intensities are plotted against the concentrations on a log10 scale and fitted using a Hill1 (Equation 9) fit to obtain k, which corresponds to the K_D in [µM].

$$y(x) = START + (END - START) * x^n/(k^n + x^n)$$

Equation 9: Hill1 Fit.
START: Start value; *END*: End value; *k*: Michaelis constant; *n*: Cooperative sites.

5.3.13.8 Surface Plasmon Resonance

To characterize the protein-protein interaction between λ5 and VPREB variants, C_H1 and λ5 variants as well as between the V_H domain and VPREB and λ5 variants, Surface Plasmon Resonance (SPR) was applied using a Biacore X100 instrument (Figure 86) (Cytiva Sweden AB, Uppsala, Sweden). The ligand each was immobilized via amine coupling chemistry at pH 4-6 onto the surface of CM5 sensor chips, while a serial dilution row of the analyte is prepared and measured by flowing over the immobilized ligand. Both, ligand, and analyte, can be applied label-free. The data is fitted using kinetics parameters in the Biacore X100 Evaluation Software (Cytiva Sweden AB, Uppsala, Sweden) and the dissociation constant, K_D, as well as on- and off-rate, k_a and k_d, are determined. The immobilization levels of the ligands were determined according to the following formula (Equation 10):

$$R_{max} = \frac{analyte\ MW}{ligand\ MW}\ x\ R_L x S_m$$

Equation 10: Immobilization Levels.
R_{max}: Binding capacity of the surface; *MW*: Molecular weight in [g mol^{-1}]; S_m: Stoichiometric ratio between analyte and ligand; R_L: Actual immobilization value.

The immobilization levels (R_L) of ligands for all ligand-analyte combinations were chosen to be roughly at an R_{max} of 100.
The technology is based on changes in the refractive index at the surface of the gold sensor chip. The refractive index increases proportionally to the increase in mass that is associated with a binding event. This is observed as a change in response, which are measured as changes in the resonance angle (δθ) of refracted light when the analyte binds to immobilized ligand and increases the density at the sensor chip. For protein-protein interactions, the change in refractive index on the surface is linearly related to the number of bound molecules. The quantification of the response signal is in resonance units (RU) and represents a defined shift in the resonance angle.
For immobilization, CM5 Chip Coupling Buffer was used and the measurement took place in Biacore Running Buffer. The measurements were conducted at 20°C on a Sensor Chip CM5

(Cytiva Sweden AB, Uppsala, Sweden). Multi cycle runs with titrations of the analytes of various concentrations were measured with an association time of 3 min, a dissociation time of 5 min and a constant flow rate of 30 µL/min. The sensor surface was regenerated between each experiment with a 30 s injection of 1.5 M KCl at a flow rate of 30 µL/min.

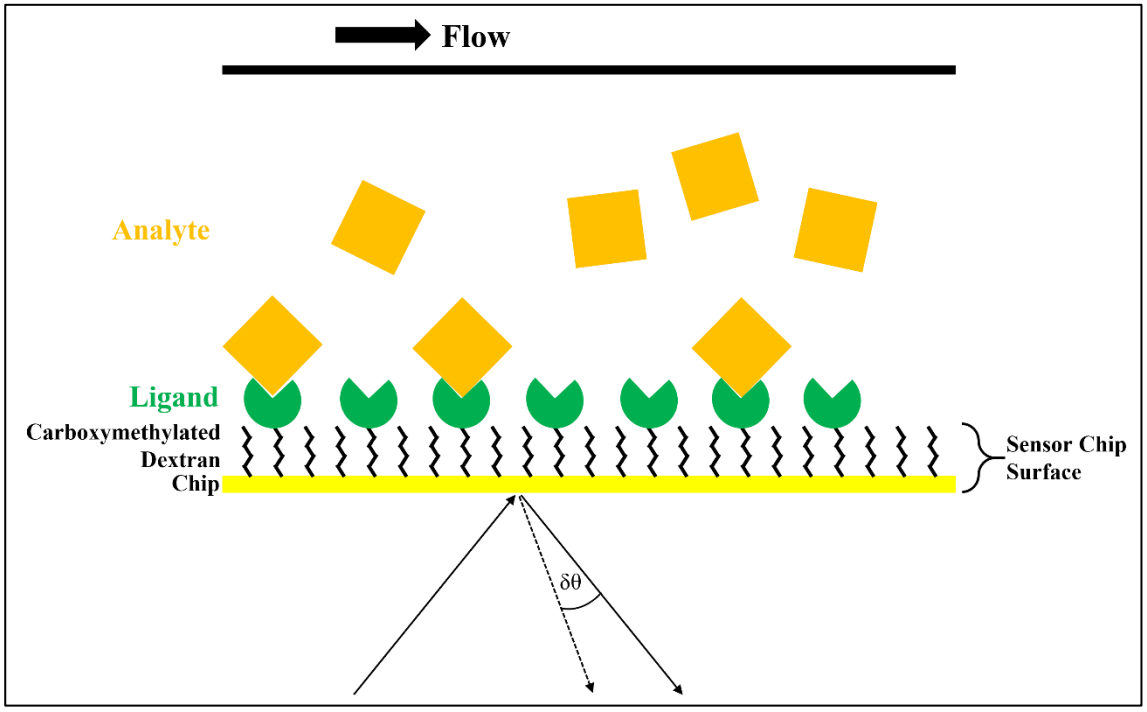

Figure 86: Schematic Overview of the SPR Workflow.
The CM5 sensor chip surface consists of a gold-layer coated with carboxmethylated dextran. The ligand gets immobilized via amine coupling to the sensor chip. The analyte is applied with a constant flow to the sensor chip. The change in the resonance angle (δθ) of refracted light when the analyte binds to the immobilized ligand is the read-out.

Binding curves were plotted after subtraction of background (binding to control flow cells and signal of the running buffer) and the sensorgrams were fitted to a 1:1 binding model using the Biacore X100 Evaluation Software (Cytiva Sweden AB, Uppsala, Sweden).

5.3.13.9 Isothermal Titration Calorimetry

Isothermal Titration Calorimetry (ITC) is a label-free method to examine the affinity between two proteins in their native states by directly measuring the heat that is either released or absorbed during gradual titration of the ligand into the sample cell containing the protein of interest (Figure 87). Furthermore, it allows the determination of binding stoichiometry, entropy, and enthalpy.
The interaction of VPREB and the additional β-strand of λ5 was analyzed using a MicroCal PEAQ-ITC 200 (Malvern Panalytical GmbH, Kassel, Germany) at 25°C. The measurement was conducted in a triplicate. For all replicates, 40 µM of VPREB were applied to the sample cell and 200 µM, 300 µM and 400 µM of the β-strand, respectively, to the syringe. Measurements took

place in HEPES Storage Buffer. From the syringe, 25 injections were done, and the released heat and binding affinities directly determined with high feedback. The syringe had a stir speed of 750 rpm and a reference power of 10 µcal/s was applied.

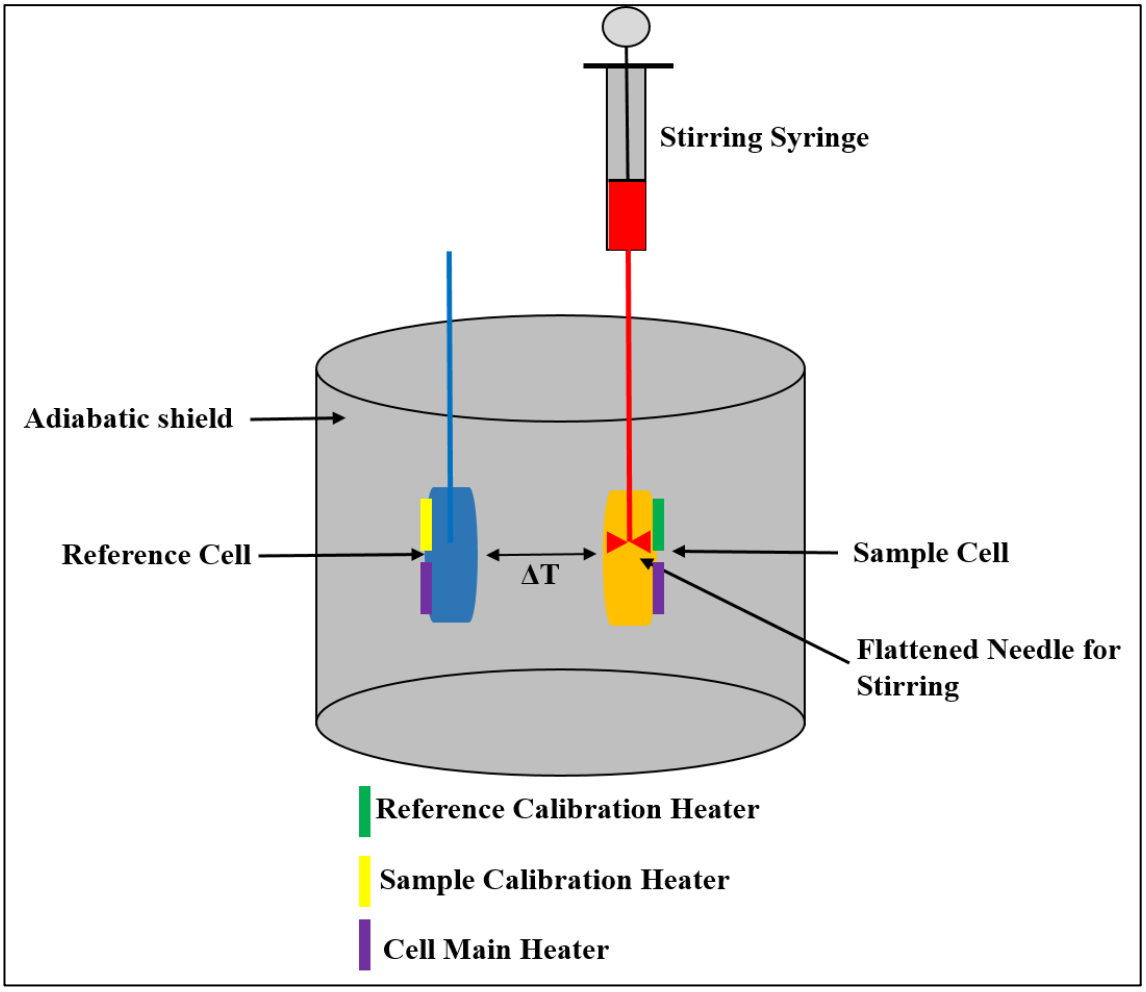

Figure 87: Schematic Overview of the ITC Workflow.
The analyte in the syringe is injected to the ligand in the sample cell. The change in temperature (ΔT) to the reference cell served to calculated the K_D between the proteins.

6. REFERENCES

Aiba, Y.; Kameyama, M.; Yamazaki, T.; Tedder, T. F. and Kurosaki, T. (2008): Regulation of B-cell development by BCAP and CD19 through their binding to phosphoinositide 3-kinase. *Blood* **111**: 1497-503.

Alberts, B.; Johnson, A.; Lewis, J.; Raff, M. and Roberts, K. W. P. (2002): **Molecular Biology of the Cell**.

Alexander, P. A.; He, Y.; Chen, Y.; Orban, J. and Bryan, P. N. (2007): The design and characterization of two proteins with 88% sequence identity but different structure and function. *Proc Natl Acad Sci USA* **104**: 11963-8.

Allman, D.; Li, J. and Hardy, R. R. (1999): Commitment to the B lymphoid lineage occurs before DH-JH recombination. *J Exp Med* **189**: 735-40.

Alt, F.; Rosenberg, N.; Lewis, S.; Thomas, E. and Baltimore, D. (1981): Organization and reorganization of immunoglobulin genes in A-MuLV-transformed cells: Rearrangement of heavy but not light chain genes. *Cell* **27**: 381-90.

Anfinsen, C. B. (1972): The formation and stabilization of protein structure. *Biochem J* **128**: 737-49.

Anfinsen, C. B. (1973): Principles that govern the folding of protein chains. *Science* **181**: 223-30.

Anfinsen, C. B. and Haber, E. (1961): Studies on the Reduction and Re-formation of Protein Disulfide Bonds. *J Biol Chem* **236**: 1361-3.

Anthony, J.; Near, R.; Wong, S.-L.; Iida, E.; Ernst, E.; Wittekind, M.; Haber, E. and Ng, S.-C. (1992): Production of stable anti-digoxin Fv in Escherichia coli. *Mol. Immunol.* **29**: 1237-47.

Araki, K. and Nagata, K. (2011): Protein folding and quality control in the ER. *Cold Spring Harb Perspect Biol* **4**: a015438.

Arnold, J. N.; Wormald, M. R.; Sim, R. B.; Rudd, P. M. and Dwek, R. A. (2007): The impact of glycosylation on the biological function and structure of human immunoglobulins. *Annu Rev Immunol* **25**: 21-50.

Avalos, A. M.; Meyer-Wentrup, F. and Ploegh, H. L. (2014): B-cell receptor signaling in lymphoid malignancies and autoimmunity. *Adv Immunol* **123**: 1-49.

Azuma, T. and Hamaguchi, K. (1976): The mechanism of reassembly of immunoglobulin G. *J Biochem* **80**: 1023-38.

Azuma, T.; Kobayashi, O.; Goto, Y. and Hamaguchi, K. (1978): Monomer-dimer equilibria of a Bence Jones protein and its variable fragment. *J Biochem* **83**: 1485-92.

Bankovich, A. J.; Raunser, S.; Juo, Z. S.; Walz, T.; Davis, M. M. and Garcia, C. K. (2007): Structural Insight into Pre-B Cell Receptor Function. *Science* **316**: 291-4.

Barger, S. W. (2016): Gene regulation and genetics in neurochemistry, past to future. *J Neurochem* **139**: 24-57.

Bartlett, A. I. and Radford, S., E. (2009): An expanding arsenal of experimental methods yields an explosion of insights into protein folding mechanisms. *Nat Struct Mol Biol* **16**: 582-8.

Bauer Jr, T. R.; McDermid, H. E.; Budarf, M. L.; Van Keuren, M. L. and Blomberg, B. B. (1993): Physical location of the human immunoglobulin lambda-like genes, *14.1*,*16.1*, and *16.2*. *Immunogenetics* **38**: 387-99.

Bauer, S. R.; Huebner, K.; Budarf, M.; Finan, J.; Erikson, J.; Emanuel, B. S.; Nowell, P. C.; Croce, C. M. and Melchers, F. (1988a): The Human Vpre B Gene is Located on Chromosome 22 Near a cluster of V Lambda Gene Segments. *Immunogenetics* **28**: 328-33.

Bauer, S. R.; Kudo, A. and Melchers, F. (1988b): Structure and pre-B lymphocyte restricted expression of the *VpreB* gene in humans and conservation of its structure in other mammalian species. *EMBO J* **7**: 111-6.

Baumal, R.; Potter, M. and Scharff, M. D. (1971): Synthesis, assembly, and secretion of gamma globulin by mouse myeloma cells. 3. Assembly of the three subclasses of IgG. *J Exp Med* **134**: 1316-34.

Behring, E. v. and Kitasato, S. (1890): Ueber das Zustandekommen der Diptherie-Immunität und der Tetanus-Immunität bei Thieren. *Dtsch Med Wochenschr* **49**: 1113-4.

Bence Jones, H. (1850): Some account of a new animal substance occurring in the urine of a patient labouring under mollities ossium. *Edinb Med Surg J* **74**: 357-68.

Bernier, G. M. and Putnam, F. W. (1963): Monomer-dimer forms of Bence Jones proteins. *Nature* **200**: 223-5.

Bertolotti, A.; Zhang, Y.; Hendershot, L. M.; Harding, H. P. and Ron, D. (2000): Dynamic interaction of BiP and ER stress transducers in the unfolded-protein response. *Nat Cell Biol* **2**: 326-32.

Bertoni, M.; Kiefer, F.; Biasini, M.; Bordoli, L. and Schwede, T. (2017): Modeling protein quaternary structure of homo- and hetero-oligomers beyond binary interactions by homology. *Sci Rep* **7**: 10480.

Bienert, S.; Waterhouse, A.; De Beer, T. A. P.; Tauriello, G.; Studer, G.; Bordoli, L. and Schwede, T. (2016): The SWISS-MODEL Repository - new features and functionality. *Nucleic Acids Res* **45**: D313-D9.

Bodelón, G.; Palomino, C. and Fernández, L. Á. (2012): Immunoglobulin domains in *Escherichia coli* and other enterobacteria: from pathogenesis to applications in antibody technologies. *FEMS Microbiol Rev* **37**: 204-50.

Bonzi, J.; Bornet, O.; Betzi, S.; Kasper, B. T.; Mahal, L. K.; Mancini, S. J. C.; Schiff, C.; Sebban-Kreuzer, C.; Guerlesquin, F. and Elantak, L. (2015): Pre-B cell receptor binding to galectin-1 modifies galectin-1/carbohydrate affinity to modulate specific galectin-1/glycan lattice interactions. *Nat Commun* **6**.

Borghesi, L. A.; Yamashita, Y. and Kincade, P. W. (1999): Heparan Sulfate Proteoglycans Mediate Interleukin-7-Dependent B Lymphopoiesis. *Blood* **93**: 140-8.

Bork, P.; Holm, L. and Sander, C. (1994): The immunoglobulin fold. Structural classification, sequence patterns and common core. *J Mol Biol* **242**: 309-20.

Bossy, D.; Milili, M.; Zucman, J.; Thomas, G.; Fougereau, M. and Schiff, C. (1991): Organization and expression of the λ-like genes that contribute to the μ-ϕ light chain complex in human pre-B cells. *Int Immunol* **3**: 1081-90.

Bossy, D.; Salamero, J.; Olive, D.; Fougereau, M. and Schiff, C. (1993): Structure, biosynthesis, and transduction properties of the Human μ-ϕL Complex: similar behavior of preB and intermediate preB - B cells in transducing ability. *Int Immunol* **5**: 467-78.

Bourne, Y.; Bolgiano, B.; Liao, D.-I.; Strecker, G.; Cantau, P.; Herzberg, O.; Feizi, T. and Cambillau, C. (1994): Crosslinking of mammalian lectin (galectin-1) by complex biantennary saccharides. *Nat Struct Biol* **1**: 863-70.

Braakman, I. and Hebert, D. N. (2013): Protein Folding in the Endoplasmic Reticulum. *Cold Spring Harb Perspect Biol* **5**: a013201.

Bradl, H. and Jäck, H.-M. (2001): Surrogate Light Chain-Mediated Interaction of a Soluble Pre-B Cell Receptor with Adherent Cell Lines. *J Immunol* **167**: 6403-11.

Bradl, H.; Wittmann, J.; Milius, D.; Vettermann, C. and Jäck, H.-M. (2003): Interaction of Murine Precursor B Cell Receptor with Stroma Cells Is Controlled by the Unique Tail of λ5 and Stroma Cell-Associated Heparan-Sulfate. *J Immunol* **171**: 2338-48.

Brewer, C. F.; Miceli, M. C. and Baum, L. G. (2002): Clusters, bundles arrays and lattices: novel mechanisms for lectin-saccharide-mediated cellular interactions. *Curr Opin Struct Biol* **12**: 616-23.

Brouns, G. S.; de Vries, E.; Neefjes, J. J. and Borst, J. (1996): Assembled Pre-B Cell Receptor Complexes Are Retained in the Endoplasmic Reticulum by a Mechanism That Is Not Selective for the Pseudo-light Chain. *J Biol* **271**: 19272-8.

Brouns, G. S.; de Vries, E.; van Noesel, C. J. M.; Mason, D. Y.; van Lier, R. A. W. and Borst, J. (1993): The structure of the μ/pseudo light chain complex on human pre-B cells is consistent with a function in signal transduction. *Eur J Immunol* **23**: 1088-97.

Brown, P. H. and Schuck, P. (2006): Macromolecular Size-and-Shape Distributios by Sedimetation Velocity Analytical Ultracentrifugation. *Biophys J* **90**: 4651-61.

Buchner, J. and Rudolph, R. (1991): Renaturation, purification and characterization of recombinant Fab-fragments produced in Escherichia coli. *Biotechnology (N Y)* **9**: 157-62.

Burrows, P. D.; Lejeune, M. and Kearney, J. F. (1979): Evidence that murine pre-B cells synthesize mu heavy chains but no light chains. *Nature* **280**: 838-40.

Burrows, P. D.; Stephan, R. P.; Wang, Y.-H.; Lassoued, K.; Zhang, Z. and Cooper, M. D. (2002): The transient expression of pre-B cell receptors governs B cell development. *Semin Immunol* **14**: 343-9.

Cenci, S. and Sitia, R. (2007): Managing and exploiting stress in the antibody factory. *FEBS lett* **581**: 3652-7.

Chang, H.; Dmitrovsky, E.; Hieter, P. A.; Mitchell, K.; Leder, P.; Turoczi, L.; Kirsch, I. R. and Hollis, G. F. (1986): Identification of three new Ig λ-like genes in man. *J Exp Med* **163**: 425-35.

Chen, J.; Herzenberg, L. A. and Herzenberg, L. A. (1991): Heparin alters the expression of different forms of immunoglobulin μ heavy chains and their associated proteins by pre-B cell lines and normal Ly-1 (CD5+) B cells. *Int Immunol* **3**: 1117-27.

Cherayil, B. J. and Pillai, S. (1991): The ω/λ5 Surrogate Immunoglobulin Light Chain is Expressed on the Surface of Transitional B Lymphocytes in Murine Bone Marrow. *J Exp Med* **173**: 111-6.

Chiariotti, L.; Salvatore, P.; Benvenuto, G. and Bruni, C. B. (1999): Control of galectin gene expression. *Biochimie* **81**: 381-8.

Chiu, J.; March, P.; Lee, R. and Tillett, D. (2004): Site-directed, Ligase-Independent Mutagenesis (SLIM): a single-tube methodology approaching 100 % efficiency in 4 h. *Nucleic Acids Res* **32**: e174.

Chothia, C.; Novotný, J.; Bruccoleri, R. and Karplus, M. (1985): Domain association in immunoglobulin molecules. The packing of variable domains. *J Mol Biol* **186**: 651-63.

Clark, P. L. (2004): Protein folding in the cell: reshaping the folding funnel. *Trends Biochem Sci* **29**: 527-34.

Coffer, P. J. and Burgering, B. M. T. (2004): Forkhead-box transcription factors and their role in the immune system. *Nat Rev Immunol* **4**: 889-99.

Coffman, R. L. and Weissman, I. L. (1983): Immunoglobulin gene rerrangement during pre-B cell differentiation. *J Mol Cell Immunol* **1**: 31-41.

Cooper, M. D. (2015): The early history of B cells. *Nat Rev Immunol* **15**: 191-7.

Cooper, M. D.; Mulvaney, D.; Coutinho, A. and Cazenave, P.-A. (1986): A novel cell surface molecule on early B-lineage cells. *Nature* **321**: 616-18.

Cox, J. S.; Shamu, C. E. and Walter, P. (1993): Transcriptional induction of genes encoding endoplasmic reticulum resident proteins requires a transmembrane protein kinase. *Cell* **73**: 1197-206.

Cox, J. S. and Walter, P. (1996): A Novel Mechanism for Regulating Activity of a Transcription Factor That Controls the Unfolded Protein Response. *Cell* **87**: 391-404.

Crick, F. (1970): Central dogma of molecular biology. *Nature* **227**: 561-3.

Dalziel, M.; Crispin, M.; Scanlan, C. N.; Zitzmann, N. and Dwek, R. A. (2014): Emerging principles for the therapeutic exploitation of glycosylation. *Science* **343**: 1235681.

Decker, D. J.; Boyle, N. E. and Klinman, N. R. (1991): Predominance of nonproductive rearrangements of VH81X gene segments evidences a dependence of B cell clonal maturation on the structure of nascent H chains. *J Immunol* **147**: 1406-11.

Dill, K. A. (1990): Dominant forces in protein folding. *Biochemistry* **29**: 7133-55.

Dill, K. A. and Chan, H. S. (1997): From Levinthal to pathways to funnels. *Nat Struct Biol* **4**: 10-9.

Dobson, C. M. (2003): Protein folding and misfolding. *Nature* **426**: 884-90.

Dolgikh, D. A.; Gilmanshin, R. I.; Brazhnikov, E. V.; Bychkova, V. E.; Semisotnov, G. V.; Venyaminov, S. Y. and Ptitsyn, O. B. (1981): Alpha-Lactalbumin: compact state with fluctuating tertiary structure? *FEBS lett* **136**: 311-5.

Dul, J. L.; Argon, Y.; Winkler, T. H.; ten Boekel, E.; Melchers, F. and Martensson, I.-L. (1996): The murine VpreB1 and VpreB2 genes both encode a protein of the surrogate light chain and are co-expressed during B cell development. *Eur J Immunol* **26**: 906-13.

Ehlich, A.; Schaal, S.; Gu, H.; Kitamura, D.; Müller, W. and Rajewsky, K. (1993): Immunoglobulin Heavy and Light Chain Genes Rearrange Independently at Early Stages of B Cell Development. *Cell* **72**: 695-704.

Ekman, A.; Niku, M.; Liljavirta, J. and Iivanainen, A. (2009): Bos taurus genome sequence reveals the assortment of immunoglobulin and surrogate light chain genes in domestic cattle. *BMC Immunol* **10**: 1-11.

Elantak, L.; Espeli, M.; Boned, A.; Bornet, O.; Bonzi, J.; Gauthier, L.; Feracci, M.; Roche, P.; Guerlesquin, F. and Schiff, C. (2012): Structural Basis for Galectin-1-dependent Pre-B Cell Receptor (Pre-BCR) Activation. *J Biol* **287**: 44703-13.

Ellgaard, L. and Helenius, A. (2003): Quality control in the endoplasmic reticulum. *Mol Cell Biol* **4**: 181-91.

Ellis, R. J. (1987): Proteins as molecular chaperones. *Nature* **328**: 378-9.

Ellis, R. J. (1996): Revisiting the Anfinsen cage. *Fold Des* **1**: R9-15.

Ellis, R. J. and van der Vies, S. M. (1991): Molecular chaperones. *Annu Rev Biochem* **60**: 321-47.

Epp, O.; Lattman, E. E.; Schiffer, M.; Huber, R. and Palm, W. (1975): The molecular structure of a dimer composed of the variable portions of the Bence-Jones protein REI refined at 2.0-A resolution. *Biochemistry* **14**: 4942-52.

Erasmus, M. F.; Matlawska-Wasowska, K.; Kinjyo, I.; Mahajan, A.; Winter, S. S.; Xu, L.; Horowitz, M.; Lidke, D. S. and Wilson, B. S. (2016): Dynamic pre-BCR homodimers fine-tune autonomous survival signals in B cell precursor acute lymphoblastic leukemia. *Sci Signal* **9**.

Erdos, G. and Dosztányi, Z. (2020): Analyzing Protein Disorder with IUPred2A. *Curr Protoc Bioinformatics* **70**: e99.

Espeli, M.; Mancini, S. J. C.; Breton, C.; Poirier, F. and Schiff, C. (2009): Impaired B-cell development at the pre-BII-cell stage in galectin-1-deficient mice due to inefficient pre-BII/stromal cell interactions. *Blood* **113**: 5878-86.

Espeli, M.; Rossi, B.; Mancini, S. J. C.; Roche, P.; Gauthier, L. and Schiff, C. (2006): Initiation of pre-B cell receptor signaling: Common and distinctive features in human and mouse. *Semin Immunol* **18**: 56-66.

Ewalt, K. L.; Hendrick, J. P.; Houry, W. A. and Hartl, F. U. (1997): In Vivo Observation of Polypeptide Flux through the Bacterial Chaperonin System. *Cell* **90**: 491-500.

Fang, T.; Smith, B. P. and Roman, C. A. J. (2001): Conventional and Surrogate Light Chain Differentially Regulate Ig μ and Dμ Heavy Chain Maturation and Surface Expression. *J Immunol* **167**: 3846-57.

Feige, M. J. and Buchner, J. (2014): Principles and engineering of antibody folding and assembly. *Biochim Biophys Acta* **1844**: 2024-31.

Feige, M. J.; Groscurth, S.; Marcinowski, M.; Shimizu, Y.; Kessler, H.; Hendershot, L. M. and Buchner, J. (2009): An Unfolded C_H1 Domain Controls the Assembly and Secretion of IgG Antibodies. *Mol Cell* **34**: 569-79.

Feige, M. J.; Groscurth, S.; Marcinowski, M.; Yew, Z. T.; Truffault, V.; Paci, E.; Kessler, H. and Buchner, J. (2008): The structure of a folding intermediate provides insight into differences in immunoglobulin amyloidogenicity. *Proc Natl Acad Sci USA* **105**: 13373-8.

Feige, M. J.; Hagn, F.; Esser, J.; Kessler, H. and Buchner, J. (2007): Influence of the internal disulfide bridge on the folding pathway of the CL antibody domain. *J Mol Biol* **365**: 1232-44.

Feige, M. J.; Hendershot, L. M. and Buchner, J. (2010a): How antibodies fold. *Trends Biochem Sci* **35**: 189-98.

Feige, M. J.; Simpson, E. R.; Herold, E. M.; Bepperling, A.; Heger, K. and Buchner, J. (2010b): Dissecting the alternatively folded state of the antibody Fab fragment. *J Mol Biol* **399**: 719-30.

Fersht, A. R. (1995): Optimization of rates of protein folding: The nucleation-condensation mechanism and its implications. *Proc Natl Acad Sci USA* **92**: 10869-73.

Fersht, A. R. (1998): Nucleation mechanisms in protein folding. *Curr Opin Struct Biol* **7**: 3-9.

Flaswinkel, H. and Reth, M. G. (1994): Dual role of the tyrosine activation motif of the Ig-alpha protein duing signal transduction via the B cell antigen receptor. *EMBO J* **13**: 83-9.

Frippiat, J.-P.; Williams, S. C.; Tomlinson, I. M.; Cook, G.; Cherif, D.; Paslier, D. L.; Collins, J. E.; Dunham, I.; Winter, G. and Lefranc, M.-P. (1995): Organization of the human immunoglobulin lambda light-chain locus on chromosome 22q11.2. *Hum Mol Genet* **4**: 983-91.

Fütterer, K.; Wong, J.; Grucza, R. A.; Chan, A. C. and Waksman, G. (1998): Structural basis for Syk tyrosine kinase ubiquity in signal transduction pathways revealed by the crystal structure of its regulatory SH2 domains bound to a dually phosphorylated ITAM peptide. *J Mol Biol* **281**: 523-37.

Galler, G. R.; Mundt, C.; Parker, M.; Pelanda, R.; Martensson, I.-L. and Winkler, T. H. (2004): Surface µ Heavy Chain Signals Down-Regulation of the V(D)J-Recombinase Machinery in the Absence of Surrogate Light Chain Components. *J Exp Med* **199**: 1523-32.

Gauthier, L.; Lemmers, B.; Guelpa-Fonlupt, V.; Fougereau, M. and Schiff, C. (1999): µ-Surrogate Light Chain Physicochemical Interactions of the Human PreB Cell Receptor: Implications for V_H Repertoire Selection and Cell Signaling at the PreB Cell Stage. *J Immunol* **162**: 41-50.

Gauthier, L.; Rossi, B.; Roux, F.; Termine, E. and Schiff, C. (2002): Galectin-1 is a stromal cell ligand of the pre-B cell receptor (BCR) implicated in synapse formation between pre-B and stromal cells and in pre-BCR triggering. *Proc Natl Acad Sci USA* **99**: 13014-9.

Georgopoulos, C. and Welch, W. J. (1993): Role of the major heat shock proteins as molecular chaperones. *Annu Rev Cell Biol* **9**: 601-34.

Gibbs, J. W. (1873): A Method of Geometrical Representation of the Thermodynamic Properties of Substances by Means of Surfaces. *Trans Conn Acad Arts Sci* **2**: 382-404.

Glockshuber, R.; Malia, M.; Pfitzinger, I. and Plückthun, A. (1990): A comparison of strategies to stabilize immunoglobulin Fv-fragments. *Biochemistry* **29**: 1362-7.

Goto, Y.; Azuma, T. and Hamaguchi, K. (1979): Refolding of the Immunoglobulin Light Chain. *J Biochem* **85**: 1427-38.

Goto, Y. and Hamaguchi, K. (1982): Unfolding and refolding of the constant fragment of the immunoglobulin light chain. *J Mol Biol* **156**: 891-910.

Gottesman, S.; Wickner, S. and Maurizi, M. R. (1997): Protein quality control: triage by chaperones and proteases. *Genes Dev* **11**: 815-23.

Goyns, M. H.; Young, B. D.; van Kessel, A. G.; de Klein, A.; Grosveld, G.; Bartram, C. R. and Bootsma, D. (1984): Regional mapping of the human immunoglobulin lambda light chain to the Philadelphia chromosome in chronic myeloid leukemia. *Leuk Res* **8**: 547-53.

Grawunder, U.; Leu, T. M. J.; Schatz, D. G.; Werner, A.; Rolink, A. G.; Melchers, F. and Winkler, T. H. (1995): Down-Regulation of *RAG1* and *RAG2* Gene Expression in PreB Cells after Functional Immunoglobulin Heavy Chain Rearrangement. *Immunity* **3**: 601-8.

Gregersen, P. K. and Behrens, T. (2006): Genetics of autoimmune diseases - disorders of immune homeostasis. *Nat Rev Genet* **7**: 917-28.

Guelpa-Fonlupt, V.; Bossy, D.; Alzari, P.; Fumoux, F.; Fougereau, M. and Schiff, C. (1994): The human pre-B cell receptor: structural constraints for a tentative model of the pseudo-light (ΨL) chain. *Mol Immunol* **31**: 1099-108.

Guex, N.; Peitsch, M. C. and Schwede, T. (2009): Automated comparative protein structure modeling with SWISS-MODEL and Swiss-PdbViewer: a historical perspective. *Electrophoresis* **30**: S162-73.

Guloglu, F. B.; Bajor, E.; Smith, B. P. and Roman, C. A. J. (2005): The Unique Region of Surrogate Light Chain Component λ5 Is a Heavy Chain-Specific Regulator of Precursor B Cell Receptor Signaling. *J Immunol* **175**: 358-66.

Guo, B.; Kato, R. M.; Garcia-Lloret, M.; Wahl, M. I. and Rawlings, D. J. (2000): Engagement of the Human Pre-B Cell Receptor Generates a Lipid Raft-Dependent Calcium Signaling Complex. *Immunity* **13**: 243-53.

Gutcher, I. and Becher, B. (2007): APC-derived cytokines and T cell polarization in autoimmune in autoimmune inflammation. *J Clin Invest* **117**: 1119-27.

Haas, I. G. and Wabl, M. (1983): Immunoglobulin heavy chain binding protein. *Nature* **306**: 387-9.

Hagiwara, S. (1996): Transgenic expression of VpreB-3 under the control of the immunoglobulin heavy chain enhancer and SV40 promoter. *Kobe J Med Sci* **42**: 1.

Hardy, R. R.; Carmack, C. E.; Shinton, S. A.; Kemp, J. D. and Hayakawa, K. (1991): Resolution and characterization of pro-B and pre-pro-B cell stages in normal mouse bone marrow. *J Exp Med* **173**: 1213-25.

Hardy, R. R. and Hayakawa, K. (2001): B cell development pathways. *Annu Rev Immunol* **19**: 595-621.

Hart, W. E. and Istrail, S. C. (1996): Fast Protein Folding in the Hydrophobic-Hydrophilic Model within Three-Eighths of Optimal. *Comput Biol* **3**: 53-96.

Hartl, F. U.; Bracher, A. and Hayer-Hartl, M. (2011): Molecular chaperones in protein folding and proteostasis. *Nature* **475**: 324-32.

Hartl, F. U. and Hayer-Hartl, M. (2009): Converging concepts of protein folding *in vitro* and *in vivo*. *Nat Struct Mol Biol* **16**: 574-81.

Haslbeck, M.; Franzmann, T.; Weinfurtner, D. and Buchner, J. (2005): Some like it hot: the structure and function of small heat-shock proteins. *Nat Struct Mol Biol* **12**: 842-6.

Hauser, J.; Wallenius, A.; Sveshnikova, N.; Saarikettu, J. and Grundström, T. (2010): Calmodulin inhibition of E2A stops expression of surrogate light chains of the pre-B-cell receptor and CD19. *Mol Immunol* **47**: 1031-8.

Hayden, T. A.; Riegert, P. and Kline, G. H. (2002): Detection of Functional V_H81X Heavy Chains in Adult Mice with an Assessment of Complementarity-Determining Region 3 Diversity and Capacity to Form Pre-B Cell Receptor. *J Immunol* **169**: 1970-7.

Helenius, A. and Aebi, M. (2004): Roles of N-linked glycans in the endoplasmic reticulum. *Annu Rev Biochem* **73**: 1019-49.

Hendershot, L. M.; Bole, D. G. and Kearney, J. F. (1987a): The role of immunoglobulin heavy chain binding protein in immunoglobulin transport. *Immunol Today* **8**: 111-4.

Hendershot, L. M.; Bole, D. G.; Köhler, G. and Kearney, J. F. (1987b): Assembly and secretion of heavy chains that do not associate posttranslationally with immunoglobulin heavy chain-binding protein. *J Cell Biol* **104**: 761-7.

Herold, E. M.; John, C.; Weber, B.; Kremser, S.; Eras, J.; Berner, C.; Deubler, S.; Zacharias, M. and Buchner, J. (2017): Determinants of the assembly and function of antibody variable domains. *Sci Rep* **7**: 12276.

Herzog, S.; Reth, M. G. and Jumaa, H. (2009): Regulation of B-cell proliferation and differentiation by pre-B-cell receptor signalling. *Nat Rev Immunol* **9**: 195-205.

Hesse, J. E.; Lieber, M. R.; Mizuuchi, K. and Gellert, M. (1989): V(D)J recombination: a functional definition of the joining signals. *Genes Dev* **3**: 1053-61.

Hetz, C. (2012): The unfolded protein response: controlling cell fate decisions under ER stress and beyond. *Nat Rev Mol Cell Biol* **13**: 89-102.

Hetz, C. and Papa, F. R. (2018): The Unfolded Protein Response and Cell Fate Control. *Mol Cell* **69**: 169-81.

Hirabayashi, Y.; Lecerf, J.-M.; Dong, Z. and Stollar, B. D. (1995): Kinetic analysis of the interactions of recombinant human VpreB and Ig V domains. *J Immunol* **155**: 1218-28.

Hochman, J.; Gavish, M.; Inbar, D. and Givol, D. (1976): Folding and interaction of subunits at the antibody combining site. *Biochemistry* **15**: 2706-10.

Hollis, G. F.; Evans, R. J.; Stafford-Hollis, J. M.; Korsmeyer, S. J. and McKearn, J. P. (1989): Immunoglobulin λ light-chain-related genes 14.1 and 16.1 are expressed in pre-B cells and may encode the human immunoglobulin ω light-chain protein. *Proc Natl Acad Sci USA* **86**: 5552-6.

Horne, C.; Klein, M.; Polidoulis, I. and Dorrington, K. J. (1982): Noncovalent association of heavy and light chains of human immunoglobulins. III. Specific interactions between VH and VL. *J Immunol* **129**: 660-4.

Horwich, A. L. and Fenton, W. A. (2019): Chaperonin-assisted protein folding: a chronologue. *Q Rev Biophys* **53**: e4.

Hozumi, N. and Tonegawa, S. (1976): Evidence for somatic rearrangement of immunoglobulin genes coding for variable and constant regions. *Proceedings of the National Academy of Sciences of the United States of America* **73**: 3628-32.

Huber, R.; Deisenhofer, J.; Colman, P. M. and Matsushima, M. (1976): Crystallographic structure studies of an IgG molecule and an Fc fragment. *Nature* **264**: 415-20.

Hurtley, S. M. and Helenius, A. (1989): Protein oligomerization in the endoplasmic reticulum. *Annu Rev Cell Biol* **5**: 277-307.

Igarashi, H.; Gregory, S. C.; Yokota, T.; Sakaguchi, N. and Kincade, P. W. (2002): Transcription from the RAG1 locus marks the earliest lymphocyte progenitors in bone marrow. *Immunity* **17**: 117-30.

Isenman, D. E.; Lancet, D. and Precht, I. (1979): Folding pathways of immunoglobulin domains. The folding kinetics of the Cgamma3 domain of human IgG1. *Biochemistry* **18**: 3327-36.

Itzhaki, L. S.; Otzen, D. E. and Fersht, A. R. (1995): The Strutcure of the Transition State for Folding of Chymotrypsin Inhibitor 2 Analysed by Protein Engineering Methods: Evidence for a Nucleation-condensation Mechanism for Protein Folding. *J Mol Biol* **254**: 260-88.

Jackson, S. E. (1997): How do small single-domain proteins fold? *Fold Des* **3**: R81-91.

Jahn, T. R. and Radford, S., E. (2005): The Yin and Yang of protein folding. *FEBS J* **272**: 5962-70.

Janeway, C. A. (1989): Approaching the asymptote? Evolution and revolution in immunology. *Cold Soring Harb Symp Quant Biol* **54**.

Janeway, C. A. and Medzitov, R. (2002): Innate immune recognition. *Annu Rev Immunol* **20**: 197-216.

Jasper, P. J.; Zhai, S.-K.; Kalis, S. L.; Kingzette, M. and Knight, K. L. (2003): B Lymphocyte Development in Rabbit: Progenitor B Cells and Waning of B Lymphopoiesis. *J Immunol* **171**: 6372-80.

Jennewein, M. F. and Alter, G. (2017): The Immunoregulatory Roles of Antibody Glycosylation. *Trends Immunol* **38**: 358-72.

Jeong, J.-Y.; Yim, H.-S.; Ryu, J.-Y.; Lee, H. S.; Lee, J.-H.; Seen, D.-S. and Kang, S. G. (2012): One-Step Sequence- and Ligation-Independent Cloning as a Rapid and Versatile Cloning Method for Functional Genomics Studies. *Appl Environ Microbiol* **78**: 5440.

Jones, D. T. (1999): Protein secondary structure prediciton based on position-specific scoring matrices. *J Mol Biol* **292**: 195-202.

Jongstra, J.; Jongstra-Bilen, J.; Tidmarsh, G. F. and Davis, M. M. (1988): The in vitro translation product of the murine lambda 5 gene contains a functional signal peptide. *Mol Immunol* **25**: 687-93.

Jumaa, H.; Hendriks, R. W. and Reth, M. G. (2005): B cell signaling and tumorigenesis. *Annu Rev Immunol* **23**: 415-45.

Jumper, J.; Evans, R.; Pritzel, A.; Green, T.; Figurnov, M.; Ronneberger, O.; Tunyasuvunakool, K.; Bates, R.; Žídek, A.; Potapenko, A.; Bridgland, A.; Meyer, C.; Kohl, S. A. A.; Ballard, A. J.; Cowie, A.; Bernardino, R.-P.; Nikolov, S.; Jain, R.; Adler, J.; Back, T.; Petersen, S.; Reiman, D.; Clancy, E.; Zielinski, M.; Steinegger, M.; Pacholska, M.; Berghammer, T.; Bodenstein, S.; Silver, D.; Vinyals, O.; Senior, A. W.; Kavukcuoglu, K.; Kohli, P. and Hassabis, D. (2021): Highly accurate protein structure prediction with AlphaFold. *Nature* **596**: 583-9.

Kabat, E. A.; Wu, T. T. and Bilofsky, H. (1977): Unusual distributions of amino acids in complementarity-determining (hypervariable) segments of heavy and light chains of immunoglobulins and their possible roles in specificity of antibody-combining sites. *J Biol Chem* **252**: 6609-16.

Kanie, T.; Abe, A.; Matsuda, T.; Kuno, Y.; Towatari, M.; Yamamoto, T.; Saito, H.; Emi, N. and Naoe, T. (2004): TEL-Syk fusion consitutively activates PI3-K/Akt, MAPK and JAK2-independent STAT5 signal pathways. *Leukemia* **18**: 548-55.

Kannan, M.; Sivaprakasam, C.; Prinz, W. A. and Nachiappan, V. (2016): Endoplasmic reticulum stress affects the transport of phosphatidylethanolamine from mitochondria to the endoplasmic reticulum in *S. cerevisiae*. *Biochim Biophys Acta* **1861**: 1959-67.

Karasuyama, H.; Kudo, A. and Melchers, f. (1990): The Proteins Encoded by the V_{preB} and λ_5 Pre-B Cell-specific Genes Can Associate with Each Other and with μ Heavy Chain. *J Exp Med* **172**.

Karasuyama, H.; Rolink, A. and Melchers, F. (1993): A Complex of Glycoproteins Is Associated with V_{preB}/λ_5 Surrogate Light Chain on the Surface of μ Heavy Chain-negative Early Precursor B Cell Lines. *J Exp Med* **178**: 469-78.

Karasuyama, H.; Rolink, A. and Melchers, F. (1996): Surrogate ligth chain in B cell development. *Adv Immunol* **63**: 1-41.

Karplus, M. and Weaver, D. L. (1976): Protein-folding dynamics. *Nature* **260**: 404-6.

Karplus, M. and Weaver, D. L. (1994): Protein folding dynamics: The diffusion-collision model and experimental data. *Protein Sci* **3**: 650-68.

Kato, I.; Miyazaki, T.; Nakamura, T. and Kudo, A. (2000): Inducible differentiation and apoptosis of the pre-B cell receptor-positive pre-B cell line. *Int Immunol* **12**: 325-34.

Kawano, Y.; Yoshikawa, S.; Minegishi, Y. and Karasuyama, H. (2005): Selection of stereotyped VH81X-{micro}H chains via pre-B cell receptor earyl in ontogeny and their conservation in adults by marginal zone B cells. *Int Immunol* **17**: 857-67.

Kawano, Y.; Yoshikawa, S.; Minegishi, Y. and Karasuyama, H. (2006): Pre-B Cell Receptor Assesses the Quality of IgH Chains and Tunes the Pre-B Cell Repertoire by Delivering Differential Signals. *J Immunol* **177**: 2242-9.

Kazman, P.; Absmeier, R. M.; Engelhardt, H. and Buchner, J. (2021): Dissection of the amyloid formation pathway in AL amyloidosis. *Nat Commun* **12**: 6561.

Kelley, L. A.; Mezulis, S.; Yates, C. M.; Wass, M. N. and Sternberg, M. J. E. (2015): The Phyre2 web portal for protein modelling, prediction and analysis. *Nat Protoc* **10**: 845-58.

Kelly, S. M.; Jess, T. J. and Price, N. C. (2005): How to study proteins by circular dichroism. *Biochim Biophys Acta* **1751**: 119-39.

Kerr, W. G.; Cooper, M. D.; Feng, L.; Burrows, P. D. and Hendershot, L. M. (1989): Mu heavy chains can associate with a pseudo-ight chain complex (ϕL) in human pre-B cell lines. *Int Immunol* **1**: 355-61.

Keyna, U.; Beck-Engeser, G. B.; Jongstra, J.; Applequist, S. E. and Jäck, H. M. (1995): Surrogate light chain-dependent selection of Ig heavy chain V regions. *J Immunol* **155**: 5536-42.

Khass, M.; Rashid, H.; Burrows, P. D.; Bridges Jr., S. L.; Javed, A. and Schroeder Jr, H. W. (2019): Disruption of the preB Cell Receptor Complex Leads to Decreased Bone Mass. *Front Immunol* **10**: 1-8.

Khorana, H. G. (1968): Synthesis in the study of nucleic acids. *Biochem J* **109**: 709-25.

Kim, P. S. and Baldwin, R. L. (1982): Specific intermediates in the folding reactions of small proteins and the mechanism of protein folding. *Annu Rev Biochem* **51**: 459-89.

Kim, Y. E.; Hipp, M. S.; Bracher, A.; Hayer-Hartl, M. and Hartl, F. U. (2013): Molecular Chaperone Functions in Protein Folding and Proteostasis. *Annu Rev Biochem* **82**: 323-55.

Kinoshita, M. (2009): Importance of Translational Entropy of Water in Biological Self-Assembly Processes like Protein Folding. *Int J Mol Sci* **10**: 1064-80.

Kitamura, D.; Kudo, A.; Schaal, S.; Müller, W.; Melchers, F. and Rajewsky, K. (1992): A Critical Role of λ5 Protein in B Cell Development. *Cell* **69**: 823-31.

Klein, M.; Kortan, C.; Kells, D. I. C. and Dorrington, K. J. (1979): Equilibrium and Kinetic Aspects of the Interaction of Isolated Variable and Constant Domains of Light Chain With the Fd´ Fragment of Immunoglobulin. *Biochemistry* **18**: 1473-81.

Kline, G. H.; Hartwell, L.; Beck-Engeser, G. B.; Keyna, U.; Zaharevitz, S.; Klinman, N. R. and Jäck, H.-M. (1998): Pre-B Cell Receptor-Mediated Selection of Pre-B Cells Synthesizing Functional μ Heavy Chains. *J Immunol* **161**: 1608-18.

Knoll, M.; Yanagisawa, Y.; Simmons, S.; Engels, N.; Wienands, J.; Melchers, F. and Ohnishi, K. (2012): The Non-Ig Parts of the VpreB and λ5 Proteins of the Surrogate Light Chain Play Opposite Roles in the Surface Representation of the Precursor B Cell Receptor. *J Immunol* **188**: 6010-7.

Kopp, M. C.; Larburu, N.; Durairaj, V.; Adams, C. J. and Ali, M. M. U. (2019): UPR proteins IRE1 and PERK switch BiP from chaperone to ER stress sensor. *Nat Struct Mol Biol* **26**: 1053-62.

Kouroku, Y.; Fujita, E.; Tanida, I.; Ueno, T.; Isoai, A.; Kumagai, H.; Ogawa, H.; Kaufman, R. J.; Kominami, E. and Momoi, T. (2007): ER stress (PERK/eIF2alpha phosphorylation) mediates the polyglutamine-induced LC3 conversion, an essential step for autophagy formation. *Cell Death Differ* **14**: 230-9.

Kreft, B.; Berndorff, D.; Böttinger, A.; Finnemann, S.; Wedlich, D.; Hortsch, M.; Tauber, R. and Geßner, R. (1997): LI-Cadherin-mediated Cell-Cell Adhesion Does Not Require Cytoplasmic Interactions. *J Cell Biol* **136**: 1109-21.

Kudo, A. and Melchers, F. (1987): A second gene, V_{preB} in the λ_5 locus of the mouse, which appears to be selectively expressed in pre-B lymphocytes. *EMBO J* **6**: 2267-72.

Kudo, A.; Pravtcheva, D.; Sakaguchi, N.; Ruddle, F. H. and Melchers, F. (1987a): Localization of the Murine λ_5 Gene on Chromosome 16. *Genomics* **1**: 277-9.

Kudo, A.; Sakaguchi, N. and Melchers, F. (1987b): Organization of the murine Ig-related λ_5 gene transcribed selectively in pre-B lymphocytes. *EMBO J* **6**: 103-7.

Kurosaki, T.; Johnson, S. A.; Pao, L.; Sada, K.; Yamamura, H. and Cambier, J. C. (1995): Role of the Syk autophosphorylation site and SH2 domains in B cell antigen receptor signaling. *J Exp Med* **182**: 1815-23.

Lang, K.; Schmid, F. X. and Fischer, G. (1987): Catalysis of protein folding by prolyl isomerase. *Nature* **329**: 268-70.

Lanig, H.; Bradl, H. and Jäck, H.-M. (2004): Three-dimensional modeling of a pre-B-cell receptor. *Mol Immunol* **40**.

Lappalainen, I.; Hurley, M. G. and Clarke, J. (2008): Plasticity within the obligatory folding nucleus of an immunoglobulin-like domain. *J Mol Biol* **375**: 547-59.

Lassoued, K.; Illges, H.; Benlagha, K. and Cooper, M. D. (1996): Fate of Surrogate Light Chains in B Lineage Cells. *J Exp Med* **183**: 421-9.

Lau, A. M.; Claesen, J.; Hansen, K. and Politis, A. (2020): Deuteros 2.0: peptide-level significance testing of data from hydrogen deuterium exchange mass spectrometer. *Bioinformatics* **btaa677**.

Laue, T. M. and Stafford III, W. F. (1999): Modern applications of analytical ultracentrifugation. *Annu Rev Biophys Biomol Struct* **28**: 75-100.

Lee, Y.-K.; Brewer, J. W.; Hellman, R. and Hendershot, L. M. (1999): BiP and Immunoglobulin Light Chain Cooperate to Control the Folding of Heavy Chain and Ensure the Fidelity of Immunoglobulin Assembly. *Mol Biol Cell* **10**: 2209-19.

Lemmers, B.; Gauthier, L.; Guelpa-Fonlupt, V.; Fougereau, M. and Schiff, C. (1999): The Human ($\psi L^+\mu^-$) proB Complex: Cell Surface Expression and Biochemical Structure of a Putative Transducing Receptor. *Blood* **93**: 4336-46.

Levinthal, C. (1968): Are there pathways for protein folding? *J chim Phys Phys-ChimBiol J Chim Phys* **65**: 44-5.

Lieber, M. R.; Ma, Y.; Pannicke, U. and Schwarz, K. (2003): Mechanism and regulation of human non-homologus DNA end-joining. *Nat Rev Mol Cell Biol* **4**: 712-20.

Lilie, H. and Buchner, J. (1995): Domain interactions stabilize the alternatively folded state of an antibody Fab fragment. *FEBS lett* **362**: 43-6.

Lilie, H.; Lang, K.; Rudolph, R. and Buchner, J. (1993): Prolyl isomerases catalyze antibody folding in vitro. *Protein Sci* **2**: 1490-6.

Lindquist, S. and Craig, E. A. (1988): The heat-shock proteins. *Annu Rev Genet* **22**: 631-77.

Liu, C. Y. and Kaufman, R. J. (2003): The unfolded protein response. *J Cell Sci* **116**: 1861-2.

Liu, Z. and Chan, H. S. (2005): Desolvation is a Likely Origin of Robust Enthalpic Barriers to Protein Folding. *J Mol Biol* **349**: 872-89.

Löffert, D.; Ehlich, A.; Müller, W. and Rajewsky, K. (1996): Surrogate Light Chain Expression Is Required to Establish Immunoglobulin Heavy Chain Allelic Exclusion during Early B Cell Development. *Immunity* **4**: 133-44.

Lorimer, G. H. (1994): GroEL structure: a new chapter on assisted folding. *Structure* **2**: 1125-8.

Ma, Y. and Hendershot, L. M. (2004): ER chaperone functions during normal and stress conditions. *J Chem Neuroanat* **28**: 51-65.

Madeira, F.; Park, Y. M.; Lee, J.; Buso, N.; Gur, T.; Madhusoodanan, N.; Basutkar, P.; Tivey, A. R. N.; Potter, S. C.; Finn, R. D. and Lopez, R. (2019): The EMBL-EBI search and sequence analysis tools APIs in 2019. *Nucleic Acids Res* **47**: W636-W41.

Mains, P. E. and Sibley, C. H. (1983): The requirement of light chain for the surface deposition of the heavy chain of immunoglobulin M. *J Biol Chem* **258**: 5027-33.

Makhatadze, G. I. and Privalov, P. L. (1993): Contribution of hydration to protein folding thermodynamics. I. The enthalpy of hydration. *J Mol Biol* **232**: 639-59.

Maki, R.; Kearney, J.; Paige, C. and Tonegawa, S. (1980): Immunoglobulin gene rearrangement in immature B cells. **209**: 1366-9.

Manning, B. D. and Cantley, L. C. (2007): AKT/PKB Signaling: Navigating Downstream. *Cell* **129**: 1261-74.

Marcinowski, M.; Höller, M.; Feige, M. J.; Baerend, D.; Lamb, D. C. and Buchner, J. (2011): Susbtrate discrimination of the chaperone BiP by autonomous and cochaperone-regulated conformational transitions. *Nat Struct Mol Biol* **18**: 150-8.

Martensson, A.; Argon, Y.; Melchers, F.; Dul, J. L. and Martensson, I.-L. (1999): Partial block in B lymphocyte development at the transition into the pre-B cell receptor stage in $V_{pre\text{-}B1}$-deficient mice. *Int Immunol* **11**: 453-60.

Martin, D. A.; Bradl, H.; Collins, T. J.; Roth, E.; Jäck, H.-M. and Wu, G. E. (2003): Selection of Ig μ Heavy Chains by Complementarity-Determining Region 3 Length and Amino Acid Composition. *J Immunol* **171**: 4663-71.

Mattei, M.-G.; Fumoux, F.; Roeckel, N.; Fougereau, M. and Schiff, C. (1991): The Human Pre-B-Specific λ-like Cluster is Located in the 22q11.2-22q12.3 Region, Distal to the IgCλ Locus. *Genomics* **9**: 544-6.

McCracken, A. A. and Brodsky, J. L. (1996): Assembly of ER-Associated Protein Degradation In Vitro: Dependence of Cytosol, Calnexin, and ATP. *J Cell Biol* **132**: 291-8.

McGuffin, L. J.; Bryson, K. and Jones, D. T. (2000): The PSIPRED protein structure prediction server. *Bioinformatics* **16**: 404-5.

McHeyzer-Williams, M.; Okitsu, S.; Wang, N. and McHeyzer-Williams, L. (2011): Molecular programming of B cell memory. *Nat Rev Immunol* **12**: 24-34.

Medzhitov, R. and Janeway, C. A. (1997): Innate immunity: impact on the adaptive immune response. *Curr Opin Immunol* **9**: 4-9.

Meffre, E.; Fougereau, M.; Argenson, J.-N.; Aubaniac, J.-M. and Schiff, C. (1996): Cell surface expression of surrogate light chain (ΨL) in the absence of μ on human pro-B cell lines and normal pro-B cells. *Eur J Immunol* **26**: 2172-80.

Meixlsperger, S.; Köhler, F.; Wossning, T.; Reppel, M.; Müschen, M. and Jumaa, H. (2007): Conventional light chains inhibit the autonomous signaling capacity of the B cell receptor. *Immunity* **26**: 323-33.

Melchers, F. (1999): Fit for life in the immune system? Surrogate L chain tests H chains that test L chains. *Proc Natl Acad Sci USA* **96**: 2571-3.

Melchers, F. (2005): The pre-B-cell receptor: selector of fitting immunoglobulin heavy chains for the B-cell repertoire. *Nat Rev Immunol* **5**: 578-84.

Melchers, F.; Karasuyama, H.; Haasner, D.; Bauer, S.; Kudo, A.; Sakaguchi, N.; Jameson, B. and Rolink, A. (1993): The surrogate light chain in B-cell development. *Immunol Today* **14**: 60-8.

Melchers, F.; ten Boekel, E.; Seidl, T.; Kong, X. C.; Yamagami, T.; Onishi, K.; Shimizu, T.; Rolink, A. G. and Andersson, J. (2000): Repertoire selection by pre-B-cell receptors and B-cell receptors, and genetic control of B-cell development from immature to mature B cells. *Immunol Rev* **175**: 33-46.

Mészáros, B.; Erdos, G. and Dosztányi, Z. (2018): IUPred2A: context-dependent prediction of protein disorder as a function of redox state and protein binding. *Nucleic Acids Res* **46**: W329-W37.

Minegishi, Y.; Coustan-Smith, E.; Wang, Y.-H.; Cooper, M. D.; Campana, D. and Conley, M. E. (1998): Mutations in the Human *λ5/14.1* Gene Result in B Cell Deficiency and Agammaglobulinemia. *J Exp Med* **187**: 71-7.

Minegishi, Y.; Hendershot, L. M. and Conley, M. E. (1999): Novel mechanisms control the folding and assembly of λ5/14.1 and VpreB to produce an intact surrogate light chain. *Proc Natl Acad Sci USA* **96**: 3041-6.

Misener, V.; Downey, G. P. and Jongstra, J. (1991): The immunoglobulin light chain related protein λ5 is expressed on the surface of mouse pre-B cell lines and can function as a signal transducing molecule. *Int Immunol* **3**: 1129-36.

Misener, V.; Jongstra-Bilen, J.; Young, A. J.; Atkinson, M. J.; Wu, G. E. and Jongstra, J. (1990): Association of IgL chain-like protein lambda 5 with a 16-kilodalton protein in mouse pre-B cell lines in not dependent on the presence of Ig H chain protein. *J Immunol* **145**: 905-9.

Montero, D.; Tachibana, C.; Winther, J. R. and Appenzeller-Herzog, C. (2013): Intracellular glutathione pools are heterogeneously concentrated. *Redox Biol* **1**: 508-13.

Morstadt, L.; Bohm, A.; Yüksel, D.; Kumar, K.; Stollar, B. D. and Baleja, J. D. (2008): Engineering and characterization of a single chain surrogate light chain variable domain. *Protein Sci* **17**: 458-65.

Mourcin, F.; Breton, C.; Tellier, J.; Narang, P.; Chasson, L.; Jorquera, A.; Coles, M.; Schiff, C. and Mancini, S. J. C. (2011): Galectin-1-expressing stromal cells constitute a specific niche for pre-BII cell development in mouse bone marrow. *Blood* **117**: 6552-61.

Mundt, C.; Licence, S.; Maxwell, G.; Melchers, F. and Martensson, I.-L. (2006): Only VpreB1, but not VpreB2, is expressed at levels which allow normal development of B cells. *Int Immunol* **18**: 163-72.

Mundt, C.; Licence, S.; Shimizu, T.; Melchers, F. and Martensson, I.-L. (2001): Loss of Precursor B Cell Expansion but Not Allelic Exclusion in *VpreB1/VpreB2* Double-deficient Mice. *J Exp Med* **193**: 435-45.

Munro, S. and Pelham, H. R. B. (1987): A C-terminal signal prevents secretion of luminal ER proteins. *Cell* **48**: 899-907.

Murphy, K. (2012): **Janeway´s Immunobiology**.

Neira, J. L. and Fersht, A. R. (1999): Exploring the Folding Funnel of a Polypeptide Chain by Biophysical Studies on Protein Fragments. *J Mol Biol* **285**: 1309-33.

Nickson, A. A. and Clarke, J. (2010): What lessons can be learned from studying the folding of homologous proteins? *Methods* **52**: 38-50.

Nishimoto, N.; Kubagawa, H.; Ohno, T.; Gartland, G. L.; Stankovic, A. K. and Cooper, M. D. (1991): Normal pre-B cells express a receptor complex of μ heavy chains and surrogate light-chain proteins. *Proc Natl Acad Sci USA* **88**: 6284-8.

Novotný, J. and Haber, E. (1985): Structural invariants of antigen binding: comparison of immunoglobulin VL-VH and VL-VL domain dimers. *Proc Natl Acad Sci USA* **82**: 4592-6.

Oettinger, M. A.; Schatz, D. G. and Baltimore, D. (1990): RAG-1 and RAG-2, adjacent genes that synergistically activate V(D)J recombination. *Science* **248**: 1517-23.

Ogawa, M.; Ten Boekel, E. and Melchers, F. (2000): Identification of $CD19^-$ $B220^+$ c-Kit^+ $Flt3/Flk\text{-}2^+$ cells as early B lymphoid precursors before pre-B-I cells in juvenile mouse bone marrow. *Int Immunol* **12**: 313-24.

Ohnishi, K. and Melchers, F. (2003): The nonimmunoglobulin portion of λ5 mediates cell-autonomous pre-B cell receptor signaling. *Nat Immunol* **4**: 849-56.

Ohnishi, K.; Melchers, F. and Shimizu, T. (2005): Lymphocyte-expressed BILL-cadherin/cadherin-17 contributes to the development of B cells at two stages. *Eur J Immunol* **35**: 957-63.

Ohnishi, K.; Shimizu, T.; Karasuyama, H. and Melchers, F. (2000): The Identification of a Nonclassical Cadherin Expressed during B Cell Development and Its Interaction with Surrogate Light Chain. *J Biol Chem* **275**: 31134-44.

Ohnishi, K. and Takemori, T. (1994): Molecular Components and Assembly of μ-Surrogate Light Chain Complexes in Pre-B Cell Lines. *J Biol Chem* **269**: 28347-53.

Okkenhaug, K. and Vanhaesebroeck, B. (2003): PI3K in lymphocyte development, differentiation and activation. *Nat Rev Immunol* **3**: 317-30.

Orengo, C. A.; Todd, A. E. and Thornton, J. M. (1999): From protein structure to function. *Curr Opin Struct Biol* **9**: 374-82.

Pace, C. N.; Fu, H.; Fryar, K. L.; Landua, J.; Trevino, S. R.; Shirley, B. A. H., Marsha McNutt; Limura, S.; Gajiwala, K.; Scholtz, J. M. and Grimsley, G. R. (2011): Contribution of Hydrophobic Interactions to Protein Stability. *J Mol Biol* **408**: 514-28.

Pace, C. N.; Shirley, B. A.; McNutt, M. and Gajiwala, K. (1996): Forces contributing to the conformational stability of proteins. *FASEB J* **10**: 75-83.

Park, Y.-H. and Osmond, D. G. (1987): Phenotype and proliferation of early B lymphocyte precursor cells in mouse bone marrow. *J Exp Med* **165**: 444-58.

Parker, M. J.; Licence, S.; Erlandsson, L.; Galler, G. R.; Chakalova, L.; Osborne, C.; Morgan, G.; Fraser, P.; Jumaa, H.; Winkler, T. H.; Skok, J. and Martensson, I.-L. (2005): The pre-B-cell receptor induces silencing of VpreB and lambda5 transcription. *EMBO J* **24**: 3895-905.

Pauling, L. and Corey, R. B. (1951a): Atomic coordinates and structure factors for two helical configurations of polypeptide chains. *Proc Natl Acad Sci USA* **37**: 235-40.

Pauling, L. and Corey, R. B. (1951b): Configuration of polypeptide chains. *Nature* **168**: 550-1.

Pauling, L. and Corey, R. B. (1951c): Configurations of Polypeptide Chains With Favored Orientations Around Single Bonds: Two New Pleated Sheets. *Proc Natl Acad Sci USA* **37**: 729-40.

Pauling, L. and Corey, R. B. (1951d): The pleated sheet, a new layer configuration of polypeptide chains. *Proc Natl Acad Sci USA* **37**: 251-6.

Pauling, L. and Corey, R. B. (1951e): The structure of synthetic polypeptides. *Proc Natl Acad Sci USA* **37**: 241-50.

Pauling, L.; Corey, R. B. and Branson, H. R. (1951): The structure of proteins; two hydrogen-bonded helical configurations of the polypeptide chain. *Proc Natl Acad Sci USA* **37**: 205-11.

Pelanda, R.; Schwers, S.; Sonoda, E.; Torres, R. M.; Nemazee, D. and Rajewsky, K. (1997): Receptor editing in a transgenic mouse model: site, efficiency, and role in B cell tolerance and antibody diversification. *Immunity* **7**: 765-75.

Pillai, S. and Baltimore, D. (1987): Formation of disulphide-linked μ_2 ω_2 tetramers in pre-B cells by the 18K ω–immunoglobulin light chain. *Nature* **329**: 172-4.

Plaxco, K. W.; Simons, K. T. and Baker, D. (1998): Contact Order, Transition State Placement and the Refolding Rates of Single Domain Proteins. *J Mol Biol* **10**: 985-94.

Plaxco, K. W.; Simons, K. T.; Ruczinski, I. and Baker, D. (2000): Topology, Stability, Sequence, and Lenght: Defining the Determinants of Two-State Protein Folding Kinetics. *Biochemistry* **39**: 11177-83.

Privalov, P. L. and Makhatadze, G. I. (1993): Contribution of Hydration to Protein Folding Dynamics. II. The entropy and Gibbs energy of hydration. *J Mol Biol* **232**: 660-79.

Ramachandran, G. N.; Ramakrishnan, C. and Sasisekharan, V. (1963): Stereochemistry of polypeptide chain. *J Mol Biol* **7**: 95-9.

Reth, M. G.; Ammirati, P.; Jackson, S. and Alt, F. W. (1985): Regulated progression of a cultured pre-B-cell line to the B-cell stage. *Nature* **317**: 353-5.

Reth, M. G.; Petrac, E.; Wiese, P.; Lobel, L. and Alt, F. W. (1987): Activation of Vκ gene rearrangement in pre-B cells follows the expression of membrane-bound immunoglobulin heavy chains. *EMBO J* **6**: 3299-305.

Richardson, J. S. (1981): The anatomy and taxonomy of protein structure. *Adv Protein Chem.* **34**: 167-339.

Richter, K.; Haslbeck, M. and Buchner, J. (2010): The Heat Shock Response: Life on the Verge of Death. *Mol Cell* **40**: 253-66.

Rolink, A.; Karasuyama, H.; Grawunder, U.; Haasner, D.; Kudo, A. and Melchers, F. (1993): B cell development in mice with a defective λ_5 gene. *Eur J Immunol* **23**: 1284-8.

Rolink, A.; Karasuyama, H.; Haasner, D.; Grawunder, U.; Martensson, I.-L.; Kudo, A. and Melchers, F. (1994): Two Pathways of B-Lymphocyte Development in Mouse Bone Marrow and the Roles of Surrogate L Chain in this Development. *Immunol Rev* **137**: 185-201.

Rolink, A. and Melchers, F. (1991): Molecular and Cellular Origins of B Lymphocyte Diversity. *Cell* **66**: 1081-94.

Rolink, A. G.; Winkler, T. H.; Melchers, F. and Andersson, J. (2000): Precursor B Cell Receptor-dependent B Cell Proliferation and Differentiation Does Not Require the Bone Marrow or Fetal Liver Environment. *J Exp Med* **191**: 23-31.

Rosam, M.; Krader, D.; Nickels, C.; Hochmair, J.; Back, K. C.; Agam, G.; Barth, A.; Zeymer, C.; Hendrix, J.; Schneider, M.; Antes, I.; Reinstein, J.; Lamb, D. C. and Buchner, J. (2018): Bap (Sil1) regulates the molecular chaperone BiP by coupling release of nucleotide and substrate. *Nat Struct Mol Biol* **25**: 90-100.

Rossi, B.; Espeli, M.; Schiff, C. and Gauthier, L. (2006): Clustering of Pre-B Cell Integrins Induces Galectin-1-Dependent Pre-B Cell Receptor Relocalization and Activation. *J Immunol* **177**: 796-803.

Rowley, R. B.; Burkhardt, A. L.; Chao, H.-G.; Matsueda, G. R. and Bolen, J. B. (1995): Syk protein-tyrosine kinase is regulated by tyrosine-phosphorylated Ig alpha/Ig beta immunoreceptor tyrosine activation motif binding and autophosphorylation. *J Biol Chem* **270**: 11590-4.

Sakaguchi, N.; Berger, C. N. and Melchers, F. (1986): Isolation of a cDNA copy of an RNA species expressed in murine pre-B cells. *EMBO J* **5**: 2139-47.

Sakaguchi, N. and Melchers, F. (1986): λ5, a new light-chain-related locus selectively expressed in pre-B lymphocytes. *Nature* **324**: 579-82.

Sanchez, M.; Misulovin, Z.; Burkhardt, A. L.; Mahajan, S.; Costa, T.; Franke, R.; Bolen, J. B. and Nussenzweig, M. C. (1993): Signal transduction by immunoglobulin is mediated through Ig alpha and Ig beta. *J Exp Med* **178**: 1049-55.

Sarmiento Alam, N. C. (2015): Structure and function of the surrogate light chain. Technical University of Munich, Munich.

Schatz, D. G.; Oettinger, M. A. and Baltimore, D. (1989): The V(D)J recombination activating gene, RAG-1. *Cell* **59**: 1035-48.

Schiff, C.; Bensmana, M.; Guglielmi, P.; Milili, M.; Lefranc, M.-P. and Fougereau, M. (1990): The immunoglobulin λ-like gene cluster (14.1, 16.1, and $F_{\lambda}1$) contains gene(s) selectively expressed in pre-B cells and is the human counterpart of the mouse λ5 gene. *Int Immunol* **2**: 201-7.

Schiff, C.; Milili, M.; Bossy, D.; Tabilio, A.; Falzetti, F.; Gabert, J.; Mannoni, P. and Fougereau, M. (1991): λ-Like and V Pre-B Genes Expression: An Early B-Lineage Marker of Human Leukemias. *Blood* **78**: 1516-26.

Schiff, C.; Milili, M. and Fougereau, M. (1989): Isolation of early immunoglobulin λlike gene transcripts in human fetal liver. *Eur J Immunol* **19**: 1873-8.

Schiffer, M.; Girling, R. L.; Ely, K. R. and Edmundson, A. B. (1973): Structure of a lambda-type Bence-Jones protein at 3.5-A resolution. *Biochemistry* **12**: 4620-31.

Schlissel, M. S. (2003): Regulating antigen-receptor gene assembly. *Nat Rev Immunol* **3**: 890-9.

Schlissel, M. S. and Morrow, T. (1994): Ig heavy chain protein controls B cell development by regulating germ-line transcription and retargeting V(D)J recombination. *J Immunol* **153**: 1645-57.

Schneider, M.; Rosam, M.; Glaser, M.; Patronov, A.; Shah, H.; Back, K. C.; Daake, M. A.; Buchner, J. and Antes, I. (2016): BiPPred: Combined sequence- and structure-based prediction of peptide binding to the Hsp70 chaperone BiP. *Proteins* **84**: 1390-407.

Schuck, P. (2000): Size-Distribution Analysis of Macromolecues by Sedimentation Velocity Ultracetrifugation and Lamm Equation Modeling. *Biophys J* **78**: 1606-19.

Seckler, R. and Jaenicke, R. (1992): Protein folding and protein refolding. *FASEB J* **6**: 2545-52.

Seidl, T.; Rolink, A. and Melchers, F. (2001): The VpreB protein of the surrogate light-chain can pair with some μ heavy-chains in the absence of the λ5 protein. *Eur J Immunol* **31**: 1999-2006.

Selkoe, D. J. (2003): Folding proteins in fatal ways. *Nature* **426**: 900-4.

Shamu, C. E. and Walter, P. (1996): Oligomerization and phosphorylation of the Ire1p kinase during intracellular signaling from the endoplasmic reticulum to the nucleus. *EMBO J* **15**: 3028-39.

Shen, Y. and Hendershot, L. M. (2005): ERdj3, a stress-inducible endoplasmic reticulum DnaJ homologue, serves as a cofactor for BiP´s interactions with unfolded substrates. *Mol Biol Cell* **16**: 40-50.

Shimizu, T.; Mundt, C.; Licence, S.; Melchers, F. and Martensson, I.-L. (2002): VpreB1/VpreB2/λ5 Triple-Deficient Mice Show Impaired B Cell Development but Functional Allelic Exclusion of the IgH Locus. *J Immunol* **168**: 6286-93.

Shinjo, F.; Hardy, R. R. and Jongstra, J. (1994): Monoclonal anti-λ5 antibody FS1 identifies a 130 kDa protein associated with λ5 and V_{pre-B} on the surface of early pre-B cell lines. *Int Immunol* **6**: 393-39.

Shirasawa, T.; Ohnishi, K.; Hagiwara, S.; Shigemoto, K.; Takebe, Y.; Rajewsky, K. and Takemori, T. (1993): A novel gene product associated with μ chains in immature B cells. *EMBO J* **12**: 1827-34.

Shoulders, M. D.; Ryno, L. M.; Genereux, J. C.; Moreco, J. J.; Tu, P. G.; Wu, C.; Yates, J. R.; Su, A. I.; Kelly, J. W. and Wiseman, R. L. (2013): Stress-independent activation of XBP1s and/or ATF6 reveals three functionally diverse ER proteostasis environments. *Cell Rep* **3**: 1279-92.

Sideris, D. P. and Tokatlidis, K. (2010): Oxidative protein folding in the mitochondrial intermembrane space. *Antioxid Redox Signal* **13**: 1189-204.

Smith, B. P. and Roman, C. A. J. (2010): The unique and immunoglobulin-like regions of surrogate light chain component λ5 differentially interrogate immunoglobulin heavy-chain structure. *Mol Immunol* **47**: 1195-206.

Solomon, A.; Weiss, D. T.; Schell, M.; Ringelberg, C.; Ch´ang, L.-Y. and Klebig, M. (1997): Identification and characterization of a human Vlambda5 (T1) germline gene that encodes structurally unique lambda light chains. *Mol Immunol* **34**: 463-70.

Stephan, R. P.; Elgavish, E.; Karasuyama, H.; Kubagawa, H. and Cooper, M. D. (2001): Analysis of VpreB Expression During B Lineage Differentiation in λ5-Deficient Mice. *J Immunol* **167**: 3734-9.

Stevens, F. J. and Argon , Y. (1999): Protein folding in the ER. *Semin Cell Dev Biol* **10**: 443-54.

Studer, G.; Rempfer, C.; Waterhouse, A. M.; Gumienny, R.; Haas, J. and Schwede, T. (2020): QMEANDisCo-distance constraints applied on model quality estimation. *Bioinformatics* **36**: 1765-71.

Su, Y.-w.; Flemming, A.; Wossning, T.; Hobeika, E.; Reth, M. G. and Jumaa, H. (2003): Identification of a Pre-BCR Lacking Surrogate Light Chain. *J Exp Med* **198**: 1699-706.

Sun, Y.; Li, X.; Wang, T. and Li, W. (2022): Core Fucosylation Regulates the Function of Pre-BCR, BCR and IgG in Humoral Immunity. *Front Immunol* **13**.

Sun, Z.; Liu, Q.; Qu, G.; Feng, Y. and Reetz, M. T. (2019): Utility of B-Factors in Protein Science: Interpreting Rigidity, Flexibility, and Internal Motion and Engineereing Thermostability. *Chem Rev* **119**: 1626-65.

Swindells, M. B.; Porter, C. T.; Couch, M.; Hurst, J.; Abhinandan, K. R.; Nielsen, J. H.; Macindoe, G.; Hetherington, J. and Martin, A. C. R. (2017): abYsis: Integrated Antibody Sequence and Structure-Management, Analysis, and Prediction. *J Mol Biol* **429**: 356-64.

Tanford, C. (1978): The hydrophobic effect and the organization of living matter. *Science* **200**: 1012-8.

Ten Boekel, E.; Melchers, F. and Rolink, A. G. (1997): Changes in the V_H Gene Repertoire of Developing Precursor B Lymphocytes in Mouse Bone Marrow Mediated by the Pre-B Cell Receptor. *Immunity* **7**: 357-68.

Ten Boekel, E.; Melchers, F. and Rolink, A. G. (1998): Precursor B Cells Showing H Chain Allelic Inclusion Display Allelic Exclusion at the Level of Pre-B Cell Receptor Surface Expression. *Immunity* **8**: 199-207.

Thompson, E. C.; Cobb, B. S.; Sabbattini, P.; Meixlsberger, S.; Parelho, V.; Liberg, D.; Taylor, B.; Dillon, N.; Georgopoulos, K.; Jumaa, H.; Smale, S. T.; Fisher, A. G. and Merkenschlager, M. (2007): Ikaros DNA-binding proteins as integral components of B cell developmental-stage-specific regulatory circuits. *Immunity* **26**: 335-44.

Tokoyoda, K.; Egawa, T.; Sugiyama, T.; Choi, B.-I. and Nagasawa, T. (2004): Cellular niches controlling B lymphocyte behavior within bone marrow during development. *Immunity* **20**: 707-18.

Tonegawa, S. (1983): Somatic generation of antibody diversity. *Nature* **302**: 575-81.

Tsai, B.; Ye, Y. and Rapoport, T. A. (2002): Retro-translocation of proteins from the endoplasmic reticulum into the cytosol. *Nat Rev Mol Cell Biol* **3**: 246-55.

Tsubata, T. and Reth, M. G. (1990): The Products of Pre-B Cell-specific Genes (λ5 and V_{preB}) and the Immunoglobulin μ Chain Form a Complex That Is Transported onto the Cell Surface. *J Exp Med* **172**: 973-6.

Tsubata, T.; Tsubata, R. and Reth, M. G. (1992): Crosslinking of the cell surface immunoglobulin (μ-surrogate light chains complex) on pre-V cells induces activation of V gene rearrangements at the immunoglobulin κ locus. *Int Immunol* **4**: 637-41.

Tsukada, S.; Saffran, D. C.; Rawlings, D. J.; Parolini, O.; Allen, R. C.; Klisak, I.; Sparkes, R. S.; Kubagawa, H.; Mohandas, T.; Quan, S.; Belmont, J. W.; Cooper, M. D.; Conley, M. E. and Witte, O. N. (2012): Deficient expression of a B cell cytoplasmic tyrosine kinase in human X-linked agammaglobulinemia. *J Immunol* **188**: 2936-47.

Übelhart, R.; Bach, M. P.; Eschbach, C.; Wossning, T.; Reth, M. G. and Jumaa, H. (2010): N-linked glycosylation selectively regulates autonomous precursor BCR function. *Nat Immunol* **11**: 759-65.

van Anken, E. and Braakman, I. (2005): Endoplasmic reticulum stress and the making of a professional secretory cell. *Crit Rev Biochem Mol Biol* **40**: 269-83.

Vanhaesebroeck, B. and Alessi, D. R. (2000): The PI3K-PDK1 connection: more than just a road to PKB. *Biochem J* **346**: 561-76.

Varadi, M.; Anyango, S.; Deshpande, M.; Nair, S.; Natassia, C.; Yordanova, G.; Yuan, D.; Stroe, O.; Wood, G.; Laydon, A.; Zidek, A.; Green, T.; Tunyasuvunakool, K.; Petersen, S.; Jumper, J.; Clancy, E.; Green, R.; Vora, A.; Lutfi, M.; Figurnov, M.; Cowie, A.; Hobbs, N.; Kohli, P.; Kleywegt, G.; Birney, E.; Hassabis, D. and Velankar, S. (2022): AlphaFold Protein Structure Database: massively expanding the structural coverage of protein-sequence space with high-accuracy models. *Nucleic Acids Res* **50**: D439-D44.

Vettermann, C.; Herrmann, K.; Albert, C.; Roth, E.; Bösl, M. R. and Jäck, H.-M. (2008): A Unique Role for the λ5 Nonimmunoglobulin Tail in Early B Lymphocyte Development. *J Immunol* **181**: 3232-42.

Vettermann, C.; Herrmann, K. and Jäck, H.-M. (2006): Powered by pairing: The surrogate light chain amplifies immunoglobulin heavy chain signaling and pre-selects the antibody repertoire. *Semin Immunol* **18**: 44-55.

Walter, P. and Ron, D. (2011): The unfolded protein response: from stress pathway to homeostatic regulation. *Science* **334**: 1081-6.

Walter, S. and Buchner, J. (2002): Molecular chaperones - cellular machines for protein folding. *Angew Chem Int Ed Engl* **41**: 1098-113.

Wang, H.; Ye, J.; Arnold, L. W.; McCray, S. K. and Clarke, S. H. (2001): A VH12 transgenic mouse exhibits defects in pre-B cell development and is unable to make IgM+ B cells. *J Immunol* **167**: 1254-62.

Wang, J.; Kang, R.; Huang, H.; Xi, X.; Wang, B.; Wang, J. and Zhao, Z. (2014): Hepatitis C virus core protein activates autophagy through EIF2AK3 and ATF6 UPR pathway-mediated MAP1LC3B and ATG12 expression. *Autophagy* **10**: 766-84.

Wang, Y.-H.; Stephan, R. P.; Scheffold, A.; Kunkel, D.; Karasuyama, H.; Radbruch, A. and Cooper, M. D. (2002): Differential surrogate light chain expression governs B-cell differentiation. *Blood* **99**: 2459-67.

Waterhouse, A.; Bertoni, M.; Bienert, S.; Studer, G.; Tauriello, G.; Gumienny, R.; Heer, F. T.; de Beer, T. A. P.; Rempfer, C.; Bordoli, L.; Lepore, R. and Schwede, T. (2018): SWISS-MODEL: homology modelling of protein structures and complexes. *Nucleic Acids Res* **46**: W296-W303.

Wendeler, M. W.; Praus, M.; Jung, R.; Hecking, M.; Metzig, C. and Gessner, R. (2004): Ksp-cadherin is a functional cell-cell adhesion molecule related to LI-cadherin. *Exp Cell Res* **294**: 345-55.

Wetlaufer, D. B. (1973): Nucleation, Rapid Folding, and Globular Intrachain Regions in Proteins. *Proc Natl Acad Sci USA* **70**: 697-701.

Wickner, S.; Maurizi, M. R. and Gottesman, S. (1999): Posttranslational Quality Control: Folding, Refolding, and Degrading Proteins. *Science* **286**: 1888-93.

Wienands, J.; Schweikert, J.; Wollscheid, B.; Jumaa, H.; Nielsen, P. J. and Reth, M. G. (1998): SLP-65: a new signaling component in B lymphocytes which requires expression of the antigen receptor for phosphorylation. *J Exp Med* **188**: 791-5.

Williams, A. F. and Barclay, A. N. (1988): The immunoglobulin superfamily-domains for cell surface recognition. *Annu Rev Immunol* **6**: 381-405.

Winkler, T. H.; Rolink, A.; Melchers, F. and Karasuyama, H. (1995): Precursor B cells of mouse bone marrow express two different complexes with the surrogate light chain on the surface. *Eur J Immunol* **25**: 446-50.

Wiseman, R. L.; Mesgarzadeh, J. S. and Hendershot, L. M. (2022): Reshaping endoplasmic reticulum quality control through the unfolded protein response. *Mol Cell* **82**: 1477-91.

Wu, T. T. and Kabat, E. A. (1970): An analysis of the sequences of the variable regions of Bence Jones proteins and myeloma light chains and their implications for antibody complementarity. *J Exp Med* **132**: 211-50.

Yancopoulos, G. D. and Alt, F. W. (1986): Regulation of the assembly and expression of variable-region genes. *Annu Rev Immunol* **4**: 339-68.

Ye, J.; McCray, S. K. and Clarke, S. H. (1996): The transition of pre-BI to pre-BII cells is dependent on the V_H structure of the μ/surrogate L chain receptor. *EMBO J* **15**: 1524-33.

Yerbury, J. J.; Stewart, E. M.; Wyatt, A. R. and Wilson, M. R. (2005): Quality control of protein folding in extracellular space. *EMBO Rep* **6**: 1131-6.

Young, J. C.; Agashe, V. R.; Siegers, K. and Hartl, F. U. (2004): Pathways of chaperone-mediated protein folding in the cytosol. *Nat Rev Mol Cell Biol* **5**: 781-91.

Zamecnik, P. C. (1962): Unsettled questions in the field of protein synthesis. *Biochem J* **85**: 257-64.

Zhang, G. and Zoya, I. (2011): Folding at the birth of the nascent chain: coordinating translation with co-translational folding. *Curr Opin Struct Biol* **21**: 25-31.

Zhang, Y.; Wienands, J.; Zürn, C. and Reth, M. G. (1998): Induction of the antigen receptor expression on B lymphocytes results in rapid competence for signaling of SLP-65 and Syk. *EMBO J* **17**: 7304-10.

Zimmermann, R.; Eyrisch, S.; Ahmad, M. and Helms, V. (2011): Protein translocation across the ER membrane. *Biochim Biophys Acta* **1808**: 912-24.

Zimmermann, S. B. and Trach, S. O. (1991): Estimation of Macromolecule Concentrations and Excluded Volume Effects for the Cytoplasm of *Escherichia coli*. *J Mol Biol* **222**: 599-620.

I. List of Figures

II. List of Tables

III. List of Abbreviations

Abbreviation	Meaning
APC	Antigen-Presenting Cell
ATF6	Activating Transcription Factor 6
ATP	Adeonsine Triphosphate
AUC	Analytical Ultracentrifugation
Bap	BiP-Associated Protein
BCAP/PIK3AP1	B-Cell PI3K Adaptor
BCR	B-Cell Receptor
BiP	Heavy Chain Binding Protein
CD	Circular Dichroism
CDR	Complementarity Determining Region
C_H	Constant Heavy Chain Domain
C_L	Constant Light Chain Domain
COPII	Coat protein II
CRD	Carbohydrate Recognition Domain
D	Diversity Gene Segment
Da	Dalton
DNA	Deoxyribonucleic Acid
E. coli	*Escherichia Coli*
ER	Endoplasmic Reticulum
ERAD	ER-Associated Degradation
ERQC	ER Quality Control
Fc	Crystallizabke Fragment
FF	Fast Flow
GAL1	Galectine-1

Abbreviation	**Meaning**
GrpE	Protein GrpE
GSH	Reduced Glutathione
GSSG	Oxidized Glutathione
h	hour
HC	Heavy Chain
HDX	Hydrogen/Deuterium Exchange
HS	Heparan Sulfate
Hsp	Heat Shock Protein
HSPG	Heparan Sulfate Proteoglycan
IB	Inlusion Body
Ig	Immunoglobulin
IGL-C	Cʎ Gene Complex
IGLL	Immunoglobulin ʎ-Like
IGL-V	Vʎ Gene Complex
IRE1α	Inositol-Requiring Enzyme 1α
ITAM	Immunoreceptor Tyrosine-Based Activation Motif
J	Joining Gene Segment
k_a	Association Rate Constant
K_D	Dissociation Constant
k_d	Dissociation Rate Constant
LC	Light Chain
MHC	Major Histocompatibility Complex
mL	milliliter
mRNA	Messenger Ribonucleic Acid
mRNA	Messenger RNA

Abbreviation	**Meaning**
MS	Mass Spectrometry
N	Native Protein
n. d.	Not determined
n. I.	No Interaction
NAC	Nascent-Chain-Associated Complex
NEF	Nucleotide Exchange Factor
NHEJ	Non-Homologous End Joining
NMR	Nuclear-Magnetic Resonance Spectrometry
NOD	Nucleotide-Binding Oligomerization Domain
O/N	Over Night
OD_{600}	Optical Density at 600 nm
PAMP	Pathogen-Associated Molacular Pattern
PDK1	3-Phosphoinositide-Dependent Protein Kinase 1
PERK	Protein Kinase RNA-Like ER Kinase
PFD	Prefoldin
PKB/AKT	Protein Kinase B
POI	Protein of Interest
PPIase	Peptidyl-Prolyl *cis/trans* Isomerase
Pre-B Cells	Precursor B Cells
Pre-BCR	Pre-B Cell Receptor
Pro-B cells	Progenitor B Cells
PRR	Pattern Recognition Receptor
Rac	Ribosome-Associated Complex
Rag	Recombinase Activating Gene
RIDD	IRE1-Dependent Decay

Abbreviation	**Meaning**
RT	Room Temperature
S1P	Site 1 Protease
sHsp	Small Heat Shock Proteins
SLC	Surrogate Light Chain
SYK	Spleen Tyrosine Kinase
T_C Cells	Cytotoxic Cells
TCR	T-Cell Receptor
TF	Trigger Factor
T_H Cells	T-Helper Cells
TLR	Toll-Like Receptor
T_m	Melting Temperature
UPR	Unfolded Protein Response
UR	Unique Region
UV	Ultraviolet
V	Variable Gene Segment
V_H	Variable Heavy Chain Domain
V_L	Variable Light Chain Domain
VLA-4	$\alpha_4\beta_1$ Integrin
VLA-5	$\alpha_5\beta_1$ Integrin
XBP1	X Box-Binding Protein 1
XBP1u	mRNA of X Box-Binding Protein 1
β-ME	β-Mercaptoethanol
ΔDU	Difference in Deuterium Uptake
τ	Time Constant

IV. ACKNOWLEDGEMENT

Ich möchte meinem Doktorvater Prof. Johannes Buchner dafür danken, dass ich die Doktorarbeit an seinem Lehrstuhl machen durfte. Für die Möglichkeit, an einem herausfordernden und zugleich sehr spannenden Forschungsprojekt arbeiten zu können, das mich nicht nur fachlich sondern auch persönlich sehr wachsen ließ.

Außerdem möchte ich dem gesamten Lehrstuhl danken, vor allem den Sekretärinnen, Margot Rubinstein und Anna Semm, die sich immer sehr liebevoll um alle Mitarbeiter gekümmert haben bzw. kümmern. Ich möchte mich außerdem bei der gesamten technischen Assistenz bedanken: Bettina Richter, Ruby Khan, Laura Meier und Anja Osterauer. Vor allem möchte ich Florian Rührnößl danken, der mit zahlreichen HDX-Messungen sowie -Auswertungen maßgeblich an dieser Doktorarbeit beteiligt war. Herzlichen Dank auch an Max Riedl und Ramona Absmeier für die AUC-Messungen. Außerdem möchte ich noch dem Arbeitskreis Klaus Richter danken, dass ihr mich so nett aufgenommen habt. Besonderer Dank gehen an Amira Ben Hadj und Lukas Schmauder, mit denen ich viele lustige Stunden verbracht habe. Zuletzt möchte ich mich noch bei „Labor/Büro 1“ im CPA bedanken, für die entspannte Atmosphäre und die anregenden Diskussionen. Hier möchte ich auch Hristo Svilenov danken, mit dem ich mir auch einige Zeit ein Büro geteilt habe und mit dem ich viele wissenschaftliche Gespräche hatte, die mich in meinem Projekt weiterbrachten.

Ein besonderer Dank geht auch an meine Kollaborationspartner, Prof. Bernd Reif und Olga Sieluzycka, für die NMR Messungen sowie Prof. Matthias Feige, Yonatan Mideksa und Nicolas Blömeke für die Zellexperimente.

Mein größter Dank geht an meine Eltern und meine Familie – dafür, dass Ihr mir die richtigen Werte mit auf den Weg gegeben und mir stets gezeigt habt, was im Leben eigentlich wirklich zählt. Danke für tatsächlich alles, Mama, vor allem aber für Dein immer offenes Ohr und die wertvollsten Ratschläge.

Ich möchte außerdem meinen Freunden danken, weil ihr einfach die Besten seid.

V. EIDESSTATTLICHE ERKLÄRUNG

Ich erkläre an Eides statt, dass ich die bei der promotionsführenden Einrichtung der Fakultät für Chemie der TUM zur Promotionsprüfung vorgelegte Arbeit mit dem Titel „Struktur und Funktion der invarianten leichten Kette (Structure and Function of the Invariant Light Chain)“ in Garching bei München, Fakultät für Chemie, Lehrstuhl für Biotechnologie unter der Anleitung und Betreuung durch Prof. Dr. Johannes Buchner ohne sonstige Hilfe erstellt und bei der Abfassung nur die gemäß § 6 Ab. 6 und 7 Satz 2 angebotenen Hilfsmittel benutzt habe.

Ich habe keine Organisation eingeschaltet, die gegen Entgelt Betreuerinnen und Betreuer für die Anfertigung von Dissertationen sucht, oder die mir obliegenden Pflichten hinsichtlich der Prüfungsleistungen für mich ganz oder teilweise erledigt.

Ich habe die Dissertation in dieser oder ähnlicher Form in keinem anderen Prüfungsverfahren als Prüfungsleistung vorgelegt.

Die vollständige Dissertation wurde in mediaTUM veröffentlicht. Die promotionsführende Einrichtung der Fakultät für Chemie hat der Veröffentlichung zugestimmt.

Die öffentlich zugängliche Promotionsordnung der TUM ist mir bekannt, insbesondere habe ich die Bedeutung von § 28 (Nichtigkeit der Promotion) und § 29 (Entzug des Doktorgrades) zur Kenntnis genommen. Ich bin mir der Konsequenzen einer falschen Eidesstattlichen Erklärung bewusst.

Mit der Aufnahme meiner personenbezogenen Daten in die Alumni-Datei bei der TUM bin ich einverstanden.

Ort, Datum, Unterschrift